Advanced cardiac magnetic resonance imaging in heart failure and coronary artery disease

Sammut, Eva Clare

Awarding institution:
King's College London

Advanced cardiac magnetic resonance imaging in heart failure and coronary artery disease

Dr Eva Sammut, MBBS

Submitted for the Degree of Doctor of Philosophy

“Science is not a body of knowledge nor a belief system; it is just a term which describes humankind’s incremental acquisition of understanding through observation. Science is awesome.”

Tim Minchin

Abstract

Recent technical developments have increased the scope for cardiac MRI as a research tool. This work presents novel approaches to the assessment of patients with coronary disease and heart failure.

The thesis explores coronary physiology and microarchitecture, ischaemia and perfusion CMR, and in particular the quantification of ischaemia. In addition, in-vivo cardiac diffusion tensor imaging is employed to characterize microarchitecture in heart failure.

This work comes to a number of conclusions.

We have been able to show, for the first time in patients with heart failure, that even in patients who have thinned and remodelled ventricles, quantitative assessment with high resolution quantitative CMR is feasible and reproducible.

Our work is also the first to perform assessment of the prognostic use of quantitative perfusion CMR - in a large group of unselected patients presenting with suspected coronary disease, we have investigated the prognostic value of a quantitative approach. This observational study proposes that this performs at least as well as visual assessment by expert readers.

Furthermore, the thesis explores the correlation between CMR and PET using a specialized cardiac phantom which simulates perfusion and a hybrid CMR-PET scanner. In this setting, we have concluded that there is excellent correlation between MR, PET and known true perfusion values.

This thesis also presents work on the use of cardiac diffusion tensor imaging in dilated cardiomyopathy, the first study to do so using a dual-phase in-vivo approach. We have been able to demonstrate significant differences in fibre and sheetlet orientation by comparison to controls. Our study used biomechanical modelling and strain data from 3D tagging CMR.

Overall this work adds to the body of knowledge of quantitative perfusion CMR analysis and cardiac DTI and merits further larger studies, particularly with regard to translation to the clinical setting.

Declaration of originality and contributions

This thesis represents part published original work

I, Eva Sammut, confirm that the work presented in this thesis is my own work.

All sources, including tables, figures and data in the thesis are referenced.

I understand that any false claim in respect of this work will result in disciplinary action in accordance with University regulations.

Papers arising from thesis and contribution:

1. 'Perfusion quantification – where are we now?'; **Sammut, E**., Zarinabad, N., Vianello, P., Chiribiri, A.; Current Cardiovascular Imaging Reports, 2014 (http://doi 10.1007/s12410-014-9278).

– first author; literature review, drafting of manuscript

2. 'Feasibility of high-resolution quanttaive perfusion CMR in heart failure'; **Sammut, E**., Zarinabad, N., Wesolowski, R., Morton, G., Chen, Z., Sohal, M., Carr-White, G., Razavi, R., Chiribiri, A.; Journal of Cardiovascular Magnetic Resonance, 2015 (https://doi.org/10.1186/s12968-015-0124-2)

– first author; responsible for data collection, analysis of functional CMR and perfusion data, drafting of manuscript.

3. 'Prognostic value of quantitative perfusion CMR'; **Sammut, E**., Villa, ADM., Di Giovine MD, G., Dancy, L., Bosio, F., Gibbs, T., Jeyabraba, S., Schwenke, S., Williams, SE., Marber, M., Alfakih, K., Ismail, TF., Razavi, R., Chiribiri, A.; JACC Imaging, 2017 (*https://doi.org/10.1016/j.jcmg.2017.07.022*)

– first author; responsible for data collection, analysis of functional CMR and perfusion data, drafting of manuscript.

4. ‘Studying Dynamic Myofiber Aggregate Reorientation in Dilated Cardiomyopathy Using In Vivo Magnetic Resonance Diffusion Tensor Imaging’; *Von Deuster, C.,* ***Sammut, E****., Asner, L., Nordsletten, D., Lamata, P., Stoeck, C.T, Kozerke, S., Razavi, R.; Circulation Cardiovascular Imaging, 2016 (http://doi: 10.1161/CIRCIMAGING.116.005018)*

– joint first author; responsible for data collection, analysis of functional CMR and tagging data, drafting of manuscript.

Table of Contents

List of figures

List of tables

Abbreviations

ATP – adenosine triphosphate

CABG – coronary artery bypass grafting

CAD – coronary artery disease

CFR – coronary flow reserve

CMR – cardiac magnetic resonance imaging

DCM – dilated cardiomyopathy

DTI – diffusion tensor imaging

FA – fractional anisotropy

FFR – fractional flow reserve

Gd – Gadolinium

HA – helix angle

HF – heart failure

ICM – ischaemic cardiomyopathy

LGE – late gadolinium enhancement

LVEF – left ventricular ejection fraction

NSTEMI – non ST-elevation myocardial infarction

STEMI – ST-elevation myocardial infarction

MBF – myocardial blood flow

MD – mean diffusivity

MPR – myocardial perfusion reserve

PCI – percutaneous coronary intervention

PET – positron emission tomography

SPECT – single photon emission computed tomography

TAC – time activity curve

TIC – time intensity curve

Acknowledgements

This work would not have been completed without the support of a number of others. I am immensely grateful to both Reza Razavi and Amedeo Chiribiri, my supervisors. They have provided the opportunity, enabled the planning, and enthusiastically supported the work, while providing vast knowledge and deep insight. They have throughout provided the critical appraisal without which robust scientific work would be impossible. I am especially grateful for the time and tireless effort they have given me. It has been an honour to have been given the opportunity to work in a great department, with its resources and intellectual energy. My time at King's has changed my outlook on a career in medicine and made me truly realize the importance of research in driving progress and providing the best care for patients.

I am humbled by the generous attitude of the patients who participated in the studies and would hope that the output in furthering and improving patient care, has justified their involvement.

I would also like to direct specific thanks to certain individuals within the department. They have given up precious time to teach and provide practical support. In particular I would like to thank Roman Wesolowski, Radomir Chabiniok, Adriana Villa and Liya Asner for their help and guidance. In addition, I would like to extend further thanks to Stephen Sinclair, Jasmine Davies and Lucy Hewett for their help with scanning of the patients.

Finally, I would like to thank my friends and family for their constant understanding of my work commitments and for the strong support network they constantly and uncomplainingly provide. They are a deep source of strength for me and I thank them all for providing compassion, understanding, entertainment and a sympathetic ear. In particular, I wish to thank Pavla and Donald, my parents, as well as Matt, for their guidance and enthusiasm through what has been a period of self-discovery and learning.

1 Introduction / rationale

This PhD project was conducted at King's College London under the supervision of Professor Reza Razavi and Dr Amedeo Chiribiri between January 2012 and August 2015. Both have provided significant help and guidance of this work.

1.1 Rationale

The initial aim of this PhD was to investigate the interplay between cardiac energetics, perfusion and structure / function, particularly in the setting of heart failure and cardiac resynchronization therapy. These factors are intertwined - weight for weight, the heart consumes more energy than any other organ in the body. In the normal heart, the heart beats around 100,000 times over each 24-hour period and pumps around 10 tonnes of blood through the body. This considerable cellular activity is fuelled by ATP, of which some 6kg is produced in 24 hours, 20 – 30 times the weight of the heart[1]. Around 65% of the ATP produced is used to power muscle contraction; the rest is used up in the production and degradation of proteins and other cellular functions[2]. The heart is primarily an aerobic organ which produces ATP in the mitochondria and which relies on a steady, adequate supply of oxygen-rich blood provided by the coronary circulation and mircoarchitecture. This enables the relentless and effective cardiac contraction of normal cardiac function. Each myocyte is particularly adapted to these high-energy demands – mitochondria make up 30% of cell volume. In addition, there is a close physical and functional coupling between the

subcellular components and a dense coronary artery tree. In essence, in the normal heart, a number of highly structured, tightly controlled systems interconnect to produce efficient continuous function.

The scenario of the energy-starved heart is well established in the pathophysiology of heart failure, due both to defects in calcium handling and excitation contraction coupling and to mitochondrial abnormalities; an imbalance between metabolic needs and energy production drives and exacerbates pump failure. The redress of the energy demand–supply balance animates therapies for heart failure; energy-sparing agents such as beta-blockers or ACE inhibitors as well as cardiac resynchronisation therapy yield long term benefit.

This interest led to the development of two projects investigating these factors in the context of dyssynchronous heart failure and cardiac resynchronization therapy (CRT). These would focus on myocardial energetics, using PET and histology, perfusion, using CMR and PET, and remodeling. The first involved a preclinical study in Aarhus, Denmark and the second a clinical study at St Thomas' Hospital, London. Both projects were extensively planned (Home Office small animal licence and granted Ethical approval) though neither came to fruition – Support was withdrawn by the Danish collaborators for the first, and there were substantial delays with tracer production for the second.

The failure to get these projects started was obviously a huge disappointment given the considerable preliminary work. The focus of the work presented is based on background work to develop an understanding, in particular of

perfusion CMR. The body of this thesis focuses first on quantitative perfusion CMR in the setting of CAD and heart failure, and secondly on cardiac diffusion tensor imaging (DTI) and 3D tagging, used to explore the changes in cardiac fibre architecture in dilated cardiomyopathy. This work aims to demonstrate feasibility of these advanced CMR approaches with a view to building on, and exploring, the interplay between the variables of cardiac energetics, perfusion and structure / function.

1.2 Thesis overview

The thesis has been divided into the following eight chapters:

Chapter 1.

Introduction and rationale for the thesis.

Chapter 2.

Summary of coronary physiology, describing normal coronary arterial system and the pathophysiology of ischaemia. Overview of the importance of the assessment of myocardial ischaemia and summary of the work done on the ischaemic cascade which has led to significant changes in practice for the management of patients with stable coronary disease. Description of studies to date on non-invasive assessment of myocardial ischaemia, focusing on those involving CMR.

Chapter 3.

This chapter consists of an overview of quantitative perfusion CMR, detailing current understanding and previous studies to date, including data published as a review article.

Chapter 4.

This chapter describes the use of high-resolution perfusion CMR in a group of patients with ischaemic and non-ischaemic cardiomyopathy and demonstrates feasibility in this cohort.

Chapter 5.

The fourth chapter details results of a large retrospective study examining the impact of quantification of perfusion results on adverse events and prognosis.

Chapter 6.

The fifth chapter describes the use of hybrid PET-MR imaging. The chapter discusses a study comparing quantitative results from PET versus CMR using a specialised dynamic cardiac perfusion phantom and a hybrid PET-MR scanner.

Chapter 7.

This chapter reviews current knowledge of cardiac microstructure and the use of diffusion tensor CMR imaging in its evaluation. The chapter also describes the results of in-vivo dual phase diffusion tensor imaging in patients with dilated non-ischaemic cardiomyopathy.

Chapter 8.

General conclusions.

2 Background

2.1 Introduction

This section includes an overview of coronary physiology and pathophysiology, the importance of myocardial ischaemia and non-invasive assessment of myocardial ischaemia.

As an introduction to the topic, one must consider the normal coronary physiology in order to then understand adaptations to coronary stenoses. An account is given of the sophisticated and specifically adapted physiology of the coronary system providing efficient delivery of oxygen to the myocardium. Alterations in blood flow through the coronary arteries due to a coronary stenosis triggers a cascade of responses to a reduced blood supply to the myocardium and to maintain the demand-supply balance. Once these adaptive processes are exhausted ischaemia and symptoms ensue. This process is exploited in stress perfusion imaging through either vasodilatation or increased oxygen demand.

The ischaemic cascade is described next. This is crucial to the appreciation of the temporal sequence of events, and the importance of ischaemia, in the setting of coronary artery disease and outlines the logic of ischaemia testing now in routine use. In early clinical practice, the application of percutaneous coronary intervention (PCI) was relatively indiscriminate, based solely on the anatomical appearance of a coronary stenosis - it took no account of the presence of ischaemia. Initial studies based on this indiscriminate application suggested that management of stable angina could as effectively be treated medically as by PCI. More recent studies have shown that PCI is beneficial in

cases of documented ischaemia. This remains a controversial and debated topic. The limitations of visual assessment of the extent of an epicardial coronary stenosis in diagnosing ischaemia in the area of supplied myocardium and use of invasive measurements of coronary flow reserve are also discussed.

Finally the strengths and limitations of the three main non-invasive modalities, CMR, PET and SPECT, are discussed, with a focus on CMR and key studies comparing SPECT or PET to CMR.

2.2 Coronary physiology

In order to be able fully to understand the pathophysiology of CAD, it is crucial to consider underlying normal cardiac physiology. The first part of this chapter will focus on the physiology of the coronary system, in particular on vasodilatory capacity and microvasculature resistance, and the adaptations to reduced coronary flow in response to coronary stenosis.

2.2.1 Physiology and pathophysiology of ischaemia

Coronary artery flow is a function of the combined factors of arterial pressure and the resistance in a given coronary artery. The physiology of the coronary circulation is complex and depends on numerous regulatory elements including nervous and metabolic control, mechanical factors including aortic pressure and heart rate, and coronary autoregulation. The difference in flow between rest and maximal vasodilatation is known as the coronary flow reserve (CFR).

It should be noted here that the terms CFR and MPR (myocardial perfusion reserve) are often used interchangeably but have fundamental differences - indeed different normal values have been obtained when using these terms. This can in part be explained by the very nature of CFR and MPR measurements, which are obtained using different techniques and are likely to provide complementary but not identical information on myocardial perfusion status. CFR is the maximum increase in blood flow [ml of blood/min] through the coronary arteries above the normal resting values and is usually measured invasively at the level of the epicardial coronary arteries. MPR is the ratio of global myocardial blood perfusion [ml of blood/g of myocardium/min] at stress versus rest, measured by microspheres or non-invasive imaging at the level of the tissue. CFR measurements represent average blood flow to the perfusion territory distal to the point where the measurements are performed, whereas MPR measurements represent the amount of blood normalized by the mass of tissue in the perfusion territory. Since CFR is obtained with measurements of blood flow in the epicardial coronary arteries, the spatial resolution of CFR measurements corresponds to the perfusion territory downstream the point where the measurements are performed. Invasive CFR measurements do not enable measurements of perfusion specifically in the subendocardium. MPR instead can be analysed with higher spatial resolution than allowed by CFR measurements, with an independent visualisation of multiple layers across the LV wall, which is a factor contributing to the elevated sensitivity of perfusion imaging modalities to the detection of ischaemia compared to invasive assessment. Given these fundamental differences between CFR and MPR, it should not surprise that

the optimal CFR cut-off is higher than the optimal MPR threshold, as CFR represents average perfusion in a larger volume of myocardium.

2.2.2 Coronary arterial system

An understanding of the anatomy and physiology of the coronary circulation is crucial to analysis of the mechanisms of ischaemia at play in CAD.

Average myocardial blood flow is calculated as the perfusion pressure (pressure difference between the ostium of left main coronary artery and coronary sinus) divided by the total coronary resistance:

$$Myocardial\ blood\ flow = \frac{Perfusion\ pressure}{Total\ coronary\ resistance}$$

In exploring this relationship, one must first consider the three functional sequential elements of the coronary arterial system: the epicardial coronary vessels, pre-arterioles and intramural arterioles. Of the three elements, only the epicardial vessels are of a calibre that can be imaged by coronary angiography.

2.2.3 Components of coronary microvasculature

The pre-arterioles and arterioles together form the microvasculature (Figure 2.1). Each section of the coronary vasculature has a specific role.There are no differing, identifying, histological features [3,4].

- The epicardial / conductive vessels (ranging in size from few millimetres to 500μm in diameter) form the largest and most proximal component. They have a capacitance function and offer little resistance to coronary blood flow when the epicardial arteries are free of CAD. During systole, these vessels dilate and increase their blood content by up to 25%. In diastole, this elastic energy is released and blood is propelled on into the distal vessel. They are responsive to flow-dependent dilatation – they respond to endothelial vasodilators released in response to changes in shear stress.
- The pre-arterioles (diameter 500-100μm) form the intermediate component, characterised by being largely extra-myocardial with a measurable pressure drop along their length. The distal pre-arterioles are the main performers of autoregulation – constricting and dilating to maintain stable blood flow despite fluctuations in perfusion pressure. Proximal pre-arterioles are responsive to flow-dependant dilatation; distal pre-arterioles are more responsive to changes in intravascular pressure. Their extra-myocardial course makes them not susceptible to diffusible metabolic metabolites.
- The intra-mural arterioles (diameter <100μm) comprise the distal component and are characterised by an even greater pressure drop along their length. Their function is to match myocardial blood supply to oxygen consumption. The arterioles play a fundamental role in the metabolic regulation of coronary blood flow. They have a high resting tone and dilate in response to the release of metabolites from the myocardium consequent on increased oxygen consumption.

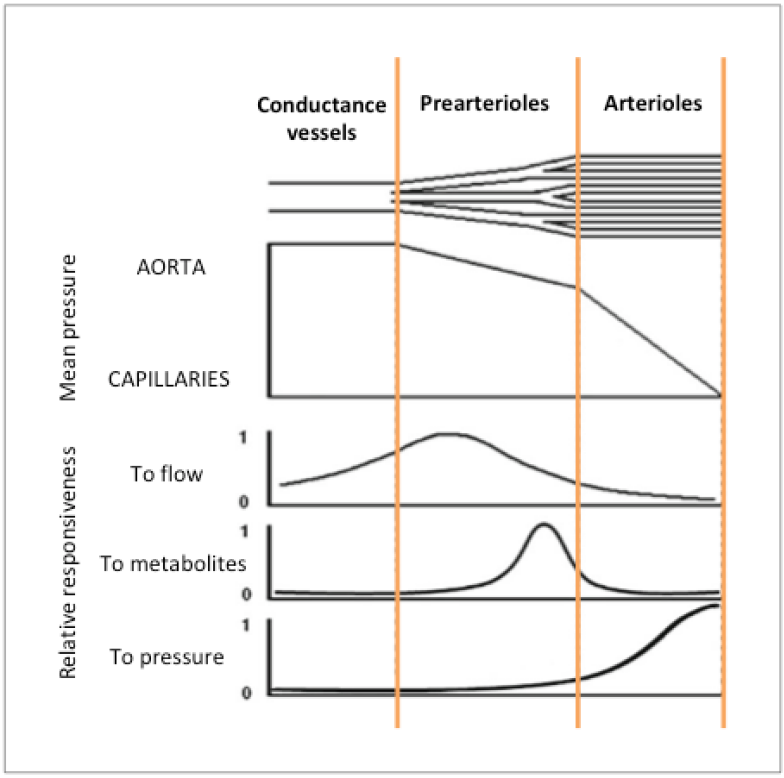

Figure 2.1 – Functional subdivision of the coronary arterial system

Schematic showing the three functional components of the coronary arterial system and their relative effects to blood flow, metabolites and pressure. ***Adapted from Camici et al.***[4]

2.2.4 Coronary resistance

Total myocardial blood flow is related to both the perfusion pressure and the total coronary resistance.

Total coronary resistance is the sum of three components: R1, R2 and R3 (see Figure 2.2).

- R1 – represents the resistance in the epicardial vessels. This contributes approximately 10% of total coronary resistance in normal

arteries. R1 may become the limiting resistance in the setting of significant CAD.

- R2 – This refers to the main resistive component and occurs at the level of the microvasculature. In basal healthy state, resistance in the pre-arterioles makes up approximately 30%, and in the arterioles 40% of total coronary resistance. When R1 rises in the setting of significant CAD, R2 will compensate, increasing vasodilatation to maintain flow to the distal myocardium.

- R3 – Unlike R1 and R2, R3 resistance is extravascular and is due to the compressive force from the myocardium during systole. During systole coronary artery flow is impeded or even reversed and venous outflow is segmented. For this reason it will vary through the cardiac cycle, and will affect the intramural components of the left coronary arterial system more than it does the right (the RV has lower pressure than LV). Furthermore, the pressure is uneven through the myocardial wall. It is highest in the subendocardium due to increased intra-cavity LV pressure and higher myocardial inotropic force at this site, causing higher intramyocardial compression, which in turn produces more severe vascular narrowing to the vessels in their course through the myocardium from subepicardium to subendocardium [5-9].

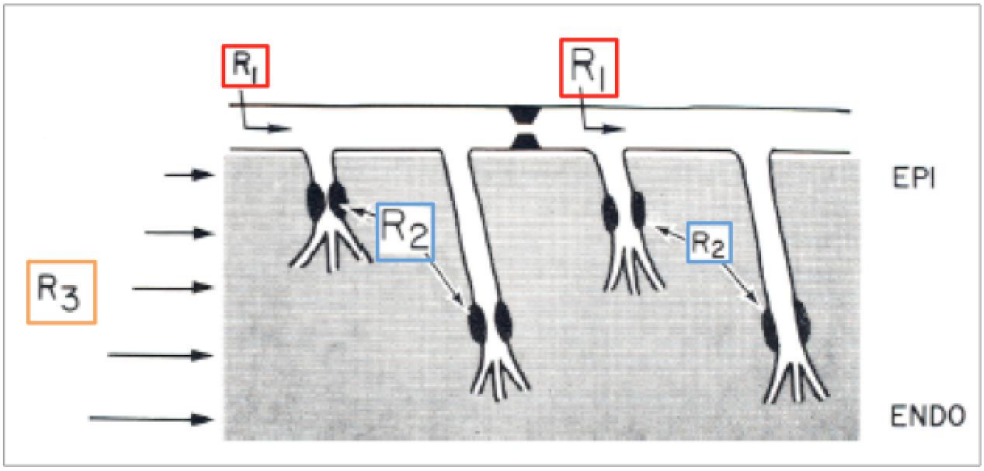

Figure 2.2 - Schematic diagram showing coronary arterial system

Left side showing the normal situation where a majority of resistance is found in the arterioles. The right side illustrates the reduction in R2 in the presence of a significant epicardial stenosis causing a rise in R1. Note the increase in R3 resistance from subepicardium to subendocardium.
***Adapted from Amedeo Chiribiri*[10].**

The third component of resistance, R3 deserves further mention. Although this site contributes the highest resistance, animal studies have shown that resting flow to the subendocardium is normally highest in this section. This is due to higher wall stress and greater oxygen demand. These factors help to explain why the subendocardium is affected first, and more severely affected in CAD, when R1 resistance is increased and R2 is maximally vasodilated.

Even in healthy hearts, there is a phasic coronary perfusion which rises in diastole and decreases in systole due to the variation of compressive forces. Despite the fluctuation, in the absence of significant CAD or small vessel disease, this does not cause subendocardial ischaemia. Similarly, in cases of tachycardia, where the diastolic component of the cardiac cycle is shortened, R3 is a factor and the subendocardium will be most affected. In the healthy heart, other resistive components will compensate for this. In tachycardia on a

background of significant epicardial stenosis, where resistive forces are already at maximal compensation, regional myocardial ischaemia may result[11,12].

2.2.5 Coronary flow reserve and CAD stenosis severity

Various studies have shown that it is not possible to use CFR at rest to assess the severity of a stenosis since compensatory vasodilation of the pre-arteriolar and arteriolar compartments are sufficient to compensate for the increase in epicardial R1 resistance[13,14].

Gould et al. used a preclinical model to measure coronary flow responses to progressive coronary artery stenosis using surgically implanted electromagnetic flow meters and comparing this to fluoroscopic images of the degree of stenosis. The group were able to demonstrate that with an increase in percentage diameter stenosis, there is a decrease in maximal coronary flow during vasodilatation[14] but that even with severe stenosis, coronary flow was relatively maintained at rest. Importantly, this group demonstrated that with moderate (50-70%) lesions, there was both a high individual variability and a relatively preserved CFR even with vasodilatation. This work elegantly demonstrates that a visually moderate stenosis may not correlate with a haemodynamically significant lesion. With more severe stenosis the CFR is significantly reduced with less variability. This is demonstrated in Figure 2.3.

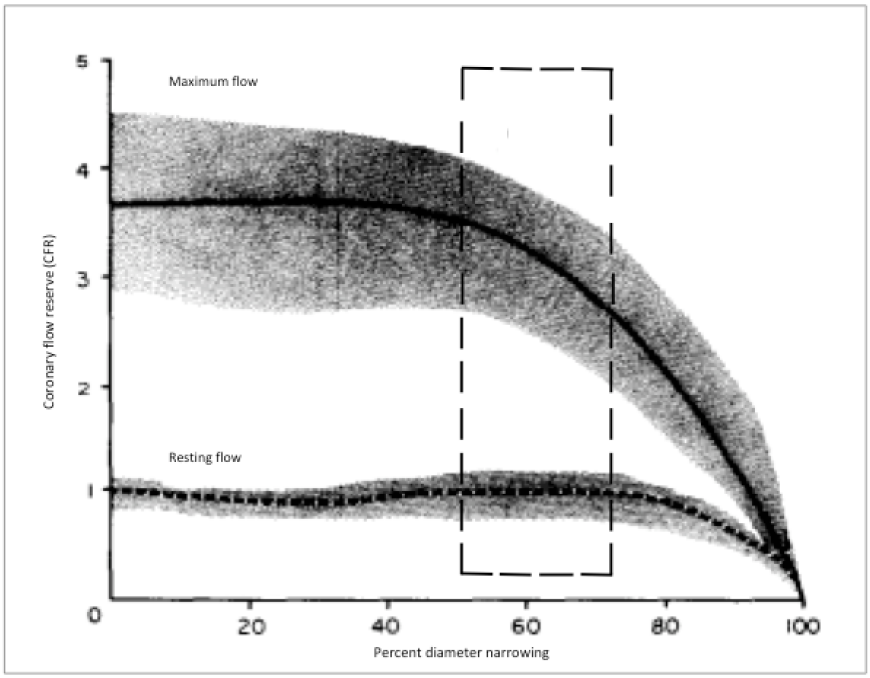

Figure 2.3 – Coronary flow reserve related to angiographic narrowing in animals

Coronary flow reserve in relation to angiographic percent narrowing of the LAD in an experimental dog model. An increase in percentage stenosis leads to decreased CFR during maximal hyperaemia. The grey region shows 95% confidence interval. Note (dotted line) that the CFR is relatively preserved in moderate stenosis.
Adapted from Gould et al.[14]

Although large animal models reflect human anatomy and physiology better than small animal experimental models, concerns have been raised with regard to differences in coronary physiology. Later studies considered the degree of stenosis and CFR in patients with CAD using PET, using either percentage narrowing from angiography or quantitative angiography[15-21].

The largest of these studies included 193 patients with previous MI and compared quantitative coronary angiography versus visual assessment of perfusion defects using PET (see Figure 2.4)[15]. The study found good correlation between coronary angiography and PET to identify areas of myocardial infarction. With increasing degrees of coronary stenosis, the PET

defect score increased with a high PET defect score being highly predictive of a severe stenosis. They also noted that there was considerable scatter of correlation, particularly in the moderate coronary stenosis range. It was postulated that this may relate to serial stenoses, collateralization, anatomical variations, visual assessment of PET imaging, inter-observer variability, and differing physiological conditions between the studies.

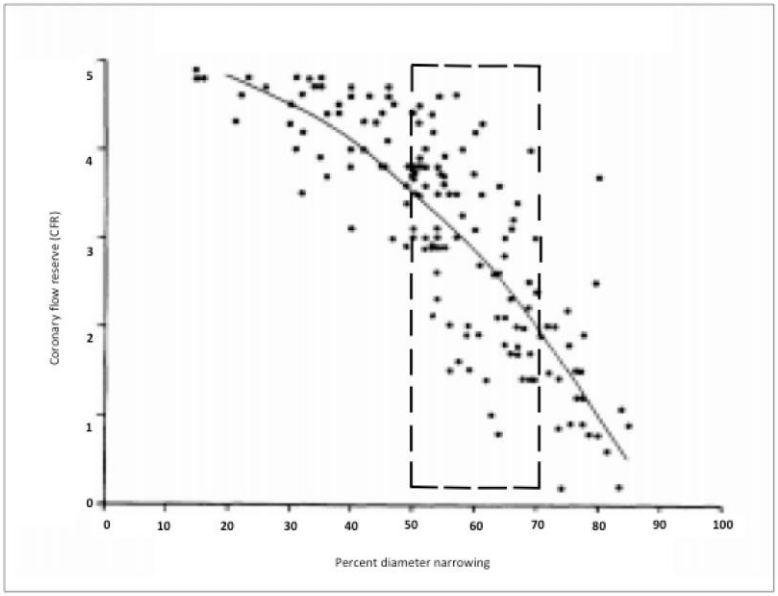

Figure 2.4 - Coronary flow reserve against percentage coronary stenosis in patients

Progressive decline in CFR with increasing severity of stenosis. Note the wide spread of data points in the moderate CAD range (dotted box).
Adapted from Demer et al.[15]

2.2.6 Myocardial energetics and the microvasculature

The heart has to sustain relentless contractile function as well as basal metabolic processes and ionic homeostasis and every day produces 6kg ATP (more than 20-30 times its own weight). There is a small ATP reserve in the

heart and due to the high turnover, the heart cycles through the entire myocardial ATP pool approximately six to eight times per minute.

The healthy adult heart is essentially an aerobic organ which produces 95% of its ATP via the tricarboxylic (TCA) cycle through oxidative phosphorylation[1]. It is consequently highly reliant on an efficient oxygen-rich blood supply – a number of adaptations help to achieve this.

The heart is adapted for aerobic metabolism with an increased number of mitochondria and the ability to use various substrates in the TCA cycle.

Since there is near maximal extraction of oxygen at rest, it is an increase in blood flow which is the variable in response to higher oxygen demand. At rest, oxygen extraction between the coronary artery and the coronary sinus is near maximal level (70-80% in contrast to 30-40% in skeletal muscle). During exercise, the myocardial oxygen consumption can increase fourfold[11,12].

At rest, myocardial blood flow is already greater than exercising skeletal muscle, underlining the need for an efficient and specialised system. The blood flow through the various components of the coronary system is closely coordinated with supply demands. In addition to the increased flow secondary to vasodilatation, cardiac muscle is endowed with a higher density of microvasculature than is skeletal muscle. Histological studies confirm that while the density of capillaries per mm^2 in peripheral muscle cells is 300-400, in the myocardium, there are 3000-4000 capillaries per mm^2 surrounding muscle fibres of relatively smaller diameter[22-24].

2.2.7 The microvasculature in ischaemia

It follows from the above that the haemodynamic implications of epicardial coronary artery stenosis largely depend on the microvasculature. The arterioles distal to a stenosis will vasodilate at rest in order to match supply to demand – this may also involve an element of steal from neighbouring vessels via collaterals. In hyperaemic / stress conditions, the arterioles distal to vessels without a stenosis will vasodilate to increase blood flow, whereas those distal to a stenosed vessel will already be at near maximal dilatation. This produces a relative imbalance in coronary flow reserve, the difference between stress (hyperaemic) blood flow, and resting blood flow. Increased oxygen demand leads to ischaemia in the area supplied by the stenosed vessel. In the presence of further increased oxygen demand the area supplied by the stenosed vessel will become more ischaemic. In this situation the contribution of previous 'steal' is diverted back to origin i.e. is not available to the ischaemic territory, further diminishing available flow to this area (see Figure 2.5).

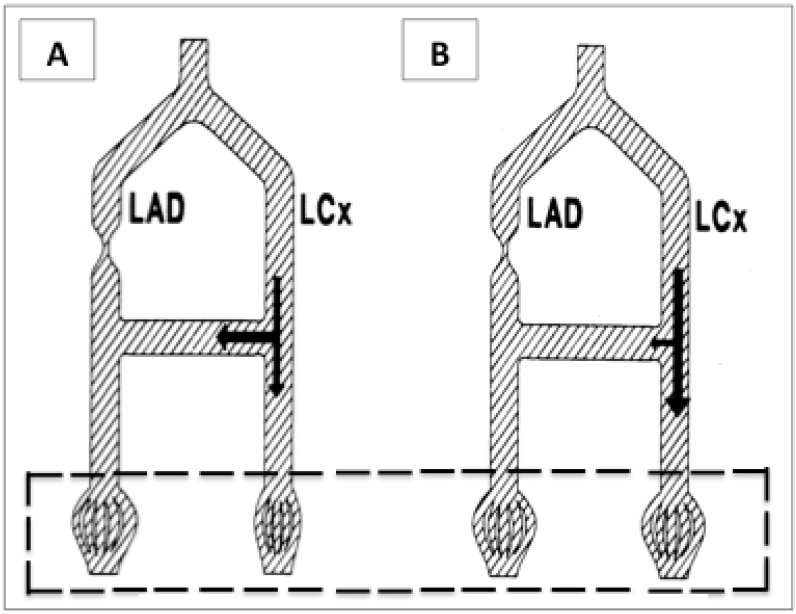

Figure 2.5 - Schematic representation to describe steal phenomenon in the presence of coronary stenosis during hyperaemia.

A - LAD artery has a stenosis, distal microvasculature vasodilates (see dotted line) and via collaterals draws blood from CX territory to maintain adequate perfusion at rest.
B- Under hyperaemia, vasodilatation of the Cx microvasculature draws more blood into the Cx territory (see dotted line). The LAD microvasculature is already at near- or maximal vasodilatation and therefore ischaemia likely to occur in this territory.
(LAD- left anterior descending artery, LCx – circumflex artery)
Adapted from Demer, et al.[15]

This sequence process explains the symptoms described by patients with stable angina. Typically this patient will report no symptoms at rest but exertion increases myocardial oxygen demand and produce symptoms of chest pain, which worsens with ongoing exertion, easing with rest.

2.3 The clinical relevance of myocardial ischaemia

Despite advances in the prevention, detection and treatment of coronary artery disease (CAD), myocardial infarction (MI) and ischaemic cardiomyopathy, coronary heart disease remains a leading cause of morbidity and mortality in developed countries. The death rate has declined due to improved treatments and an ageing population. The number of patients living with stable angina and heart failure continues to increase.

Myocardial ischaemia is at the centre of this cardiovascular mortality and has been the subject of investigation by numerous groups over several decades.

2.3.1 The ischaemic cascade

The concept of the ischaemic cascade refers to the sequence of events whereby ischaemia is triggered by an imbalance between oxygen supply and demand. This leads to impaired diastolic then systolic dysfunction, ECG changes and culminates in anginal chest pain and potentially myocardial infarction. This cascade is key to understanding the approach to stable coronary artery disease[27].

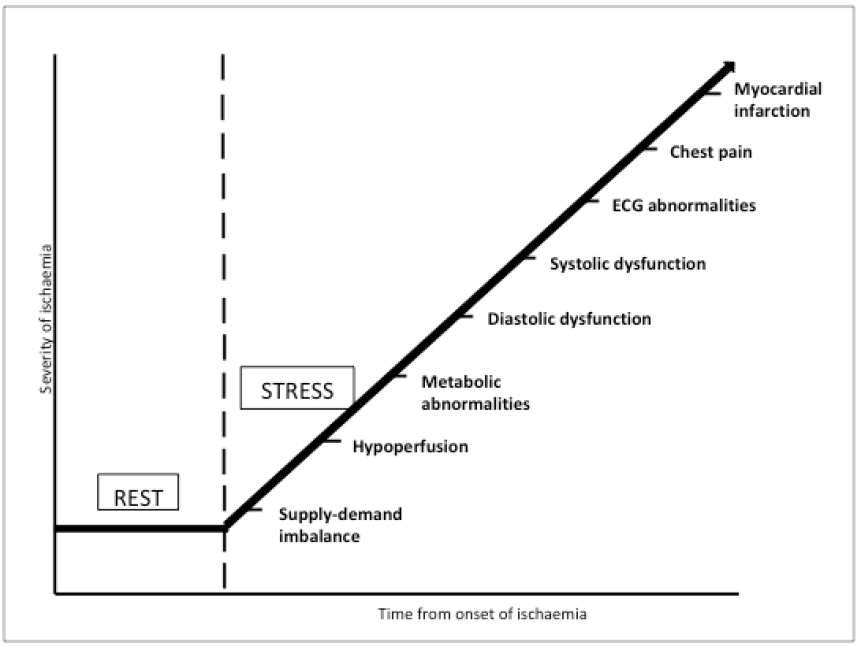

Figure 2.6 – Schematic representation of the ischaemic cascade

Figure demonstrating the temporal dispersion of events in the ischaemic cascade. ***Adapted from Nesto et al.*** [27]

The majority of early studies investigated animal or human models of coronary occlusion, namely 'supply ischaemia' by means of invasive epicardial coronary artery balloon occlusion assessed in terms of the changes in cardiac compliance (diastolic function) and contractility (systolic function) using echocardiography, invasive haemodynamic measures and ECG tracing. These studies demonstrated the temporal distribution of events and showed that typical symptoms of angina did not occur universally. These observations proposed that identification of events before the onset of chest pain and appreciation of changes seen with ischaemia-reperfusion could relate to cardiac function[25-28].

Later studies used atrial pacing tachycardia or exercise, where the myocardial demand for oxygen is increased, to demonstrate the same temporal sequence of events in 'demand ischaemia'[29-32]. Once again, the presence of anginal chest pain was found to be an insensitive and unreliable marker of the presence of ischaemia when correlated with the other events noted in the cascade.

In subsequent years, and with the development of nuclear imaging techniques and the use of dobutamine echocardiography for perfusion, investigators were able to start to identify specific, discrete, regions of hypoperfusion and link these directly to the other changes described in the ischaemic cascade – previously only implied by other studies – and demonstrated that hypoperfusion occurred earlier in the cascade and was a more sensitive marker than the development of regional wall motion abnormalities[29-37].

2.3.2 STEMI and unstable coronary syndromes

The term 'coronary artery disease' encompasses a group of conditions which include ST-elevation myocardial infarction (STEMI), unstable acute coronary syndromes (non-ST elevation myocardial infarction (NSTEMI) and unstable angina) and stable angina. The use of revascularisation procedures and medical therapy varies, depending upon which condition predominates.

In patients with STEMI, where there is acute complete occlusion of a coronary artery, timely reperfusion is key. A number of studies have shown that timely percutaneous coronary intervention (PCI) provides management superior to that of the alternative strategy of thrombolysis and leads to reduced infarct size, preservation of left ventricular function and reduced incidence of

morbidity and death[38-46]. Similarly, in acute coronary syndromes, an invasive approach is generally favoured over medical therapy. This remains a debated topic[47-53].

2.3.3 Stable angina

The use of early revascularisation in place of medical therapy has been clearly shown to be beneficial in cases of STEMI and in several studies looking at unstable coronary syndromes and angiography is embedded in current standard National Institute for Clinical Excellence (NICE), European Society of Cardiology (ESC) and American heart association (AHA) clinical care guidelines. In the setting of stable angina, guidelines advocate revascularisation only in patients who remain symptomatic after optimisation of medical therapy, lifestyle intervention and risk factor modification. Nevertheless, percutaneous coronary intervention (PCI) continues to be frequently performed in patients with stable angina referred for coronary angiography. This continues to be a heavily debated issue and one which has been controversial for some years with contradictory evidence for either revascularisation or optimised medical therapy in these patients. The key studies will be presented here.

2.3.4 Key studies demonstrating importance of the presence of ischaemia

The Asymptomatic Cardiac Ischaemia Pilot Study randomised patients with stable angina and coronary anatomy suitable for revascularisation, into one of three treatment strategies: angina-guided drug therapy (183 patients), angina plus ischaemia-guided therapy (183 patients), or revascularisation by PCI or

CABG (192 patients)[54]. It was demonstrated that the lowest mortality at two years was recorded in the revascularisation group (1.1%), followed by the ischaemia-guided group (4.4%) and the angina-guided group (6.6%), with corresponding proportions for death, MI or recurrent cardiac hospitalisation, as shown in Figure 2.7.

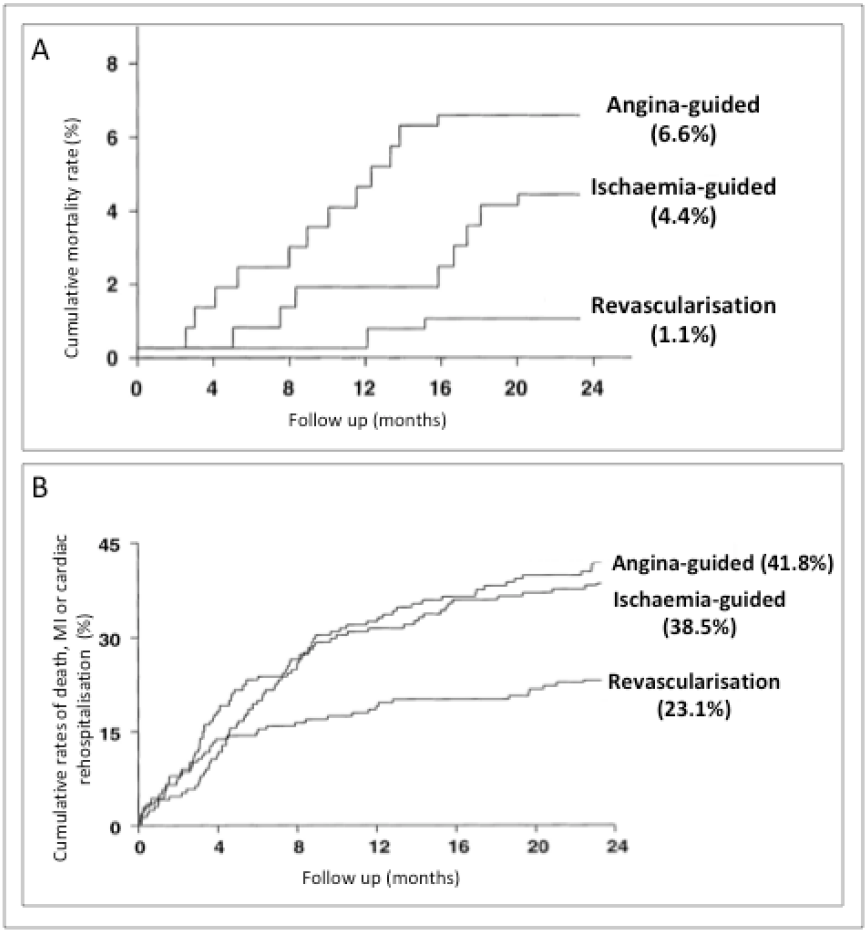

Figure 2.7 - Outcomes - ACIP study

A – Two-year cumulative mortality rates for three treatment strategies
B- Two year cumulative rates of death, MI or cardiac rehospitalisation for three treatment strategies
The lowest mortality at two years was recorded in the revascularisation group, followed by the ischaemia-guided group and finally the angina-guided group.
Adapted from ACIP study[54]

It is important to note that the eligibility criteria for the ACIP study included only patients with evidence of inducible ischaemia during pharmacological or exercise stress and at least one episode of asymptomatic ischaemia on ambulatory ECG. Furthermore, during the study period medication was uptitrated according to clinical evidence of ischaemia suggesting that the benefit of revascularisation could be linked to the presence of ischaemia, a theme which will become more apparent as further studies are described.

A meta-analysis conducted around the same time by Katritis et al. which included the work by Davies et al, pooled the results of 11 randomised studies, comprising 1476 patients who received PCI and 1474 patients who received medical therapy for CAD[55]. This, in contrast, concluded that overall there was no significant difference between the treatment strategies with regard to mortality, cardiac death, myocardial infarction (MI) or revascularisation rates during follow up. A possible survival benefit was seen only in patients who had recently had an MI. However, it must be noted that the studies included were heterogenous with regard to inclusion and exclusion criteria and methodology and therefore it may be difficult to draw a reliable conclusion from this data.

The SWISS-II trial prospectively studied patients with recent STEMI or NSTEMI, one- or two-vessel CAD and ischaemia on stress imaging and investigated the merits of revascularisation (with balloon angioplasty) versus medical therapy[56]. This concluded that at 10 years post follow-up, revascularisation (96 patients versus 105 patients on optimal medical therapy)

resulted in a reduction of death, non-fatal MI and symptom-driven revascularisation, as well as long term preservation of cardiac function. The benefit was apparent at the 2-year point and survival curves were seen to diverge continuously during follow up. Once again, this supported the use of revascularisation where there was objective evidence of ischaemia.

The Clinical Outcomes Utilitizing Revascularisation and Aggressive Drug Evaluation (COURAGE) trial was the first large multi-centre study specifically designed to compare optimal medical therapy plus PCI with optimal medical therapy alone in patients with stable coronary artery disease[57]. 2287 patients were randomly assigned to undergo either PCI and medical therapy or medical therapy alone with a median follow up of 4.6 years. The primary finding of this study was that the cumulative primary event rate was similar in the two groups with no clear benefit conferred by PCI (p=0.62). Specifically, there were no significant differences for the composite endpoint of death, myocardial infarction and stroke, and for hospitalisation due to acute coronary syndromes or MI (see Figure 2.8). Furthermore, sub-analysis of even the more severely narrowed coronary stenoses, showed that PCI was still not effective in reducing rate of death or MI.

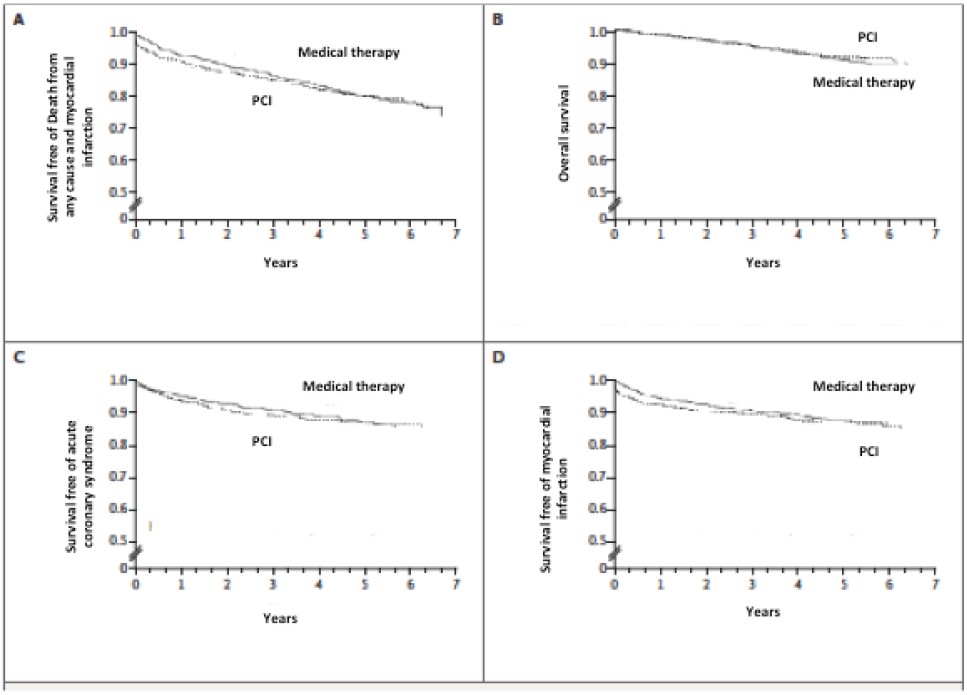

Figure 2.8 – Outcomes - COURAGE sub study

A- Estimated 4.6 year rate of composite primary outcome of death from any cause and non-fatal MI (19.0% PCI group, 18.5% medical therapy group),
B- Estimated 4.6 year rate of death from any cause (7.6% PCI group, 8.3% medical therapy group),
C- Estimated 4.6 year rate of hospitalisation for acute coronary syndrome (ACS) (12.4% PCI group, 11.8% in medical therapy group),
D- Estimated 4.6 year rate of acute myocardial infarction (13.2% PCI group, 12.3% medical therapy group).
No survival difference was observed between medical or revascularisation therapy.
Adapted from COURAGE study[57]

There was a substantial reduction in the prevalence of angina in both groups during follow up. Rates of freedom from angina were in favour of the PCI group throughout most of the study period but at 5 years this difference was non-significant.

This was an important study whose outcome was somewhat surprising. Interpretation must take into account the exclusion of patients with severe angina or marked ischaemic changes on initial screening exercise test. It

could therefore be argued that this may have excluded patients in whom the addition of PCI could have been beneficial.

2.3.5 Ischaemic burden in stable coronary artery disease

Over the same period the use of ischaemia testing was increasingly advocated on the basis of earlier studies facilitating a growing understanding of its impact on clinical outcomes. The simple presence or absence of a perfusion defect demonstrated by any imaging modality technique has been shown to be relevant to prognosis[58-61]. However, in more recent years, this has been refined to consideration of the relevance of the ischaemic burden. This was considered in two important studies which will be discussed below. These demonstrated that, while the presence of significant ischaemia was relevant, severity and extent of ischaemic myocardium was also relevant.

2.3.6 Key studies demonstrating the importance of ischaemic burden

A study by Hachamovitch et al. set out to assess the relationship between the amount of inducible ischaemia and survival benefit achieved with medical therapy versus that achieved by revascularisation[62]. This large retrospective observational study included 10,627 patients with no previous MI or revascularisation, who underwent exercise or adenosine single photon emission computed tomography (SPECT) to detect inducible ischaemia and then went on to be revascularised or receive medical therapy. These patients were divided into two groups: those receiving either medical therapy (9956 patients) or revascularisation (671 patients; CABG 325 patients, PCI 346 patients). All included patients were within 60 days of the SPECT study with a

relatively short follow up period (1.9 +-0.6 years). The study noted that patients sent for revascularisation had a greater burden of cardiovascular risk factors and this is a bias inherent to the observational nature of the study. The key finding was that, albeit with a relatively short term follow up, patients without inducible ischaemia treated medically had a very low risk of adverse events but that with increasing degrees of inducible ischaemia, the mortality rate increased in patients treated medically. As shown in Figure 2.9 and Figure 2.10 below, this study demonstrated a survival advantage with revascularisation over medical therapy in those with an ischaemic burden of >12.5%, with medical therapy being favoured below this threshold. There was significant benefit of revascularisation over medical therapy in those with >20% ischaemic myocardium.

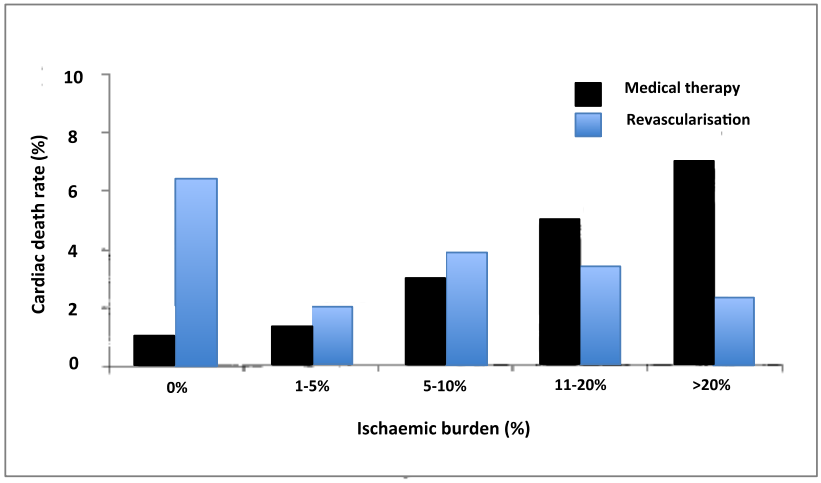

Figure 2.9 – Cardiac death according to ischaemic burden

Observed cardiac death rates over the follow up period in patients undergoing revascularisation versus medical therapy as a function of the amount of inducible ischaemia.
In those with ischaemic myocardium of 10% or more there was a significant benefit of revascularisation over medical therapy >20%.
Adapted from Hachamovitch et al.[62]

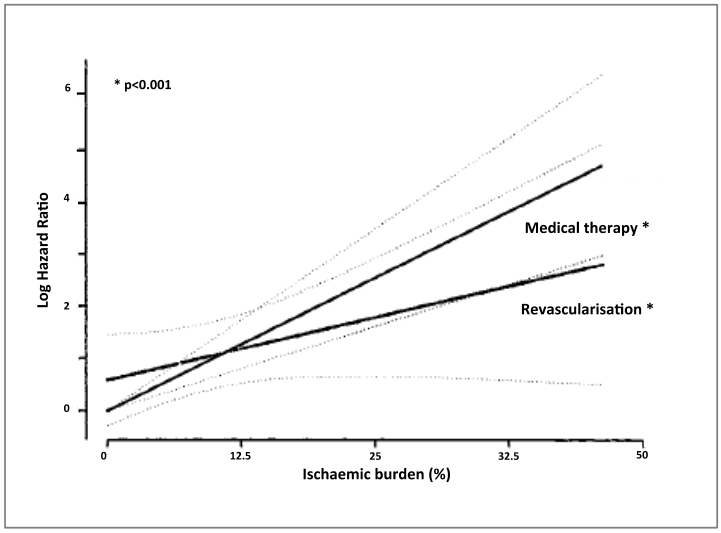

Figure 2.10 - Log hazard ratio according to ischaemic burden

Log hazard ratio for revascularisation versus medical therapy as a function of percentage ischaemic myocardium based on a Cox proportional hazard model. There was a survival advantage of patients with no or little inducible ischaemia with medical treatment. This was lost at a threshold of 10-12.5% ischaemic myocardium, above which the survival benefit favoured revascularisation.
Adapted from Hachamovitch et al.[62]

The relevance of ischaemic burden in guiding management of patients with stable CAD was further elaborated by the results of a substudy of the COURAGE trial[63]. This reported data on a subset of 314 patients of the main COURAGE trial who underwent SPECT at baseline and at 6-18 months follow-up. Substudy entry criteria included patients with at least one epicardial coronary artery stenosis of >70%. Importantly, on subanalysis of the patient characteristcs of the nuclear substudy population, the enrolled patients reported less severe angina than did the main cohort. The pre-treatment percentage of ischaemic myocardium was similar in those randomised to each group, with a similar number (about a third) of patients with moderate to severe baseline ischaemia burden assigned to either PCI or medical therapy alone. Patients who achieved a significant reduction of

ischaemia in response to medical therapy were less likely to crossover to PCI from the medical group (in contrast, 21% patients crossed over from the medical therapy group to have PCI and of these 80% had exhibited no significant reduction in ischaemic burden), or undergo repeated PCI from the PCI group (whereas 15% patients randomised to PCI had repeat revascularisation of whom 75% had exhibited no significant ischaemia reduction). The addition of PCI to medical therapy was more effective in producing a measureable reduction of ischaemia at follow up scan (33% & 19% respectively, $p<0.0001$). The unadjusted rate of death or non-fatal MI for patients exhibiting significant reduction in ischaemia with either treatment strategy was 13.4% compared to 24.7% of patients for those without significant ischaemia reduction. The unadjusted event-free survival improved regardless of the original randomisation group or treatment received (see Figure 2.11). This was measured by a reduction in the absolute amount of ischaemia by at least 5%, This clearly demonstrated that a reduction in ischaemia of >5%, especially in those with more severe baseline ischaemia resulted in fewer adverse events - the 5% cut-off was identified on the basis of previous observational studies[64,65].

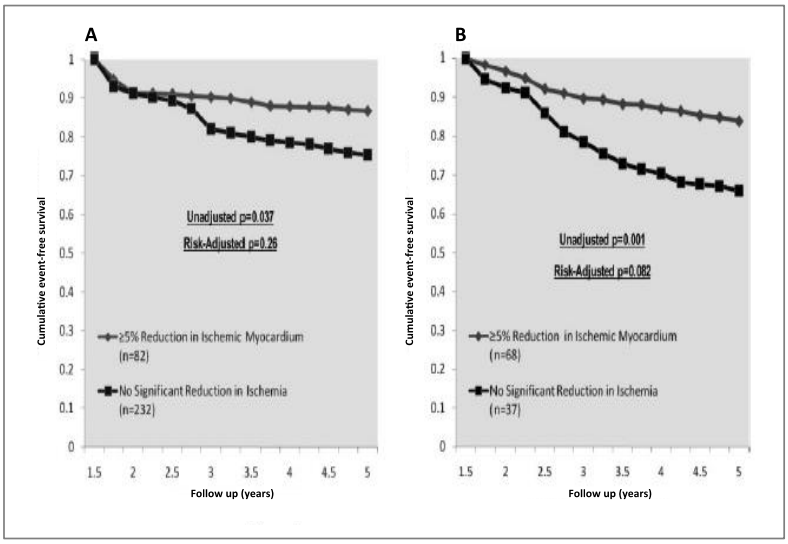

Figure 2.11 – Survival curves (COURAGE substudy)

Kaplan Meier curves for event free-survival according to reduction in ischaemic burden >5% at follow up for patients in either treatment group.

A – showing survival for patients with >5% reduction in ischaemia at follow up

B - showing K-M survival for patients with >5% reduction in ischaemia when baseline ischaemic burden was moderate or severe

Survival was improved in those who demonstrated >5% reduction in ischaemia, particularly if moderate-severe ischaemia was present at baseline.

Adapted from COURAGE substudy[63]

In summary, this reinforced the views of those proposing revascularisation as the superior treatment arm by demonstrating that PCI was more effective at reducing ischaemic burden and that a significant reduction in ischaemia with either treatment resulted in fewer adverse events. Despite being underpowered to specifically investigate differences in clinical outcome according to change in ischaemic burden, the COURAGE substudy would for many years stimulate investigation into the importance of using ischaemia as a guide to revascularisation.

Despite this, many have been critical of the COURAGE study design and findings and this has remained a debated topic.

The recent ORBITA trial, published in 2017, is also relevant to this same issue[66]. The study aimed to evaluate whether there was a placebo effect of PCI and again compare PCI to medical therapy in stable CAD. It identified 230 patients with symptoms of stable angina and a single severe (>70%) coronary stenosis. Patients were initially given several weeks of optimal medical therapy then randomized to either complete revascularistion with PCI (guided by FFR at the discretion of the operator) or a sham procedure where patients underwent FFR only and further medical therapy. There was no demonstrable increase in exercise time increment or peak VO2 between groups, and no deaths in either group over the follow up period of 6 weeks. This study is particularly interesting as it is the first placebo controlled PCI trial, using contemporary medication and PCI techniques and again challenges the premise that PCI provides benefit over medical therapy.

The ISCHEMIA trial[67] is currently in recruitment stage and its findings eagerly awaited. This is a large multi-centre study which will again compare PCI and medical therapy. In contrast to the COURAGE study, the ISCHEMIA patients will be enrolled on the entry criterion of moderate to severe ischaemia .

2.3.7 Invasive assessment of myocardial ischaemia

As studies drew attention to the importance of myocardial ischaemia as an index and other studies seemed to suggest that revascularisation in the absence of ischaemia may not be of benefit, it became clearer that visual assessment of angiography may be insufficient. It was postulated that some

lesions may not be haemodynamically significant nor flow-limiting despite appearing moderately to severely narrowed. Alternatively the simple explanation could be that angiography is a two-dimensional imaging modality and therefore difficult to judge visually. It became apparent that even quantitative analysis of angiography in terms of percentage narrowing could be flawed as the result of collateralisation of vessels and changes in vasomotor tone, or by the absence of a reference diameter in those with diffuse disease which could make the use of luminal assessment alone potentially misleading. In clinical practice, the issue is further complicated by the presence of complex CAD such as multi-vessel disease, previous coronary artery bypass grafting and reduced left ventricular function. In parallel there is a growing appreciation that, setting aside issues of cost, the risks inherent to PCI including stent thrombosis or peri-procedural MI and stroke which, despite the advent of newer drug-eluting stents, are not negligible[68,69]. These factors discourage the use of unnecessary PCI.

Although studies had suggested that intervention should be guided by the presence of myocardial ischaemia, the widespread availability of advanced non-invasive imaging techniques to assess myocardial ischaemia was limited until relatively recently. In consequence, interventional cardiologists developed more sophisticated invasive techniques and the ability to assess flow in each coronary artery directly during coronary angiography.

Fractional flow reserve (FFR) is achieved with a microscopic transducer mounted on a wire which can be placed in a coronary artery and, under maximal hyperaemia, measures the relationship between the flow proximal

and distal to a narrowing. The FFR compares the pressure distal and proximal to a stenosis and is expressed as a fraction of the proximal pressure. A normal value is therefore 1.0, with lower values indicating a degrees of stenosis. There is no absolute value that establishes a threshold for significance however most studies have used a cut-off of 0.75 to 0.80. Collateralisation of a vessel may mean that a visually severe lesion is non-significant since adequate blood flow is delivered to the relevant portion of myocardium; FFR is able to take this into account. It should be noted that small vessel disease, diffuse coronary artery disease, exercise induced vasospasm or left ventricular hypertrophy may underestimate FFR value[70].

A number of studies have investigated the use of FFR in comparison to other measures in guiding intervention[71-74].

One such study investigated 45 patients with moderate coronary artery lesions and atypical chest pain and compared results of exercise testing, thallium SPECT, dobutamine stress echocardiography and quantitative coronary angiography with FFR measurements[75]. There was no significant difference in minimal luminal diameter or percentage of the stenosis in the FFR >0.75 and <0.75 groups. In all 21 patients with an FFR <0.75, reversible myocardial ischaemia was demonstrated on at least one non-invasive test. All but one patient with an FFR <0.75 underwent revascularisation and repeat non-invasive tests were subsequently negative for reversible ischaemia. In contrast, in 21 of the 24 patients with an FFR measurement of >0.75 or higher, all tests for reversible ischaemia were negative. These patients did not undergo revascularisation and were followed for a period of 14±5 months

during which no ischaemic events were noted. This study was important in supporting the use of FFR in patients where chest pain was not typical and where angiographic findings could be considered equivocal.

2.3.8 Key studies investigating FFR to guide revascularisation

Two key studies, DEFER[76] and Fractional Flow Reserve versus Angiography for Multi-vessel Evaluation (FAME) [77-79], assessed the use of FFR versus visual assessment alone to guide PCI in patients with single and multi-vessel coronary artery disease.

DEFER was an international, multicentre prospective randomised study which enrolled 325 patients with stable angina and a visually measured stenosis of >50% in a native vessel measuring >2.5mm in diameter, with no evidence of reversible ischaemia documented by another test in the preceding two months[76]. Patients were either randomised to deferral (167 patients) or performance (158 patients) of PCI (see Figure 2.12) and were followed up for 5 years.

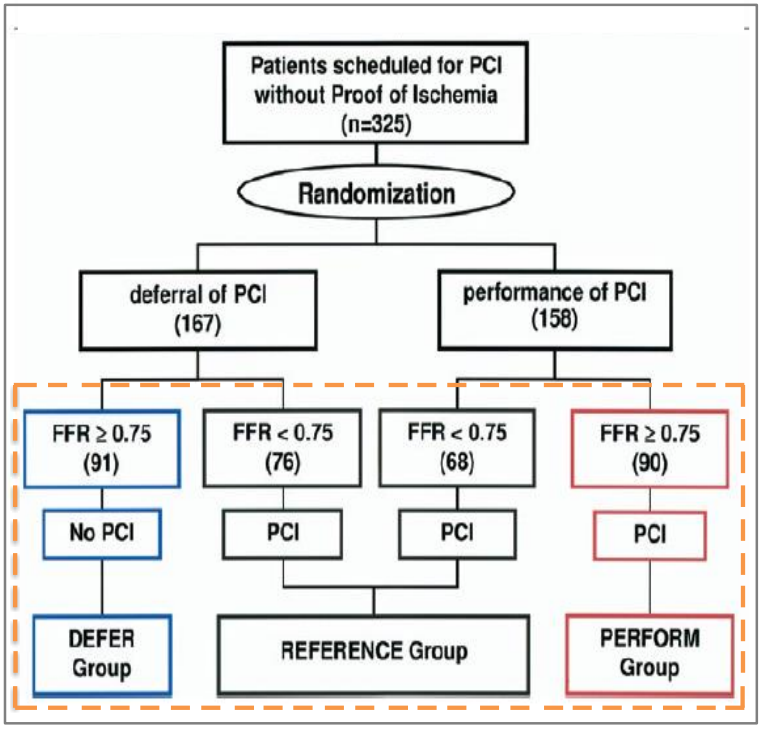

Figure 2.12 – DEFER study flowchart

Study design, randomisation and definition of the three groups (dotted orange line).

Adapted from DEFER study[76]

In order to minimise bias, patients were randomised to deferral or performance of PCI once enrolled, and before any physiological measurement. All patients then underwent FFR measurement. If this was below 0.75, randomisation was ignored and patients received PCI to that vessel (Reference group, 144 patients). Those remaining with an FFR above 0.75 either received no PCI (Defer group, 91 patients) or PCI (Perform group, 90 patients). Baseline characteristics were similar between the two groups. Follow up was performed at 1, 3, 6, 12, 24 and 60 months.

The average FFR measurement in the Reference group was 0.57+/-0.16, with a smaller average percentage diameter of stenosis but with too much overlap between groups to serve as a useful predictor. The stenosis severity and

average FFR in the Defer and Perform groups were similar (0.86+-0.06 versus 0.87+-0.07 respectively), see Figure 2.13.

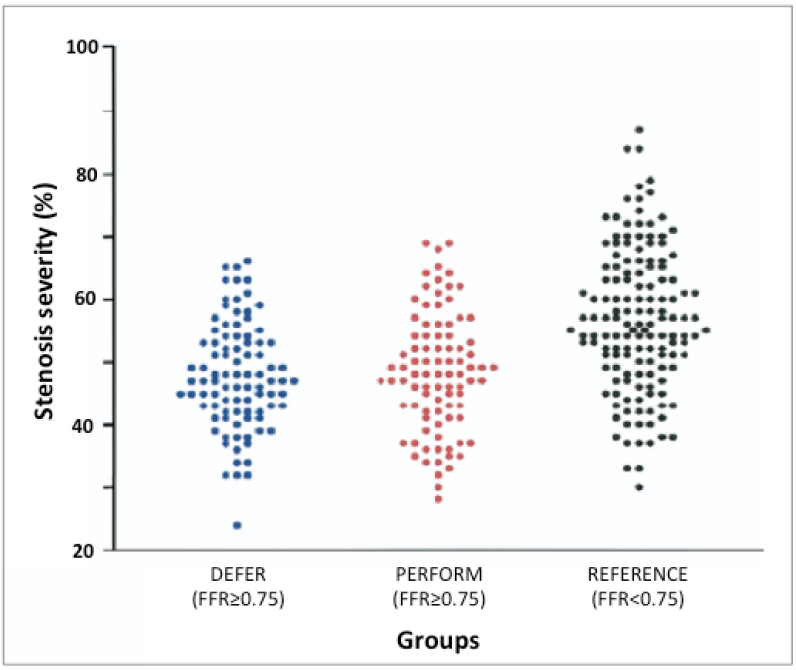

Figure 2.13 – Fractional flow reserve in three groups studied – DEFER study

DEFER study cohort - stenosis severity at baseline in three groups assessed by coronary angiography
Adapted from DEFER study[76]

None of the patients in the Defer group had an adverse event (death, MI, CABG or coronary angioplasty) during the follow up period. By contrast, in the Perform group, 5 patients suffered an event. In the Reference group, there were 12 patients with an adverse event. This was non-significant compared to the Perform group (p=0.61) but significantly different to the Defer group (p=0.004). At 5 year follow up, despite PCI, survival of patients in the Reference group was significantly lower (see Figure 2.14) than in the

combined Perform or Defer groups (61% versus 76% respectively, p=0.03). Importantly, there was no significant difference in survival over 5 years between the Perform and Defer groups (73% versus 79% respectively, p=0.52).

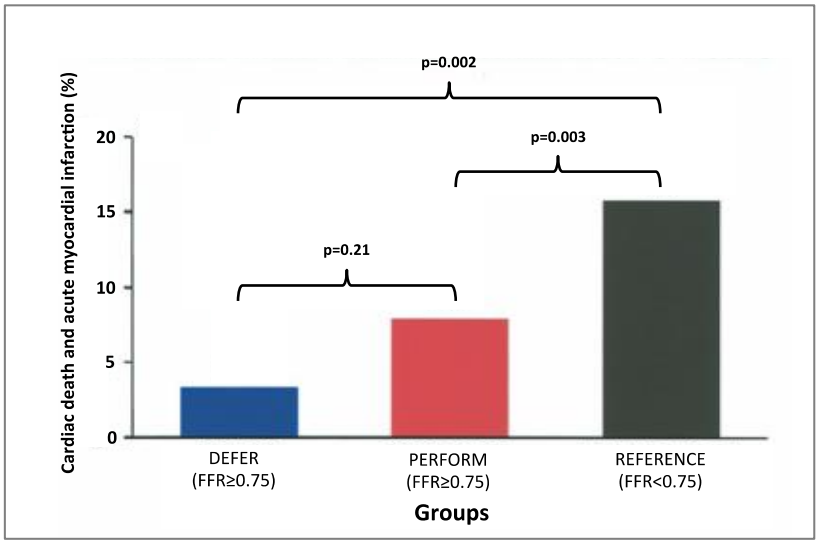

Figure 2.14 - Cardiac death and acute MI rate in the three groups – DEFER study

In patients with a functionally significant stenosis, (i.e. - FFR <0.75) managed with PCI, the incidence of cardiac death or acute myocardial infarction at 5 year follow up was five times higher than in patients with a negative FFR who were managed medically (15.7% versus 3.3%, p=0.002)
Adapted from DEFER study[76]

The patients in the Reference group recorded the most symptomatic improvement. In those with a negative FFR, there was also a benefit in symptoms of angina but interestingly this was more pronounced in the Defer group, even at the two-year point. In summary, the results demonstrated that PCI of a non-functionally significant stenosis is neither of prognostic nor of symptomatic benefit. It is important to note that this was a relatively small study but that nonetheless provided important findings.

The authors of the DEFER study later published 15-year follow up data. At this long follow up, the mortality rate was similar between the three groups. The rate of non-fatal MI was lowest in the Defer group. This showed that even long term, no adverse event was associated with avoidance of PCI to a functionally non-significant stenosis[80].

The FAME study further advanced this work and was designed to evaluate the role of FFR in the management of patients with multi-vessel CAD[77-79]. This tackled the important issue of interventional cardiologists being faced with patients with multi-vessel CAD having to determine which vessel warranted treatment. Data was collected on 1005 patients with multi-vessel CAD (luminal stenosis >50% in more than one of the three main epicardial arteries) who underwent PCI, either by angiography alone or by angiography on the basis of FFR measurements. Patients from the angiography alone group underwent PCI of all affected vessels on the basis of angiographic appearance, whereas patients in the FFR guided group underwent PCI only to stenoses with an FFR measurement <0.80.

In total 496 patients assigned to the angiography-guided group, and 509 patients were assigned to the FFR-guided group for final analysis. At one year, the primary endpoint, a composite of death, MI and repeat revascularization, occurred in 91 patients in the angiography-guided group (18.3%) and 67 patients in the FFR-guided group (p=0.02). The event-free survival is shown in (see Figure 2.15). Significantly more stents were placed in the angiography group (2.7+-1.2 versus 1.9+-1.3, p<0.001) with

comparable procedural times and mean length of stay leading to a significant cost benefit in favour of the FFR guided group ($p<0.001$)[78].

At 5 year follow-up, the group reported a similar rate of major adverse cardiac events between the angiography-guided and FFR-guided groups. Though the initial advantage of an FFR-guided strategy had been lost, the patients in this group underwent less PCI suggesting that an FFR-guided approach was both safe and resulted in fewer stenting procedures[79].

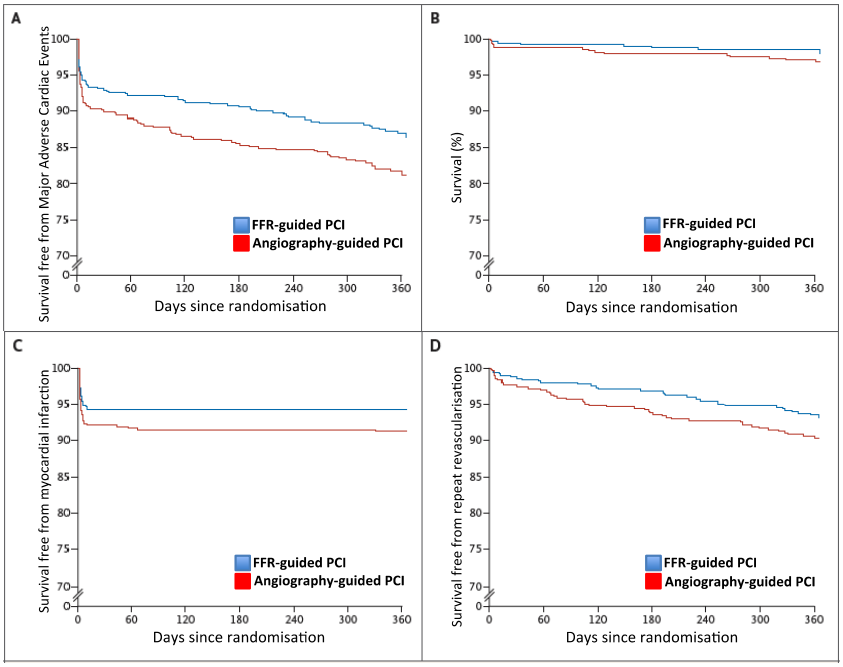

Figure 2.15 – Survival curves comparing angiography versus FFR-guided revascularisation (FAME study)

Kaplan Meier curves showing improvements in FFR-guided treatment group in terms of major adverse cardiac events (A), overall survival (B), survival free from MI (C) and survival free from repeat revascularisation (D) compared to angiography alone.

Adapted from FAME study[81]

2.4 Non-invasive imaging of myocardial ischaemia

Most clinicians now accept that the assessment of CAD ideally takes into account both anatomical and functional information in guiding revascularisation decisions.

In the management of non-invasive assessment of myocardial ischaemia, a number of options are available each with inherent merits and pitfalls. The choice of test used will of course also be based on the clinical scenario, local expertise and availability.

The four main non-invasive imaging modalities for the assessment of myocardial ischaemia are:

CMR,

Positron Emission Tomography (PET),

Single Photon Emission Computed Tomography (SPECT), and

Echocardiography

2.4.1 Use of stressor agents in imaging

There are two ways in which ischaemia can be appreciated by non-invasive imaging – both target points of the ischaemic cascade – vasodilator stress, to identify areas of hypoperfusion, or inotropic stress, to identify regional wall motion abnormalities. As described previously, the use of vasodilator stress is more sensitive since it targets an earlier point in the ischaemic cascade curve[27,36].

2.4.1.1 Vasodilator stress

The changes in blood flow in response to stress agents which cause vasodilatation can be visualised by means of SPECT, PET or perfusion CMR.

2.4.1.1.1 Perfusion CMR

Perfusion CMR perfusion imaging is based on the delivery of a contrast agent to the myocardium after intravenous injection under hyperaemic conditions, usually with adenosine. The imaging sequence is started shortly after injection of the contrast agent peripherally. The scan captures simultaneous basal, mid and apical LV cross-sectional slices with dynamic beat-to-beat imaging. The term 'first pass' is used to identify the images obtained on first passage of contrast first in the ventricles and then in the myocardium. The contrast is Gadolinium-based, which passes readily from the blood to the interstitial space (it does not enter intact cells and is therefore termed 'extracellular') at a rate proportional to blood flow. The acquired images show a delayed wash-in of contrast to the area of myocardium served by the narrowed vessel which is most severe in the endocardium[82,83]. This yields a contrast between areas of stress-induced hyperaemic myocardium and areas of reduced coronary reserve and relatively reduced perfusion due to differences in contrast concentration.

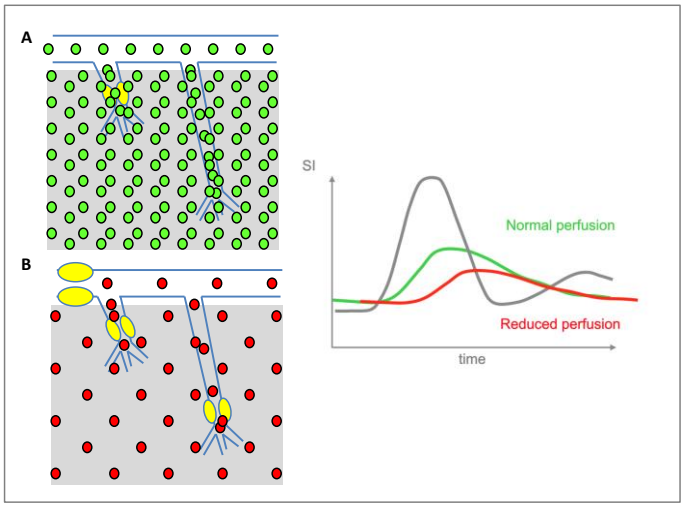

Figure 2.16 - Schematic showing difference in normal and hypoperfused myocardium

Left panel –
A – normal vessel with green dots indicating Gadolinium contrast molecules readily passing into the blood vessels then into the extracellular space.
B- stenotic epicardial vessel with fewer Gadolinium contrast molecules resulting in lower myocardial Gadolinium concentration.
Right panel – shows the relative signal intensity curves whereby the hypoperfused region reaches a lower and later peak in Gadolinium concentration.
Adapted from Amedeo Chiribiri[10]

The acquisition of rest images is obtained after an interval of approximately 10-15 mins. This second acquisition is identical to the first but without the vasodilatory influence of adenosine. This identifies rest perfusion defects likely to represent areas of scar (or artefact). Quantitative analysis of these images also enables calculation of myocardial perfusion reserve. The interval between the stress and rest acquisitions can be used for functional and flow imaging. Following the rest acquisition an additional dose of contrast agent is usually administered for late gadolinium enhancement imaging.

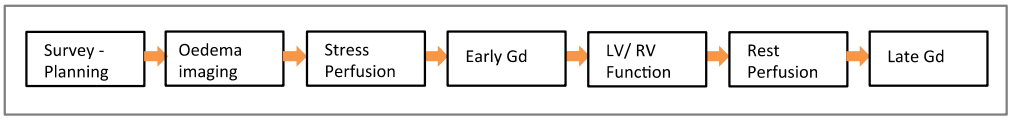

Figure 2.17 - Schematic diagram showing scan sequence for a stress perfusion CMR

Taken from clinical scan protocols, St Thomas' Hospital, King's College London

2.4.1.1.2 Perfusion CMR sequences

The signal generated, and how it relates to the myocardial blood flow is also a function of the specific CMR sequence used. Perfusion CMR images were previously acquired using an inversion recovery pulse sequence – this can be used to null the tissue signal not exposed to Gadolinium and therefore creates a difference between normal and hypoperfused myocardium – these sequences however unfortunately require long acquisition which limits the temporal resolution and the number of slices possible within one cardiac cycle.

Newer sequences tend to use a saturation recovery sequence where a saturation pre-pulse is given to null the myocardium then images are taken as the tissue relaxation recovers. This type of sequence is faster and permits an increase in the acquired in-plane spatial resolution while allowing multi-slice acquisition, at some expense in loss of the contrast between normal and hypoperfused myocardium. The saturation pre-pulse is triggered by the QRS complex and nulls the longitudinal magnetisation of the tissues. The tissue will then start to recover, at a speed which is proportional to the local T1 values. During first-pass, the concentration of gadolinium increases at a speed proportional to blood flow, and this reflects in the T1 of the tissue.

Areas of normal tissue will have received more contrast agent and will have a shorter T1 than hypoperfused regions. These two regions will therefore recover at different speeds and the hypoperfused region will reach a lower peak than normal tissue. After the saturation pre-pulse, 90-120 ms are allowed for the recovery of longitudinal magnetisation, before the first image is acquired. Image acquisition can start in any phase of the cardiac cycle, after the initial saturation-recovery time has elapsed. This is controlled by a different parameter, the trigger delay[84].

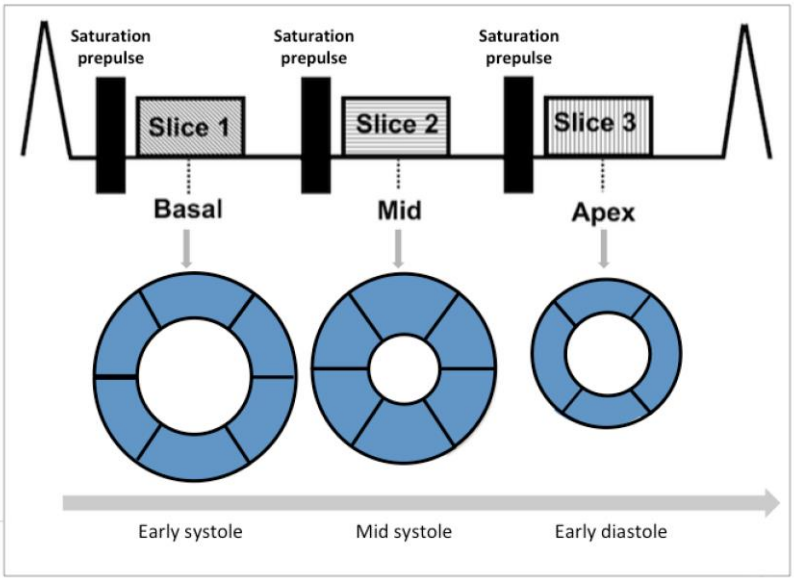

Figure 2.18 - Schematic showing typical image sequence for 2D perfusion CMR

Saturation recovery sequence where a saturation pre-pulse is given to null the myocardium then images are taken as the tissue relaxation recovers. The saturation pre-pulse is triggered by the QRS complex and nulls the longitudinal magnetisation of the tissues. The tissue will then start to recover, at a speed which is proportional to the local T1 values. During first-pass, the concentration of gadolinium increases at a speed proportional to blood flow, and this reflects in the T1 of the tissue. After the saturation pre-pulse, 90-120 ms are allowed for the recovery of longitudinal magnetisation, before the first image is acquired. Image acquisition can start in any phase of the cardiac cycle, after the initial saturation-recovery time has elapsed. This is controlled by a different parameter, the trigger delay. Stress and rest perfusion images are usually acquired using a 2D imaging technique, and 3 short axis slices are usually acquired in basal, mid and apical geometry. Each slice will be imaged at a different point in the cardiac cycle.
Adapted from Motwani et al.[84]

2.4.1.1.3 Visual assessment of perfusion CMR

In the clinical setting, visual assessment of stress, rest and late gadolinium imaging are used in combination to report on the presence of 'non-inducible' perfusion defects. These are seen on stress and rest perfusion imaging and typically correspond to scar on late gadolinium imaging provided this is not related to artefact. Likewise, 'inducible' perfusion defects - seen on stress but not rest perfusion imaging and not corresponding to, or extending beyond areas of scar on late gadolinium enhancement imaging – are also identifiable. Myocardial perfusion is seen to fill from subepicardium towards the subendocardial layer with successive heartbeats. Perfusion defects are seen to be arising from the subendocardium or transmural and, in the case of CAD, are located in the distribution of a coronary territory, typically affecting more than one slice.

2.4.1.1.4 Advantages of CMR for stress perfusion imaging

One of the key features of CMR is its higher spatial resolution of CMR compared to other imaging modalities. In the field of perfusion CMR this is a clear advantage as CMR lends itself to the identification of subendocardial perfusion defects, potentially invisible to other modalities. Newer CMR sequence protocols, utilising high-resolution sequences can also reveal transmural gradients in perfusion and identification of subendocardial defects. As will be discussed later, this is an advantage in particular in patients with heart failure, where the left ventricular wall is thinned and the ventricle remodelled and high spatial resolution is required to resolve subendocardial ischaemia.

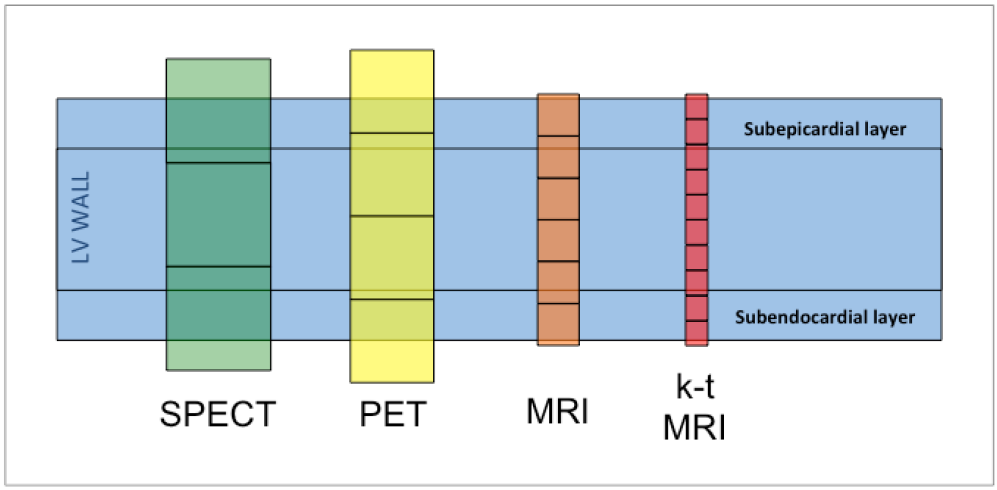

Figure 2.19 - Schematic showing the different spatial resolution of SPECT, PET and MRI

Diagram demonstrating the improved spatial resolution of MRI, in particular of a high-resolution sequence, compared to SPECT and PET. This is an important consideration in heart failure where the myocardial wall can be thinned.

The images are acquired first under hyperaemic conditions then again at rest in order to be able to compare, visually or quantitatively, the difference. If done quantitatively, the stress value is divided by the rest value to produce the myocardial perfusion reserve (MPR). In SPECT or PET, blood flow is recorded by means of a radioactive tracer, and in CMR by Gadolinium contrast agent, both injected through a peripheral vein and recorded at first-pass entering the myocardium dynamically.

In practice, both in CMR and in nuclear imaging, the most commonly utilised stress vasodilator agent is adenosine, delivered as an infusion to produce hyperaemic responses. It has a short half-life of less than ten seconds, with peak hyperaemic effect within two minutes.

Other potential agents include dipyridamole and regadenoson but these are less commonly used. Dipyridamole has been shown to be a less potent

vasodilator with a more variable response than adenosine[85-87]. In a practical sense regadenoson is easier to use than adenosine as it is given as a single bolus injection and is safe but its vasodilator effects are longer-lasting than those of adenosine. The washout periods before acquisition of rest images and time constraints make it a less popular agent in some centres and it can impact on MPR measurements from stress and rest perfusion estimates [88,89].

In hearts with normal coronary arteries, blood (and contrast agent) will rapidly pass from the aorta to each part of the myocardium in a uniform manner, washing in from the subepicardium to subendocardium. In contrast, areas served by epicardial coronary vessels with significant stenosis, show little or no effect from vasodilator. Comparison of such an area with a healthy territory provides visual evidence of the difference in perfusion. The more severe and proximal the stenosis, the more transmural and extensive the perfusion defect.

2.4.1.2 SPECT versus CMR

Until recently, when CMR became more widely available, SPECT was the most commonly employed technique for non-invasive assessment of ischaemia.

The CE-MARC and MR-IMPACT I and II studies compared SPECT directly with CMR and will be summarised below.

The CE-MARC study was the first large prospective study using angiography as the reference method to compare CMR with SPECT with regard to ability to predict major adverse cardiovascular events[90]. Patients with stable angina underwent stress and rest adenosine CMR and Tc (technetium) SPECT as well as coronary angiography. The primary outcome of this study was to determine the ability of a multi-parametric CMR protocol (rest and stress perfusion, left ventricular function, coronary magnetic resonance angiography, late gadolinium enhancement) to detect clinically significant coronary heart disease as measured by angiography. The secondary outcome was a comparison of multi-parametric CMR and SPECT (rest and stress perfusion, left ventricular function) using angiography as the reference. Perfusion CMR images were analysed visually. Of 752 patients, 628 patients had analysable CMR, SPECT and angiography data. 39% patients had significant CAD (defined as >70% coronary stenosis of one of the main coronary arteries or >50% left main stem, measured by quantitative angiography). The key finding of the study showed that, by comparison with SPECT, sensitivities and negative predictive values of the CMR protocol were significantly in favour of CMR ($p<0.0001$ for both), with no significant difference in specificity or positive predictive value ($p=0.916$ and 0.061 respectively). For the receiver-operating curve (ROC) analysis, stress perfusion CMR significantly outperformed SPECT (AUC 0.89, 95% CI 0.86-0.91), see Figure 2.20. Stress perfusion CMR was better than SPECT even when the angiographic cut-off value for a clinically significant stenosis was adjusted to 50% or greater for any main epicardial vessel or when multi-vessel CAD was considered. This was a necessary and important study in direct comparison of these

techniques but has been criticised by some due to the single site design, which carries inherent limitations, and the reported under-performance of SPECT compared to other published studies[91].

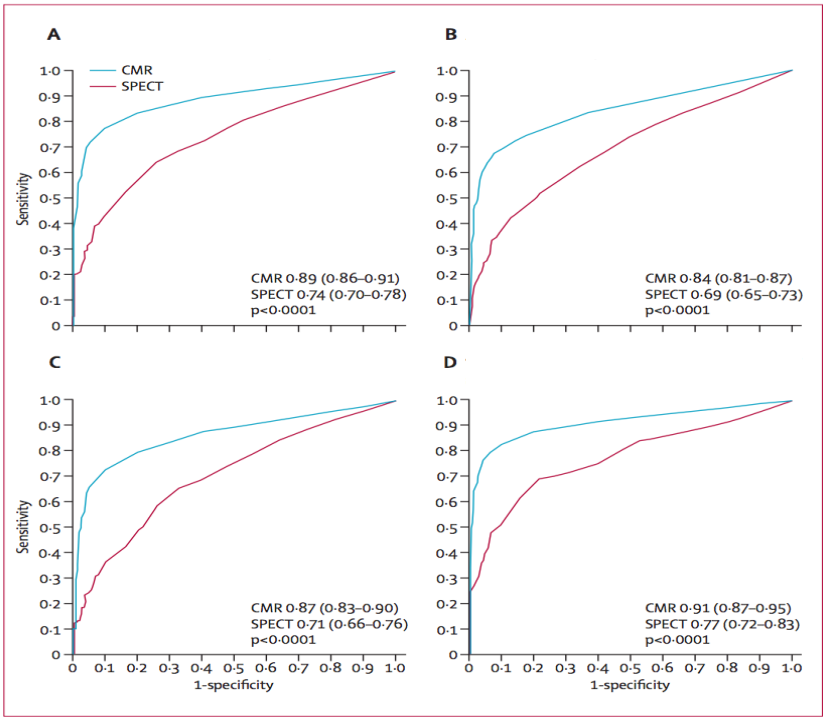

Figure 2.20 - Receiver operator curves – CE-MARC study

Receiver operator curves from SPECT versus CMR for the whole cohort
A- angiographic cut-off ≥50% LMS; ≥70% for LAD, Cx, & RCA
B- angiographic cut-off ≥50% for LMS, LAD, Cx, and RCA
C- patients with single-vessel disease
D- patients with multi-vessel (two or three vessel) disease
(LMS - left main stem, LAD - left anterior descending, Cx - circumflex artery, RCA - right coronary artery)
Adapted from CE-MARC[90]

Published a few years earlier, the MR-IMPACT trial also aimed to compare the two modalities using coronary angiography as the reference[92]. Perfusion CMR was assessed visually by experts. Patients who had recorded positive in a clinically indicated SPECT scan, or had undergone a clinically-indicated coronary angiogram were eligible. As a result of the entry criteria, this study

recruited a highly selected and higher risk population, evidenced by the high prevalence of CAD (77% patients had CAD, 31% had history of PCI). A total of 225 patients were considered suitable for analysis of SPECT versus CMR. The results suggested equal performance of gated SPECT versus CMR for the detection of significant CAD in this higher risk patient group, with CMR performing better when ungated SPECT studies were included.

The MR-IMPACT II study built further on this data and again sought to evaluate the diagnostic performance of perfusion CMR versus SPECT using coronary angiography as the standard reference[93]. This was a large multi-centre, multi-vendor study with 515 patients recruited to 33 American and European sites. This included patients who were scheduled for a clinically indicated SPECT scan or coronary angiogram and included patients with previous myocardial infarction. Perfusion CMR was assessed visually. The primary endpoint was non-inferiority of CMR compared to SPECT for the detection of CAD. Unlike the MR-IMPACT study, patients were included irrespective of the result of the SPECT scan and therefore the population was more representative of a general cohort with 48.8% of patients having significant CAD with a coronary stenosis >75%, and 29% patients having had previous MI. In total 465 patients underwent all three investigations and were included in final analysis.

The findings echoed the findings of the CE-MARC study and concluded that CMR was non-inferior to SPECT for the detection of CAD in terms of sensitivity but that SPECT was more specific.

In summary, these studies showed that visually assessed stress perfusion CMR performed better than SPECT in terms of sensitivity with similar specificity (somewhat favouring SPECT). There was also the advantage of eliminating exposure to ionising radiation and the ability to assess the detailed morphology of cardiac structure. These factors supported more widespread use of CMR to assess myocardial ischaemia.

2.4.1.3 PET versus CMR

Perfusion CMR can be assessed by direct visualisation of first pass of Gadolinium contrast agent or, like PET, can be assessed semi- or fully-quantitatively. Quantification of perfusion CMR will be discussed in more detail in a later chapter but, in essence, can provide stress, rest and myocardial perfusion reserve (MPR) estimates, measured either semi- or fully quantitatively.

In brief, PET is performed in combination with CT or MRI scanning for attenuation correction and, anatomical localisation and co-registration of images. One of several suitable short-lived metabolically active, or freely diffusible radioactive tracers is injected to the patient to measure stress and rest myocardial perfusion blood flow and myocardial perfusion reserve (MPR). This exposes the patients to ionising radiation from the PET tracer, and the CT scan when performed, and requires an on-site cyclotron if tracers such as ^{15}O-water or ^{13}N-ammonia are to be used. Previous studies have demonstrated a sensitivity and specificity of PET for the detection of CAD of around 90% and in consequence, PET is considered the non-invasive reference method for perfusion measurements[18-21].

Due to the lack of widespread use of PET in the clinical setting for myocardial ischaemia assessment, studies comparing the techniques have been limited. These studies have used semi- or fully quantitative CMR analysis and will be discussed in more detail in the next chapter.

2.4.1.4 SPECT versus PET versus CMR

In a meta-analysis, SPECT, PET and CMR were compared[94]. This reviewed 3635 studies and found 166 met the inclusion criteria- that the test was used as a diagnostic test for obstructive CAD with angiography as the standard reference. This resulted in analysis of 17,901 patients and 114 SPECT, 37 CMR, and 15 PET studies. Patient-based analysis per imaging modality demonstrated pooled sensitivities of 88 % for SPECT, 84 % for PET, and 89 % for CMR; pooled specificities were 61 %, 81 %, and 76 %, respectively. This demonstrated a high sensitivity of all modalities with a broader range of specificity but emphasised that CMR has a role to play in this area.

2.4.1.5 FFR versus CMR

Lockie et al. studied 42 patients with suspected CAD[82]. Visual and quantitative assessment of perfusion CMR was compared with invasive fractional flow reserve findings (FFR). FFR was measured in all vessels where the stenosis was >50% narrowed visually. The results demonstrated that visual assessment of perfusion with CMR performed well against FFR - the FFR in territories deemed to be normal by visual assessment of perfusion was 0.93±0.09 versus an FFR of 0.59±0.22 in vessels with visual evidence of a perfusion defect. This produced a sensitivity of 0.82 and specificity of 0.94

for detection of an FFR <0.75 for visual analysis. Similarly, quantitative analysis also performed well – the MPR for territories with an FFR <0.75 was 1.35±0.5 versus an MPR of 2.2±0.5 for those with a normal FFR. This produced a sensitivity and specificity of 0.80 and 0.89 respectively for quantitative analysis. Linear regression analysis suggested that quantitative measurements correlated better with FFR measurements than visual analysis. The optimal MPR value to detect lesions with an FFR <0.75 was found to be 1.58.

The MR-INFORM (MR Perfusion Imaging to Guide Management of Patients with Stable Coronary Disease) study has compared outcomes between patients treated according to the result of either a perfusion CMR or an FFR result[95]. This study compared the revascularisation rates and outcome of patients randomised either to an FFR-guided approach or a CMR perfusion-guided approach. In total, 918 patients were enrolled and followed up for 1 year. Preliminary results show that both groups demonstrated a very low event rate with similar performance of both tests. This showed that patients can safely be managed by either approach. Importantly, the CMR-guided group underwent significantly fewer revascularisation procedures suggesting that a CMR-guided approach will avoid unnecessary invasive intervention. This study is likely to produce significant advance in the application of CMR to guide management.

2.4.1.6 Invasive angiography versus CMR

Several studies have specifically tested perfusion CMR against invasive coronary angiography. While this is reasonable at judging severity at the extremes of mild or severe CAD, its use in the moderate range this is open to scrutiny, even if assessed quantitatively. Many of these studies were performed at a time where this was either not appreciated or when additional means of assessing the severity of coronary lesion were not available - most would now argue that fractional flow reserve is the reference standard for invasive assessment of coronary artery stenosis.

Ishida et al. studied 104 patients referred for coronary angiography with suspected CAD and no prior history of MI and reported a sensitivity of 0.90 and specificity 0.85 for perfusion CMR[96]. Pilz et al. presented similar sensitivity and specificity on a series of 176 patients with stable angina (0.96 and 0.83 respectively) compared to angiography and concluded that perfusion CMR was highly accurate as a gatekeeper for patients with intermediate CAD[97].

Some groups have examined the use of adenosine for evaluation regional wall motion abnormalities. In one of these studies, it was demonstrated that DSMR was superior in the induction of regional wall motion abnormalities compared to adenosine - adenosine stress CMR is capable of detecting regional wall motion abnormalities but only identifies high-grade coronary stenosis using coronary angiography as the reference[98].

2.4.2 Inotropic stress

The assessment of inducible ischaemia may also use dobutamine, an inotrope which increases myocardial oxygen demand and uses regional wall function as the endpoint to indicate ischaemia. It is only applicable to CMR and echocardiography.

Dobutamine CMR can be performed at low dose for assessment of viability, alone or in combination with LGE imaging, or can be used at high-dose as alternative to stress perfusion CMR to assess for ischaemia.

Though not routinely performed in combination, there is evidence of improved diagnostic accuracy when perfusion CMR is added to high dose DSMR for the evaluation of patients with intermediate coronary stenosis, especially when a high-spatial resolution sequence is used[99-101].

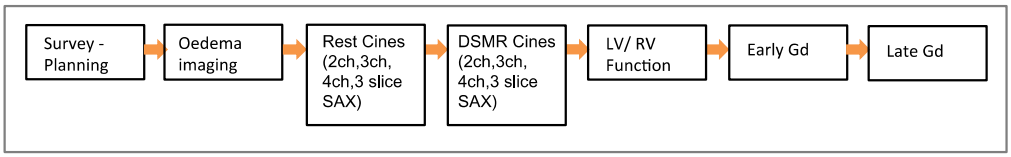

Figure 2.21- Schematic diagram showing scan sequence for a stress DSMR

Taken from clinical scan protocols, St Thomas' Hospital, King's College London
If viability is the main question, low dose DSMR is performed, if ischaemia is the concern and if clinically indicated, high-dose DSMR is performed.

This is performed using either dobutamine at low dose (up to 10 mcg/kg/min) or high dose (up to 40 mcg/kg/min). Low dose dobutamine stress by echo (DSE) or by CMR (DSMR) is used to simulate recruitment of hibernating regions by demonstrating areas improve under stress with increased wall motion and thickening – this can be used alone, or in the setting of CMR in

combination with LGE images[102-104]. High dose DSMR is used as an alternative to perfusion CMR to look for regional wall motion abnormalities at peak stress. The target for a high-dose DSMR is to achieve target heart rate and this can be promoted with the addition of atropine during the scan. At low dose DSE or DSMR, a region can be seen to improve but at a higher dose of dobutamine the ischaemic region is seen to worsen in contractility – a so-called biphasic response.

Exercise can also be used to drive increase in oxygen demand but is not practically feasible in CMR due to patient positioning and movement within the MRI bore. In echocardiography, patients can be asked to cycle while being scanned in place of pharmacological stress.

2.4.3 The importance of a negative stress CMR

In work by Jahnke et al. 513 patients underwent both adenosine and high-dose dobutamine stress perfusion CMR with a median follow up of 2.3 years[59]. This team found that the three-year event free survival was 99.2% in patients with a normal adenosine and dobutamine stress CMR, and 83.5% in those with an abnormal test. Ischaemia detected by CMR was found to be an independent predictor of cardiac events - multivariate analysis showed that an abnormal test carried significant incremental value over other recognised clinical risk factors.

A meta-analysis of 19 studies including over 11,000 patients with a mean follow up of 32 months showed that patients with an abnormal stress (vasodilator or dobutamine) CMR test had a 7.7-fold increased incidence of MI and a 7-fold increased risk for cardiovascular death compared to those

without demonstrated ischaemia. A negative CMR implied a very low risk of adverse events[58].

Similarly, a second meta-analysis performed the same year reported on 14 studies including over 12,000 patients. This demonstrated a high negative predictive value for MI and cardiac death of a CMR showing no evidence of ischaemia on vasodilator or dobutamine CMR - 98.1% and an annualised event rate of only 1%[105].

Nandalur et al. also performed a meta-analysis which pooled results of 37 studies (2191 patients) using visual, semi-quantitative and fully-quantitative perfusion CMR analysis and DSMR against angiography and concluded that perfusion CMR has a sensitivity and specificity of 91% and 81% respectively, and that DSMR has a sensitivity and specificity of 83% and 86% respectively[106].

The growing impact of CMR in the clinical setting was highlighted in the Euro-CMR Registry which studied over 11,000 patients in Germany. This showed that CMR is a safe test, with diagnostic image quality in 98% patients and has an impact on subsequent patient management in nearly two-thirds of patients[107,108].

2.5 Conclusion

In summary, this chapter introduces the concepts and themes on which subsequent chapters are based. The assessment of ischaemia is relevant and sensitive to early detection of coronary artery disease and appears to

have prognostic benefit in decisions regarding revascularisation. The use of ischaemia testing is relevant also to the avoidance of unnecessary revascularization and appears superior to visual assessment of coronary stenosis, in particular in the moderate range. The use of perfusion CMR is increasingly prevalent, largely due to the multi-parametric capability and the high spatial resolution of the technique. Visual assessment of ischaemia by perfusion CMR compares well with invasive and other non-invasive techniques, with corresponding prognostic benefit. In addition perfusion CMR can be quantified, bringing the additional potential of absolute, objective measurements of perfusion – this will be discussed in the subsequent chapter.

3 Quantitative perfusion CMR

3.1 Introduction

The quantitative analysis of perfusion CMR was first described over 20 years ago but its use has been limited to research. As discussed in the previous chapter, both semi and fully quantitative CMR have been shown to compare well with the reference method of non-invasive perfusion (PET) in healthy volunteers[109] and patients[110-113].

This chapter will discuss the evidence supporting the use of quantitative perfusion CMR analysis, the different approaches to quantification of perfusion CMR data and finally will explore the barriers limiting its transition to routine clinical use. This chapter includes a published review article - Eva Sammut is first author and was responsible for literature review and involved with manuscript drafting.

3.2 Quantitative perfusion CMR

The search for quantitative measures of perfusion by CMR is motivated by the desire to obtain observer-independent and reproducible measures of myocardial perfusion status. The advantages of a quantitative approach include assessment of global disease. In broad terms, there are two ways to quantitatively assess perfusion CMR – semi-quantitatively, and fully quantitatively. Both have been shown to be reproducible from studies investigating intra- an inter-reader variability[114-117].

3.3 Linearity of signal intensity and gadolinium contrast

It is important to appreciate that, for semi-quantitative assessment to be even possible, signal intensity in both the blood (input) and myocardium (output) should be proportional to the concentration of the contrast agent. Unfortunately, as will be outlined, linear relationship is only observed at lower Gadolinium concentration levels. At higher levels, the signal intensity is seen to saturate and loses its relationship to contrast agent concentration.

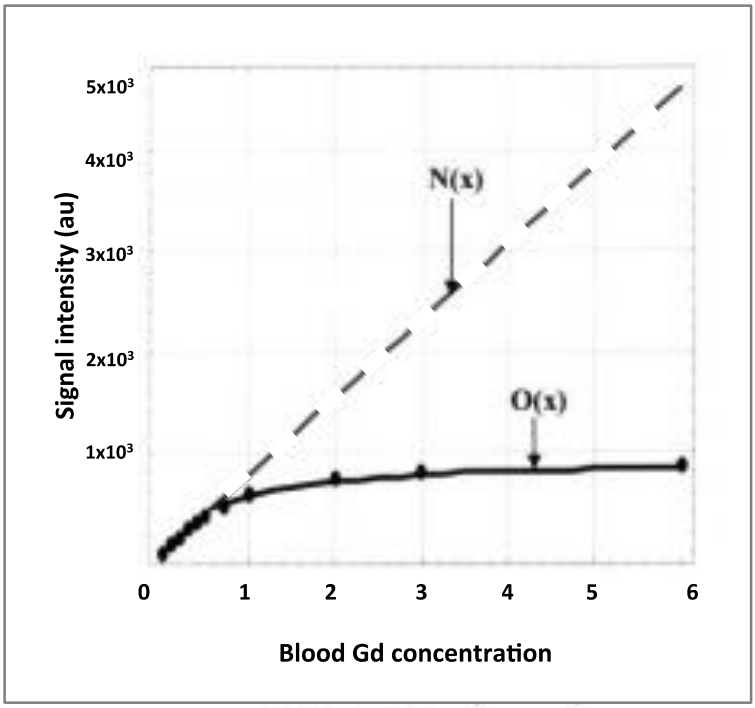

Figure 3.1 – Figure showing relationship between signal intensity and Gadolinium concentration

Demonstrates findings of an experiment on human blood samples using a saturation recovery MRI sequence showing blood signal intensity (SI) plotted against Gadolinium (Gd) concentration. The measured relationship is shown on Ox line and shows the signal with is initially linear but saturates at high Gd concentration. Nx shows the theoretical, projected linear relationship between the SI and Gd concentrations, extrapolated from the lower concentration data points on Ox.

Adapted from Ichihara et al.[118]

Since perfusion CMR is judged visually in the clinical setting, it is desirable to maximise the contrast to noise ratio (CNR) in the myocardium – this requires a large Gadolinium (Gd) dose. A higher contrast to noise is preferable for visual assessment but the loss of relationship between signal intensity and Gd concentration at higher doses, precludes direct quantification of signal to calculate Gd concentration and in turn perfusion. The dosage regime of Gadolinium used in previous studies has ranged from 0.025 – 0.15mmol/kg which is adequate to identify areas of hypoperfusion by visual assessment[119]. Lower doses make visual assessment suboptimal[120].

3.4 Semi-quantitative analysis of perfusion CMR

Semi-quantitative analysis, the simplest quantitative approach, plots the signal intensity (SI) against the time of the dynamic perfusion images. This provides a number of indices – the maximal SI; contrast appearance time; time to maximal SI; area under the SI curve and steepness of the upslope of the SI curve.

The most widely used index is the upslope of the SI curve which measures the speed of wash-in of contrast agent as an index for blood flow. In view of the saturation of signal at higher Gd doses, in semi-quantitative analysis, higher values are extrapolated from the start of the SI slope and a linear fit curve is created. Upslope analysis has been compared against angiography, FFR, microspheres and PET – it has been shown to reproducible between sites and can accurately discriminate between normal and hypoperfused

regions but some studies suggested an underestimation of semi-quantitative CMR analysis against other modalities[110,121-126].

3.5 Key studies - semi-quantitative perfusion CMR

Giang et al. compared angiography with upslope analysis in 94 patients and showed a sensitivity of 93% and specificity of 75%[121]. Rieber et al. studied 43 patients with known or suspected CAD and compared upslope analysis against angiography alone versus FFR angiography and concluded that CMR was capable of detecting haemodynamically significant lesions with a high sensitivity and specificity (88% and 90% respectively)[122]. Nagel et al. described the accuracy of upslope analysis on 84 patients referred for angiography, with a high prevalence of CAD and reporting sensitivity of 0.88 and specificity of 0.90[123]. Schwitter et al. used PET and angiography to assess upslope analysis and found that CMR was able to identify patients with CAD even when hypoperfusion was limited to the subendocardial layer, with a sensitivity and specificity of 91% and 94% respectively compared to PET, and 87% and 85% respectively compared to quantitative angiography[110]. Al-Saadi et al. used upslope analysis against angiography to define an optimal MPR threshold of 1.5 and then prospectively tested this threshold in a second group and reported a sensitivity, specificity and diagnostic accuracy of 90%, 83%, and 87% respectively[124]. Ibrahim et al. studied a group of patients with angiographically-documented CAD with CMR and PET and found that upslope analysis underestimated MPR values compared to PET with a sensitivity, specificity and diagnostic accuracy of

86%, 84% and 85% respectively[125]. Plein et al. reported on 92 patients and 10 healthy volunteers and a high diagnostic accuracy of upslope analysis with AUC 0.908, sensitivity 88% and specificity 82% compared to angiography[126].

Lee et al. used an in-vivo dog model to compare semi-quantitative analysis of CMR and SPECT against the preclinical invasive reference standard of microspheres[127]. At rest they demonstrated homogenous regional microsphere concentrations and, using upslope analysis, CMR and SPECT performed similarly. When the circumflex artery flow was reduced by >85%, both CMR and SPECT showed marked perfusion abnormalities. Importantly, when the circumflex was occluded by 50%, a perfusion defect was seen only on CMR. There was a linear relationship between the CMR signal intensity curves and microsphere flow rate over the range of flow limitation. This highlights the ability of CMR to appreciate moderate as well severe degree of stenosis, visually apparent as a subendocardial rather than transmural defect. This result is somewhat surprising given one would not typically expect a perfusion abnormality for a 50% lesion. Nevertheless, as described in the previous chapter, moderate lesions can be flow limiting underlining the importance of ischaemia assessment with CMR or FFR.

Schwitter et al. prospectively studied a group of 41 patients with suspected stable angina, using MR perfusion, analysed semi-quantitatively, and ^{13}N-ammonia PET against coronary angiography[110]. 18 healthy volunteers also underwent perfusion CMR to generate reference values for transmural and subendocardial perfusion levels. The group concluded that first pass CMR

perfusion reliably detects and quantifies CAD, and includes the ability to identify subendocardial perfusion abnormalities. They reported a sensitivity and specificity for perfusion CMR of 91% and 94% respectively for patients with reduced CFR as defined by PET, and 87% and 85% respectively compared to coronary angiography. There was a linear relationship between PET and MR in detecting the number of hypoperfused segments when considering no, one-, two- and three-vessel disease, with a tendency to underestimation by CMR (see Figure 3.2). ROC analysis demonstrated that semi-quantitative CMR data are highly reliable in the detection of significant CAD (see Figure 3.3).

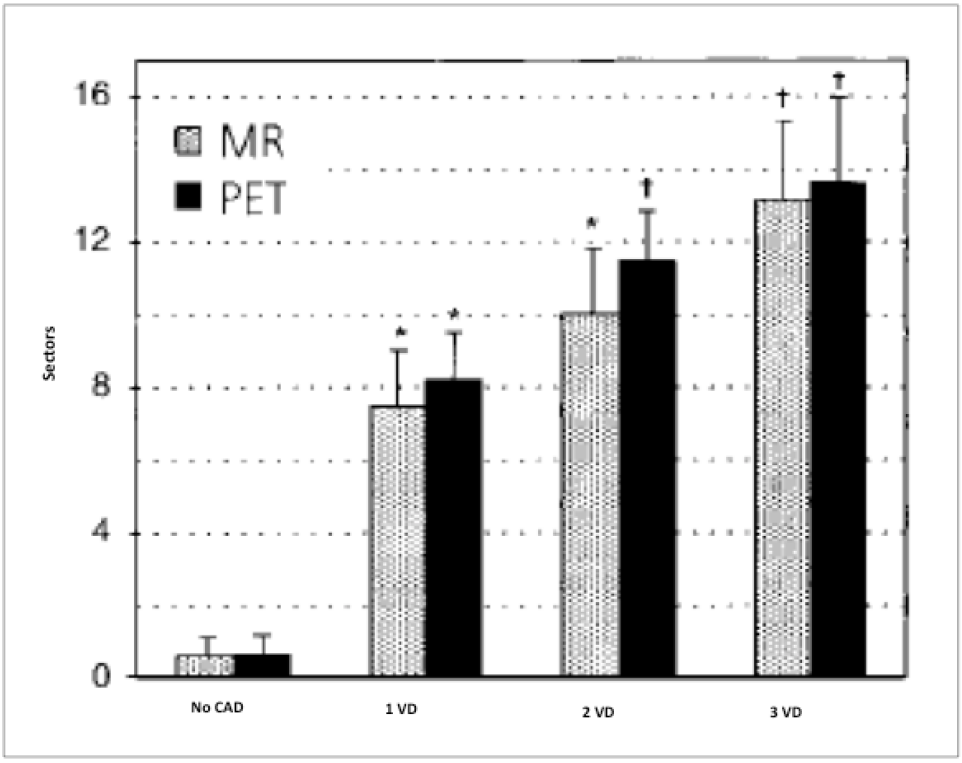

Figure 3.2 – Bar chart comparing results of CMR versus PET

Bar chart summarising number of positive segments identified by each technique. With progressive increase in extent of CAD, both techniques identify increasing extent of ischaemia, with slightly higher values seen with PET.
1VD- one vessel disease, 2VD – two vessel disease, 3VD – three vessel disease
Adapted from Schwitter et al.[110]

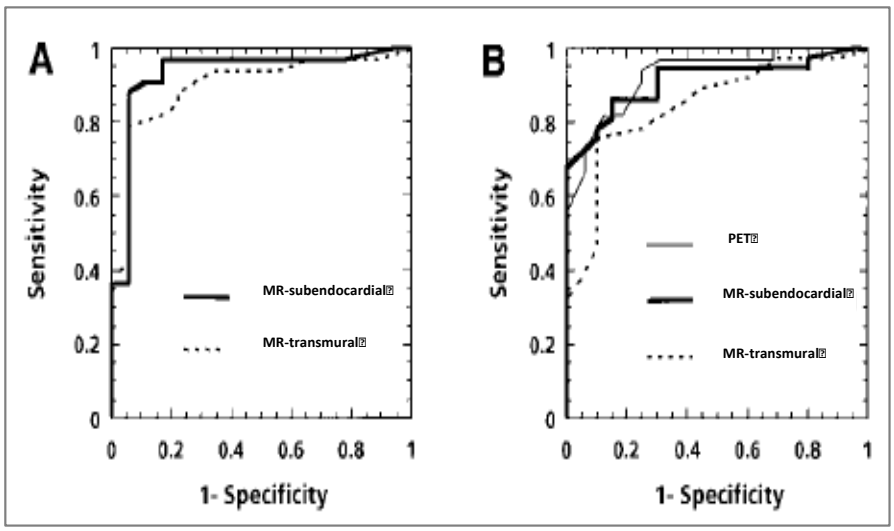

Figure 3.3 – Comparison of semi-quantitative CMR to PET or angiography

A – MR detection of haemodynamically significant CAD by PET (>1 sector with CFR <1.65, n=51)
B - diagnostic accuracy of MR and PET are similar compared to angiography (>1 coronary artery >50% stenosis, n=57).
Adapted from Schwitter et al.[110]

3.5.1 Transmural perfusion analysis

A different approach to exploit and quantitate high-resolution perfusion CMR data has been proposed by Hautvast et al.[128]. This is based on the measurement of perfusion imbalances between endocardial and epicardial myocardial layers. Following accurate motion correction and segmentation of the LV wall, an algorithm calculates the transmural perfusion gradient G(α,t) frame-by-frame during first-pass wash-in of contrast agent (t) and in every myocardial transmural sector α according to the following formula:

$$G(a,t) = \frac{I_{epi}(a,t) - I_{endo}(a,t)}{I_{transm}(a,t)} * 100\%$$

where $I_{epi}(\alpha,t)$ is the signal intensity curve in the LV endocardial layers, $I_{endo}(\alpha,t)$ is the signal intensity curve in the LV epicardial layers and $I_{transm}(\alpha,t)$

is the average transmural signal intensity curve in the LV. The transmural perfusion gradient is expressed as a percentage of transmural redistribution of myocardial blood flow between layers. The optimal diagnostic threshold has been identified in comparison with FFR and then validated in an independent cohort of patients. A transmural perfusion gradient of 20% identifies the presence of haemodynamically significant CAD with a sensitivity of 0.78, specificity of 0.94, diagnostic accuracy of 0.86 for in a per-segment analysis and of 0.89, 0.83, and 0.86 in a per-patient analysis, respectively[129].

Transmural perfusion gradient analysis offers a series of advantages over other methods used for quantitative analysis. It does not require administration of a diluted pre-bolus or the acquisition of rest perfusion images. Additionally, it is more robust to image homogeneity due to variations in the B1 field, different coil configurations, different schemes of contrast agent administration, field strength, and the acquisition pulse sequence[128,129].

3.6 Fully quantitative analysis

Fully quantitative analysis permits absolute measurement of myocardial blood flow during stress and at rest for the calculation of myocardial perfusion reserve (MPR). Once again, accurate quantification must overcome the loss of a linear relationship between signal intensity and higher blood Gadolinium concentration. As only a small proportion of the injected Gadolinium will pass from the blood pool to the myocardium, the ideal situation is achievement of a high dose of Gd in the myocardium, to maximise contrast to noise in the myocardium, and a low dose in the blood pool in order to minimise saturation

effects. This is unobtainable with a single injection but has been addressed by two approaches:

The dual bolus approach using administration of lower concentration pre-bolus of Gadolinium to measure the blood pool (arterial input function), followed by a full strength main bolus from which the myocardial signal is then calculated[130].

A more recent dual sequence approach involves a short saturation low resolution image acquired for each heart beat to measure the arterial input function. This is followed by a higher resolution long saturation recovery image for myocardial signal intensity[131].

These approaches will be discussed in more detail later.

The analysis of quantification data requires complex mathematics, each with limitations and assumptions, and these will be discussed later in the chapter.

3.6.1 Quantitative CMR versus PET

The current reference method of choice for quantitative analysis of perfusion is PET. As discussed in previous chapters, the alternative of CMR is attractive in view of the ability to obtain quantitative perfusion measurements by CMR, with its higher spatial resolution, as well as detailed functional and viability data, within a single examination and without the use of ionising radiation.

Only few studies have compared PET with fully quantitative CMR.

A good correlation between MPR derived from PET and MRI was noted in a study by in which 10 healthy individuals underwent PET and MRI at rest and dipyridamole stress – a linear relationship was found between the two

methods with a correlation coefficient of 0.96 however MRI measurements under-estimated perfusion compared to PET[109].

A key study directly comparing PET and CMR was performed by Morton et al.[111]. A cohort of 41 patients was studied comparing fully quantitative CMR and PET perfusion measurements, performed on independent scanners on the same day. This was the first study comparing a fully quantitative approach to CMR analysis with PET. It was demonstrated that calculation of MPR by the two techniques produced similar values but that absolute stress and rest MPR values differed between the two methods. It has since been suggested that this can be ascribed to differences between approaches to assessing and quantifying perfusion by CMR and PET techniques including specific tracer properties, modelling assumptions, fitting methods and parameter constraints[132].

Miller et al. compared a number of methods described for full quantification of perfusion CMR against rubidium-82 PET in 18 patients, 9 of whom had significant CAD[112]. The median time between studies was 7 days (IQR 4-25 days). The data was analysed on a voxel-wise basis. They showed no significant difference between the methods in terms of myocardial blood flow calculation, though the Fermi method showed the closest correlation with PET values. There was a linear relationship with PET values using all methods however each CMR method under-estimated stress and rest estimates compared to PET. This was largely cancelled out when calculating MPR.

In a very recent study by Engblom et al. 21 patients with stable CAD underwent CMR and [^{13}N]NH_3 PET sequentially, on the same day[113]. Perfusion CMR was analysed quantitatively using methods which will be described in more detail later in the chapter. There was good agreement between global and regional myocardial perfusion and MPR between the two modalities, as shown below in Figure 3.4. Importantly, due to recent technological post-processing advances, this was done using a highly automated CMR analysis pipeline – a factor which has previously limited translation to more widespread use and will be discussed.

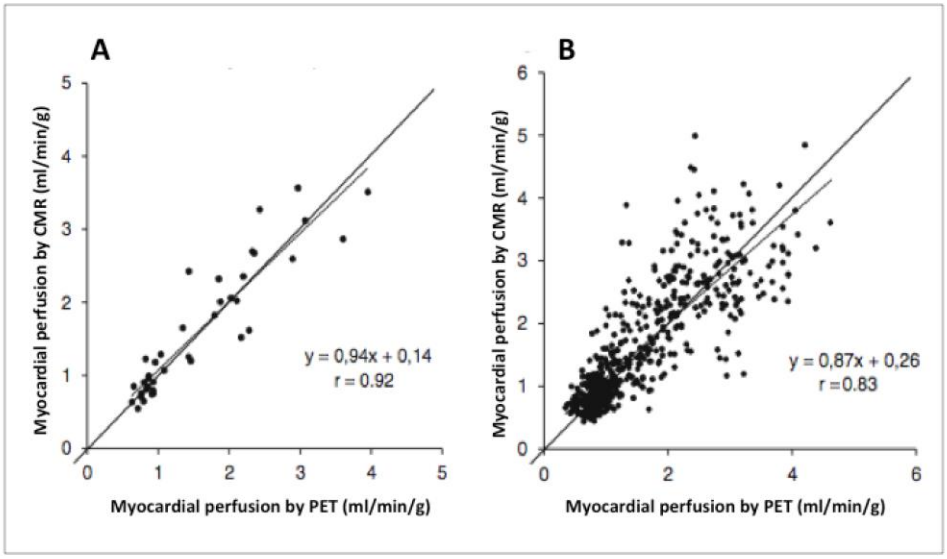

Figure 3.4 – Correlation between fully quantitative CMR and PET

Scatter plot demonstrating a good correlation between quantitative CMR versus PET
A - global myocardial perfusion by CMR versus PET
B - regional myocardial perfusion by CMR versus PET
Adapted from Engblom et al.[113]

In summary, previous studies comparing fully quantitative CMR against PET have suggested that there is a linear relationship between values derived from either modality, with a suggestion that CMR appears to underestimate values by comparison with PET. MPR values obtained by quantitative CMR correlate better than stress or rest values[109-113]. The complex mathematics and tracer properties required in both modalities would appear to have inherent errors which cancel each other out. These aspects require further investigation, refinement and validation.

3.7 Perfusion quantification – where are we now?

The following section is taken from a review article summarising the principles and methods used to quantify perfusion CMR. In the final section of the chapter, an important new approach is described.

3.7.1 Principles of perfusion quantification by CMR

Perfusion quantification is based on the indicator-dilution principle. “A known quantity of an indicator is injected into a fluid flowing at unknown rate through a system of unknown volume. Fluid is sampled or monitored at one or more points downstream from the plane of introduction and the concentration of indicator, diluted by the parent fluid, is measured as a function of time”[133]. In perfusion CMR, the indicator is a gadolinium-based contrast agent injected via a peripheral vein. As the concentration of contrast at the ostium of the coronary arteries is not known, the quantity is estimated by measuring the arterial first-pass time-intensity curve (arterial input function, AIF) in the left

ventricle or ascending aorta. Myocardial blood flow is monitored as a function of the measured myocardial time-intensity curve.

First-pass CMR perfusion series are usually acquired using a dynamic T1-weighted sequence, designed to generate a contrast between areas of stress-induced hyperemic myocardium and areas of relatively reduced perfusion, based on the different speed of inflow of blood and gadolinium over time, as described in the previous chapter.

3.7.1.1 Quantification by signal deconvolution

The relationship between the AIF and the myocardial time intensity curve is defined by the following convolution equation:

$$C_{myo}(t) = C_{AIF}(t) * h(t)$$

where C_{myo} (t) is the myocardial time-intensity curve, C_{AIF} (t) is the arterial input function and $h(t)$ is the myocardial tissue impulse response.

In essence, the arterial input and myocardial input functions are convolved, a mathemetical process, to produce a curve. Myocardial perfusion can be estimated from the above equation by model-based or model-independent signal deconvolution - this is done by producing a large number of curves which are then matched to the convolved signal curve - the best fit represents the h(t) - this is taken as the perfusion rate.

3.7.1.2 Model-based deconvolution

Model-based deconvolution is considerably complex and is based on tracer-kinetic modelling. The circulatory system is divided in different compartments and a transfer constant (K^{trans}) is defined which physiologically reflects the

combination of perfusion, blood volume and capillary permeability to the contrast agent[134]. In most implementations, the intravascular and extracellular compartments are considered, although single-compartment models have also been described by the assumption of a fast exchange of contrast agent between the vessels and the interstitial space during first-pass. The Patlak method[135] is a specific implementation of a single-compartment pharmacokinetic model which has been adapted to perfusion CMR quantification[118].

Model-based deconvolution methods rely on a correct estimate of K^{trans}. This parameter is difficult to assess in-vivo including in animal models. Some preclinical studies have been conducted in canines[136-138]. The different characteristics in microscopic anatomy between the human and canine coronary microcirculation and a number of different physiological factors preclude direct application of assumptions on K^{trans} to human studies.

3.7.1.3 Model-independent deconvolution

Model-independent deconvolution was originally developed for intravascular contrast agents studying brain perfusion. It has gained popularity as an alternative to model dependent deconvolution for myocardial perfusion assessment in the last few years. Perfusion is estimated without considering the tracer-kinetic modelling, using a variety of different deconvolution methods (Fermi function modelling, B-spline basis, exponential basis and autoregressive moving average model – ARMA) to constrain the results.

3.7.1.4 Fermi function modelling

Fermi function modelling appears to be the most favorable method for model-independent deconvolution quantification[139-141]. First proposed by Wilke et al.[142] and Jerosch Herold et al.[143], this method for perfusion quantification is based on the observed similarity between the impulse response, $h(t)$, for an intra-vascular tracer and shape of the Fermi function (Figure 3.5). Fermi function modelling is robust in application to different scanning and modelling parameters. Moreover, this method has been shown to be precise and to have a consistent outcome independent of the spatial resolution level and of the level of noise[141,144].

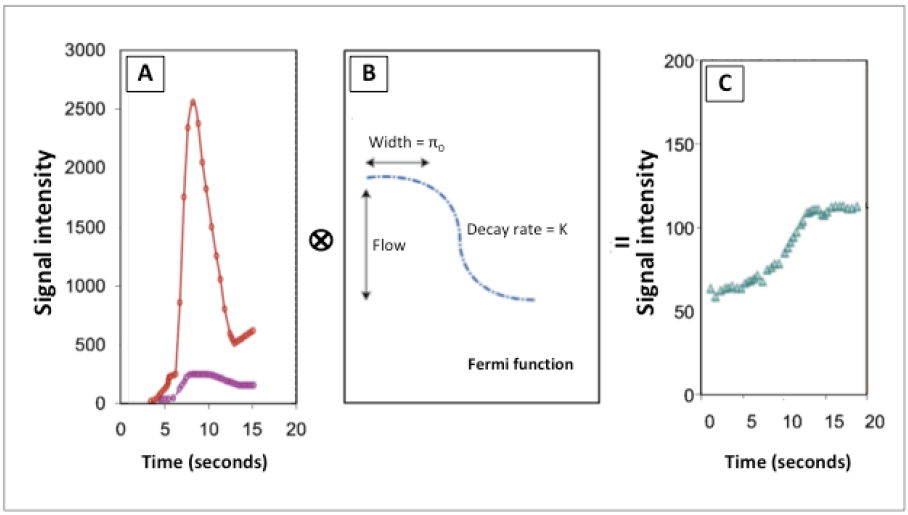

Figure 3.5 – Schematic demonstrating the use of Fermi function deconvolution with a dual-bolus approach

A- The prebolus is made up of 10% full dose according to bodyweight, this can then be multiplied to achieve the predicted peak of the arterial input function without the effect of saturation. To minimize contrast to noise, the signal from the main bolus is used for the myocardial signal.
B- The deconvolution process extracts the myocardial transfer function by iteratively convolving the scaled signal intensity of the LV cavity by using a three-parameter Fermi transfer function until the myocardial enhancement can be predicted
C- The transfer function characterizes the myocardial circulation that transforms the delivery of contrast material into the LV cavity (input) into the observed myocardial enhancement (output).

3.7.1.5 B-spline basis deconvolution

Jerosch-Herold et al.[145] later developed a model-independent deconvolution method based on B-spline functions and stabilized the solution by using Tikhonov regularization. B-spline model-independent deconvolution has been compared with other analysis methods in a number of studies, both for segmental and high-resolution (voxel-wise) quantification[141,144].

3.7.1.6 Exponential basis deconvolution

Exponential functions can be used as the base function for the model-independent deconvolution. Keeling et al. initially used decaying exponential functions in order to estimate perfusion of the brain[146]. This approach has also been validated against a hardware cardiac perfusion phantom, where perfusion values are known, and was demonstrated to provide accurate quantification of myocardial blood flow[147].

3.7.1.7 ARMA (Auto regressive moving average model)

Autoregressive-moving-average (ARMA) modelling is a linear algebraic technique without any direct curve fitting and a limited number of parameters. ARMA approach achieves the required model accuracy with a lower order approximation than other modelling methods[141,144,148]. As a result, ARMA is faster than other methods of analysis and avoids convergence issues.

An accurate comparison of Fermi function modelling with the other algorithms for model-independent deconvolution was made possible by the availability of a novel perfusion phantom, capable of a realistic simulation of myocardial perfusion and providing true validation for absolute perfusion measurements[149]. Sensitivity of all these deconvolution methods to their order and modelling parameter has more recently been tested against simulated data and a blood-perfused explanted pig heart with microspheres[141,150]. This demonstrated that the choice of method and its order depend on several factors including signal-to-noise ratio of the data, computational burden and desired accuracy of the results. The Fermi model was found to be the most favourable as all of the modelling parameters are either fixed or they will be determined during deconvolution process. Moreover it has shown to have good correlation with the real perfusion values. The ARMA model with the correct choice of order was superior to other methods including Fermi with better accuracy and less computational burden.

3.7.2 Saturation effects and contrast agent injection schemes

A number of critical assumptions need to be made in order to enable quantitative perfusion analysis. The indicator-dilution principle can be applied to perfusion CMR quantification under the presumption of a linear dose-signal response for gadolinium during first pass.

Dosages of gadolinium in the range of 0.05-0.1 mmol/kg of body weight are required to generate images with sufficient contrast-to-noise ratio for visual and quantitative analysis. Though single-bolus approaches in this concentration range were previously used with good diagnostic accuracy

compared with invasive coronary angiography and FFR[82]. Ichihara et al. have shown that these can result in significant saturation effects in the AIF[118]. Saturation effects lead to elevated and non-physiological perfusion estimates. For this reason, this approach is not currently considered adequate for accurate quantitative analysis.

Several approaches have been proposed in order to overcome the limitations of first-pass signal saturation effects. Some studies have used lower doses (0.025-0.05 mmol of gadolinium per kg of body weight) of contrast agent in combination with strongly T1 weighted sequences[143,151]. Despite a reduction in saturation effects, this approach is limited by the low myocardial contrast-to-noise ratio. Others have proposed strategies to correct for signal saturation using magnetization modeling[152,153].

3.7.2.1 Dual-bolus

Currently, the most commonly implemented approach is the dual-bolus method. This consists of a combination of the low and high dosage approaches, using two consecutive injections of contrast agent. The first low dosage injection enables the acquisition of a non- saturated AIF. The second high-dosage injection elicits a sufficient myocardial signal response for visual and quantitative assessment[154-158]. This approach has been shown to permit accurate perfusion estimates[155] but can potentially be limited by the need for a state-of-the-art gadolinium injector and more patient preparation time. In addition it is more prone to blurring by respiratory motion over the time taken to acquire the images. Ishida et al.[130] devised a universal dual-bolus injection scheme that resolves these issues and can be easily employed in a clinical

setting. The dual-bolus approach is based on a combination of a bodyweight-adjusted and high-dose main bolus of contrast agent preceded by the injection of a low dose pre-bolus having the same volume of the bolus and only 10% of the concentration of gadolinium. The injector is filled with saline solution. Both the pre-bolus and the main bolus are loaded using a 3-way tap in a large bore tube connected between the injector and the patient. A 25-second pause was found to be a near optimal delay between the first and the second injection, avoiding overlap between the first and the second bolus while minimizing the duration of the acquisition (see Figure 3.6).

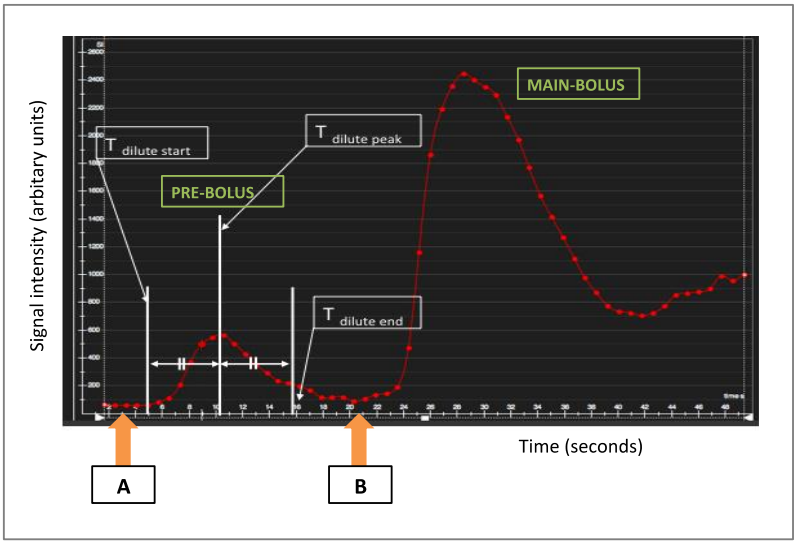

Figure 3.6 - Schematic showing the dual bolus approach

Prebolus (10% concentration) is given at Point A.
After a 25 second pause the main bolus (Point B) is given.

3.7.2.2 Dual-sequence

An alternative to the dual-bolus approach is the dual-sequence method. The dual-sequence approach is simple to use since AIF saturation is avoided at the time of image acquisition and it allows optimization of parameters for

blood and myocardium. In each cardiac cycle a low-resolution image is acquired to measure the AIF with a short saturation-recovery time after the R-wave. This is then followed by the acquisition of high-resolution images with longer saturation-recovery time to measure the myocardial signal with high contrast. In order to quantify perfusion, the signals must be converted to Gadolinium concentration units (using Bloch simulation look-up table correction, and for the arterial input function, also correction for T2* recovery) in order to have common scaling between AIF and myocardial signals. The signals can then be convolved - from here, the same deconvolution process as described above can be used whereby many simulated curves are produced and the best fit curve represents perfusion. The dual-sequence method has been shown to provide accurate measurement of the AIF when using high-dose and single-injection protocols and has the potential to become the preferred protocol of acquisition[131,159,160]. Dual-sequence protocols are not yet available from all vendors and this is likely to be the main factor limiting its application.

3.7.3 High-resolution sequences and quantification

Important physiological factors could limit the clinical application of quantitative perfusion. These factors are mainly related to the spatial resolution used for the acquisition and for the analysis of the data.

Myocardial ischaemia affects the inner (endocardial) layers of the LV wall myocardium earlier and more severely than the outer (epicardial) layers[161]. Perfusion CMR has an intrinsically high spatial resolution - higher than SPECT and PET. This enables the independent visualization of multiple

transmural myocardial layers and therefore visualization of subendocardial ischaemia[83,162]. Visual assessment enables a highly accurate diagnosis of haemodynamically significant CAD[90,92,93,163]. Visual assessment exploits the high spatial resolution of CMR perfusion images, identifying areas of subendocardial delayed and reduced signal intensity relative to the epicardial layers and to normal neighbouring segments. Subendocardial localization of perfusion defects and the epicardial to endocardial wash-in of signal during first pass are features that help to identify true perfusion defects.

A few studies have demonstrated the advantages of using high-resolution perfusion CMR sequences in comparison with standard sequences when visual assessment is used to make a diagnosis[164,165].

When segmental quantitative analysis is performed from these high-resolution images, the spatial resolution of the images is only partially exploited as the signal intensity is sampled from transmural areas of myocardium or from the inner (subendocardial) half of the LV myocardium. The time intensity curves from subendocardial ischaemic areas are averaged in variable proportions with signals originated in more superficial and likely less ischaemic layers, resulting in partial-volume effects and reduced sensitivity.

In order to preserve the improved spatial resolution enabled by CMR when quantifying, high-resolution quantification has been proposed by Zarinabad and Chiribiri et al.[166] and by Hsu et al.[140]. High-resolution, voxel-wise myocardial perfusion quantification allows for the detection of subendocardial perfusion abnormalities and offers additional information on the heterogeneity of myocardial perfusion. Moreover, the combination of absolute quantification and preserved high-resolution has the potential to allow calculating the true

ischaemic burden (a combination of severity and extent of myocardial ischaemia), limiting partial volume effects or the influence of other factors such as the geometry of the LV wall. This is particularly important in patients with LV hypertrophy or previous infarcts. Moreover, high-resolution, voxel-wise quantification has the potential to enable quantitative perfusion assessment also in patients with heart failure, regardless of remodelling and thinning of the LV wall.

A potential limitation of high-resolution, voxel-wise quantification is the low signal-to-noise ratio typical of high-resolution datasets. This could result in inaccuracies of myocardial blood flow quantification or make quantification impossible. Simulations performed on patients' data however have shown that voxel-wise analysis offers the most accurate diagnostic results and that the potential loss of diagnostic information due to the decreasing signal-to-noise ratio is counterbalanced by preserving the spatial information regarding presence and distribution of ischaemia[144].

3.7.4 Factors limiting the clinical translation of quantitative perfusion

Over recent decades perfusion CMR imaging sequences have become more sophisticated. This has offered the ability to visually assess perfusion abnormalities more precisely. In parallel, various dosing regimes, acquisition protocols and analysis algorithms focusing on quantitative analysis have been developed. Despite validation of perfusion CMR quantitative analysis against invasive measures such as FFR[82,152,167,168], against microspheres[140,155] and

more recently against PET[111-113] there remain very few patient studies in the literature. Quantitative perfusion analysis is superior to visual assessment in the evaluation of patients with advanced multi-vessel CAD[120]. Further study on other patient groups is warranted to establish further beneficial applications of quantification. More recently, Mordini et al. have shown that quantitative stress perfusion CMR outperforms semi-quantitative measures of perfusion and visual assessment in comparison with quantitative coronary angiography. These findings suggest a potential clinical role for quantitative stress perfusion CMR[169].

The main obstacle to more widespread implementation of quantitative perfusion CMR is the lack of standardisation. There is heterogeneity in acquisition and dosing protocols, analysis methods and software available for post-processing across centres. There is now a reasonable body of work to support a standardized approach to drive this forward. Table 1 summarises the evidence from the literature on quantitative perfusion CMR (shown at end of chapter).

This table underlines the limited number of studies including human subjects assessed with quantitative analysis and the heterogeneity of reference standards and deconvolution algorithms. Most of these studies included healthy volunteers and appraised the technical feasibility of quantitative perfusion rather than the clinical usefulness.

From the point of view of acquisition, dual-bolus protocols can already be used in most centers without the need to acquire new software or hardware, with the drawback of a slightly higher complexity in the preparation of the scan. Dual-sequence protocols are simpler to implement and have the

potential to become the preferred acquisition protocol for quantitative perfusion assessment but widespread use remains limited by availability of specialized hardware on cardiac scanners.

While Fermi function modelling appears to be the most accurate method for model-independent deconvolution and the optimal analysis parameters have been validated[141,144], each centre relies on a different implementation, custom filtering and modelling parameters. Moreover, the lack of commercial software is road-blocking for centres that do not have significant expertise in signal processing and the capability to build their own software tools. This is coupled with the need for expertise to implement a robust approach to quantitative analysis in a centre. Arguably the development of a standardized approach would enable user-independent, and ultimately more reproducible analysis, which would be less reliant a clinician with years of experience.

High-resolution, voxel-wise perfusion assessment enables the assessment of the true ischaemic burden and is soon likely to become the preferred method for quantitative CMR perfusion analysis, particularly if coupled with full LV coverage enabled by 3D perfusion sequences[170-172]. The optimal diagnostic criteria to recognize prognostically relevant ischaemia using these novel methods will need to be explored further with clinical studies.

3.7.5 In-line quantitative myocardial perfusion mapping

Since publication of this review, Peter Kellman's group has reported an important development in perfusion quantification. This uses a dual sequence approach and runs on the MRI scanner. It is able to produce fully automated, high-resolution (voxel-wise), almost instantaneous (within 1.5 minutes) MBF

maps. The process is implemented via the open-source Gagetron framework[173] and integrated inline on the scanner with motion-corrected perfusion images to produce stress, rest and MBF maps without any user interaction.

This method has been validated in an MRI phantom, small numbers of healthy volunteers and patients. It has been shown to be feasible and reliable with low variability of calculated perfusion estimates[159]. One study used a phantom to validate signal correction[159], and tested the method in healthy volunteers[159]. A second study (previously described above) by Engblom et al.[113] compared perfusion measurements from PET to CMR.

This analysis pipeline is currently only deployed on selected scanners and is currently only available via one scanner provider. Nevertheless, this development has the potential to make perfusion quantification significantly simpler, faster and available to less expert centres and will be a major step in the more widespread use of quantitative perfusion CMR clinically.

3.8 Conclusion

Accurate quantification of perfusion has been the goal of many investigators for over two decades. Over this period, numerous imaging protocols, contrast agent dosage schemes and analysis methods have been developed. Regrettably, this has resulted in a lack of standardization which has hindered more widespread application, including multi-centre collaboration and comparisons. Quantification has been well validated against a number of invasive and non-invasive methods. The recent development of rapid, fully

automated quantification of perfusion represents a significant step towards translation to the clinical setting.

Part of this chapter consists of work that has been published:

***Sammut, E.,** Zarinabad, N., Vianello, P., Chiribiri, A.*

'Perfusion quantification – where are we now?'

Current Cardiovascular Imaging Reports, 2014 (http://doi 10.1007/s12410-014-9278).

Eva Sammut is first author on the publication and was responsible for literature review and draft of the manuscript.

Table 1 - Summary of Pubmed results on quantitative perfusion CMR (2014)

Author, Reference	Number of human subjects	Reference standard used	Deconvolution method used	Key findings
Miller et al. JCMR 2014[112]	9 patients with significant CAD, 9 healthy volunteers	Rubidium-PET (patients only)	Fermi function deconvolution, TSVD, first-order Tikhonov regularisation with b-spline	Complex quantification gives similar MBF estimation compared to simple factors such as AIF location and inter-observer variability. Under-estimation of estimated MBF with deconvolution compared to PET findings.
Mordini et al. JACC Imaging 2014[169]	67 patients referred for assessment of myocardial ischaemia	Invasive coronary angiogram	Fermi function deconvolution	Fully quantitative analysis has high diagnostic accuracy for detecting obstructive coronary artery disease and outperforms semi-quantitative

				measures and qualitative methods.
Chiribiri et al. JACC Imaging 2013[129]	67 patients referred for assessment of myocardial ischaemia, training group 30 patients	Invasive coronary angiography with FFR (in vessels with visual stenosis >50%)	N/A	Transmural perfusion gradients threshold of 20% has similar accuracy to visual assessment Significant correlation with FFR findings to identify haemodynamically-significant coronary stenosis.
Morton et al. JACC 2012[111]	41 patients referred for assessment of myocardial ischaemia	N13-Ammonia PET, invasive coronary angiography	Fermi function deconvolution	Good correlation between myocardial perfusion reserve PET and CMR and similar accuracy in detecting significant stenosis. Weak correlation between absolute perfusion values from PET and CMR.

Zarinabad et al. MRM 2012[141]	5 patients with suspected CAD, 2 healthy volunteers	Invasive coronary angiography	Fermi function, b-spline, exponential, ARMA deconvolution	Voxel-wise quantitative analysis is feasible and can detect areas of abnormal myocardial perfusion. Highest error seen with B-spline method. Fermi most robust method to noise.
Hsu et al. JACC 2012[140]	5 patients with confirmed CAD, 1 healthy volunteer	Invasive coronary angiography	Model-constrained deconvolution	Myocardial blood flow can be quantified on a pixel-level. Good correlation of method against microspheres (preclinical component)
Patel et al. JACC 2010[120]	41 patients with abnormal nuclear stress scan	Invasive coronary angiography	Fermi function deconvolution	Quantitative analysis differentiates moderate from severe coronary stenosis. Superior to visual assessment.

				Improved inter-observer agreement with quantitative compared to visual assessment.
Cullen et al. JACC 1999[174]	20 patients with angiographically proven CAD; 5 normal volunteers	Invasive coronary angiography	Tracer kinetic model	Possible to differentiate normal subjects from patients with CAD and may help decide significance of coronary lesions.

Papers using quantitative perfusion CMR in human subjects from Pubmed. The list of studies was retrieved using the following query: “("heart"[MeSH Terms] OR "heart"[All Fields]) AND ("perfusion"[MeSH Terms] OR "perfusion"[All Fields]) AND “deconvolution”[All Fields]” – last interrogation 17 April 2014.

4 Feasibility of perfusion CMR in heart failure

4.1 Introduction

This chapter will consider the use of perfusion CMR in the setting of heart failure. The evaluation of myocardial perfusion status in patients with HF can be challenging due to the LV remodelling and wall thinning, the presence of scar, and respiratory artefacts.

In this chapter we present a study of the use of high-resolution quantitative perfusion CMR in patients with heart failure, who have thinned and remodeled ventricles. We have put forward the hypothesis that, using higher spatial resolution sequences combined with higher resolution analysis, the assessment of quantitative perfusion is feasible – meaningful and reproducible - even in patients with heart failure with thin walled and remodeled ventricles. Eva Sammut is first author on the publication and contributed to the study design, experimental work and draft/review of the manuscript.

4.2 Aetiology of heart failure

Around 900,000 individuals in the UK currently have heart failure and almost as many patients have evidence of damaged hearts while not displaying the clinical features of heart failure. The recorded incidence and prevalence of heart failure have been steadily increasing. This is due to a combination of improved diagnostic tests and better treatment, and survival, of patients with acute myocardial infarction as well as an ageing population generally.

Heart failure is a complex clinical syndrome produced by impaired pumping or compliance of the heart. This leads to failure in the form of either reduced

ejection fraction (HFrEF) or with preserved ejection fraction but reduced relaxation (HFpEF). Either will produce the same collection of clinical signs and symptoms with evidence of fluid overload but the underlying pathophysiology is significantly different. HFpEF is attracting increasing interest, but the bulk of previous work has focused on HFrEF and this is most pertinent to the work of this thesis and will be considered here – henceforth, the term heart failure will be used to refer to HFrEF.

4.2.1 Ischaemic cardiomyopathy

The most common cause of heart failure is coronary artery disease – namely ischaemic cardiomyopathy. Occlusion of a coronary artery causes scarring of the ventricular wall and this region will not contract normally, resulting in reduced pumping action of the heart. The concept of myocardial 'stunning' is worth mentioning – an area supplied by an occluded artery will, in the acute phase after revascularisation, be hypocontractile and when re-examined at a later stage will show signs of partial or complete improvement. Myocardial 'hibernation' is also recognised - an ischaemic region will downregulate its contraction in order to match its function to the reduced available oxygen. As discussed previously, the subendocardium is most susceptible to ischaemic insult and the scar pattern seen in ischaemic cardiomyopathy reflects this with a pattern of late gadolinium enhancement extending from the subendocardium to transmural in regions supplied by a coronary artery. The specific segments supplied by each coronary artery can vary from person to person but are fairly consistent overall (see Figure 4.1).

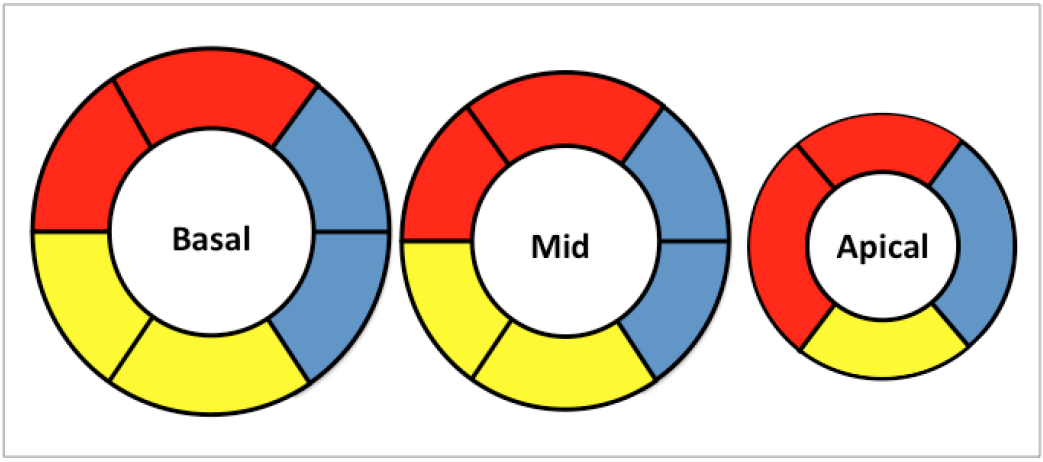

Figure 4.1 - Schematic diagram showing the typical distribution of myocardial territories

Schematic diagram showing the typical distribution of myocardial territories according to coronary artery in AHA 16-segment model.
(Red –Left anterior descending artery, Yellow – Right coronary artery, Blue – Circumflex artery)

Late gadolinium enhancement imaging is used to identify the radial and transmural extent of scar. This allows assessment of viability if revacsularisation is performed i.e. the likelihood of recovery of a segment with impaired contractility. The concept of viability is based principally on a paper by Kim et al.[181]. This used an instrumented canine model to investigate the association between transmurality of scar and recovery after revscularisation. They demonstrated that in those with <25% transmurality LGE there was good functional recovery, but that >75% transmurality there was poor recovery, with an almost 50:50% chance of recovery in those with around 50% transmurality as shown below (Figure 4.2).

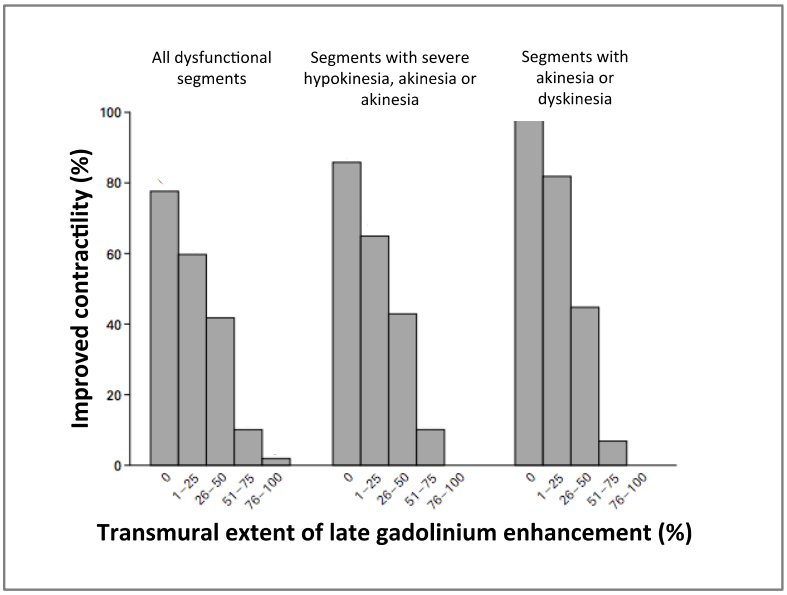

Figure 4.2 – Bar graph of relationship between LGE and improvement in contractility after revascularization

Bar graph showing relationship between transmural extent of LGE before revascularisation and likelihood of improved contractility after revascularisation (804 dysfunctional segments, 462 segments with at least severe hypokinesia and 160 segments with dyskinesia or akinesia)
Adapted from Kim et al.[181]

4.2.2 Non-ischaemic cardiomyopathy

Non-ischaemic cardiomyopathies encompass a range of non-coronary related conditions which also cause impairment of systolic function. This term encompasses: idiopathic dilated cardiomyopathy; alcohol or toxin related cardiomyopathy; or genetically induced dilated cardiomyopathies. The pattern of scar in non-ischaemic cardiomyopathies differs from that seen in ischaemic cardiomyopathy. One may find no late gadolinium enhancement or there may be mid or epicardial scar or fibrosis at the superior and/or inferior LV-RV insertion points. In addition, if scar is present it will not correspond to a coronary artery territory.

Morphologically, aside from scar, in both ischaemic and non-ischaemic cardiomyopathy there is progressive chamber dilatation which may lead to functional valvular regurgitation. Typically, there is thinning of the ventricular wall thickness with overall increase in LV mass – a process known as eccentric remodelling.

4.3 Perfusion CMR in heart failure

4.3.1 Spatial resolution

Within the field of perfusion CMR, several technical developments have refined the sequences. The use of an advanced sequence such as *kt* sensitivity encoding and a 3-Tesla scanner allows considerable improvement in spatial resolution with improved image quality, signal-to-noise, contrast-to-noise and reduction in the transmural extent of dark-rim artefacts compared to standard imaging sequences, particularly at 3T, in patients with normal LV function[164,165,182,183].

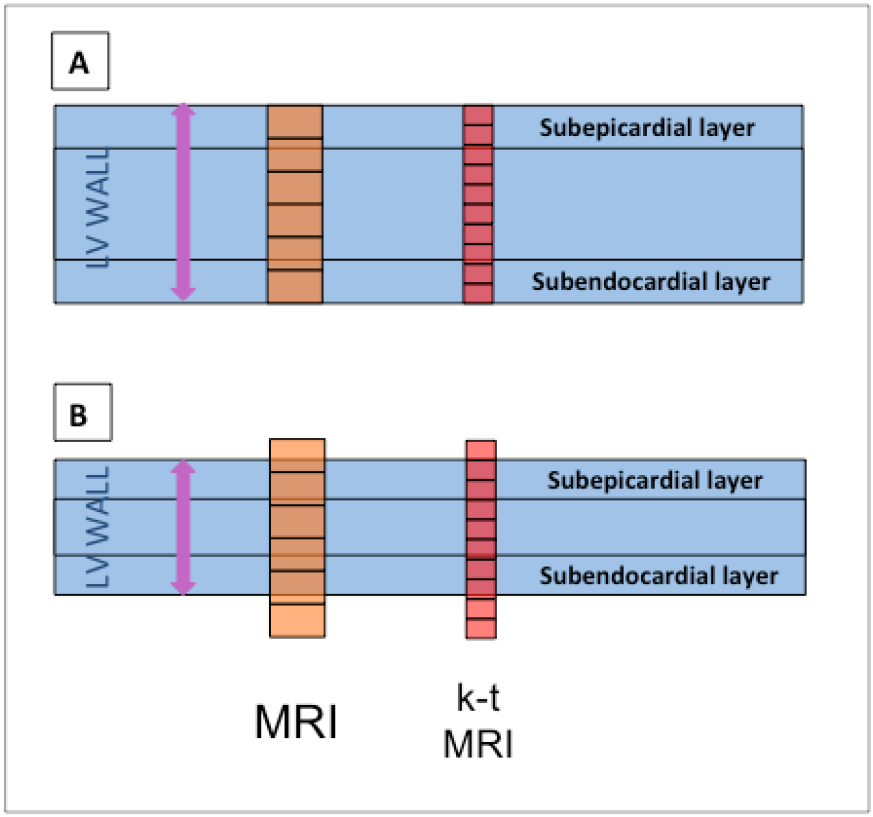

Figure 4.3 - Schematic showing importance of a high resolution technique in patients with heart failure

Schematic showing importance of a high resolution technique in patients with heart failure with thinned ventricular walls - A – Shows a normal left ventricular thickness where both standard and high resolution CMR are able to differentiate the myocardial layers, B – Shows reduced left ventricular wall thickness to demonstrate that a higher resolution technique is better able to appreciate these layers.

4.3.2 Voxel-wise analysis

Furthermore, advances in the quantification methods have allowed analysis on a voxel, rather than segmental level. This approach has the potential to capture more detailed information on the location, extent and transmurality of coronary perfusion with less impact from spatial averaging effects but comes with possible compromise of lower signal to noise.

A previous study by Schuster et al. used an explanted porcine model to evaluate a voxel-wise approach and high-resolution CMR sequence compared to microspheres, the invasive reference of coronary perfusion[184]. It was shown that this was feasible and was able to distinguish between normal and hypoperfused myocardium. The values obtained for segmental analysis compared well to microsphere data at both 1.5- and 3-Telsa The same group used an explanted pig heart model to investigate the different deconvolution quantification algorithms using a voxel-wise approach and found that all methods appear to correlate well with MBF by microspheres. Others studied patients with voxel-wise perfusion and compared results to PET and found that all methods compared similarly though all underestimated MBF compared to PET[111-113]. In a study by Hsu et al. an experimental canine model was used to evaluate voxel-wise perfusion maps and again showed correlation though a degree of under-estimation compared to microsphere data. In the same study, a group of patients with significant CAD showed regional blood flow decreases and transmural perfusion gradients in territories served by stenotic coronary arteries[140]. In a more recent study, Villa et al. used a high-resolution imaging sequence and analysed patients with hypertrophic cardiomyopathy using voxel-wise perfusion assessment combined with voxel-wise scar correction and showed that this combined approach improves sensitivity of detection of quantitative perfusion analysis by reducing the under-estimation of MPR through scar-related hypoperfusion[185].

4.3.3 Respiratory artefacts

Perfusion assessment in patients with HF can be further complicated by a well-recognised irregularity in respiratory motion and reduced tolerance to breath-holding[186-188]. These are also key components to obtaining diagnostic-quality images. In a study by Morton et al.[164] whilst showing that visual analysis was superior with a higher-resolution sequence with better image quality, signal to noise and contrast to noise, there was a non-significant trend towards more respiratory artefact with the high-resolution sequence.

4.4 Feasibility of high-resolution quantitative perfusion analysis in patients with heart failure

The combination of a high-resolution sequence with voxel-wise quantification has the potential to assess perfusion even in the context of reduced LV wall thickness however it has been raised as a concern that respiratory artefacts may limit the use of these sequences in heart failure patients. We recognised the importance of a specific study into the use of perfusion quantification in this group of patients. Our aim, in the following study was to test the feasibility of 3T *kt* high-resolution and voxel-wise quantitative perfusion CMR in a group of patients with heart failure.

4.4.1 Methods

We identified a group of patients referred for perfusion CMR to assess HF aetiology. Consecutive patients from one scanner at our site were selected where a dual bolus contrast regime and stress and rest images were acquired.

Patients were then retrospectively classified on the basis of the aetiology of HF as ischaemic (LVEF<50% with scar arising from the subendocardium or transmural in a location corresponding to a coronary territory) or non-ischaemic (LVEF<50%, either no scar or mid-myocardial or epicardial scar [189]. A group of patients with normal LV function (LVEF >50%) referred with suspected coronary artery disease were used as control subjects. Patients with normal LV function and ischaemic cardiomyopathy included underwent a coronary angiogram either before or after the CMR scan.

All included patients provided written consent (09/H0802/78) and the study was conducted in accordance with the Declaration of Helsinki.

4.4.1.1 Imaging parameters

Images were acquired on a Philips Achieva 3T (TX) system, equipped with a 32-channel cardiac phased array receiver coil (Philips, Best, the Netherlands). First pass perfusion imaging consisted of a high-resolution *kt* turbo-gradient echo sequence (imaging parameters: shortest echo time (range 1.35 to 1.54ms), shortest repetition time (range 2.64 to 3.12ms), 18° flip angle, 90° saturation prepulse, 120ms prepulse delay, typical TR 2.6ms, typical TE 0.9ms, typical spatial resolution 1.2x1.2x10mm.

Three short-axis slices (basal, mid and apical) were acquired during each heartbeat, covering 16 of the standard myocardial segments (segment 17 was excluded). Stress imaging preceded rest imaging by 14±2min (range 10 to 19 min). To acquire stress imaging, 140 μg/kg/min of adenosine was administered intravenously for 4 min. Imaging commenced 3 min into the infusion and continued during the acquisition of the images. Perfusion data was acquired during first pass injection of 0.075mmol/kg Gadobutrol (Gadovist, Schering,

Germany) at 4ml/minute followed by a 20ml saline flush. A dual bolus contrast agent scheme was used to correct for signal saturation of the arterial input function as previously described[130]. The CMR scan protocol included late gadolinium enhancement imaging for all subjects after a top up dose of contrast agent to a total dose of 0.2 mmol of gadolinium/kg of body weight in accordance with SCMR guidelines[190].

4.4.1.2 Visual analysis

The studies were analyzed visually by two independent experts blinded to all other data. CMR scans were classified positive for ischaemia in the presence of a perfusion defect (>60 degrees in either the basal or mid-ventricular slices, or >90 degrees in the apical slice) which was transmural, or involving ≥2 adjacent myocardial segments according to the criteria set out by Hussain et al.[95]. In cases of disagreement, the observers reviewed the images together and a consensus was reached. Late gadolinium enhancement and rest perfusion scans were then used to differentiate between stress-induced perfusion abnormalities and scar-related perfusion defects.

4.4.1.3 Quantitative analysis

An experienced operator, blinded to visual assessment and other clinical data, performed quantitative analysis using software and methods developed and previously validated against phantom and PET data[111,141]. The implementation of high-resolution signal intensity (SI) analysis required accurate respiratory motion correction and myocardial contour delineation. Respiratory motion was corrected using affine image registration by maximization of the joint correlation between consecutive dynamics within an automatically determined region of interest. A temporal maximum intensity projection was calculated to serve as a

feature image for automatic contour delineation. The operator then manually optimized the automatically generated contours to avoid partial volume effects at the endocardial and epicardial border, as previously described[147]. Areas of subendocardial dark-rim artefact occurring at the point of arrival of the main bolus of contrast agent in the LV were carefully selected and excluded from the segmentation.

Quantitative perfusion analysis was performed by Fermi deconvolution according to the methods described by Wilke et al.[142] and Jerosch-Herold et al.[143] where time curves for the tissue impulse response function, *h(t)*, were fitted to the Fermi function with the following analytical expression:

$$h(t) = R\left[\frac{1}{e^{(t-\tau_0-\tau_d)k}+1}\right] u(t-\tau_d)$$

using a Marquardt-Levenberg nonlinear least square algorithm by letting *k, R* and τ_0 vary and keeping τ_d fixed. In the above equation $u(t-\tau_d)$ is the unit step function. The τ_d accounts for the delay time between the appearance of the signal in the LV blood pool and myocardial region of interest (ROI)[166]. τ_0 characterizes the width of the shoulder of the Fermi function during which little or no contrast agent had left the ROI. *R* is the index of contrast agent influx parameter and k represents the decay rate of $h(t)$ due to contrast agent washout. Using the above equation, myocardial blood flow (MBF) estimates are calculated as $h(t)$ at $t = 0$.

Myocardial perfusion reserve (MPR) was calculated by division of stress perfusion rate by rest perfusion rate.

In addition, voxel-wise MPR results from the epicardial half (outer 50% transmural thickness) and from the endocardial half of each segment (inner 50%

transmural thickness) were averaged and the endocardial to epicardial CFR ratio (endocardial MPR/epicardial MPR) was calculated.

4.4.1.4 Image quality

A visual score was given for image quality of each dataset using a four-point scale: 1—poor, 2—fair, 3—good, and 4— excellent. The severity of respiratory artefacts and dark rim artefacts were also scored on a four-point and three-point scale respectively. For respiratory artefacts: 1 – non-diagnostic; 2 – severe artefacts but diagnostic; 3 – mild artefacts; 4 – no artefacts. For dark rim artefacts: 1 - circumferential; 2 - segmental; 3 - absent.

4.4.1.5 Statistical analysis

Data is presented as mean and standard deviation. Group means were compared using paired and unpaired Student *t* test and 1-way ANOVA as appropriate. The statistical analyses were performed using PASW software for Macintosh (IBM, Chicago, Illinois, version 21). Mann-Whitney and Chi-squared tests were used to test the qualitative measurements for statistical significance, with a p value threshold of 0.05.

4.4.2 Results

A total of 91 subjects were studied. This included 58 patients with HF (LVEF 39±10%) and 33 patients with normal LV function (Normal LV group) (LVEF 64±5%). In the HF group, on the basis of the CMR scan, 30 patients (51.7%) had a final diagnosis of ischaemic cardiomyopathy (ICM) and the remaining 28

subjects had a final diagnosis of non-ischaemic cardiomyopathy (NICM). Demographics and CMR structural findings are given in in Table 2 (shown at end of chapter).

4.4.2.1 Visual analysis

In the ICM group, 25/30 (83%) patients showed evidence of a perfusion abnormality. Of these 19/25 (76%) patients showed stress-induced perfusion abnormalities, either extending beyond an area of scar or in an area served by a separate coronary territory. On segmental analysis, there were 73 segments showing stress-induced perfusion abnormalities (4.06±2.05/patient). 90 segments showed scar-related perfusion abnormalities (4.29±2.13/patient).

In the NICM group, no visual perfusion abnormalities were reported and 7/28 patients (for a total of 25 segments) showed late enhancement with a non-ischaemic-pattern[189].

15/33 (46%) patients in the Normal LV group showed stress-induced perfusion abnormalities, with a total number of 105 positive segments (6.4±4.5/ patient). No patients from the Normal LV group showed scar on late gadolinium enhancement images.

4.4.2.2 Quantitative analysis

4.4.2.2.1 Stress and rest perfusion estimates

Detailed results of stress and rest quantitative analysis are reported in Table 3 (shown at end of chapter). No significant difference in visually normal segments was observed between groups, with an average stress perfusion rate of

2.2±1.0ml/g/min in the ICM group, 1.9±0.8ml/g/min in the NICM group and 2.3±1.3ml/g/min in the Normal LV group (p= 0.18).

In the ICM group, there was a significant difference in stress perfusion rate between visually normal and abnormal non-scarred segments (2.2±1.0ml/g/min vs 1.8±0.9ml/g/min, p=0.02). The presence of ischaemic scar was associated with significantly reduced perfusion rate compared to visually normal segments (1.5±0.8ml/min vs 2.2±1.0ml/g/min; p=0.005).

Within the Normal LV group, the difference in stress perfusion rate between visually normal and abnormal non-scarred segments was less pronounced and not statistically significant (2.3±1.3ml/g/min vs 1.6±0.8ml/g/min, p=0.08).

There was no significant difference in stress perfusion values between the ICM and Normal LV groups in visually abnormal segments (p=0.47).

Examples of high-resolution, voxel-wise perfusion maps are given in Figure 4.4 and Figure 4.5.

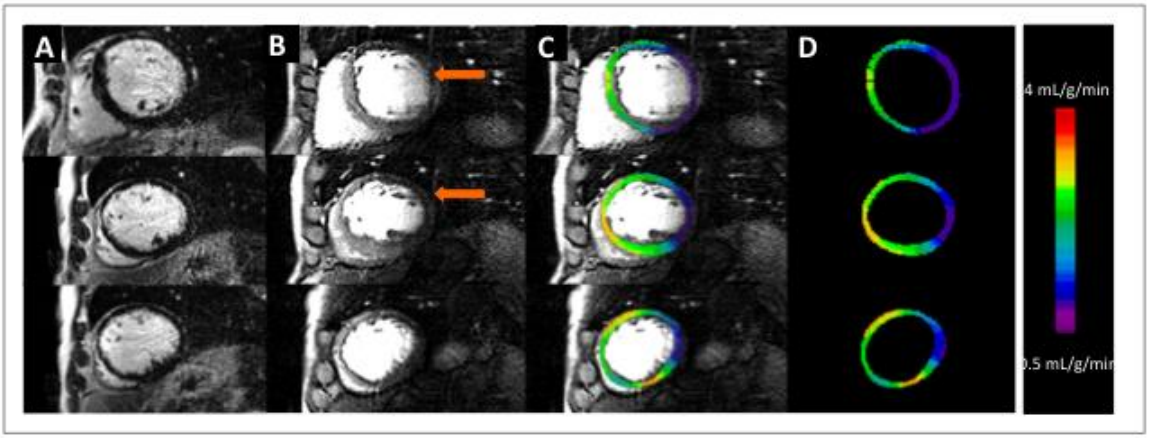

Figure 4.4 - Perfusion images from a heart failure patient

Images from a heart failure patient with a circumflex artery lesion causing a perfusion abnormality extending from base to mid to apex (from top to bottom row). Images in column B show perfusion images, column D shows perfusion maps, column C shows the superimposed images. Column A shows the corresponding late gadolinium enhancement images. Note the respiratory artefact (orange arrows).

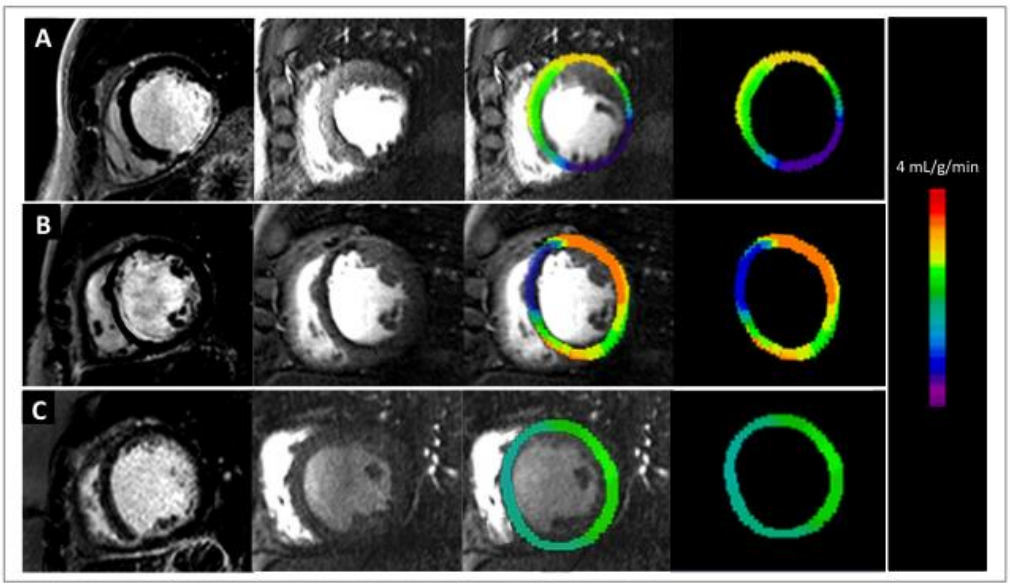

Figure 4.5 - Perfusion images seen from three different heart failure patients

Perfusion images seen from three different heart failure patients (rows A-C).
Acquired CMR perfusion image in second column, perfusion map in far right column and superimposed images in third column Corresponding late gadolinium images in far left column. Row A shows thinning of the mid inferior wall with matched ischaemia in the territory of the RCA, Row B shows a perfusion defect in the LAD territory matched to subendocardial scar. Row C shows homogenous perfusion in a patient with a dilated and remodelled ventricle.

4.4.2.2.2 Myocardial perfusion reserve

Detailed results of MPR analysis are also reported in Table 3 (shown at end of Chapter).

No significant difference in visually normal segments was observed between groups, with an average MPR of 2.3±0.8 in the ICM group, 2.2±0.9 in the NICM group and 2.6±1.1 in the Normal LV group (p= 0.19).

In the ICM group, there was a significant difference in MPR between visually normal and abnormal non-scarred segments (2.3±0.8 vs 1.8±0.9, p=0.04). The presence of ischaemic scar was associated with significantly reduced perfusion reserve compared to visually normal segments (1.68±0.08 vs 2.3±0.8, p=0.004).

Similarly, within the Normal LV group, the difference in MPR between visually normal and abnormal non-scarred segments was statistically significant (2.6±1.1 vs1.7±0.8, p=0.04).

There was no significant difference in MPR values between the ICM and Normal LV groups in visually abnormal segments (p=0.62).

4.4.2.2.3 Endocardial-epicardial CFR ratio

There was no significant difference in the endo-epi MPR ratio in visually normal segments across groups with an endo-epi MPR ratio of 1.05±0.16 in ICM patients, 1.02±0.04 in NICM patients and 1.00±0.06 in Normal LV patients (p=0.57).

There was a significant difference in endo-epi CFR ratio between visually normal and visually abnormal non-scarred segments in both the ICM and

Normal LV groups (ICM group: 1.04±0.09 versus 0.96±0.12 respectively, p=0.02; Normal LV group: 1.00±0.05 versus 0.93±0.06 respectively, p=0.02).

4.4.2.3 Coronary angiography

The results of invasive coronary angiography and perfusion CMR in relation to coronary artery territories, including Kappa results, are detailed in Table 4.

4.4.2.4 Image quality

Detailed results of overall image qualitative assessment, respiratory arterfacts and dark rim artefacts are given in Figure 4.7 and in Table 5 below. No significant differences were observed between groups. The average angular extent of dark rim artefact was 27° (range 9-41°).

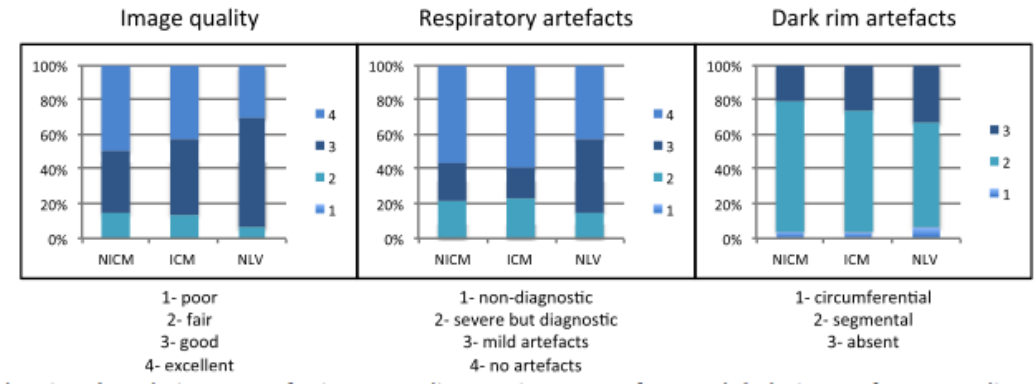

Figure 4.6 – Figure showing the relative scores for image quality

Figure showing the relative scores for qualitative image quality, respiratory artefacts and dark rim artefacts according to group.

Table 5 - Table showing results of the Chi-squared tests for qualitative assessment of image quality according to group

	Chi-square	P value
Overall image quality	2.559	0.6342
Respiratory artefacts	5.359	0.2524
Dark rim artefacts	1.863	0.7609

4.4.3 Discussion

This study revealed a number of novel findings. Most importantly, it demonstrated the feasibility of quantitative first-pass perfusion analysis in patients with heart failure using a combination of high-resolution *kt* 3T acquisition methods and high-resolution voxel-wise quantification. There were significant differences of MPR between visually normal and abnormal segments in both ICM and Normal LV groups. In the ICM group stress perfusion values were also statistically significant between visually normal and abnormal segments. This was not the case in the Normal LV group. This could be explained by the relatively low number of subjects positive for ischaemia included in the study. It is in keeping with previous validation studies that compared CMR perfusion and PET, showing good correlation for MPR values and weaker correlation for absolute stress perfusion values. This may relate to differences in the methods used for quantification such as the tracer properties,

model assumptions, fitting methods and parameter constraints. MPR cancels out a degree of variability and this may help explain our results[132].

CMR is now well established for the evaluation of patients with coronary disease and heart failure. Perfusion CMR is increasingly used to determine aetiology of heart failure and to plan patient management. Further, CMR is now well established for the evaluation of patients with CAD. The detection of ischaemia is rapidly becoming one of the main indications for CMR examination[108]. Studies have also shown that even in non-ischaemic cardiomyopathy the presence of ischaemia has implications for the occurrence of adverse events[191,192].

As described, perfusion CMR has been previously shown to be at least as accurate as nuclear perfusion imaging in patients with angina[92,93] and quantitative perfusion CMR has been validated against FFR[82,167], microspheres[156], Single Photon Emission Computed Tomography (SPECT)[127] and Positron Emission Tomography (PET) [111-113].

To our knowledge, there are limited studies using quantitative analysis and no previous studies focusing on perfusion in patients with heart failure using CMR. Only a few studies, using PET, have been performed specifically exploring perfusion abnormalities in patients with HF and these have produced conflicting results[193-195]. Van Den Heuvel et al. studied a group of NICM patients using PET and showed a similar perfusion rate at rest but reduced global myocardial perfusion reserve (MPR) versus a group of healthy controls[193]. In contrast, Neglia et al. showed a reduced MPR at rest as well as during pacing and pharmacological stress in patients with NICM[195]. The concept that, even in NICM, the presence of silent ischaemia may contribute to progressive

impairment of LV function was supported by the conclusions of a study by Tio et al. Patients with NICM were assessed with PET and dobutamine stress[196]. In this study, MPR was significantly higher in segments with higher contractile reserve and lower in the segments which did not change or deteriorated with stress. Our study reveals a trend towards a lower MPR in normal segments.

Non-invasive assessment of myocardial perfusion in patients with HF can be challenging for a number of reasons. In cases of advanced HF the LV wall is often thinner and remodeled, requiring higher spatial resolution for reliable identification of subendocardial areas of stress-induced ischaemia or areas of peri-infarct ischaemia. PET is considered the reference standard for in-vivo quantitative perfusion assessment. However, it is limited by the intrinsically lower spatial resolution and this could be an important limiting factor for the assessment of dilated and remodelled ventricles.

Perfusion CMR, and in particular 3T kt, offers higher spatial resolution and arguably is best placed to identify areas of ischaemia in these patients. In addition, the advantage of CMR over other techniques to directly visualise scar enables more precise assessment of peri-infarct ischaemia. This reduces the risk of including scarred areas in segmental averages of perfusion. Perfusion rate in areas of scar was found to be reduced and this aspect could result in false positive ischaemia results.

We observed a non-significant trend towards lower perfusion rates in visually normal segments of patients with NICM, which would be in keeping with the results previously obtained by PET. This comparison is beyond the scope of the study and would merit investigation in future work.

Importantly, our results demonstrate a significant endocardial-epicardial CFR ratio in ischaemic segments, even in patients with HF who have thinned and remodelled ventricles. This is in keeping with findings of a study by Parodi et al. where microspheres were injected into the hearts of patients at time of transplantation, demonstrating the presence of a transmural gradient of perfusion even in the presence of extensive LV remodelling[197]. To our knowledge, our data is the first to show that non-invasive quantification of myocardial perfusion in multiple independent layers of myocardium is feasible also in this group of patients.

The *kt* sequences used in this study are more vulnerable to respiratory artefact than are other perfusion sequences. We did not observe this effect in our study, which may be a reflection of good patient coaching and careful selection of the time for the breathhold command.

4.4.4 Study limitations

1) This was a feasibility study. Visual assessment was the only reference standard. Nevertheless, visual assessment is considered the clinical diagnostic standard for perfusion CMR evaluation and extensive validation is available against Fractional Flow Reserve (FFR), invasive angiography, SPECT and PET.
2) This study consisted of a small number of patients and in some patients the degree of heart failure was mild. By current criteria many would have represented patients within the HFmrEF group. Our results demonstrate that a high resolution quantitative approach is feasible in this cohort but this cannot be generalised to patients with more severe LV function. A

study exploring the use of this technique in a larger number of patients would be needed to explore this further.

3) Patients included in this study who had normal LV function were referred for a CMR on the basis of symptoms or cardiovascular risk factors – some had diabetes or hypertension and therefore could not be considered a true control group given recognised abnormalities in perfusion seen in these patients.
4) It is not straightforward to extend our results to other CMR sequences and field-strengths, or to standard (segmental) quantitative analysis methods. The quantification process may need to be adjusted for other field strengths and perfusion sequences and this could form part of future work.

4.5 Conclusion

In summary, the use of perfusion CMR continues to increase and the quality of sequence imaging has advanced in parallel. There are a number of challenges in scanning patients with heart failure, namely thinner LV walls, and breathing and respiratory artefacts. The advances in CMR have enabled high resolution imaging quality; alongside this the ability to analyse the data on a voxel level can potentially overcome some of these challenges.

The study described demonstrates that the combination of 3T *kt* high-resolution perfusion CMR with high-resolution voxel-wise quantitative analysis appears feasible in heart failure patients. This approach permits preservation of additional information gained from improved spatial resolution, a feature of

crucial importance in heart failure in order to be able to appreciate sub-endocardial perfusion defects.

Part of this chapter consists of work that has been published:

***Sammut, E**., Zarinabad, N., Wesolowski, R., Morton, G., Chen, Z., Sohal, M., Carr-White, G., Razavi, R., Chiribiri, A.*

'Feasibility of high-resolution quantitative perfusion analysis in patients with heart failure'

Journal of Cardiovascular Magnetic Resonance, 2015 (https://doi.org/10.1186/s12968-015-0124-2)

Eva Sammut is first author on the publication and was responsible for data collection, study design, experimental work and draft/review of the manuscript.

Table 2 - Table showing demographic data and structural CMR findings for subjects studied

	NICM group	ICM group	Normal LV (NLV) group	P value NICM vs ICM group	P value NICM vs NLV group	P value ICM vs NLV group	P value between all groups
Male Gender %	65%	82%	67%	-	-	-	-
Age (years+/- SD)	58±14	63±12	54±18	0.78	0.77	0.08	0.79
BSA (m^2+/- SD)	1.86±0.21	1.96±0.19	1.90±0.19	0.27	1.00	0.70	0.27
LV EDV (ml/m^2+/- SD)	102±28	112±33	71±18	0.48	<0.0001*	<0.0001*	<0.0001*
LV ESV (ml/m^2+/- SD)	63±26	73±31	25±8	0.16	<0.0001*	<0.0001*	<0.0001*
LVEF (%+/- SD)	39±9	37±10	65±4	0.06	<0.0001*	<0.0001*	<0.0001*
LV mass (g/m^2+/- SD)	73±18	70±18	55±13	1.00	0.001*	0.006*	0.001*
RV EDV (ml/m^2+/- SD)	80±22	74±20	72±18	0.88	0.39	1.00	0.30
RV ESV (ml/m^2)	40±20	35±16	28±10	0.54	0.008*	0.24	0.01*

Table 3 - Table showing rest, stress and MPR perfusion values for groups studied

	Visually normal segments	Visually abnormal, non-scarred segments	Visually abnormal, scarred segments	p-value Normal vs non-scarred segments	p-value Normal vs scarred segments
Stress perfusion Normal LV group (ml/g/min)	2.3±1.3	1.6±0.8	-	0.08	-
Stress perfusion NICM group (ml/g/min)	1.9±0.8	-	-	-	-
Stress perfusion ICM group (ml/g/min)	2.2±1.0	1.8±0.9	1.5±0.7	0.02*	0.006*
Rest perfusion Normal LV group (ml/g/min)	0.86±0.30	0.9±0.4	-	0.83	-
Rest perfusion NICM group (ml/g/min)	0.90±0.19	-	-	-	-
Rest perfusion ICM group (ml/g/min)	1.0±0.4	1.0±0.4	0.9±0.4	0.25	0.83
CFR Normal LV group	2.6±1.1	1.7±0.8	-	0.04*	-
CFR NICM group	2.2±0.8	-	-	-	-
CFR ICM group	2.3±0.8	1.8±0.9	1.7±0.7	0.04*	0.004*

Table 4 – Table showing results of coronary angiography versus perfusion results according to group

Group	LAD territory				Cx territory				RCA territory			
	CAD on angio	LGE only	iPD (no LGE/ beyond LGE)	Kappa (significance)	CAD on angio	LGE only	iPD (no LGE/ beyond LGE)	Kappa (significance)	CAD on angio	LGE only	iPD (no LGE/ beyond LGE)	Kappa (significance)
ICM group	25/30 (85%)	12/25 (48%)	11/25 (44%)	0.462 (p=0.003)*	11/30 (37%)	4/11 (36%)	4/11 (16%)	0.603 (p=<0.001)*	13/30 (43%)	9/13 (69%)	6/13 (46%)	0.718 (p=<0.001)*
Normal LV group	16/33 (48%)	0/33	6/16 (38%)	0.382 (p=0.005)*	11/33 (33%)	0/11	6/11 (55%)	0.615 (p=<0.001)*	13/33 (39%)	0/13	6/13 (46%)	0.510 (p=0.001)*

5 Prognostic value of quantitative perfusion CMR

5.1 Introduction

This chapter will describe the shift in focus on the ischaemic burden in the management of CAD. This will conclude with the first published study to examine the prognostic value of a quantitative approach compared to visual assessment. As faster, more automated, perfusion CMR analysis becomes possible, prognostic data is an important component in driving the impetus to translate quantitative perfusion CMR to the clinical setting. This chapter includes a large observational study comparing quantitative and visual perfusion analysis in terms of their prognostic value. We proposed that the use of a quantitative approach would provide similar or incremental prognostic value compared to visual assessment, and potentially over other recognised risk factors, due to its ability to objectively identify ischaemia. Eva Sammut is first author on the publication and contributed to the study design, experimental work and draft/review of the manuscript.

5.2 Ischaemic burden thresholds according to modality

The mere presence of ischaemia as identified on visual analysis has been shown to relate to prognosis. In recent years the extent and severity of ischaemia, the ischaemic burden, have become a focus.

On the basis of a number of large nuclear studies, ≥10% ischaemic myocardium is considered the risk threshold associated with an increase in adverse events. Several studies have demonstrated that in patients with a burden of ischaemia above this threshold, there appears to be an advantage of revascularization

over medical therapy and that a reduction in ischaemia with treatment appears to be associated with lower incidence of adverse events[62,63,198-202].

The thresholds of ischemic burden defined by SPECT have been extrapolated to other imaging modalities such as CMR and echocardiography. Evidence validating these thresholds for CMR is lacking and different studies have applied different thresholds[95,203]. A meta-analysis by Shaw et al, proposed that for stress perfusion CMR, moderate to severe ischaemia could be defined as >2/16 AHA segments, >4/32 segments by perfusion MR (This assumes that the 16 AHA segments are further subdivided into subendocardial and subepicardial halves, which yields a total of 32). Using DSMR this threshold is >3/16 dysfunctional segments[203].

The quantitative approach also requires consideration of the optimal threshold to define ischaemia. There is no consensus on this and it has remained an obstacle to clinical application of quantitative CMR. In a study by Lockie et al. MPR measurements by CMR were compared to fractional flow reserve measurements and this suggested an optimal cut off of <1.58 to define ischaemia, with a sensitivity of 0.80 and specificity of 0.89[82]. A similar cut-off (<1.5) was also suggested in an earlier study comparing angiographic severity of CAD versus semi-quantitative measurements of MPR by CMR[124].

Two important studies are will be key in developing specific indications and thresholds to be used for cardiovascular imaging in the setting of CAD. The MR-INFORM (MR Perfusion Imaging to Guide Management of Patients with Stable Coronary Disease) trial[95] randomized patients to be guided for the need of revascularization either by CMR or the FFR and showed that guiding the

management of patients with suspected CAD based on CMR result was safe and resulted in fewer invasive procedures – the full results are awaited. The ISCHEMIA (International Study of Comparative Health Effectiveness with Medical and Invasive Approach) trial[67] is a large randomized multi-centre study designed to further investigate the benefit of revascularization compared to medical therapy in those with moderate to severe ischaemia on stress testing by SPECT, echocardiography or CMR. This study is still in the recruitment phase but will aim to use contemporary non-invasive ischaemia modalities, medical therapy and percutaneous techniques to explore once again the impact of PCI over medical therapy in light of the controversies and criticisms of previous studies and the persistence of the use of PCI for patients with stable angina.

5.3 The importance of cross-modality validation

A number of important considerations must be taken into account when considering the optimal test to assess ischaemia.

5.3.1 Target

A comparison of tests which use either dobutamine or vasodilator stress is likely to produce differing results due to their differing targets on the ischaemic cascade – as discussed in earlier chapters perfusion abnormalities will be more extensive and occur earlier in the ischemic cascade whereas regional wall motion abnormalities are associated with more severe stenosis and occur later in the cascade[36].

5.3.2 Spatial resolution

The extent of ischaemia can be imaged both radially and transmurally although it is also important to consider the spatial resolution and endocardial definition of each technique. This is substantially lower in nuclear imaging techniques and echocardiography by comparison to CMR. Furthermore, within CMR there have been substantial improvements in spatial resolution, and therefore of visually-determined appreciation of subendocardial perfusion defects. Studies employing direct comparison of ischaemic burden by CMR using a standard and high-resolution technique, show that the accuracy of MPR is greater with a high resolution technique in patients with angiographic three-vessel disease[204]. High-resolution sequences were also better correlated with semi-quantitative angiographic scores than standard resolution[205]. More recently, analysis of these higher resolution images has also been described on a voxel-wise level and has compared favourably with the invasive reference of microspheres in an explanted pig heart model[140,184].

5.3.3 Inducible versus non-inducible perfusion defects

The presence of scar can complicate ischaemia assessment. Scarred areas are not considered ischaemic. Assessment of ischaemia in these areas is either 'matched' and therefore considered non-inducible or extends beyond the scar and represents peri-infarct ischaemia. This relies on direct visualization of scar and a high spatial resolution, both possible only in CMR. In the clinical setting this is usually achieved by simple visual assessment. Initial studies are available that suggest that combined high-resolution assessment of quantitative perfusion and late gadolinium enhancement images by CMR is feasible and may further improve the technique[206].

5.3.4 Whole heart coverage

In the context of assessment of the ischaemic burden it is important to note that nuclear techniques provide whole heart coverage whereas in perfusion CMR, only three or four short axis, non-contiguous slices are acquired. This is the standard clinical approach; slices which include basal, mid and apical LV are felt to provide a representative picture of the left ventricular myocardium. Calculation of the total ischaemic burden is therefore an extrapolation using CMR and it can be argued that the assessment of ischaemic burden may be incomplete and therefore imprecise. Substantial work has been directed into overcoming the numerous technical challenges involved in the acceleration of data acquisition without significant loss in image quality. Newer 3D perfusion sequences permit whole heart 3D first pass perfusion with all slices being acquired at the same point in the cardiac cycle. Initial reports suggest good correlation between semi-quantitative angiographic scores, FFR and ischaemic burden calculated by 3D perfusion CMR[171,172,207]. Compromise in spatial resolution is inevitable – wider coverage is exchanged for inferior resolution - and one should compare high resolution 2D approach versus 3D whole heart perfusion CMR. A study comprising 27 patients performed direct comparison of high-resolution 2D and whole heart 3D perfusion CMR (both visually assessed). This delivered promising results with a strong correlation and broad agreement between 2D and 3D with regard to calculated ischaemic burden[208]. Initial studies have also shown that quantitative assessment of 3D perfusion CMR is feasible and with high diagnostic accuracy[170]. Larger datasets and further comparison between these approaches are required to explore this further.

5.3.5 Field strength

In the context of CMR there is some evidence suggesting that perfusion CMR is more accurate when performed at higher magnetic field strengths – studies have shown that at 3T both sensitivity and specificity are improved compared to 1.5T perfusion CMR. This is likely to be due to improved signal to noise and contrast to noise ratios resulting in better detection of subendocardial perfusion and reduced occurrence of dark rim artefacts[182]. This study was performed using visual assessment and would benefit from revisiting with quantitative analysis in due course.

5.4 Calculation of ischaemic burden by perfusion CMR

In the clinical setting perfusion CMR is assessed visually. Although both visual and quantitative analysis can provide data on ischaemic burden, visual analysis is subject to variation in reader expertise. The quantitative approach has been shown to be less susceptible to inter-observer variation[120]. This is particularly an issue in multi-vessel CAD. The appearance of balanced ischaemia where all segments are hypoperfused can potentially lead the reader to provide a false negative result. Data is now available suggesting diagnostic superiority of quantitative CMR perfusion analysis specifically in the setting of multi-vessel coronary disease[120]. Patel et al. studied a group of 30 patients who had undergone a positive nuclear test and were scheduled for coronary angiography. Patients underwent a stress perfusion CMR, using a dual bolus approach; quantification was performed by Fermi deconvolution. In single vessel disease >50% severity, quantitative and visual analysis performed

similarly (83% versus 80% respectively). Likewise, for single vessel disease >70% severity (77% versus 67% respectively). A stepwise reduction in MPR was noted with increasing severity of single vessel CAD and the authors were able to define cutoff values according to stenosis severity, yielding an area under the curve of 0.82 for the detection of CAD >50% (optimal MPR threshold 1.85) and 0.77 for CAD >70% (optimal MPR threshold 1.55). Importantly, patients with three vessel CAD had a higher burden of ischaemia as assessed by quantitative analysis than those with single vessel disease (60% versus 25%, p=0.02) whereas no difference could be detected with visual assessment (31% versus 21%, p=0.26).

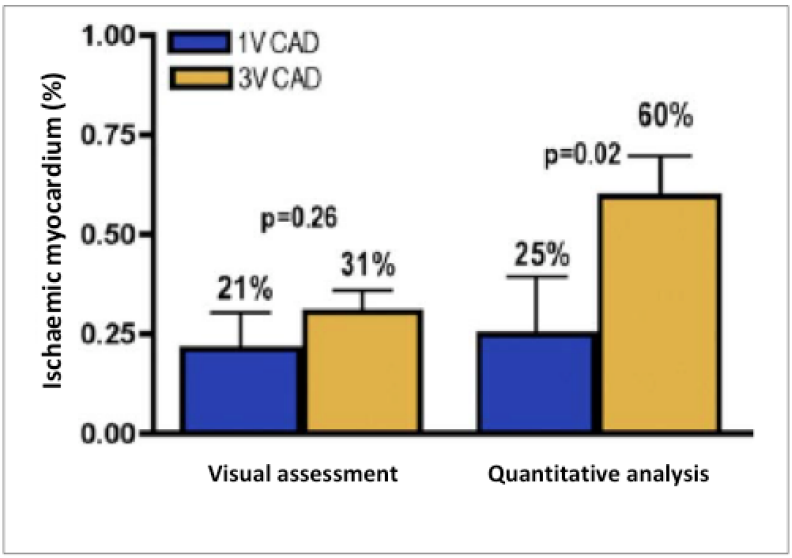

Figure 5.1 - Bar chart showing differences between visual and quantitative analysis when considering single or multi-vessel disease

In single vessel disease, quantitative and visual analysis performed similarly. In contrast, in patients with multi-vessel CAD there was a significant difference between the two approaches, favouring quantitative analysis.
Adapted from Patel et al.[120]

5.5 Prognostic value of perfusion CMR

The following section describes an observational clinical study, performed as part of this thesis, which compared the prognostic value of quantitative CMR perfusion against visual assessment in a group of unselected patients with suspected CAD.

5.5.1 Methods

5.5.1.1 Study design

Patients with suspected CAD referred on a clinical basis to the King's College London CMR Service at St Thomas' Hospital (Guy's and St Thomas' NHS Trust) between January 2009 and January 2015 were considered for enrolment. Consecutive patients who underwent a clinical CMR scan comprising assessment of cardiac function, ischaemia testing with high-resolution dual bolus adenosine stress and rest perfusion imaging followed by late gadolinium enhancement (LGE) imaging were included in the study. Patients in whom regadenoson was used were excluded from the study since the half-life of the drug has the potential to result in the acquisition of rest perfusion images with a degree of residual hyperemia, potentially resulting in the underestimation of MPR[88,89].

The study was conducted in accordance with the Declaration of Helsinki (2000) and was approved by the National Research Ethics Service. All patients provided written informed consent.

The start of the follow-up was defined as the date of the CMR scan. The primary endpoint was as a composite of cardiovascular death (defined as death due to

myocardial infarction, heart failure or ventricular arrhythmia), non-fatal myocardial infarction (MI defined as clinical acute coronary syndrome with associated ECG changes and elevation of serum biomarkers of myocardial necrosis to >99th percentile of the assay upper limit of normal[209], aborted sudden cardiac death (SCD, defined as documented ventricular fibrillation or sustained ventricular tachycardia with hemodynamic compromise requiring defibrillation or cardioversion not associated with acute myocardial infarction), and late revascularisation (percutaneous coronary intervention (PCI) or coronary artery bypass grafting (CABG) >90 days after the start of follow-up). In order to avoid the potential effect of a positive CMR result leading to early revascularisation, we excluded procedures within 90 days of the CMR scan from the endpoint definition revascularization[59,210]. Patients who did not experience events were censored at the point of last follow-up. Where patients experienced more than one event, only the first event was considered.

Follow-up was performed through interrogation of electronic patient records and patient notes. All events were adjudicated by consensus of three physicians blinded to CMR data. Mortality and cause of death were obtained from the Office for National Statistics and through review of medical records, death certificates and post-mortem data where available.

5.5.1.2 Image acquisition

Patients were asked to refrain from nicotine and caffeine-containing foods and beverages for 24 hours prior to the scan. Standard 2, 3 and 4-chamber cine images were acquired during breath hold. Contiguous short-axis slices were acquired from the base to the apex for calculation of left ventricular (LV) volumes, function and mass. Following 4 minutes of adenosine (140mcg/kg/min,

increased to 210mcg/kg/min if there was an inadequate response[211]), stress perfusion data were acquired in 3 short-axis slices with a saturation-recovery k-t sensitivity encoding [k-t SENSE] accelerated gradient-echo method[212], covering 16 of the standard myocardial segments (segment 17 was excluded).

A dual-bolus contrast agent scheme was used to correct for signal saturation of the arterial input function as previously described[130]. In brief, 0.0075 mmol/kg gadobutrol (Gadovist, Bayer, Berlin, Germany) was administered as a pre-bolus at peak stress with imaging of the arterial input function. First-pass perfusion data were then acquired after the injection of 0.075 mmol/kg gadobutrol at 4 ml/second followed by a 20 ml saline flush. Rest perfusion imaging was performed after a minimum of 15 minutes following the stress acquisition prior to acquisition of late gadolinium enhancement imaging according to Society of Magnetic Resonance (SCMR) guidelines[190]. LGE imaging was performed after a further dose of contrast agent, to a total dose of 0.2 mmol/kg gadobutrol.

5.5.1.3 Image analysis

Ventricular volumes, atrial size, and left ventricular mass were calculated and normalized to body surface area (CVI42, v5.1.1, Circle Cardiovascular Imaging, Calgary, Canada). Segmental mass was measured in end-diastole and expressed as percentage of total LV mass and was used in the calculation of the ischaemic burden.

Visual assessment was performed using stress and rest perfusion and LGE images with consensus of two SCMR level III accredited physicians using the standard 16-segment AHA model and standardized reporting criteria. Scans were reported visually on a clinical basis and therefore baseline clinical data were available to the observers performing visual assessment.

A perfusion abnormality was defined visually according to the criteria previously described in the MR-INFORM (MR Perfusion Imaging to Guide Management of Patients with Stable Coronary Disease) study[95] as a delayed wash-in of contrast persisting for ≥5 dynamics in 1 or more AHA segment compared with normal remote myocardium. Since the spatial resolution of CMR allows for appreciation of subendocardial versus transmural perfusion defects, each of the 16 AHA segments were subdivided into an endocardial and epicardial half resulting in a total of 32 segments to allow more accurate calculation of ischaemic burden. Segments in which LGE was present were excluded from ischaemia assessment.

Surface coil intensity correction was performed prior to quantification using pre-contrast imaging data[153]. Time signal-intensity curves were extracted using commercially available software (CVI42).

Quantitative analysis was performed blinded to baseline clinical data.

Quantitative perfusion analysis was performed by Fermi-constrained deconvolution according to the methods described by Wilke et al.[142]

and Jerosch-Herold et al.[143] where time-signal intensity curves for the tissue impulse response function, h(t), were fitted to the Fermi function using a Marquardt-Levenberg nonlinear least squares algorithm according to the following analytical expression:

$$h(t) = R\left[\frac{1}{e^{(t-\tau_0-\tau_d)k}+1}\right]u(t-\tau_d)$$

by letting k, R and τ_0 vary and keeping τ_d fixed. In the above equation, u(t − τd) is the unit step function. The τ_d accounts for the delay time between the

appearance of the signal in the LV blood pool and myocardial region of interest (ROI). T_0 characterizes the width of the shoulder of the Fermi function during which little or no contrast agent had left the ROI. R is the index of contrast agent influx parameter and k represents the decay rate of h(t) due to contrast agent washout. Using the above equation, myocardial blood flow (MBF) estimates are calculated as h(t) at t=0. Myocardial perfusion reserve (MPR) was calculated as the ratio between stress and rest MBF estimates[166].

Ischaemia was defined as segments with MPR<1.5, according to previously validated criteria[82].

5.5.1.4 Statistical methods

The statistical analysis was performed by two of the authors (SS and TI). Data for categorical variables are presented as frequencies and percentages. Data for continuous variables are presented as mean±standard deviation (SD) or as medians and interquartile range (IQR) depending on normality. The study cohort was stratified according to the presence or absence of events during follow-up.

Differences between categorical variables were evaluated using Fisher's exact test. Comparisons between continuous variables were performed with the independent samples Student t-test or using the Wilcoxon rank-sum test as appropriate. Two-tailed p values <0.05 were considered significant.

Survival risk classifiers were built using a penalized Cox proportional hazards models with L1-(Lasso) penalty. Double-loop cross-validation with 500 re-starts was used to obtain robust unbiased estimates of predictive strength as outlined by Simon et al.[213]. A baseline model was built containing established prognostic variables - age, gender and LGE - as un-penalized independent variables. LV ejection fraction (LVEF), revascularisation within 90 days and pre-scan

revascularization also entered the baseline model and were subject to penalization[214]. None of these penalized variables were found to provide predictive information, and therefore were not retained in the final model specification. The baseline model was then extended to include the visual ischaemic burden or MPR ischaemic burden. The predictive performance of the resulting enriched models was evaluated by 10-fold cross-validation with 500 re-starts[213]. Survival probabilities were derived for each patient for the 2-year time point. The 2-year time point was chosen on the basis of ≥75% cohort having follow-up of 869 days (2.4 years). Cross-validated receiver-operator characteristic curves were created for each model at 2 years and the associated cross-validated area under the curve (AUC) determined[215]. Patients were classified into the three categories: low (<1%), intermediate (1-3%) and high (>3%) risk as specified by current ACC guidelines[216]. Cross-validated categorical net reclassification improvement (NRI) and integrated discrimination improvement (IDI) reclassification metrics were then computed for the two perfusion models in relation to the baseline model[217].

After establishing the independent predictive value of each measure of perfusion as a continuous covariate, the perfusion measures were dichotomized using a threshold of ≥2 segments for visual ischaemia and ≥10% for ischaemic MPR[203]. Model performance was re-assessed as previously using cross-validated Cox regression and reclassification metrics for the 2-year time point.

Kaplan-Meier-curves were produced for time to the composite endpoint to visualize the discriminative power of LGE and perfusion measurements.

All statistical analysis was performed with R version 3.3.0 (R Core Team (2016)).

5.5.2 Results

A total of 434 patients met the inclusion criteria: 24(5.5%) were lost to follow-up and 15(3.5%) were excluded due to poor image quality. The baseline clinical and CMR characteristics of the final cohort of 395 patients stratified by event status are listed in Table 5. Patients tended to be middle-aged (58±13 years), mostly male (70%), with the majority having known hypertension (59.5%), hypercholesterolemia (54.7%) and approximately one in five had diabetes (19.7%). About one third of the patients had had previous revascularisation either by PCI or CABG. About one third (34.9%) of the patients had stress-induced perfusion abnormalities on visual assessment and 35.4% were positive for LGE. In total, 40 patients underwent revascularisation within 90 days (7 CABG, 33 PCI, median 30 and 36 days respectively post CMR) and these events were excluded from subsequent analysis.

The median follow-up was 460 days[IQR 190-869]. Overall, 52 patients met the primary endpoint: 39 patients underwent revascularisation after 90 days (23 elective PCI for stable angina, median 196 days after CMR[IQR 135-240]; 5 unplanned PCI due to unstable angina, 220 days after CMR[IQR 140-704]; 10 patients underwent elective CABG, 188 days after CMR[IQR 148-282]), 1 patient had unplanned CABG due to unstable angina, 190 days after CMR). Other events consisted of non-fatal MI in 7 cases, 896 days after CMR[IQR 56-1160] (leading to unplanned revascularisation in 3 subjects), 4 cardiovascular deaths, 508 days after CMR[IQR 186-856] and 2 aborted SCD at 16 and 443 days after CMR.

The baseline cross-validated Cox regression model found the linear predictors to be age, gender and LGE as follows:

$$\sim 0.025 * \text{age} + 2.993 * \text{gender} + 0.616 * \text{LGE}$$

The addition of visual ischaemic burden as a continuous covariate yielded a linear predictor of:

$$\sim 0.028 * \text{age} + 3.108 * \text{gender} + 0.563 * \text{LGE} + 1.423 * \text{visual}_{\text{ischaemic burden}}$$

The corresponding model for MPR ischaemic burden as a continuous covariate was:

$$\sim 0.02 * \text{age} + 2.722 * \text{gender} + 0.678 * \text{LGE} + 2.490 * \text{MPR}_{\text{ischaemic burden}}$$

The addition to the baseline model of dichotomized visual ischaemic burden using a threshold of ≥2 segments yielded a model of:

$$\sim 0.019 * \text{age} + 2.949 * \text{gender} + 0.486 * \text{LGE} + 1.374 * \text{visual}_{\geq 2 \text{ segments}}$$

The corresponding model for dichotomized MPR ischaemic burden using a threshold of ≥10% ischaemic myocardium was:

$$\sim 0.016 * \text{age} + 2.486 * \text{gender} + 0.497 * \text{LGE} + 1.761 * \text{MPR}_{\geq 10\%}$$

Ischaemia assessment by visual or quantitative analysis significantly improved predictive performance by comparison with the baseline model alone. When established clinical thresholds were utilized, there were further significant improvements in model performance.

Figure 5.2 illustrates the ROC curves for 2-year outcome for the continuous and dichotomized visual and quantitative perfusion results. This translated into a

significant improvement in risk reclassification (Figure 5.3). Kaplan-Meier curves illustrating survival in patients stratified according to LGE and dichotomized visual and quantitative perfusion findings are shown in Figure 5.4.

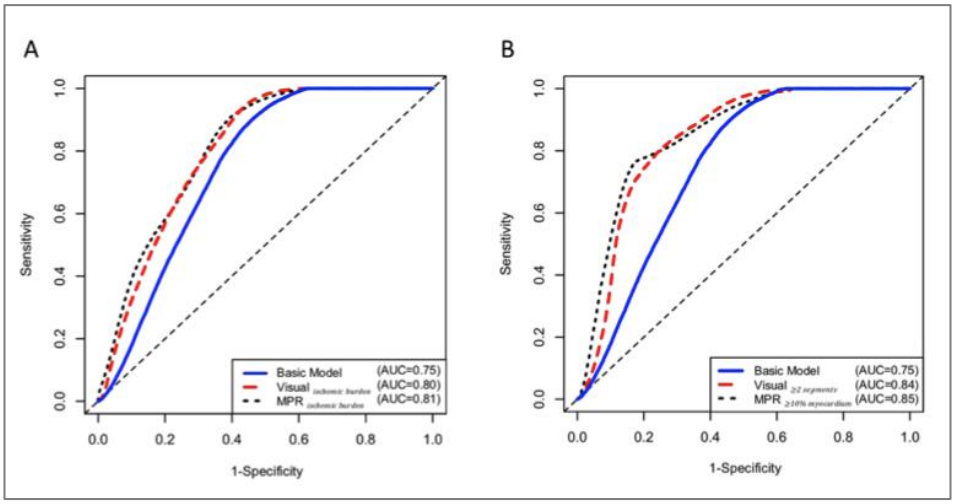

Figure 5.2 - Receiver-operator characteristic curves for 2-year outcome for visual and quantitative analysis

Receiver-operator characteristic curves for 2-year outcome for the baseline cross-validated Cox regression model and for the extended models including visual and ischaemic burden (MPR, myocardial perfusion reserve) as a continuous (Panel A) or dichotomized covariate (Panel B)

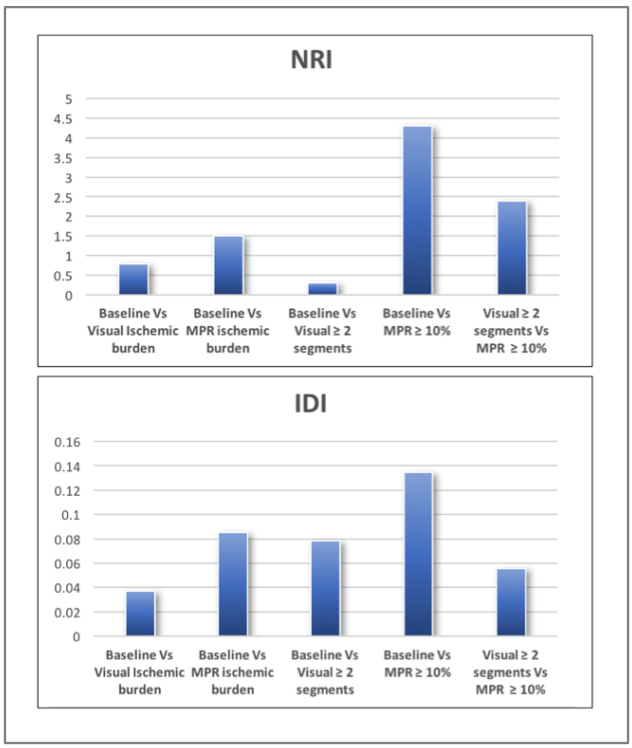

Figure 5.3 - Cross-validated categorical net reclassification improvement (NRI) and integrated discrimination improvement (IDI) reclassification

Cross-validated categorical net reclassification improvement (NRI) and integrated discrimination improvement (IDI) reclassification for the baseline and the perfusion models.

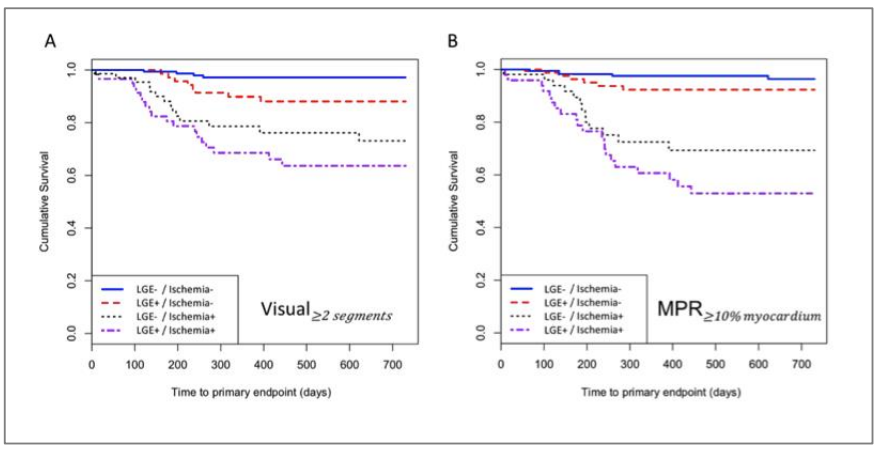

Figure 5.4 - Kaplan-Meier curves illustrating survival in patients according to dichotomized visual and quantitative analysis

Kaplan-Meier curves illustrating survival in patients stratified according to LGE and dichotomized visual (Panel A) and quantitative (Panel B) ischaemic burden.

On further analysis of the concordance of results obtained from visual and quantitative analysis, the incidence of primary events was noted to be highest in the context of concordant positive tests (53.9% of the total events) and the lowest event rate was observed in patients negative in both tests (9.6%). In the case of disagreement, we observed a higher number of patients meeting the primary endpoint when classified as positive on quantitative analysis (23.1%) compared with those positive only on visual assessment (13.5%).

5.5.3 Discussion

The described study represents the first to address the prognostic benefit of quantitative analysis of stress perfusion CMR. A quantitative approach has previously been shown to significantly improve diagnostic performance over visual assessment specifically in the setting of multi-vessel coronary artery disease[120]. Our data demonstrate that a quantitative approach is also superior to visual assessment in an unselected group of patients from a prognostic perspective. Moreover, our data demonstrate the independent prognostic value of ischaemic burden measurements over and above LGE assessment, highlighting the strength of CMR as a multi-parametric technique.

In this study, both visual and quantitative analysis were performed in a high-volume tertiary centre, and by experts. It is a significant finding that the semi-automated quantitative analysis performed similarly, if not slightly better, than visual assessment performed by expert readers. This is of increasing relevance as recent technical advances in image reconstruction and analysis techniques are likely to permit the robust full automation of quantitative analysis in coming years[159,218]. The findings have important implications for facilitating the rapid

and more widespread adoption of stress perfusion CMR by less experienced centers and readers, and allowing realisation of the full prognostic value of perfusion quantification.

It is encouraging that there were only a small number of non-analyzable cases in the study (3.5%). This was mainly due to respiratory motion, a known limitation of the high-resolution *k-t* accelerated techniques used in this study[219]. The advent of novel motion correction techniques is likely to ameliorate this further[220].

We found that the consensus-based threshold of ≥10% ischemic myocardium or ≥2 abnormal segments can be validly extrapolated from nuclear medicine to CMR[203]. The use of these thresholds not only improved model predictive performance, but also translated into significant reclassification of patient risk using established risk categories. This is a reassuring finding since important studies such as MR-INFORM and the ISCHEMIA (International Study of Comparative Health Effectiveness with Medical and Invasive Approach) Trial are employing these criteria[67,95].

In this study, abnormal perfusion was defined by an MPR<1.5. This threshold has previously been validated against FFR[82] and is very similar to the optimal threshold found in some PET studies in patients with angina requiring revascularization[221].

5.5.4 Study Limitations

1. This was a single-center study, performed at a tertiary hospital with a high-volume CMR service. The single-center design permitted

standardization of the pharmacologic stress protocols and of the acquisition methods.

2. This was an observational study which could suffer potential inherent bias but nevertheless represents a real-world scenario. Consecutive patients fulfilling the entry criteria were included but may have constituted a selected group.
3. A dual-bolus approach was used, justified by the need to minimize signal saturation effects in the arterial input function. It is recognized that the relative complexity of this approach makes it more difficult for less experienced centers to adopt. The emergence of dual-sequence acquisition schemes and other advances may render this less of a barrier in the future[131,159,160].
4. Mirroring previous clinical studies where visual CMR results may have influenced revascularisation decisions, we excluded early revascularisation events (within 90 days) from the primary composite endpoint[59,210]. All scan reports were issued within 5 days with a median time of 36 days between scan to revascularisation in patients undergoing early revascularisation. On this basis, we feel that the cut-off of 90 days appears to be reasonable in our cohort for minimizing the CMR result influencing revascularisation. Furthermore, we would suggest that were it present, any bias would have favored a visual analysis approach as this was used for clinical decision-making. Although all endpoints were adjudicated blind to CMR data and in our modelling, and early revascularisation was not a significant predictor of outcome, we cannot

exclude the possibility that the impact of ischaemia may have been underestimated in the presence of prompt revascularisation.

5. The presence of severe ischaemia, defined as vasodilator-induced systolic dysfunction by CMR, was previously shown to predict poor prognosis in a large series of patients and to identify a subgroup of patients who benefitted most from revascularisation. A comprehensive evaluation of the ischaemic cascade, including induced-systolic dysfunction, was not performed in this study.
6. Finally, this study focuses solely on the use of CMR perfusion and uses visual assessment as the clinical reference standard. CMR perfusion was not directly compared with other modalities such as PET or SPECT. PET remains the non-invasive reference method for quantitative perfusion measurements. However, it is not widely used clinically, involves significant cost and uses ionising radiation. SPECT is more widely available but also uses ionising radiation and has lower spatial resolution than CMR. Visual and quantitative CMR analysis have been shown to perform similarly or better to these modalities in other studies but a direct comparison was not possible in this study.

5.6 Conclusion

In recent years there has been growing appreciation of the importance not only of the presence but also the severity and extent of ischaemia as a prognostic marker. There is a growing body of evidence supporting more widespread use of quantitative analysis, which lends itself well to calculation of ischaemic burden

both in terms of extent and severity. Quantitative analysis of perfusion CMR has now been demonstrated to be robust and reproducible, increasingly automated and, importantly advantageous over visual assessment in selected groups of patients.

The study presented here provides further support for the introduction of quantitative CMR perfusion analysis to the clinical setting. It supports the use of current consensus-based prognostic ischaemic burden thresholds for perfusion CMR. Quantitative perfusion analysis performed similar to, or when using a threshold based approach, better than visual assessment. In this study, the use of quantitative analysis provided incremental value over other recognized risk factors such as the presence of late gadolinium enhancement in an unselected cohort of patients.

This study should provide a basis to performing larger, multi-centre prospective studies to explore the prognostic implications of quantitative CMR perfusion analysis.

Part of this chapter consists of work that has been published:

***Sammut, E**., Villa, ADM., Di Giovine MD, G., Dancy, L., Bosio, F., Gibbs, T., Jeyabraba, S., Schwenke, S., Williams, SE., Marber, M., Alfakih, K., Ismail, TF., Razavi, R., Chiribiri, A.*

'Prognostic value of quantitative perfusion CMR'

JACC Imaging, 2017 (https://doi.org/10.1016/j.jcmg.2017.07.022)

Eva Sammut is first author on the publication and was responsible for data collection, image analysis and draft of the manuscript.

Table 5 - Baseline clinical and MR characteristics of study cohort

Variable	No Event (n=343, 86.8%)	Event (n=52, 13.2%)	Total (n=395, 100%)	P-value
Age, years	57.6±13.2	63.3±11.8	58.3±13.1	0.019
Sex, Male (n, %)	226 (65.9)	51 (98.1)	277 (70.1)	<0.001
Body Mass Index, kg/m^2	1.95±0.23	2.00±0.20	1.96±0.23	0.612
Risk Factors (n, %)				
Diabetes Mellitus	66 (19.2)	12 (23.5)	78 (19.7)	0.575
Hypertension	201 (58.6)	34 (66.7)	235 (59.5)	0.368
Current Smoker	63 (18.4)	10 (19.2)	73 (18.5)	0.849
Ex-Smoker	31 (9.0)	4 (7.7)	35 (8.9)	1.000
Hypercholesterolemia	180 (52.5)	36 (72)	216 (54.7)	0.025
Previous PCI/CABG	101 (29.2)	34 (65.4)	135 (34.2)	<0.001
PCI/CABG within 90 days	36 (10.5)	4 (7.7)	40 (10.1)	0.804
Atrial Fibrillation	36 (10.5)	10 (19.2)	46 (11.6)	0.100
CMR Characteristics				
LVEDV, ml	152[130-183]	156[125-195]	153[129-183]	0.462
Indexed LVEDV, ml/m^2	78 [67-91]	79 [65-96]	79 [67-91]	0.790
LVESV, ml	60 [47-82]	65 [41-97]	60 [46-84]	0.223
Indexed LVESV, ml/m^2	30 [24-40]	32 [22-47]	31 [24-41]	0.374
LVEF, %	60 [53-66]	59 [44-67]	60 [52-66]	0.121
LV Mass, g	107 [88-134]	115 [97-134]	109 [90-134]	0.086
Indexed LV Mass, g/m^2	55 [46-66]	60 [50-67]	56 [47-56]	0.075
RVEDV, ml	149[126-174]	143[114-170]	147[124-174]	0.185
Indexed RVEDV, ml/m^2	75 [64-87]	73 [60-88]	31 [23-38]	0.178
RVESV, ml	62 [44-77]	57 [46-78]	61 [44-77]	0.671
Indexed RVESV, ml/m^2	31 [23-39]	31 [22-38]	31 [23-38]	0.610
LA size, cm^2	23 [20-26]	22 [18-27]	23 [19-26]	0.944
RA size, cm^2	20 [17-23]	21 [18-24]	20 [17-23]	0.464

Resting Heart Rate, min^{-1}	71.8±14.2	68.7±13.5	70.8±14.0	0.182
Stress Heart Rate, min^{-1}	96.8±17.4	90.9±16.1	95.6±17.6	0.042
Rest Systolic BP, mmHg	137.9±22.7	137.4±22.2	137.9±22.4	0.859
Rest Diastolic BP, mmHg	79.3±12.5	74.9±10.9	78.6±12.5	0.097
Stress Systolic BP, mmHg	132.9±20.6	131.8±19.8	132.8±20.4	0.652
Stress Diastolic BP, mmHg	74.5±12.5	74.5±9.8	74.5±12.2	0.763
Visual Ischaemic Burden, %	14.7±29.2 0 [0-12.5]	29.6±28.2 25 [0-50]	17.2±29.7 0 [0-25]	<0.001
MPR Ischaemic Burden, %	6.09±14.6 0[0-4.9]	25.1±22.0 23.4[1.3-39.0]	8.35±16.7 0[0-8.5]	<0.001

6 Hybrid PET-CMR imaging

6.1 Introduction

This chapter will focus on the use of hybrid imaging to make a more direct comparison between PET and MR using a specialized cardiac phantom. Nuclear imaging modalities suffer a number of drawbacks: they use ionising radiation, they have limited spatial resolution by contrast with CMR, they are inferior in terms of assessment of cardiac chamber dimension and functional analysis, they cannot directly visualise scarred regions and finally, the availability of PET is restricted to large centres with an on-site cyclotron for tracer production. These factors make CMR an attractive alternative. Previous studies, described in previous chapters, have suggested that CMR is non-inferior to SPECT[90,92,93,127]. Previous studies comparing quantitative measurements of coronary flow reserve using PET and MR have demonstrated a good correlation between the modalities when considering coronary flow reserve (CFR) [111-113]. There is however a lesser correlation of absolute stress and rest estimates and this has been ascribed to specific tracer properties, modelling assumptions, fitting methods and parameter constraints[132]. Previous studies comparing PET and CMR can also been criticised on the basis that the MR and PET scans were performed in sequence, in some cases on different days.

Part of this chapter consists of work that has been published - Eva Sammut is second author on the publication and contributed to the study design, experimental work and draft/review of the manuscript. The published study serves primarily as a feasibility study of the first simultaneous PET-MR acquisitions from a dynamic cardiac perfusion phantom but in addition allows direct correlation of perfusion quantification between modalities against a true

perfusion rate – a situation not possible in-vivo, but providing a basis for future in-vivo work.

6.2 PET-CT

Multi-modal imaging is not a new concept. Indeed, PET scanners have been combined with CT scanners for over a decade[222]. The addition of CT allowed combination of functional PET data with high-resolution, three-dimensional anatomical data, yielding more accurate attenuation correction, and localisation of tracer uptake within a single examination. Studies have demonstrated clear advantages to the use of a combined approach[223-225]. Initial studies used only a low-dose CT scan for attenuation. More recently, the use of full, diagnostic-quality CT improved yield, at the cost of more radiation to the patient[226].

PET-CT remains a clinically applicable combined tool particularly in the field of oncology but does suffer from limitations. Despite use of the same scanner, the PET-CT scans are performed in sequence rather than simultaneously. This increases overall scan time. Most importantly, this sequential scanning can be problematic in terms of attenuation correction and co-registration due to breath-hold pattern and patient movement. This can significantly compromise accuracy of quantification of radiotracer activity[227-230].

6.3 Hybrid PET-MR imaging

Recent technical developments have led to the development of systems which combine PET and MRI imaging. These systems do allow simultaneous imaging, providing temporal correlation of dynamically acquired data from both

modalities. This improves cross-modality validation, reduces scan time relative to independent CMR and PET-CT scans, and reduces exposure to ionising radiation since the CT component is eliminated[231]. MRI also brings the advantage of superior tissue characterisation in contrast to CT, an important factor in the main applications of PET: oncology and cardiology. From a cardiac perspective the unrivalled ability to acquire high-resolution functional information, such as ventricular function and mass, myocardial scar, make it an attractive option to examine pathophysiology in more depth. The use of advanced MRI techniques such as phosphorus spectroscopy with MRI combined with the functional metabolic information from PET confer the same advantages.

Studies comparing PET-MR with PET-CT within the field of oncology have been encouraging[232,233].

Over the past decade, both PET and MRI technologies have been developed further. Currently available sequences show a dramatic improvement in spatial resolution of MRI and high sensitivity PET allows enables detection of minute amounts of radiotracer in-vivo.

6.3.1 Challenges of hybrid PET-MR

The combination of PET and MR into a single system has also come with several challenges. Commercially viable units are now available in few centres in the UK.

The PET and MRI subsystems have the potential to degrade one another. The PET scanner hardware may disrupt the homogeneity of the magnetic field and

produce distortion of the applied gradient field causing a loss of image quality and artefacts. In turn, the magnetic field at the centre of MRI imaging can affect the PET scanner by distorting the path of electrons through the photomultiplier tubes (PMTs) used in conventional PET scanners. The role of the PMT is to transform the visible light produced in the scintillator into an electric signal detectable by PET electronics. A number of detector design modifications have been proposed to address this[234].

Attenuation, traditionally performed using CT, has proved to be a challenge using PET-MR and here too a number of techniques have been proposed which include CT-based atlas or MR based attenuation[235-240].

Finally, physical restrictions are also a consideration since the size of the bore in the MRI scanner is already modest and cardiac coils must also be placed on the patient. One of the main challenges has been to try to incorporate the PET component without reducing the size within the bore even further. In practice, this is currently achieved by installing a PET insert in a magnet designed to equip a wide bore MRI scanner. This allows the system to have a bore with a diameter of 60 cm, suitable for most patients.

6.3.2 Challenges specific to cardiac PET-MR

Cardiac imaging is more challenging than imaging of other organs as it has three, rather than one, potential sources of motion – respiration, cardiac contraction, and voluntary or involuntary patient movement. Eliminating the effect of cardiac and respiratory motion in PET-MR has been addressed via a number approaches[241-244].

6.3.3 Clinical PET-MR

The bulk of work to date using hybrid PET-MR has been conducted in animals and has yielded encouraging results. In the clinical setting, most work has addressed brain or oncologocal imaging which does not carry the same variables as cardiac imaging. The use of clinical hybrid PET-MR in the field of cardiology is however steadily increasing.

The feasibility of using hybrid PET-MR imaging to identify areas of non-viable myocardium using [^{18}F]-FDG has been studied. It has been proposed that the mismatch between FDG uptake and scar by late gadolinium enhancement (LGE) could be used to define the area at risk if used in patients post acute myocardial infarction[245-247].

In chronic myocardial infarction, areas of reduced uptake of [^{18}F]-FDG and LGE have been shown to correlate well, including a recent study focusing on viability using a hybrid PET-MR system[248].

The use of hybrid PET-MR to assess perfusion is limited. Initial results appear to suggest similar outcomes between PET-CT and PET-MR when comparing quantification of myocardial blood flow - a recent study Kero et al. in 10 patients with suspected CAD demonstrated a high intra-class correlation coefficient of 0.98[249].

In a recent study, 12 patients who had undergone SPECT showing rest perfusion defects were scanned with PET-MR using [^{18}F]-FDG and LGE, and results were compared to SPECT versus CMR methods[250]. The hybrid approach showed good correlation with the CMR approach for identifying normal, scar and ischaemic segments, with poor correlation between SPECT and CMR. Compared to CMR alone there was reclassification of 19.2%

segments using a hybrid approach with a significant impact on downstream revascularisation. CMR perfusion routinely images only three slices. PET is able to take into account three-dimensional whole heart. When both modalities are used in combination, more comprehensive imaging is obtained and complimentary information is yielded with consequent benefit in assessment.

PET-MR systems have also been used to image myocarditis, sarcoidosis, cardiac tumours, and Takotsubo cardiomyopathy using glucose uptake as a surrogate for inflammation or a metabolically active lesion[251-254]. Finally, a number of studies have used PET-MR to image coronary or carotid plaques which may be vulnerable to rupture[255,256].

6.4 Feasibility of simultaneous PET-MR perfusion using a novel cardiac perfusion phantom

The background described above formed the basis of the subsequent study conducted at King's College London as part of this. In brief, the study aimed to compare simultaneous perfusion quantification from the two modalities using a physiologically validated phantom and hybrid PET-MR scanner.

6.4.1 Methods

6.4.1.1.1 Phantom

The custom designed perfusion phantom used in this study was designed and built at King's College London as a prototype[149]. It was designed to simulate physiological volumes and conditions to provide a reference method for quantification techniques using delivery of a known perfusion rate. The cardiac

perfusion phantom has previously been validated to provide data suitable for quantitative analysis. It has been employed in MR quantification[141] and in comparison with CT perfusion[257]. In essence: water is pumped through an MR-safe myocardial perfusion phantom placed in the scanner. The phantom is representative of the large thoracic vessels and of the heart of a 60kg subject. It is composed of four cardiac chambers (120 ml each) and associated thoracic vessels (aorta, pulmonary artery, pulmonary vein, vena cava). A schematic representation detailing the phantom and supporting precision pumping and monitoring mechanisms, is shown below in Figure 6.1.

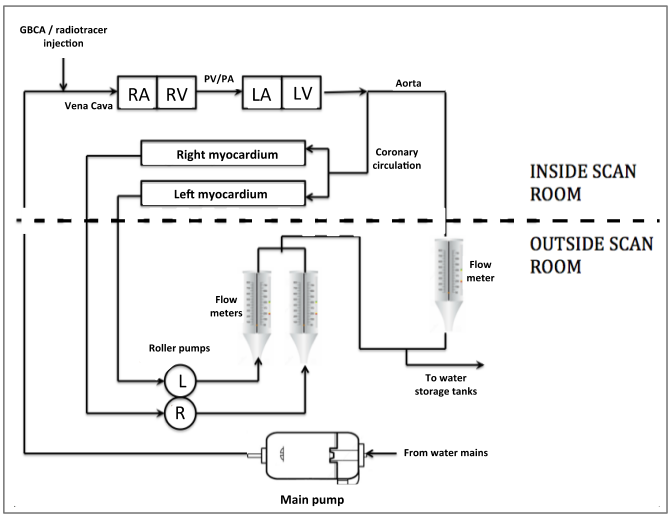

Figure 6.1 - Basic schematic representation of the cardiac phantom

Basic schematic representation of the phantom showing the control unit outside the scan room and the phantom components inside the PET-MR scanner. VC = vena cava, PA/PV-pulmonary artery/vein, RA/LA=right/left atrium, RV/LV-right/left ventricle.
Adapted from Chiribiri et al.[149]

Myocardial perfusion is monitored in real time by flow meters which continuously sample the flow rate by means of high-precision digital flow meters (Atrato,

Titan, Sherborne, United Kingdom) These flow meters also provide adjustment of the speed of rotation of roller pumps through a feedback mechanism. Perfusion values are obtained by means of measurement of the distribution volume for the radioactive tracer and for the Gadolinium-based contrast agent (GBCA, Gadovist®, Bayer HealthCare, Berlin, Germany). The flow rate is then divided by this value. All pump controls and flow/perfusion rates are handled remotely from a custom-written LabVIEW application (LabVIEW Professional Development System 2014, National Instruments, Austin TX, USA) controlled from a dedicated remote workstation using an iPad application (Dashboard for LabVIEW, National Instruments, Austin TX, USA).

In this study, no radiotracer or GBCA re-entered the system after injection. The model was non-recirculating and this permitted study of first-pass myocardial perfusion data.

6.4.1.1.2 Scanning parameters

PET-MR imaging was performed on a 3T Siemens Biograph mMR scanner (Siemens Healthcare GmbH, Erlangen, Germany). The MR sequence consisted of a clinically utilized imaging protocol, (a 2D TurboFLASH saturation recovery gradient echo sequence; TE=1 ms, TR=164 ms, Flip angle=10^{o}, slice thickness=6 mm, voxel size=1.875 mm, matrix size 144x192 voxels), with temporal resolution of 1 image per cardiac beat. MR data was acquired in a single transverse plane identified by markings on the phantom, the locations of which corresponded to a known dispersion volume for the GBCA and radiotracer. Cardiac output flow rate was set to 3 litres/minute, with true myocardial perfusion rates (hereon denoted P_T) set to 1, 2, 3, 4 and 5 ml/g/min.

A previously validated dual-bolus protocol was used for GBCA injection, with a pre-bolus of 0.001 mmol/kg of GBCA injected before a main bolus of 0.01 mmol/kg, (based on the weight of a 60kg patient)[130]. A minimum pause of 30 seconds was allowed between the pre-bolus and the main bolus of GBCA to ensure return to baseline values of signal in the vascular and myocardial compartments.

3D PET data was acquired in a single list-mode file and re-binned into short frames during the peak influx and washout phases (60 x 3 seconds) with longer frames towards the end of the washout phase (12 x 15 seconds). PET image frames were reconstructed using the standard manufacturer-issued filtered back-projection (FBP) algorithm available on the scanner (344 x 344 matrix, Gaussian smoothing filter of 4 mm. The resulting PET voxel sizes were 2.086 mm x 2.086 mm x 2.031 mm). Attenuation correction of PET data was provided by the standard dual-point VIBE T1-weighted Dixon sequence available on the mMR scanner front end[239]. Total attenuation of the phantom was low as there was no attenuating material surrounding the phantom.

A mean of 207.8±9 MBq was injected in order to exclude potentially confounding dead-time effects in the PET detectors. After preloading of $[^{18}F]F^-$ into the tubing, the main bolus of GBCA and $[^{18}F]F^-$ was injected simultaneously via a contrast injection system (Spectris Solaris, Bayer AG, Leverkusen, Germany) through the vena cava tubing of the phantom. Simultaneous dynamic PET-MR imaging was performed for a total of 300 seconds. A single simultaneous PET-MR acquisition was performed at each P_T step, and each step was repeated in order to gauge repeatability of the phantom. Following each scan, water was pumped through the myocardial compartments of the phantom for a minimum of 60

seconds between experiments to ensure a complete washout of GBCA and radiotracer before the next scan.

6.4.1.1.3 Image Analysis

Dynamic PET images were analysed in PMOD v 3.7 (PMOD Technologies, Zurich, Switzerland) to produce time-activity curves (TACs). 2D MR images were analysed in OsiriX (OsiriX 64-bit, version 8.0.2, Pixmeo SARL, Geneva, Switzerland) to produce time-intensity curves (TICs). A region of interest (ROI) of 1.6 cm (tubing diameter) was placed over the aorta of the phantom, and ROIs of 4 cm diameter were placed over the left and right myocardial sections, ensuring inclusion of the entire section of the vessel and tissue compartment in the segmentation. Positioning of ROIs on the PET image plane corresponding to the MR image plane was determined from fusion of the dynamic 3D PET and 2D summed dynamic MR images using PMOD. ROIs were placed on PET images over the same spatial area as the MR ROIs. The PET volumes of interest (VOIs) were 6.093 mm thick (3 PET slices) in the axial-dimension in order to match the slice thickness of the MR data (6 mm). All PET data were decay-corrected to the scan start time. We obtained a set of TACs and TICs for the aorta and myocardial compartments over the range of P_T.

6.4.1.1.4 MR perfusion calculation

In-house software was used for perfusion quantification (Labview 2014 for Mac, National Instruments, Austin, USA). A model-independent deconvolution approach was used to calculate the tissue impulse response function, providing results in units of 1/second and was not scaled to be in units of ml/g/min. In brief: relative perfusion can be calculated based on the central volume principle using a signal deconvolution method[143].

The TIC for the myocardial uptake function, *M(t),* can be calculated from the TIC for the arterial input function, $C_{in}(t)$, convolved with the tissue impulse response function *h(t),* in which $C_{out}(t)$ denotes the contrast concentrations in the venous out-perfusion:

$$M(t) = \int_0^t C_{in}(t-\tau) \cdot h(t)dt = \int_0^t [C_{in}(\tau) - C_{out}(\tau)]d\tau$$

We performed this calculation using the pre-bolus curve, $C_{in}(t)$, as an input function, in order to minimize the effect of signal saturation by the main bolus of higher GBCA concentration, (an effect which has been noted in previous work) and with this phantom at high GBCA dosages[130,149]. In the range of physiological concentration used in the pre-bolus injection, MR signal intensity is proportional to GBCA concentration. The tissue impulse response function *h(t)* has the shape of an exponential decay. MR relative perfusion measurements were calculated from the *h(t)*) when *h(t=0)*, i.e. at the peak point of the exponential decay. The delay between the arterial input TIC and the myocardial TIC was accounted for in the model[144].

6.4.1.1.5 PET perfusion calculation

PET data was modelled using a one-tissue compartment model characterized by a one blood compartment, one tissue compartment and two rate constants K_1 (uptake rate constant in units of ml/g/min) and k_2 (clearance rate from tissue to blood constant in units of min^{-1}). For this phantom study, using $[^{18}F]F^-$ we assume an extraction fraction of 1.0 due to the lack of any metabolic processes, and thus the K_1 constant is entirely representative of perfusion. In order to

eliminate any prospective bias, PET and MR data was analysed independently by two authors blinded to the true myocardial perfusion rates, P_T.

The terms ‘flow’ and ‘perfusion’ have been used interchangeably in both PET and MR literature. Owing to the fact that rates of liquid through our phantom were calibrated in ml/g/min (i.e. units of perfusion) and K_1 values from PET kinetic modeling were in the same units, we have opted for consistency in terminology and have used the term ‘perfusion’ rather than ‘flow’ (i.e. units of ml/min).

6.4.2 Results

6.4.2.1.1 Simultaneous imaging

As the PET acquisition is fully 3D (25.8 cm field of view), all myocardial chambers can be visualized simultaneously. Figure 6.2 illustrates the rapid passage of radiotracer from right atrium to ventricle, through the pulmonary circulation and into the left atrium and ventricle and exiting through the aorta.

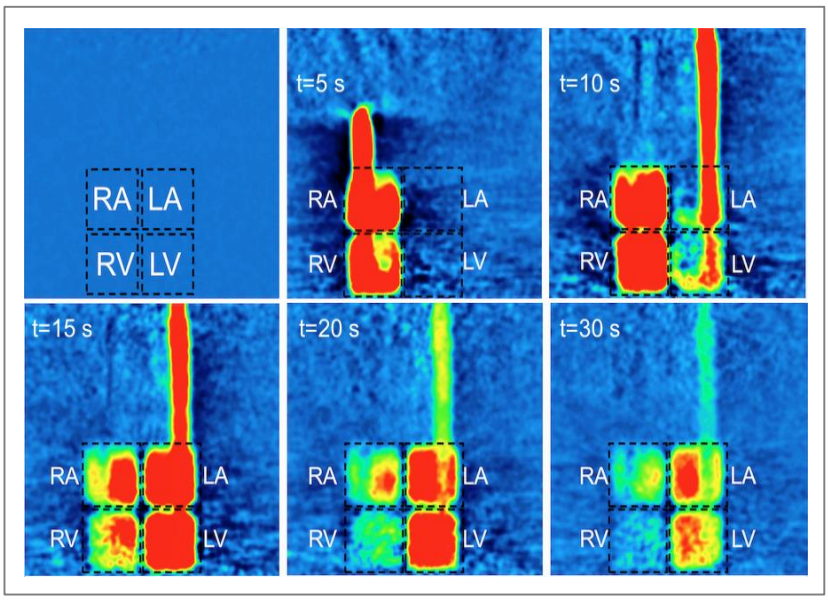

Figure 6.2 - Single coronal PET slice from the 3D phantom acquisition

Single coronal PET slice from the 3D phantom acquisition at a cardiac output rate of 3 L/min, showing an example of radiotracer distribution in the myocardial chambers at increasing post-injection time points. All images are shown at the same windowing and level.
(RA/LA=right/left atrium, RV/LV-right/left ventricle)

Figure 6.3 displays a fused transaxial image of the single MR slice with the corresponding merged 3 PET slices covering the same axial extent. The inset image of Figure 6.3 shows the passage of MR contrast only, which temporally matches the distribution of PET radiotracer. The expected GBCA and PET radiotracer distribution through the phantom can be seen at increasing time points of the 2D MR imaging sequence and fused PET-MR images detailing the first pass dynamics of the phantom.

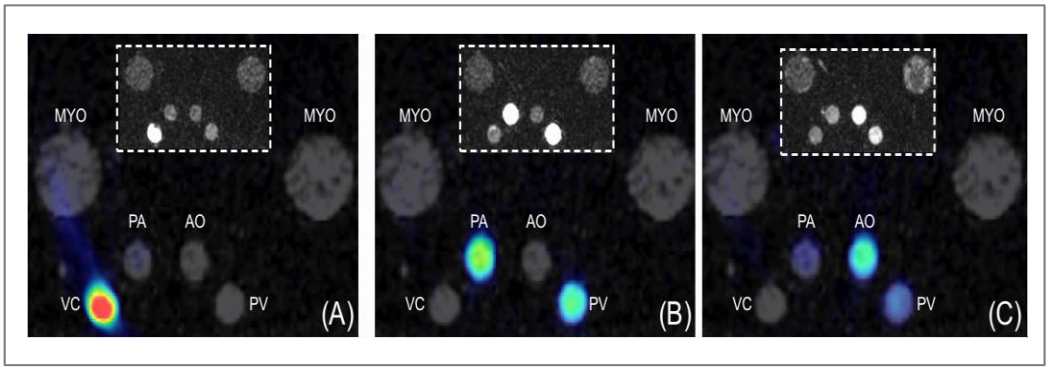

Figure 6.3 - Example of fused PET-MR images

Example of fused PET-MR images showing dynamics of GBCA and radiotracer transfer through the phantom. (A) – bolus in the VC (t=0 s). (B) – out-perfusion from the RV through the PA (t=3 s), (C) – coronary circulation to the PV (t=5 s) and the aorta (AO).
Inset images show the time distribution of GBCA only.

Image processing of the ROI/VOIs to produce TACs and TICs enables comparison of resulting mean PET kBq/ml to MR signal intensity during transit of the GBCA and radiotracer, as shown in Figure 6.4.

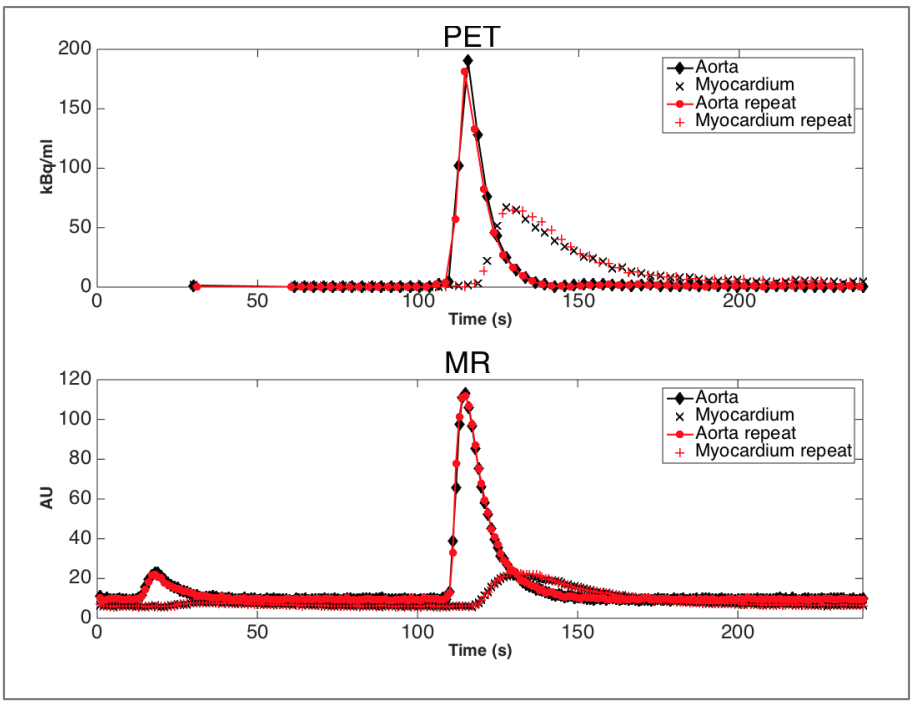

Figure 6.4 – Comparison of PET mean activity and MR mean signal time intensity curves

Comparison of mean activity concentration (kBq/ml) time activity curves (TAC) and mean MR signal (AU) time intensity curves (TIC) acquired from the phantom VOIs (PET-top) and ROIs (MR-bottom). Data are presented for simultaneous PET and MR acquisitions for a myocardial perfusion rate, P_T = 4 ml/g/min and cardiac output of 3 L/min. Repeat scan data using ROI and VOI in the same positions are also plotted and show a high level of repeatability. Error bars are omitted in order to improve visual clarity of overlapping traces.

As the repeat injection of [^{18}F]F$^-$ and GBCA was performed using the same timings and methodology as the first test, the time traces produced by both PET and MR data were similar. Although omitted from Figure 6.4 for clarity, for a single P_T of 4 ml/g/min, one standard deviation of the mean PET activity concentration from the VOI varied over time from ±2 to ±24%, while that of the MR mean ROI signal intensity varied over time from ±13% to ±29%. Standard deviations were similar for other values of P_T.

Figure 6.5 shows a comparison of the input functions from both imaging methods normalised by their respective maximum signal intensities:

- first between the peak of GBCA and the radiotracer (A),

- second between the MR pre-bolus peak (used for the MR perfusion analysis) and a time-shifted PET TAC overlaid to provide comparison (B), and

- finally a normalized comparison of the functions obtained from the myocardial chamber (C). These traces show that the input functions for both PET and MR models have similar characteristics but with clear difference in transit time, potentially due to higher mass and viscosity of the GBCA.

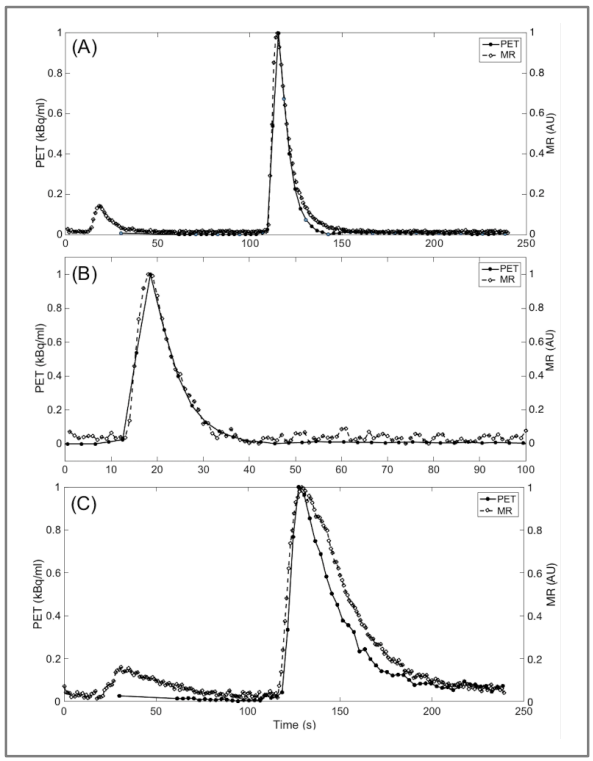

Figure 6.5 – Comparison of AIFs derived from PET and MR signal traces

Comparison of normalized (respective maximum signal intensity) AIFs derived from both PET and MR signal traces at a myocardial perfusion rate of 4 ml/g/min and cardiac output of 3 l/min. Image (A) represents the input functions from the main MR bolus and PET bolus, showing a longer washout of GBCA than radiotracer in the main bolus. Image (B) details the MR prebolus with the same PET bolus as (A) but time-shifted to provide comparison. Image (C) details the simultaneous curves from the myocardial compartment showing a clear difference in transit time, potentially due to higher mass and viscosity of the GBCA.

6.4.2.1.2 Perfusion calculations

PET datasets were used to calculate perfusion (ml/g/min) via K_1, and MR datasets to calculate relative perfusion values via *h(t=0)* as described above. Resulting K_1 and *h(t=0)* and are shown in

Table 6 below.

Table 6 - Results and repeatability of simultaneous quantification by PET or MR using cardiac phantom

	PET				MR	
P_T (ml/g/min)	K_1 (ml/g/min)	K_1 SE (%)	k_2 (l/min)	k_2 SE(%)	*h(t=0)* (s^{-1})	h(t=0) SE (%)
1	1.14	3.8	0.96	7.83	0.132	4.019
2	1.93	2	1.62	1.71	0.213	4.141
3	2.94	1.55	2.44	2.05	0.279	3.346
4	3.81	2.41	3.20	2.93	0.339	3.834
5	5.14	1.83	4.43	3.35	0.403	2.985
REPEAT						
1	1.18	0.5	0.99	7.68	0.133	3.953
2	2.07	1.87	1.87	1.74	0.201	3.112
3	2.98	2.6	2.60	2.06	0.293	4.526
4	3.98	3.21	3.21	2.16	0.384	4.259
5	5.07	4.44	4.43	3.48	0.457	3.214

Figure 6.6 shows three plots detailing the relationship between K_1 and P_T, *h(t=0)* and P_T and also *h(t=0)* and K_1. The results show that K_1 is linearly related to P_T (R^2=0.99), and that *h(t=0)* is also linearly related to both P_T and K_1 (R^2 values of 0.99 in both cases).

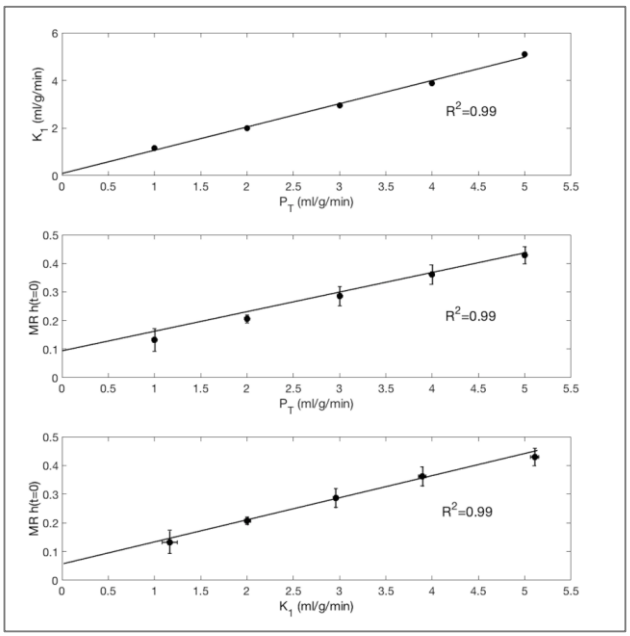

Figure 6.6 – Plots demonstrating linear relationship between true perfusion rate (P_T), and PET (K_1) and MR (*h(t=0)* data

Top - Resulting K_1 values from a single compartment model for PET data plotted against P_T.
Middle – MR values of *h(t=0)* from model-independent deconvolution for MR images plotted against the range of P_T. Bottom - MR values of *h(t=0)* plotted against the range of K_1 from PET kinetic modelling.

6.4.3 Discussion

We performed PET-MR tests using a specialized cardiac phantom allowing assessment of myocardial perfusion measurements with both imaging modalities from simultaneously acquired data. Both PET and MR are accurate tools for the assessment of myocardial ischaemia, but there are drawbacks inherent to each technique. For instance, in MR derivation of fully quantitative

perfusion units is still a complex process due to the relationship between signal intensity and gadolinium contrast and dependence on acquisition sequence[258]. In addition, dynamic imaging favours 2D images. This means that perfusion calculations cannot be representative of the entire volume. In PET, the cost of the perfusion exam can be prohibitive. The procedure requires access to short-lived radiotracers and thus access to a cyclotron. There is also a not insignificant radiation dose associated with the radiotracer. Although the principles of image formation between MR and PET are based on entirely different physical principles, we have shown that similar TACs and TICs from the arterial and myocardial compartments can be obtained from a single short acquisition. Furthermore, it has been possible to show that the results obtained with the employed MR and PET models are linearly related to the true myocardial perfusion rate, P_T.

The phantom is physiologically faithful and therefore enables exploration of some relevant aspects of perfusion dynamics of the human heart. Figure 6.2 and Figure 6.3 demonstrate the distribution of both GBCA and radiotracer through the right side of the cardiac chambers followed by the left, with perfusion through the myocardial compartments following shortly after. Simultaneous traces of PET activity concentration and MR signal intensity seen in Figure 6.4 demonstrates the transit of radiotracer and GBCA through the phantom, showing the simultaneity of PET and MR signals that can be achieved in this phantom. Our data also confirms that when a dual bolus approach is used in MR, linear perfusion estimates to those obtained in PET are achievable.

In this study, we adopted a dual-bolus injection scheme previously described and validated by our group[130,150]. The results of this study demonstrate that this

approach results in MR input functions which are very similar in shape and transit time to the reference standard PET input functions, as demonstrated in Figure 6.5. The myocardial compartment TAC and TIC match closely in terms of wash-in. Nevertheless, the MR TIC is observed to have a longer transit time than the radiotracer. We propose that this may be due to the higher particle mass and viscosity of the GBCA in contrast to the radiotracer.

One of the main benefits of the phantom model is its reproducibility. Table 6 demonstrates that repeat acquisitions at the same P_T give similar TAC and TIC. Upon calculation of perfusion via PET, K_1 values were in the range of 1.2%-7.5% of each other. A similar repeatability is shown in MR data with a repeatability of 0.6%-13% for *h(t=0)*. PET measurements at P_T = 1 ml/g/min showed an overestimation of P_T by 16%. The P_T rates of 2, 3, 4 and 5 ml/g/min were accurate to K_1 values to within a maximum of 2.65%, indicating good precision for repeated measurements and also good accuracy to P_T values above 1 ml/g/min. Variation in the true measurement of P_T = 1 ml/g/min due to physical inconsistency of the roller pumps may account for the larger differences at this value of P_T, and will be investigated in the next generation of the phantom currently under development. Although *h(t=0)* values represent relative perfusion measurement and were not scaled to represent absolute perfusion units, their relationship to P_T and K_1 can be clearly observed in Figure 6.6, which records the linear relationship found between *h(t=0)* and K_1, as well as *h(t=0)* and P_T.

Total analysis time of each series of PET images was approximately 30 minutes, and MR images were approximately 5-10 minutes. Owing to the geometrical differences between phantom and patient images, semi-automated

PET analysis software could not be used. Furthermore, PET images were re-binned into short frames of 3 seconds because of the rapid transit of the radiotracer in water. In a clinical image we expect to have to analyse a lower amount of data and frames.

Attenuation correction is a major issue in clinical PET-MR imaging and the focus of much research[235-240,259]. In this work, we utilised GBCA for the bolus injection, and in clinical studies the concentration would be far higher. Previous work by our group has shown that despite large concentrations of GBCA up to 65 mM (presenting the scenario of GBCA bolus in the left ventricle simultaneously with the PET radiotracer), the effect of attenuation of gamma photons by GBCA on quantified activity concentration (kBq/ml) in the final reconstructed images is less than 5% when compared to no GBCA present[260].

We believe that by providing a standardized setup and known perfusion rates, results, claims and hypotheses from clinical studies can be further investigated. Previous studies have shown that MPR calculated from independent CMR and PET scans have been shown to correlate well. There was a weak correlation between absolute CMR perfusion at stress and rest[111]. This may indicate that errors in quantification have a similar effect on stress and rest perfusion MBF values but are cancelled by calculation of the MPR. Future experiments could verify this finding by the exclusion of physiological variation. The phantom also allows comparison of kinetic models given the known ground truth of perfusion rates, and the potential for development of new hybrid kinetic models employing both PET and MR data. Another potential advantage of the approach is the possibility to address differences in the way images are acquired and modality-

specific artefacts, such as saturation effects in MR or attenuation correction in PET.

Knowledge of the relationship between P_T, K_1 and $h(t=0)$ may allow the creation of a modality-specific calibration curves. Particularly in the case of perfusion MR, this could allow converting the results of the deconvolution operation from seconds^{-1} to ml/g/min of perfusion. This approach could prove of value as a substitute for current approaches based on constraining the deconvolution operation[144,147]. This may lead to an improvement in the correlation between absolute MBF values measured with MR and PET.

6.4.4 Study limitations

1. The use of the phantom in this work for simultaneous PET-MR acquisitions as a surrogate for clinical acquisitions presents some fundamental limitations. Despite the fact that the TIC and TAC curves are similar in appearance for this simplified phantom study, it may not be the case for clinical studies in a human cohort due to the mechanism of transport of radiotracer (intracellular) and GBCA (extracellular). Therefore the phantom study serves to provide preliminary investigation into the standardized comparison between PET and MR perfusion values in a controlled simulation. The phantom model used in our experiments is not able to capture the broad range of body structures and physiological states that may be present in a clinical setting and as such represents an oversimplification of the cardiovascular system which cannot detail true myocardial diffusion or radiotracer uptake.

2. Despite a good correlation between PET and MR perfusion, there remain fundamental differences between the calculation methodology between the MR model-independent deconvolution approach and perfusion as calculated from a single compartment PET model. As is the mechanism with PET radiotracers, no separate tissue compartment exists, for example one with well-defined mechanical properties such as a membrane. Therefore true intracellular uptake cannot be simulated. Strategies would be required in order to simulate the kinetics of other perfusion tracers that undergo metabolic processes such as [^{13}N]NH_3 or [^{18}F]Flurpiridaz. Efforts will made to create myocardial compartments within the phantom, which would allow a more accurate approach to kinetic modeling.
3. We performed only 1 repeat acquisition of each P_T in this feasibility study. Repeat measurements would allow the calculation of a repeatability coefficient for both the PET and MR datasets.
4. The current phantom model setup is unable to reproduce the multiple sources of image artefacts in PET-MR such as the effects of motion due to respiration or cardiac contraction. Thus the phantom creates an environment free of these potentially confounding effects focusing only on the assessment of the perfusion dynamics within the cardiac compartments. Translation of calibrations from the phantom to the clinical setting should be treated with caution. Confounding factors from clinical data may include the use of respiratory correction via importation an average cine CT or using MR-based navigators[261] or employing MR motion-field based cardiac motion correction employed in PET

reconstruction[262]. Efforts to apply these techniques specifically to quantitative dynamic PET-MR cardiology are in their infancy, although some techniques are currently under development for static imaging[246,263].

6.5 Conclusion

The advances in PET and MR technology have paved the way for the combination of these modalities and to allow the strengths of each to be harnessed simultaneously. One of the additional benefits is the ability to directly compare results of parameters such as perfusion from each without concerns in physiological variations which may occur with a time lag between studies.

Though in its infancy this represents an exciting opportunity and preliminary preclinical and clinical results have been encouraging. The experiments performed in this study demonstrate similar first-pass dynamics of both the PET and MR contrast agents. Importantly, we have also established a correlation between perfusion quantification of the PET time-activity traces using a kinetic model, relative MR perfusion using a deconvolution model and the true manually set myocardial perfusion rate. This work contributes to the growing body of knowledge on PET-MR and will inform future clinical studies.

The phantom used in this study has the potential for improving standardisation of perfusion measurements, analysis routines, development of imaging protocols and potential calibration of MR perfusion.

7 Excitation-contraction coupling and the cardiac microarchitecture

7.1 Introduction

Previous chapters have detailed the tightly coordinated vasodilatory capacity and the relevance of myocardial ischaemia to cardiac function. Electrical impulse propagation and the cardiac microstructure are also highly coordinated to deliver effective cardiac output. In heart failure, these precisely synchronized systems are disrupted. This chapter will discuss heart failure from the perspective of excitation-contraction coupling and the cardiac microarchitecture.

This chapter will describe the highly structured system at cellular and tissue level, underlining the need for adequate and continuous ATP supply and an efficient supply of oxygen-rich blood.

The bulk of this chapter will focus on the use of cardiac diffusion tensor imaging, an advanced CMR technique for in-vivo imaging of cardiac myofibres. This will include a study which examines myofibre architecture in dilated cardiomyopathy and proposes insights into the underlying mechanistic processes using dual heart-phase cardiac DTI, 3D tagging and biomechanical modelling. We proposed the hypothesis that there would be structural differences at a myofibre level that would relate to the reduced cardiac contractility seen patients with DCM. Furthermore, we hypothesised that these changes could adaptive in preserving function in DCM. Eva Sammut was joint first author on the publication and was responsible for patient recruitment and scanning, and involved in analysis and drafting of the manuscript.

7.2 Excitation-contraction coupling

Excitation-contraction coupling is a vast topic which can only be summarised here. As suggested by the term, excitation-contraction coupling (ECC) refers to the physiological process of conversion of an electrical stimulus to a mechanical response. This is central to the heart's ability to generate adequate contractile force.

In the myocardium the action potential is produced by spontaneous depolarisation of the pacemaker cells in the sino-atrial (SA) node (in contrast to the skeletal muscle cell where membrane depolarisation is triggered by neuronal activity). From the SA node, the electrical impulses excite the right atrium and spread to the atrio-ventricular (AV) node. The impulse then travels through the Bundle of His, which has the special quality of rapid electrical transmission, and to the left and right bundles, which depolarise the left and right ventricle respectively, almost simultaneously. This process is initiated by excitation-contraction coupling (ECC), a cascade of events which triggers shortening of many sarcomeric units - contractile units composed of actin and myosin filaments within each myocyte to produce cardiac contraction. Individual myocytes are interconnected by intercalcalated discs (made up of three types of cell-cell junction - fascia adherens, desmosomes and gap junctions) – the gap junctions facilitate electrical communication from one myocyte to the next, producing smooth coordinated contraction of the myocardium. The myofibre arrangement is also crucial to the maximising the force of contraction and the volume of blood ejected from the ventricles in systole.

On depolarisation, sodium ion influx triggers opening of L-type calcium (Ca^{2+}) channels on the myocyte cell membrane. The influx of calcium ions to the cell

via L-type channels binds to, and activates, ryanodine R2 (RyR2) channels located on the sarcoplasmic reticulum (SR) causing further release of stored calcium[264,265]. This phenomenon is known as Ca2+ induced-Ca2+ release (CICR). The transient local increase in cytosolic calcium concentration due to release of stored Ca2+ from the SR is known as a calcium spark. When one RyR receptor is activated this leads to another and another being activated - a wave of Ca2+-induced activation, the whole cell CA2+ transient, spreads across the cell causing contraction of the sarcomere[264]. The majority of calcium release into the cytoplasm is from the SR with a ratio of stored versus influx in the region of 10:1, with a smaller amount of Ca2+ entering the cell via the Ca^{2+}/Na^{2+} exchanger pump[266].

An increase in cytosolic Ca^{2+} binds to troponin C which modulates the troponin complex on the sarcomere and exposes a binding site on the actin molecule. The myosin head binds to ATP using myosin ATPase and attracts the actin filaments towards the centre of the sarcomere – the actin and myosin filaments slide over one another and shorten myocyte length.

This is a continuous process which occurs as long as cytosolic calcium concentration remains high. Ca^{2+} is actively removed from the cytosol predominantly by the sarcoplasmic reticulum ATP-dependent (SERCA) pump, the sodium-calcium exchanger pump (NCX), the sarcolemmal Ca2+ ATPase, and via the mitochondria. The relative proportion of each Ca^{2+} removal method depends on the species studied – in humans, the predominant removal mechanism is via the SR Ca^{2+} ATPase (around 70%), with around 28% related to the NCX pump and only around 1% is removed by other methods[267].

To maintain homeostasis, the Ca^{2+} released in the cytoplasm must be thoroughly removed within each cardiac cycle. This results in removal of calcium ions from the troponin complex, and inhibits the actin-binding site, thus restoring the relaxed sarcomere length.

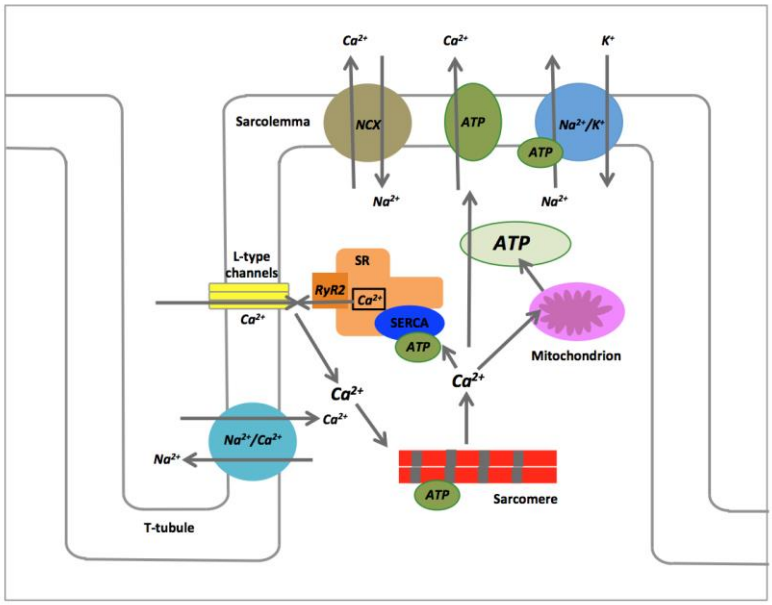

Figure 7.1 - Schematic representation of excitation-contraction coupling

Schematic representation of excitation-contraction coupling. Ca2+ enters the cell via L-type channels which triggers release of stored Ca2+ from the sarcoplasmic reticulum (SR) via the ryanodine R2 (RyR2) channels. Ca2+ also enters the cell via the Ca2+/Na+ exchanger pump. The Ca2+ transient is used for sarcomeric shortening (cardiac contraction). Ca2+ is removed from the cytoplasm via the SR SERCA pump, Na2+/Ca (NCX) pump and via the Ca2+ ATP pump.
Adapted from Bers et al.[267]

CICR is dependent on tight coupling between the L-type and RyR2 channels, primarily achieved by a highly organised dense network of T-tubules, invaginations of the sarcoplasmic reticulum which penetrate the cell. This close physical proximity of channels facilitates almost instantaneous, synchronous excitation of the sarcomeric units within each myocyte. The other major factor is

adequate availability of ATP since ECC requires considerable amounts of energy. The main cellular energy consumers are the myosin ATPase of the contractile filaments, the NCX pump, and the SR Ca^{2+} ATPase[268]. Even at rest, ECC consumes vast amounts of energy - during maximal workload, there is turnover of the entire ATP pool each couple of seconds[265,269-271].

7.3 Excitation-contraction coupling in heart failure

It is accepted that lesser and slower contraction of individual cardiomyocytes contributes to reduced overall contractility in heart failure[272,273]. Fundamental to this is a decrease in Ca^{2+} transients due to a lesser Ca^{2+} release from the SR upon L-type channel activation[274,275]. This is related to decreased SR Ca^{2+} content, leakage of the RyR channels, reduced activity and expression of SERCA function or increased NCX pump activity[276-278].

Excitation-contraction coupling occurs primarily at the sites of T-tubule/ sarcoplasmic reticulum junction. In heart failure there is reduced density, dilatation or abnormal orientation of the T-tubule network. The loss of T-tubules results in dyssynchronous release of sarcolemmal calcium due to a physical uncoupling of the L-type and RyR receptors. Loss of T-tubule integrity has been linked directly to the progression of heart failure[279].

.

7.4 Cardiac deformation

The complex muscle structure of the heart is made up of cardiomyocytes which contract upon an electrical stimulus. During contraction, there is motion in three

orthogonal directions – longitudinal, circumferential and radial - each myocyte thickens in diameter and shortens in length, producing shortening in the longitudinal and circumferential direction and concurrent thickening in the radial direction. In the healthy heart, using tagging CMR (this will be discussed in more detail later in the chapter) the left ventricle has been shown to shorten 15-20% in the longitudinal and circumferential direction and thicken 30-40% in the radial direction. There is also simultaneous rotation of the heart - when viewed from base to apex the base moves in an anti-clockwise direction and the apex in a clockwise direction[280]. 'Twist' is defined as the difference between rotation at the base (negative angle) and at the apex (positive angle). This is typically 10-15 degrees. 'Torsion' is twist normalized to long axis length. More rotation is noted at the apex than the base and in the subendocardial layer relative to the subepicardium[280]. This complex, spiral, motion leads to the stroke volume being expelled efficiently from the cavity. The difference between end-diastolic and end systolic function, represented as a percentage, equates to the left ventricular ejection fraction.

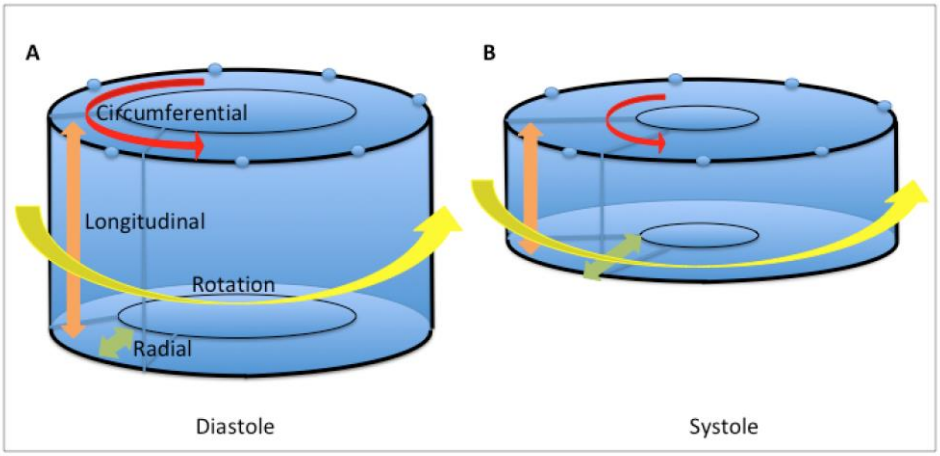

Figure 7.2 - Schematic diagram depicting the three orthogonal components of myocardial motion

The three components of myocardial deformation are longitudinal, circumferential and radial strain. During systole, the heart shortens in the longitudinal and circumferential directions and increases in the radial direction. In addition, the heart rotates during contraction.

7.4.1 Myocardial strain

CMR anatomical cine-imaging permits high-resolution appreciation of the subendocardial and subepicardial borders which can be manually segmented to provide accurate measures of left ventricular volumes and used to calculate ejection fraction, left ventricular mass and wall thickness. Global measures do not adjust for regional wall motion abnormalities. Furthermore, identification of a regional wall motion abnormality does not consider whether a region is actively contracting or whether it is passively 'pulled' by an adjacent region. In addition, rotation of the heart and through-plane motion can make visual interpretation challenging.

In recent years, there has been significant interest in more detailed, quantitative assessment of myocardial deformation, and calculation of strain and strain rate. Strain is defined as "a dimensionless quantity produced by the application of a stress in terms of a fractional change from the unstressed dimension". Put

another way, strain, for which the symbol ε is used (with L the length of the object after deformation and L_0 its original length), can be expressed:

$$Strain = \frac{L - L0}{L}$$

Strain can be measured invasively using surgically embedded radio-opaque markers[281-284] or ultrasound crystals (sonomicrometres) [285,286] into the myocardium, and plotting their movement in the cardiac tissue using fluoroscopy or ultrasound. This can only be applied to animal models, cannot be applied repeatedly and the implants may themselves alter the local tissue dynamics.

Strain can be assessed non-invasively by echocardiography using Doppler imaging or speckle tracking, or using CMR phase contrast imaging[287-289] or myocardial tagging sequences.

7.4.2 Myocardial tagging

Myocardial tagging is used to evaluate the dynamic deformation of lines or grids superimposed on the myocardium during the cardiac cycle. First introduced in 1988 by Zerhouni et al.[290], it involves modulation of the tissue magnetization using specific radiofrequency prepulses to create visible markers, seen as grids or parallel lines, on the myocardium which can be imaged and tracked over time. To eliminate influence by respiratory motion this is typically done during a breath-hold with a navigator sequence to ensure a similar cardiac position within the thorax.

A number of different sequences are available for tagging (SPAMM, DENSE, DANTE, HARP, CSPAMM, SENC). Each of these has been refined to improve resolution, signal-to-noise and scan time.

In 2D tagging, the tagging lines are applied perpendicular to the imaging plane to perturb the longitudinal magnetization at specific locations (creating the grid) without affecting the magnetisation of surrounding regions. These 'lines' are initially black due to the magnetization saturation and move with the tissue producing images through the cardiac cycle. Since tagging lines represent alterations in the longitudinal magnetization, they fade with relaxation due to exponential decay of T1. As a result, tagging is better quality at 3-Tesla than at 1.5-Tesla (longer T1 time at higher field strength) and is better pre-contrast (contrast shortens T1 relaxation). 2D tagging is the most commonly used tagging method whereby a stack of short axis images is acquired and a 3D reconstruction is created by means of data interpolation. The disadvantage of 2D tagging is its susceptibility to through-plane motion where a point moves out of the imaging plane and may be incorrectly assigned to another point. 3D tagging involves application of three orthogonally-orientated tagged cine lines to cover the entire LV permitting calculation of three-dimensional displacement fields free of the issue of through-plane motion. 2D tagging can be assessed visually but the significant advantage of tagging is the potential for quantification of the three components of myocardial motion – longitudinal, radial and circumferential strain – and torsion.

Normal strain values vary but different groups have reported similar average values[291,292]. Results from tagging data compare to measurements from speckle tracking[293] and sonomicrometers[294]. There has been much interest in

the clinical relevance of strain and this may provide insight into cardiac mechanics and also complement standard indices of pump function such as ejection fraction. Longitudinal strain has been noted to be abnormal in cases of: heart failure with normal ejection fraction[295]; chemotherapy-related cardiotoxicity[296]; cardiac amyloidosis[297]; hypertrophic cardiomyopathy[298] and Takotsubo cardiomyopathy[299]. A meta-analysis, pooling 16 studies (5721 patients) on heart failure, acute MI and valvular heart disease, has shown global longitudinal strain to be a stronger predictor of mortality than LV ejection fraction[300]. The degree of torsion is also a useful and interesting index. A number of studies have shown that in dilated cardiomyopathy, rotation of the heart has an inverted pattern or is reduced[301-304].

7.5 Cardiac microstructure in the healthy heart

In 1965, Grant et al. stated that “the search for an accurate and detailed picture of the muscular architecture of the left ventricle is by no means trivial”[305]. The myocardium consists of a three-dimensional functional syncytium of branching and inter-connecting myocytes embedded in a predominantly collagen matrix. Myocytes are clustered into myocyte aggregates which cannot be truly defined as distinct fibres but which are separated by collagen sheetlets[305-307]. These laminar sheetlets (previously called sheets) each consist of a layer of five to ten branching myocytes which interconnect with neighbouring layers. The connection of myocytes between layers is most prominent at the epicardium and decreases significantly through the mid wall and subendocardium with a heterogenous extension of sheetlets through the LV wall. Sheetlets are

orientated perpendicular to the local myocyte plane and appear to fall into two distinct populations, generally perpendicular to one another[308,309] – these are not however completely separate and are seen to intersperse in the mid myocardium[310,311].

In the left ventricle, the overall direction of myocyte aggregates is found to follow a helical arrangement (see Figure 7.3). These run in opposite directions at subendo- and subepicardial level. The helix is right-handed (positive angulation) at subendocardium and transitions to being left-handed (negative angulation) at the subepicardum with myofibre aggregates in the mid LV layer being orientated transversely[312].

The helical arrangement is consistent with the torsion direction noted macroscopically in the epicardium because of greater epicardial muscle mass and a greater moment arm around the long axis[292]. The helical arrangement of the myocytes is expressed as the helix angle– this is taken to be the angle between the locally defined transverse plane and the angle of the principal myofibre direction.

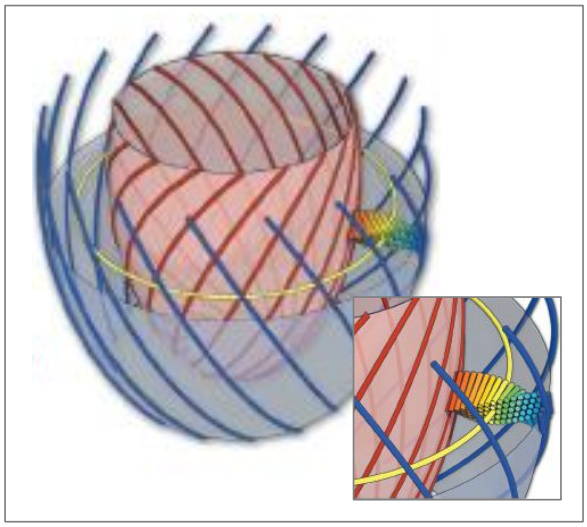

Figure 7.3 - Schematic diagram showing helical arrangement of epicardial and endocardial myofibres

Subendocardial and subepicardial myofibres follows a helical arrangement which run in opposite directions. The mid LV myofibres are arranged transversely.
Myocytes are clustered into myocyte aggregates separated by collagen sheetlets. These laminar sheetlets each consist of a layer of five to ten branching myocytes which interconnect with neighbouring layers.
Adapted from Nielles-Vallespin et al.[313]

7.6 Cardiac contraction

Individual myocytes have been shown to shorten by only around 15% and thicken by around 8% during systole[307]. This does not fully account for the magnitude of myocardial wall thickening known to be at least 30%[313]. In order to explain this discrepancy, it has been proposed that there is dynamic rearrangement of the helical arrangement of the myofibres and, furthermore, that the cleavage planes between the myocytes allow for sliding of the sheetlets in respect to one another with cardiac contraction[314,315]. Indeed, in early work by Spotninz et al. the number of myocytes across the ventricular wall was seen to increase from end diastole to end systole. This supports the theory of a dynamic

rearrangement during cardiac contraction[316]. Other studies have used confocal micrography to show that there is a reduction in resistance to shear stress during contraction which facilitates radial thickening[317,318]. Cardiac myofibre arrangement has been examined using animal models with hearts arrested in systole and diastole. This demonstrated that in diastole, the myofibre aggregates are aligned more tangentially to the epicardial surface and in systole they assume a more transverse orientation[315,319]. Changes in both the helix angle and sheetlet angle during contraction have been observed but it is the sheetlet angle that is generally considered to be the principal component responsible for macroscopic LV wall thickening (see Figure 7.4).

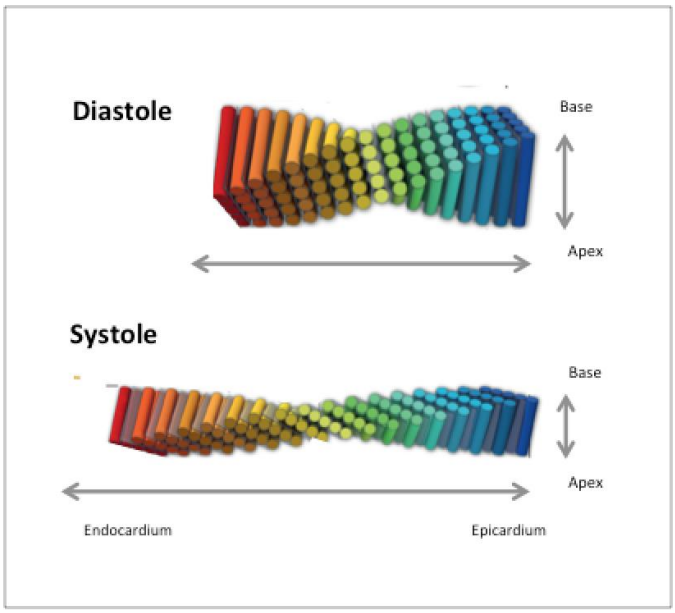

Figure 7.4 - Schematic diagram showing dynamic alteration in myofibre alterations during cardiac contraction

Myocytes are clustered into myocyte aggregates separated by collagen sheetlets. These laminar sheetlets each consist of a layer of five to ten branching myocytes which interconnect with neighbouring layers.
During cardiac contraction, there is shortening of the ventricle from base to apex with concurrent wall thickening, related predominantly to a more transverse sheetlet angulation in systole.
Adapted from Nielles-Vallespin et al.[313]

7.7 Diffusion tensor imaging

Diffusion tensor imaging (DTI), also known as diffusion tractography, is a CMR technique which permits study of tissue microstructure in-vivo.

In-vivo DTI is well established for imaging of static organs such as neurological tracts in the brain[320,321]. The base premise of DTI involves the imaging of the diffusion of water. When this is not bound to tissue, water will diffuse at the same rate in all directions – this can be visualized as a sphere. In contrast, within a tissue, water will diffuse more freely in one direction than in others - this is known as the phenomenon of anisotropy. This produces a different diffusion characteristic which will be seen to progress in different directions and this can be used to create a map of diffusion. In can, in turn, be applied to an image of the structure of interest - the displacement probability of diffusing water molecules within the tissue is measured and the arrangement of the mean direction of water diffusion can be reconstructed.

Cardiac DTI is acquired as a series of 2D short axis slices which can then be reconstructed in 3D form. In cardiac DTI, the use of diffusion-sensitising sequences permits calculation of a set of three eigenvectors (see Figure 7.5).

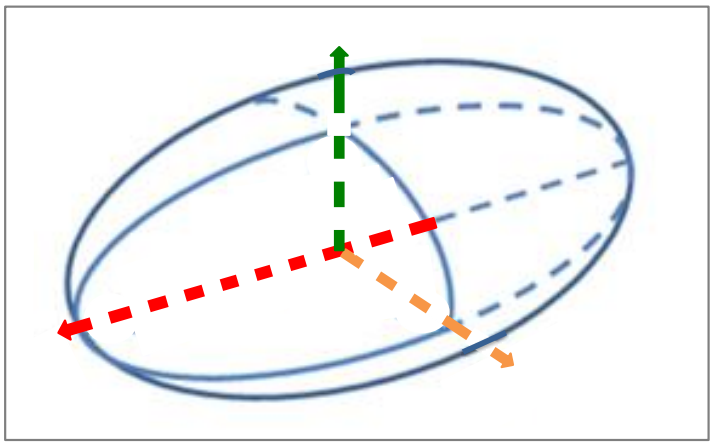

Figure 7.5 - Schematic showing the three orthogonal eigenvectors used in DTI

Three orthogonal eigenvectors are used in DTI to create a map of water diffusion in a tissue of interest. In cardiac DTI, the first eigenvector (red arrow) represents the mean intravoxel myofibre orientation from which the helix angle can be calculated, the second eigenvector (orange arrow) represents the sheetlet orientation from which the mean intravoxel sheetlet angle can be calculated and the third eigenvector (green arrow) represents the sheet normal direction.
Adapted from Tseng et al.[322]

Water will diffuse more readily along the myofibre and therefore the first, largest eigenvector (E1) represents the average local myocyte orientation within the voxel. The second, and second largest, eigenvector (E2) corresponds to the average local sheetlet direction. E1A is the angle relative to the local wall tangent plane and represents the mean helix angle. E2A is mean intra-voxel sheetlet angle. The third eigenvector is the sheet-normal which is perpendicular to the helix and sheet plane (also known as the transverse angle).

Scalar metrics such as mean diffusivity (MD) and fractional anisotropy (FA) permit characterisation of structural integrity by recording the degree of free diffusion in a tissue as a general measure- 'diffusivity' is the average of the sum of eigenvalues; 'fractional anisotropy' is an index which reflects the degree of anisotropy within a voxel (the difference by which the tissue diffusion compares to an idealised sphere).

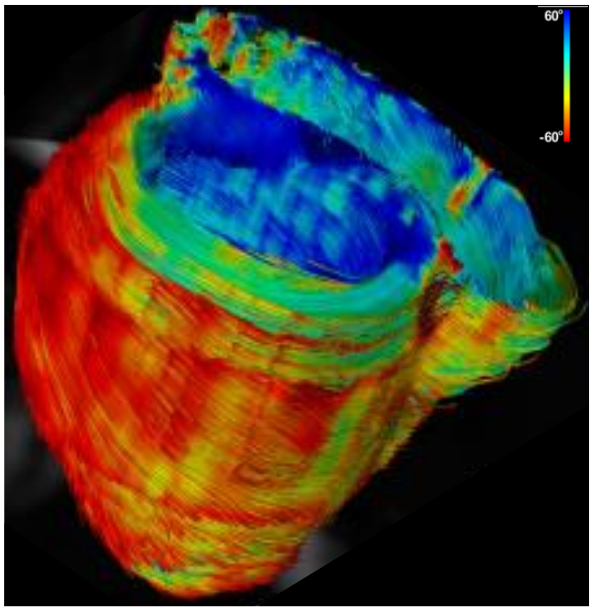

Figure 7.6 – Example of reconstructed 3D whole heart DTI image

Reconstructed 3D whole heart image representing measured helix angles from in-vivo cardiac DTI. Note the change in colour indicates the helix angle, with variation from subendocardium to subepicardium.
Adapted from Mekkaoui et al.[323]

7.7.1 Challenges of cardiac DTI

The application of DTI to a moving tissue, in particular the heart, is more challenging than in a static organ such as the brain.

The relaxation time of the myocardium is significantly shorter than in the brain. This imposes significant restrictions on the echo time that can be used. Secondly, inhomogeneity of the B0 field is increased in the thorax, particularly at higher field strengths, by comparison with the brain. This leads to higher incidence of artefacts which can affect the diffusion-weighted images. Finally, the application of DTI in a beating heart with respiratory motion and displacement of the myocardium during cardiac contraction is even more

challenging - the diffusion of water is several orders of magnitude smaller than bulk motion.

Until relatively recently, cardiac DTI was only feasible in an ex-vivo model in order to counter some of the challenges described above. These early studies showed that cardiac DTI was possible without destruction of the myocardial architecture and was validated against histological examination[315,324,325]. It was demonstrated that the first and second eigenvectors correlated with histological findings of the mean orientation of the myofibres and sheetlet direction respectively. Other studies have used animal models to explore pathophysiology. These studies have used ex-vivo cardiac DTI in experimental models of myocardial infarction and myocardial ischaemia[323-325]. Most studies have been performed in experimental preclinical models and though animals can be examined more extensively, there are conflicting reports on similarities myofibre architecture between species[323,326].

Ex-vivo cardiac DTI suffers from various limitations related to: the method/ duration of fixation of the tissue; the cardiac phase in which the heart was fixed (ie in a systolic or diastolic state) and the absence of normal loading conditions. This has stimulated the search for ways to overcome the limitations.

7.7.2 Challenges of in-vivo cardiac DTI

The sequences used for ex-vivo images (pulsed gradient spin echo/ Stejskal-Tanner sequences) are highly motion sensitive and therefore would not be suitable - the signal relating to diffusion would be overwhelmed by bulk motion.

A number of other sequences have been proposed. The most commonly used approach is the dual-gated stimulated echo acquisition mode (STEAM) sequence. The physics principles related to this sequence are beyond the

scope of this thesis. In essence these involve three excitation pulses applied over two successive heartbeats. This sequence is relatively insensitive to cardiac motion but is not robust in arrhythmia, as it requires a regular R-R interval and matched cardiac position between the two pulses. The STEAM sequence has been criticised on the grounds that the use of two successive heart beats is inefficient in producing a signal and there is loss of signal between the two RF pulses. In addition to respiratory motion, cardiac DTI in the beating heart is also affected by cardiac contraction and strain. The need for specific correction of strain continues to be a debated issue but there is agreement that strain produced by myocardial deformation has an impact on diffusion measurements. An effective in-vivo cardiac DTI sequence would be capable of the following:

> Encoding of diffusion in a very short time period so that the myocardium is almost immobilized at the time of contraction, and
>
> Insensitivity to diffusion outside of the time of encoding period so that the diffusion measurement will not be affected by motion effects from times outside of the diffusion encoding period[327].

This is a particular concern when using the STEAM sequence for in-vivo imaging given the relatively long acquisition time. One proposed approach to resolve this is to image at the so-called 'sweet-spot' – a time point, individual for a subject, where the temporal mean of strain approaches zero thereby eliminating the effect of strain[318,328]. Typically this is at the mid-systolic or mid-diastolic phase of the cardiac cycle. Ex-vivo studies have shown significant dynamic rearrangement of myofibre architecture during cardiac contraction and recent years have seen growing interest in performing dual-phase in-vivo

cardiac DTI where the fibre architecture can be examined in systole and diastole. Some studies have shown that at peak systole the results of diffusion DTI, in particular the sheetlet angles, are significantly affected at end-systole unless strain is measured and specifically corrected for[329]. Other studies have shown that the effect of strain compares well to ex-vivo measurements if measured at the sweet-spots, where strain is negligible and therefore not a factor[313,330].

In-vivo cardiac DTI has been used to report normal ranges of helix and sheetlet angles in healthy hearts[331-334]. Pathological conditions such as myocardial infarction, hypertrophic cardiomyopathy and, more recently, dilated cardiomyopathy have been investigated with in-vivo cardiac DTI[313,330,335-337]. In-vivo cardiac DTI has been shown to be reproducible in healthy hearts and also in patients with hypertrophic cardiomyopathy[333,338].

A number of ex-vivo and in-vivo cardiac DTI studies have shown that there is a limited degree of change in helix angle between systole and diastole but a more significant change in the sheetlet angle[315]. The sheetlet dynamics have been shown to be abnormal in ex-vivo experimental canine models of ventricular dyssynchrony and rodent models of dystrophy, and more recently in in-vivo work of hypertrophic cardiomyopathy and dilated cardiomyopathy[313,330,337].

With these studies as background, we performed the following study with the specific aim of exploring the use of dual phase in-vivo cardiac DTI alongside 3d myocardial tagging for strain correction in a group of patients with dilated

cardiomyopathy. Furthermore, we used biophysical modelling to try to gain further insight into the mechanism.

7.8 Dilated cardiomyopathy

Dilated cardiomyopathy (DCM) is an umbrella term which encompasses a range of acquired and hereditary diseases but by definition is unrelated to obstructive epicardial coronary disease. On a macroscopic level, regardless of aetiology, DCM results in a cascade of events propagated by ventricular chamber enlargement and progressive contractile dysfunction. Over time, the heart loses the ability to compensate for the loss of contractile force and clinical manifestations become apparent. In addition, activation of neurohormonal pathways exacerbates cardiac haemodynamic abnormalities and leads to adverse cardiac remodelling or end organ damage. The clinical course is variable but is progressive and largely irreversible. The decline of cardiac function brings a risk of sudden cardiac death from malignant arrhythmias. Despite developments in understanding and treatment approaches, the disease is not yet fully characterised and prognosis remains poor. On a cellular level, regardless of aetiology, histological findings tend to be non-specific, with hypertrophy and elongation of myocytes, reduced density of myofibrils, cellular necrosis, and fibrosis[339]. An understanding of the structural adaptations and maladaptations, and pathophysiological responses of the condition in-vivo remains a prime aim of development of new approaches to therapy.

7.9 Studying dynamic myofibre reorientation in dilated cardiomyopathy

7.9.1 Methods

7.9.1.1 Study Protocol

Patients with non-ischaemic dilated cardiomyopathy were enrolled at St Thomas' Hospital, King's College London. The criteria for DCM included left ventricular ejection fraction (LVEF) below 50%, no myocardial scar on previous cardiac MR scan, and a previous invasive coronary angiogram confirming unobstructed epicardial coronary arteries. All patients were taking maximally tolerated medical therapy at the time of enrolment. Age-matched healthy volunteers without a history of cardiac events were enrolled as the control group at the University Hospital Zurich. Imaging, at both sites, was performed on 1.5T Philips Achieva systems (Philips Healthcare, Best, The Netherlands) equipped with 32-channel cardiac receiver arrays. Written informed consent was obtained from all subjects prior to imaging, and the study protocol was approved by the ethics committees of King's College London and the Canton of Zurich.

Prior to diffusion imaging, balanced steady state free precession (bSSFP) cine data (spatial resolution 2x2x15 mm^3, temporal resolution 30 ms) was acquired in two-chamber and short-axis view of the left ventricle (LV). On cine images, subject-specific mid-diastolic and peak-systolic time points were visually determined. To assess cardiac function, a contiguous stack of short-axis cine images from apex to base was acquired (spatial resolutions 1.6x1.6x8 mm^3, temporal resolution 30 ms).

7.9.1.1.1 Diffusion Tensor Imaging

Diffusion weighted imaging was performed in short-axis view orientation using stimulated echo acquisition mode (STEAM) imaging with single shot echo planar image (EPI) readout[340]. The imaging plane was placed at mid-ventricular level and the acquisition was ECG triggered to peak systole and mid diastole. Consistent levels of breath holding were ensured by respiratory navigator gating (gating window 5 mm). Eight signal averages for each diffusion direction were acquired within a single breath hold. A total of ten optimized diffusion directions were encoded (25) with a b-value of 350 s/mm^2, resulting in 22 breath holds for two cardiac phases. Parameters of the diffusion sequence were: field-of-view: 309×129 mm^2, in-plane resolution: 2.5×2.5 mm^2, slice thickness: 8 mm, TE/TR 18 ms/2 R-R intervals, partial Fourier factor 0.65.

7.9.1.1.2 Motion Imaging

Tissue motion and strain were quantified using three-dimensional complementary spatial modulation of magnetization (CSPAMM) tagged imaging, employing a segmented echo planar imaging readout[341]. Three tagged cine image volumes were acquired in two long and one shot axis plane sequentially, covering the whole LV. Data acquisition was navigator gated (acceptance window 15 mm) within three consecutive breath holds, each spanning over 18 heartbeats. Imaging parameters were as follows: field-of-view: 108x108x108 mm^3, spatial resolution: 3.5x7.7x7.7 mm^3, tag line distance: 7 mm (EPI factor 7, 3 excitations per heart phase), temporal resolution: 20 ms. Geometrical stack alignment of all tagged volume images was performed by incorporating navigator offsets and rigid image registration.

7.9.1.1.3 Data Analysis

Functional Analysis

Left and right ventricular volumes and ejection fraction, and left ventricular mass were calculated by manual drawing of end-diastolic and end-systolic contours on short-axis images excluding the papillary muscles (CVI software, Circle Cardiovascular Imaging Inc., Canada). Left ventricular wall thickness was measured at end diastole and end systole in the mid LV, at the level of the papillary muscles.

Diffusion Tensor Analysis

Upon image registration, systolic and diastolic diffusion tensors were determined taking into account diffusion weighting of the "b=0 s/mm^2" image[342]. Systolic diffusion tensors were corrected for myocardial strain, as previously reported[329]. Upon tensor calculation, helix, transverse and sheet angles were computed as described in the supplemental material.

For each diffusion tensor, a locally normalized transmural position was calculated. Helix angles (HA) were binned along ten equidistant transmural positions, followed by linear regression to determine the slope of the transmural HA course. To avoid partial voluming effects at the endo- and epicardial boundaries, data points from 80% of the inner myocardium were used for data fitting. HA ranges were computed as differences between maximum (endocardial) and minimum (epicardial) HA values within the 80% transmural interval. MD, FA, HA slope and transverse angles (TA) were evaluated in the whole left ventricle for each cardiac phase and reported as median and interquartile ranges across both groups. Radial and axial diffusivities were

computed similarly and are reported in the supplemental material. Sheetlet angles were evaluated in the anterior-septal region in the proximity of the surface coils to reduce the impact of noise as a confounding factor. Sheetlet angles are reported as histograms for both cohorts (see Figure 10.10).

Motion and Strain Analysis

On the 3D tagging data, endo- and epicardial contours of the LV were manually defined while excluding papillary muscles. Longitudinal and circumferential strain were determined by contour tracking utilizing the SinMod algorithm (TagTrack, GyroTools LLC, Zurich, Switzerland)[343]. Radial strain was evaluated by the Harmonic Phase algorithm[344]. Cardiac torsion was normalized to long-axis length as described previously[345]. Circumferential and radial strains are given in the mid ventricular region. Longitudinal strain was computed across the whole LV.

Biomechanical Modelling

Two idealised geometric models of the LV truncated at the base were created using the average measurements (end-diastolic long and short-axis lengths, wall thickness and cavity volumes). The two models represent an average of the control and DCM populations. Fibre distributions were chosen to match the average end-diastolic HA slopes observed in the respective cohorts. Figure 7.7 shows both models as well as the HA maps in short-axis view.

Sheet angle (E2A) distributions were chosen to match the frequencies observed in the data at end diastole, with idealised transmural variation based on previous studies (6,31) changing from 0° to 90° between endocardium and midwall, and

from -90° to 0° between midwall and epicardium. Passive inflation and active contraction of the ventricle were simulated using computational biomechanical models[346]. The impact of dilatation and increased sphericity on the changes of HA slopes was explored and compared between the groups. Additionally, strain and torsion were measured in both models with varying HA slopes to investigate whether the changes in fibre orientation were in part responsible for the differences seen in these parameters.

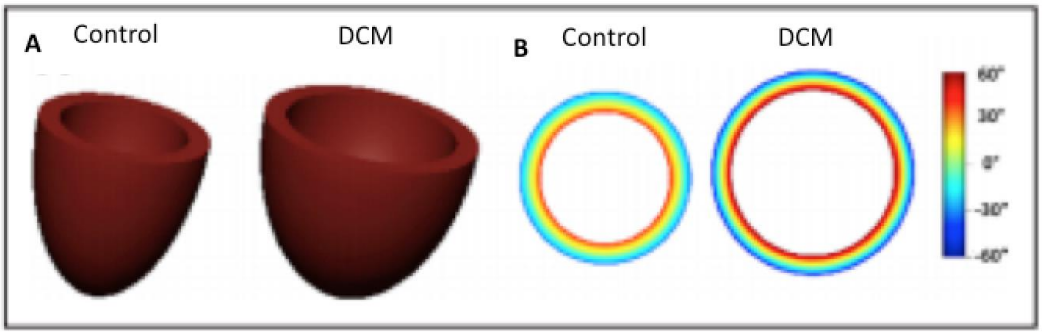

Figure 7.7 - Idealised LV models used for biomechanical modelling

A - Idealised LV models used for biomechanical modelling of healthy and DCM hearts.
B - Idealised helix angle maps based on average end-diastolic measurements in controls and DCM patients.

7.9.1.1.4 Statistical Analysis

Differences between diastolic/systolic parameters and DCM patients/controls were determined by a Wilcoxon signed-rank and Wilcoxon rank-sum test, respectively. A p-value below 0.05 was considered statistically significant.

7.9.2 Results

A total of 15 patients and 10 healthy subjects were recruited. Nine patients and nine healthy volunteers were scanned successfully and comprised the final cohort. Datasets were rejected due to either technical issues or breathing motion related signal loss in the diffusion weighted images.

Demographics and clinical characteristics are given in Table 7 (shown at end of chapter). The DTI data are summarized in Table 8 (shown at end of chapter).

7.9.2.1.1 Helix angles

Figure 7.8 shows example helix (E1A) and sheetlet (E2A) angle maps for a control subject and DCM patient in diastole and systole. Histograms of HA distributions for both cohorts are displayed in Figure 7.9. A change towards steeper HAs during contraction is seen in the controls, whereas inconsistent dynamic change between heart phases is observed in the patients. Bin counts of diastolic HAs close to zero degrees were reduced in DCM relative to healthy controls. The corresponding transmural HA slopes are shown.

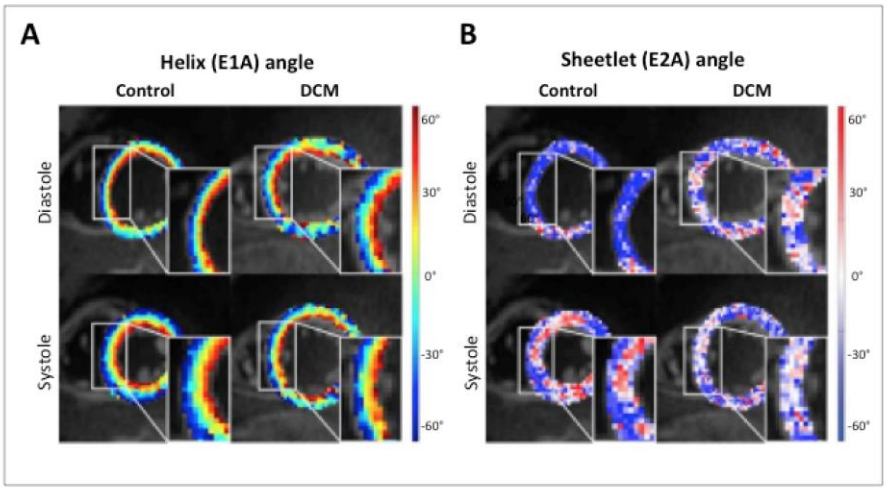

Figure 7.8 - Comparison of helix angle and sheetlet maps acquired in diastole and systole

Example of helix (E1A) angle and sheetlet (E2A) maps acquired in diastole and systole from control versus DCM patient.

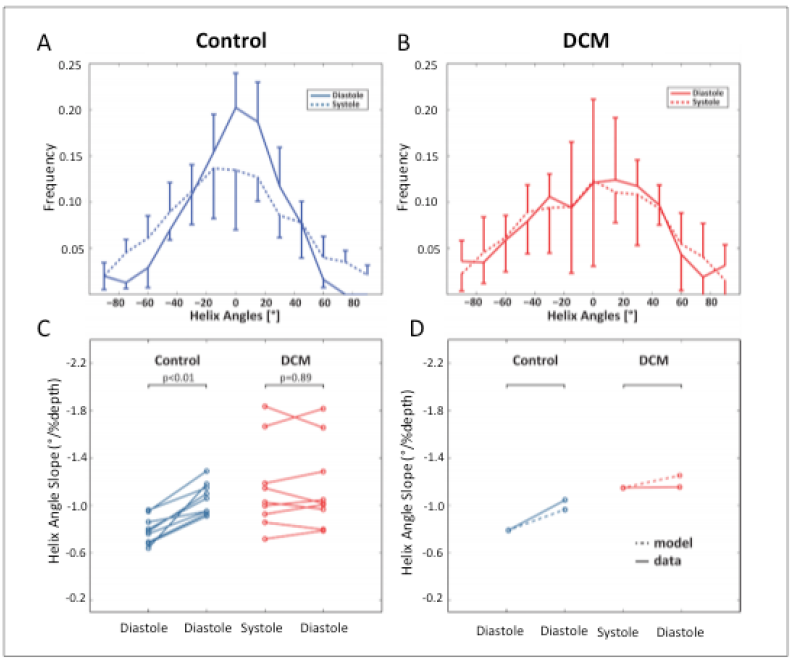

Figure 7.9 - Histograms of diastolic and systolic helix angles for controls and DCM patients

Histograms of diastolic and systolic helix angles for controls (a) and DCM patients (b). While a shift towards steeper helix angles is seen in the systolic healthy heart, systolic and diastolic distributions are similar in the DCM case. Error bars indicate interquartile ranges across the subjects. c) Corresponding transmural helix angle slopes in diastole versus systole for the control and DCM groups. d) Diastolic and systolic helix angles for control and DCM modelling as compared to the data.

In diastole, the HA slope was significantly steeper in the patients when compared to controls (-1.02±0.53°/% depth versus -0.78±0.22°/% depth, $p<0.01$).

In systole, there was a significant increase in maximum endo- and epicardial HA in the controls suggesting a more longitudinal alignment of myofibre aggregates with cardiac contraction. This resulted in a significant increase in HA slope in the control group from diastole to systole (-0.78±0.22°/% depth to -1.06±0.23°/% depth, $p<0.01$). In contrast, there was no significant change in HA slope from diastole to systole in the DCM patients (-1.02±0.53°/% depth to -1.01±0.59°/% depth, $p=0.89$).

7.9.2.1.2 Sheetlet angles

Histograms of E2A sheet angle distributions for controls and DCM patients are shown in Figure 7.10 . A change in E2A angles towards a broader distribution during contraction is seen in the control group, whereas reduced dynamic change between diastole and systole is observed in the DCM patients. Bin counts of diastolic sheetlet angles close to zero degrees are reduced in DCM relative to healthy controls.

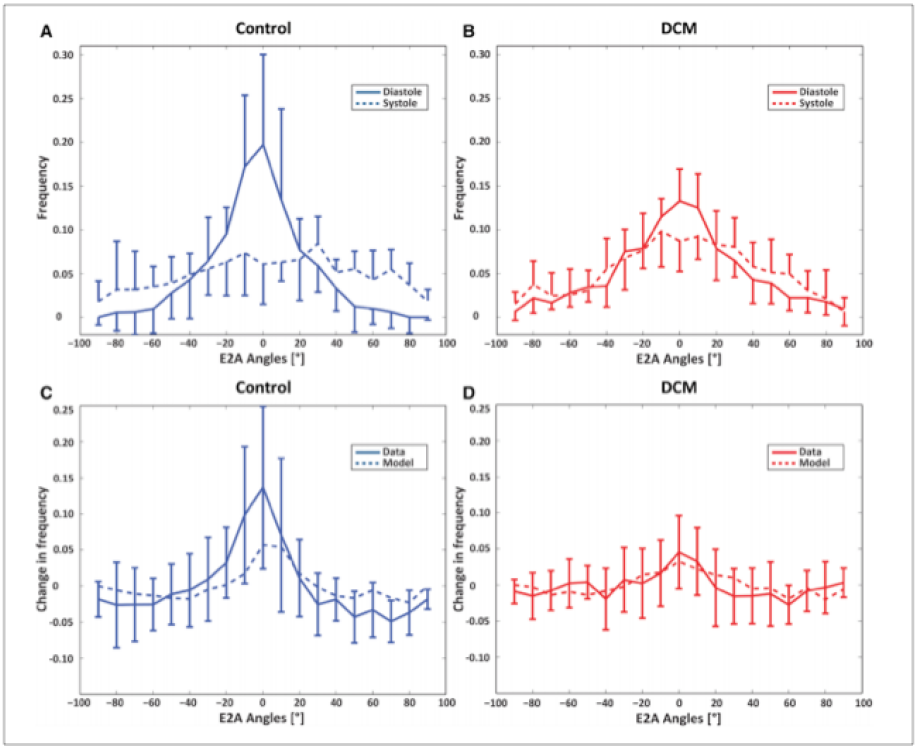

Figure 7.10 - Histograms of diastolic and systolic E2A sheetlet angles for controls and DCM patients

Histograms of diastolic and systolic E2A sheet angles for controls (a) and DCM patients (b). The sheet angle distribution is broader in the systolic healthy heart compared to diastole, whereas systolic and diastolic distributions are similar in the DCM case. Histograms of change between diastolic and systolic E2A distributions for controls (c) and DCM patients (d). Controls exhibit a marked change in E2A as opposed to little change in DCM patients. Model results follow a similar trend. Error bars indicate interquartile ranges across the subjects.

7.9.2.1.3 Transverse angles

Transverse angles are distributed around zero degrees indicating the expected circumferential alignment of the fibre aggregates (shown in Table at end of chapter).

7.9.2.1.4 Mean diffusivity (MD) and fractional anisotropy (FA)

In both diastole and systole, there was lower FA in the DCM group than in the controls (diastole 0.56±0.07 versus 0.63±0.05 respectively, $p<0.04$; systole

0.58±0.08 versus 0.62±0.07 respectively, p=0.56). There were no significant differences in FA between cardiac phases in either group.

There was a trend towards higher MD in the DCM group relative to controls (diastole 1.17±0.22x10^{-3}mm^2/s versus 1.09±0.12x10^{-3}mm^2/s, p=0.23; systole 1.23±0.34x10^{-3}mm^2/s versus 1.09±0.27x10^{-3}mm^2/s, p=0.27). There were no significant differences in MD between cardiac phases in either group.

7.9.2.1.5 Torsion and strain

Table 8 reports maximum torsion and strain for both groups. Figure 7.11 shows the median torsional deformation and cardiac strain parameters over the cardiac cycle. Longitudinal, circumferential and radial strains were all significantly reduced in the DCM group compared to the controls. Table 9 shows the torsion and strain values according to group.

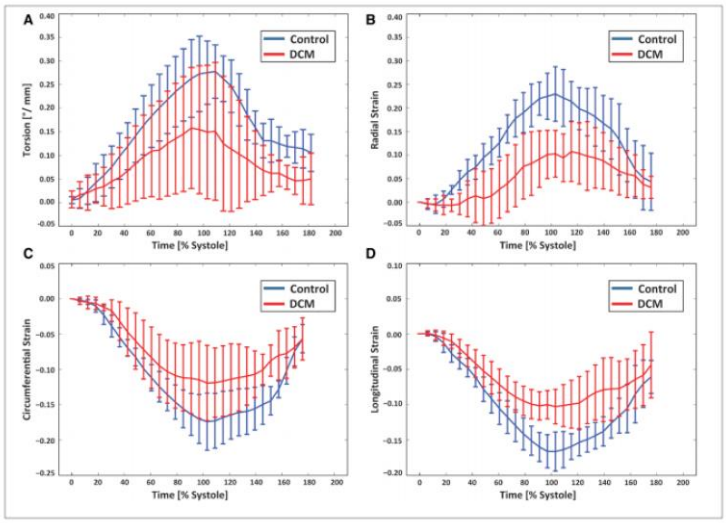

Figure 7.11 – Torsion and strain over cardiac cycle for both groups

Time course of myocardial torsion (a), radial (b), circumferential (c) and longitudinal (d) strain for DCM and control. Error bars indicate interquartile ranges across the subjects.

Table 9 – Table showing maximum torsion and strain for both groups

	DCM group (N=9)	Control group (N=9)	P value (DCM vs Control)
Max torsion (°/mm)	0.17±0.19	0.28±0.09	<0.02*
Max radial strain	0.11±0.02	0.25±0.04	<0.01*
Min circumferential strain	-0.12±0.07	-0.17±0.04	<0.01*
Min longitudinal strain	-0.10±0.03	-0.17±0.04	<0.01*

Mean (systolic and diastolic) HA slope was correlated against maximum torsion, LVEF and longitudinal strain. The correlations were found to be limited in both groups (Figure 7.12). In the patient group there was a trend towards reduced torsion and longitudinal strain with increased HA slope compared to controls. LVEF was found to remain on a constant 40% for HA slopes of about 1.0°/% transmural depth. This decreased to 15% with increased HA slope.

In the control group, values for peak torsion were spread by approximately 15% around 0.30°/mm and the values for longitudinal strain were in the range of 0.15-0.19 for the controls compared to 0.07-0.17 for the DCM patients. LVEF values in controls were densely distributed around 58±7%.

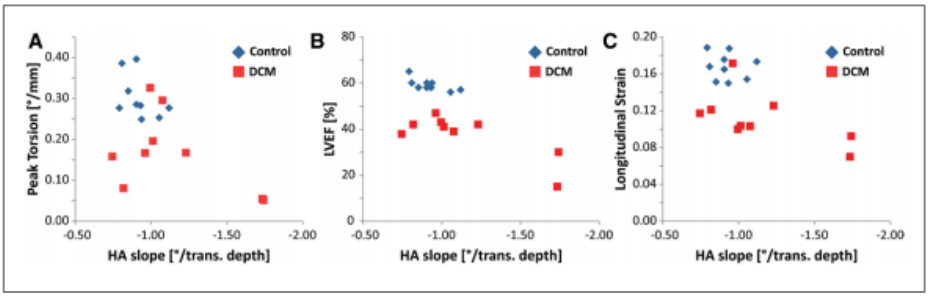

Figure 7.12 – Helix angle in relation to torsion, LV ejection fraction and longitudinal strain

Peak torsion (a), left-ventricular ejection fraction (LVEF) (b) and (negative) longitudinal strain (c) as a function of normalized helix angle (HA) slope. A trend towards lower torsion (a), LVEF (b) and longitudinal strain (c) with increasing helix angle slope is seen in the DCM group.

7.9.2.1.6 Biomechanical Modelling

The active contraction phase was simulated for the healthy and the DCM models in order to understand the differences in the HA changes between end-diastolic and end-systolic states. Both models were progressively activated at respective end-systolic volumes, and the change in HA slopes at the endo- and epicardial surfaces was recorded. Figure 7.9 shows the results for the two models. The model supports the observation from the data, the slope change is higher in controls in contrast to that in DCM patients

The change in E2A distributions between diastole and systole is illustrated in Figure 7.10 . A significant change is observed in controls (up to 0.13/0.06 in data/model), whereas the distribution for DCM patients remains largely unchanged (up to 0.03/0.03 in data/model), reflecting the trend seen in the data.

The next modelling objective addressed a possible explanation of the observed changes in HAs by the dilatation and remodelling seen in DCM hearts. To this end, the control LV was inflated from its reference volume to the DCM model reference volume. The measured HAs at the larger volume was steeper, but the

change was too low to explain the difference between the measured control and DCM HA slopes (0.03°/%depth, see Figure 7.13).

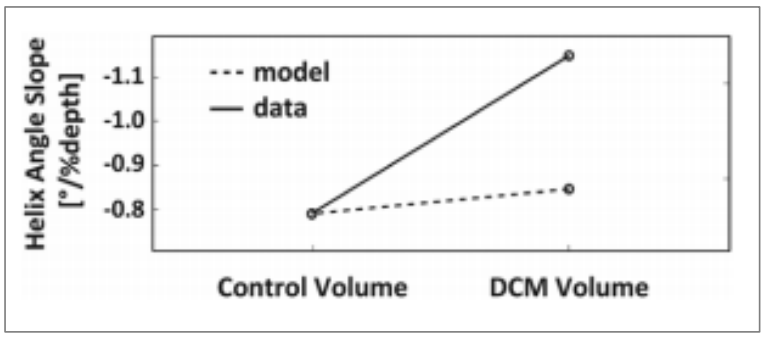

Figure 7.13 – Comparison of change in helix angle between actual and modelled data

Change in helix angle slope caused by passive inflation of the control LV model to DCM model cavity volume as compared to measured difference in control and DCM helix angle slopes. Volume change alone does not explain observed differences between the two cohorts.

When repeated for the DCM LV, a more spherical geometry, and inflated to twice the cavity volume, a larger change in HA was observed (0.1°/%depth). Nevertheless, the DCM modelled result was still significantly lower than the values observed in the data (0.36°/%depth difference calculated between control and DCM DTI data). This suggests that LV size and shape do not appear to be entirely responsible for the steepening of HAs seen in DCM patients in comparison with controls.

Finally, we aimed to investigate whether the change in HA was contributing to the reduced torsion and strain or was a compensatory factor in preserving cardiac function (see Table 10). Strain and torsion were evaluated in each model with both control and DCM HA distributions. The results are shown in Table 9. These results show that in the DCM group, when simulating with steeper angles, torsion was reduced and strain values were unchanged. A

similar pattern was demonstrated in the control group. This suggests that steeper angles do not play a compensatory role in aiding cardiac contraction and that torsion impairment is exacerbated with steeper angles in hearts of either geometry. It is worth noting that the values of strain and torsion do not directly compare to those from the data though there are clearly similar trends and this likely reflects the use of an idealised non-patient specific model.

Table 10 - Biomechanical modelling torsion and strain results according to shape and helix angles

	Control shape/ Control helix angles	Control shape/ DCM helix angles	DCM shape/ Control helix angles	DCM shape/ DCM helix angles
Max torsion (°/mm)	0.24	0.19	0.13	0.10
Max radial strain	0.41	0.43	0.23	0.23
Min circumferential strain	-0.18	-0.18	-0.11	0-.10
Min longitudinal strain	-0.04	-0.05	-0.05	-0.06

7.9.3 Discussion

In this study, the dynamic change of myofibre aggregate orientation in DCM patients and healthy controls was investigated using in-vivo dual phase cardiac DTI. A statistically significant change of myocyte orientation between diastole and systole was found in the control group. The longitudinal fibre alignment during contraction is assumed to optimize cardiac pumping efficiency and has been described previously using in-vivo and ex-vivo DTI data and

histology[315,318,329,347]. In contrast to healthy controls, the change in HA from diastole to systole was found to be far less pronounced in DCM patients and was not statistically different between both heart phases. On average, diastolic myofibre aggregate orientation had a more longitudinal orientation in DCM patients relative to healthy controls. Seven out of nine DCM patients showed comparable systolic HA configurations relative to healthy controls. In the two remaining patients, clearly increased HA slopes in both cardiac phases were recorded. One might speculate that this elevated longitudinal myocyte orientation could result from advanced remodelling as these two patients were considerably older (76 and 77 years) when compared to the mean age of the patient population (60±14 years), and had the poorest LVEF. Accordingly, this could be due to successive elongation of myocytes and reduced contractility. Similar reorientation was previously described by Tseng et al.[336] in hypertrophic hearts, but this has not been confirmed by more recent data[330].

In addition, we demonstrated that there are differences in sheet angle pattern between the groups. In the controls, sheet angle distribution changes dynamically between systole and diastole with a broader distribution in systole. The systolic and diastolic distributions in the DCM patients are, however, similar between the two cardiac phases.

In general, cardiac pumping performance in the DCM patients was significantly reduced compared to the controls as quantified by a number of parameters: LVEF, maximum torsion, longitudinal, radial and circumferential strain. Particularly low values for LVEF, torsion and strain values were recorded for the two patients with elevated HA slopes. Our data on maximum torsion in DCM patients and controls is in good agreement with literature values[302].

As well as the clinical and gross structural changes seen in DCM, the effects of myofibre aggregate reorientation must be considered alongside well-recognised subcellular changes such as microarchitecture disarray. Histologically, heart failure is characterised by myocyte elongation, reduced myocyte density and fibrosis. These changes have been correlated with ex-vivo DTI results in previous studies[348,349]. The observed trend towards increased MD and decreased FA supports the presence of reduced myofibril density and cellular necrosis.

Using biomechanical modelling we were able to reproduce similar trends between the model and the data. There were differences of changes in HA when activating the model relative to the in-vivo findings prompting for further work including patient-specific geometries and myofibre aggregate data as well as myocyte modelling at the microscale. The use of biomechanical modelling was twofold. First, an attempt to understand whether the size and/or shape of the ventricle could be responsible for the altered steep angle of the myofibre aggregates in diastole. Second, an investigation of the implications of fibre alterations were investigated, in particular whether these are beneficial or detrimental to efficient cardiac contraction. Initial tests showed that even pronounced dilatation of the heart is not sufficient to produce the observed differences in HA between the groups. We noted however that the correlation between simulated and actually measured myofibre aggregate orientation improves, when simulating a dilated, more spherical heart. Furthermore, the biomechanical simulations show that the reduction in torsion appears to be exacerbated by steeper HAs with no improvement or deterioration in strain. This was found in both LV models and suggested that this factor is independent of

the changes to LV size and shape. Even in a dilated and remodelled heart the steeper angles are not beneficial to maintaining longitudinal, radial or circumferential strain or torsion. The exacerbated deterioration in strain and torsion observed in the DCM group may thus reflect underlying subcellular changes that were beyond the scope of this study.

There is little correlation with any of the single parameters tested against the change in HA slope in the subjects studied. This suggests that a composite of factors such as dilatation, poor systolic function and the recognised subcellular alterations seen in DCM may be responsible for this structural rearrangement. Further studies would be needed to confirm this.

In summary, this study demonstrates that there are changes in diastolic myocyte orientations and, importantly, that there is reduced and inconsistent dynamic reorientation during cardiac contraction in DCM patients relative to healthy hearts. We have been able to show that the change in left ventricular shape does not entirely explain the difference seen in HA slope between DCM patients and controls. We have also demonstrated findings that suggest that steeper HAs do not confer a compensatory adaptation in terms of cardiac contraction. Overall, our findings provide new insight into the structural alterations within the living heart in DCM and underline the importance of MR diffusion tensor imaging to gain deeper understanding of cardiac disease.

7.9.4 Study Limitations

1. The DCM patient cohort in this study was small and though all had a diagnosis of non-ischaemic cardiomyopathy the aetiology may be heterogeneous. Clinical, morphological and functional data were variable and, accordingly, a large variation of HA distribution was recorded.

2. Overall the patients studied present a form of milder DCM and therefore our results cannot provide a complete picture of changes in myofibre aggregate architecture in all stages of DCM. Similarly, the impact of medical therapy cannot be appraised due to the small sample size but this would be an interesting avenue of future work. In addition some of the measurements were taken only in specific regions of the myocardium to reduce low signal-to-noise effects and therefore may not be representative of the entire myocardium should there be heterogeneous changes.
3. Because of scan time constraints, the imaging resolution of cardiac DTI was relatively coarse (2.5x2.5x8 mm^3) and partial voluming effects were inherent at the endo- and epicardial borders. To reduce the impact of this effect, edge voxels were excluded from the analysis.
4. The limitations in time scan, and patient cooperation also meant that only one slice could be acquired using cardiac DTI (taking approximately 1 hour per patient) and that all patients were not successfully scanned. The time taken to perform the scans makes cardiac DTI unfeasible currently in routine clinical use. Faster acquisition is likely to change this situation and encourage translation to the clinical setting.

A paper since the publication of the study above deserves specific mention[313].

This elaborate study had two components – first: in-vivo cardiac DTI was performed in porcine models at six to nine time points in the cardiac cycle; second continuous cardiac DTI was performed in-situ after cardiac arrest by either potassium chloride (which arrested the heart in a diastolic configuration) or barium chloride (which arrested the heart in diastole initially then underwent a single slow cardiac contraction and remained contracted).

A number of important findings were reported.

As suggested by others previously, the study showed that, in normal hearts, the major change in myocardial wall thickening was an increase in the sheetlet angle (E2A) – this was seen in both the in-vivo group and in the potassium chloride versus barium chloride arrested ex-vivo group, with similar values. This correlated with histological analysis of sheetlet angles. The slowly contracting barium chloride arrested group was compared to the in-vivo group in order to examine the changes in wall thickness and the effect of strain. The estimated effect of strain was in the order of 17%. These workers were reassured by the finding that sheetlet angle change was similar in both the arrested and the in-vivo hearts. This suggested a small effect of strain on measured E2A values. On histological examination, the previously described helical pattern of fibre orientation was shown to change little from systole to diastole in both in-vivo and ex-vivo hearts.

In parallel to this study, in-vivo dual-phase cardiac DTI was performed on a group of volunteers, on patients with hypertrophic cardiomyopathy and on dilated cardiomyopathy with particularly interesting findings. The findings in healthy subjects reflected those seen in the porcine work with significant change

in sheetlet angle from diastole to systole. In hypertrophic cardiomyopathy, the sheetlet angle was higher than controls in diastole with similar values in systole. In contrast, in dilated cardiomyopathy, there was a similar sheetlet angle in diastole but lower sheetlet angle change in systole. Importantly the study showed similar reductions in longitudinal, radial and circumferential strain in both disease groups compared to controls and the changes in sheetlet angle exceeded the estimate of the effect of strain. This suggests that hypertrophic cardiomyopathy represents a form of disease whereby the hearts are permanently in a more systolic, contracted state whereas in dilated cardiomyopathy the hearts are permanently in a more diastolic state. This may account for the predominant diastolic impairment seen in hypertrophic cardiomyopathy as opposed to the predominant systolic impairment seen in dilated cardiomyopathy.

7.10 Conclusion

The arrangement of the cardiac microstructure is complex, highly organized and fundamental to cardiac function. The arrangement of the myocardial myofibres and sheets contributes significantly to efficient ventricular function and in recent years, there has been increasing interest in characterising differences between normal and diseased or injured hearts. This can be assessed non-invasively with diffusion tensor imaging (DTI) which relies on the anisotropy of the myocytes and the diffusion of water. The development of in-vivo cardiac DTI has presented a number of challenges but has also provided new insights into the nature of dynamic alterations of myocyte architecture in vivo in health and

disease. This study adds to the body of literature on this topic and shows a loss of dynamic helix and sheetlet reorientation. Using biophysical modeling we have been able to suggest that in part it is the altered geometry which causes these changes and that furthermore, this altered structural arrangement and dynamic rearrangement appears to be maladaptive and exacerbates reduced contractile parameters. This is an area for future work using patient specific models.

Part of this chapter consists of work that has been published:

*Von Deuster, C., **Sammut, E**., Asner, L., Nordsletten, D., Lamata, P., Stoeck, C.T, Kozerke, S., Razavi, R.*

'Studying dynamic myofiber aggregate reorientation in dilated cardiomyopathy using in-vivo magnetic resonance diffusion tensor imaging'

Circulation Cardiovascular Imaging, 2016 (http:// doi: 10.1161/CIRCIMAGING.116.005018)

Eva Sammut is joint first author on the publication and was responsible for data collection, involved in image analysis and drafting of the manuscript.

Table 7 – Patient demographics and CMR data

	DCM group (N=9)	Control group (N=9)	P value (DCM vs Control)
Male	7	7	-
Age (years)	61±24	51±11	0.052
Heart rate (beats/min)	66±16	62±13	0.38
BSA (m^2)	1.8±0.2	1.8±0.5	0.75
iLV EDV (ml/m^2)	84±48	83±18	0.48
iLV ESV (ml/m^2)	57±47	31±10	<0.01*
LVEF (%)	41±11	58±7	<0.01*
iLV mass (g/m^2)	78±22	53±17	<0.02*
iRV EDV (ml/m^2)	72±38	82±28	0.40
iRV ESV (ml/m^2)	36±18	32±9	0.40
RVEF (%)	55±13	61±7	0.063
LV diastolic wall thickness (mm)	9±1	9±1	0.96
LV systolic wall thickness (mm)	10±2	12±4	0.054

* denotes significance

BSA: Body Surface Area, iLV EDV: indexed Left Ventricular End Diastolic Volume, iLV ESV: indexed Left Ventricular End Systolic Volume, LVEF: Left Ventricular Ejection Fraction, iLV mass: indexed Left Ventricular mass, iRV EDV: indexed Right Ventricular End Diastolic Volume, iRV ESV: indexed Right Ventricular End Systolic Volume, RVEF: Right Ventricular Ejection Fraction, LV: Left Ventricle. Reported values are median±interquartile range.

Table 8 – Diffusion tensor data according to group

	DCM group (N=9)	Control group (N=9)	P value		
			DCM (diastole vs systole)	Controls (diastole vs systole)	DCM vs controls
Diastolic HA slope [°/Trans. depth]	-1.02±0.53	-0.78±0.22	0.89	<0.01*	<0.01*
Systolic HA slope [°/Trans. depth]	-1.01±0.59	-1.06±0.23	-	-	0.90
Diastolic HA range [°]	74±44	54±16	0.82	<0.01*	<0.02*
Systolic HA range [°]	76±45	77±14	-	-	0.97
Diastolic TA [°]	0±25	-2±17	0.82	0.43	0.40
Systolic TA [°]	0±30	-1±24	-	-	0.63
Diastolic MD [$x10^{-3}mm^2/s$]	1.17±0.22	1.09±0.12	0.43	0.50	0.23
Systolic MD [$x10^{-3}mm^2/s$]	1.23±0.34	1.09±0.27	-	-	0.27
Diastolic FA	0.56±0.07	0.63±0.05	0.36	0.30	<0.04*
Systolic FA	0.58±0.08	0.62±0.07	-	-	0.56

* denotes significance

HA: Helix Angle, TA: Transverse Angle, MD: Mean Diffusivity, FA: Fractional Anisotropy. Reported values are median±interquartile range.

8 Conclusion

In conclusion, this thesis presents a number of original studies which have explored the use of quantitative perfusion, CMR and cardiac DTI.

We have been able to show that quantitative assessment with high resolution quantitative CMR is feasible and reproducible in patients with heart failure. Given the prevalence of HF and increasing reliance on CMR to evaluate patients, this small study is the first to test this specific hypothesis and these initial results are encouraging.

Quantitative analysis is not a new technique but, despite multiple validation studies, has resisted attempts to move it out of the research arena and into the clinical setting. The thesis also presents a large observational study which has conducted the first assessment of the prognostic use of quantitative perfusion CMR. This study has shown that this performs at least as well as visual assessment by expert readers. The study establishes a significant base for larger randomised studies. The increasingly prevalent automatisation of the analysis pipeline, combined with prognostic data should enable translation to the clinical setting.

PET remains the non-invasive reference standard of assessment of perfusion. Nevertheless the improved tissue characterisation, and the structural and functional information provided by MRI has increased the attraction of MRI for perfusion assessment in particular for patients with coronary disease.

Previous studies have suggested an imperfect correlation between PET and MR. We have explored this correlation using a specialized cardiac phantom which simulates perfusion (with known true perfusion rates) and a hybrid MR-PET scanner. Despite differing methods of analysis, we have demonstrated excellent correlation between MR, PET and known true perfusion values.

This thesis also presents work on the use of cardiac diffusion tensor imaging in dilated cardiomyopathy. This used a dual-phase, in-vivo cardiac DTI approach, biomechanical modelling and strain data from 3D tagging CMR. We were able to demonstrate and document significant differences in fibre architecture between subjects and controls. This has shed light on the interplay between cardiac structure and function in health and disease and is the basis for further exploration of therapeutic targets or biomarkers. Time constraints and issues of patient cooperation prevent this being available for clinical use for the present, but there is scope for developing this further.

In conclusion, this work has presented a number of studies focusing on quantitative perfusion analysis and cardiac DTI. All research is incremental, building on the work of others and in turn serving as a platform for further advance. Our work has provided much scope for further exploration of the clinical applicability of these techniques.

9 References

1. Neubauer S. The failing heart--an engine out of fuel. *New England Journal of Medicine*. 2007;356:1140–1151.

2. Stanley WC. Myocardial Substrate Metabolism in the Normal and Failing Heart. *Physiological Reviews*. 2005;85:1093–1129.

3. Camici PG, Crea F. Coronary microvascular dysfunction. *New England Journal of Medicine*. 2007;356:830–840.

4. Camici PG, d'Amati G, Rimoldi O. Coronary microvascular dysfunction: mechanisms and functional assessment. *Nat Rev Cardiol*. 2015;12:48–62.

5. Toyota E, Koshida R, Hattan N, Chilian WM. Regulation of the coronary vasomotor tone: What we know and where we need to go. *J Nucl Cardiol*. 2001;8:599–605.

6. Fuchs M, Ertl G, Falcke A. Changes of collateral perfusion pressure and segmental coronary resistances during reactive hyperemia in anesthetized dogs. *Pflugers Arch*. 1983;399:285–289.

7. Chilian WM, Marcus ML. Phasic coronary blood flow velocity in intramural and epicardial coronary arteries. *Circulation Research*. 1982;50:775–781.

8. Hoffman JI, Spaan JA. Pressure-flow relations in coronary circulation. *Physiological Reviews*. 1990;70:331–390.

9. Marcus ML, Wilson RF, White CW. Methods of measurement of myocardial blood flow in patients: a critical review. *Circulation*. 1987;76:245–253.

10. Chiribiri A. High-resolution non-invasive assessment of myocardial perfusion in the human heartby cardiovascular magnetic resonance. *PhD thesis 2010*. 2010;:1–280.

11. Spaan J, Kolyva C, van den Wijngaard J, Wee ter R, van Horssen P, Piek J, Siebes M. Coronary structure and perfusion in health and disease. *Philos Trans A Math Phys Eng Sci*. 2008;366:3137–3153.

12. BERNE RM. REGULATION OF CORONARY BLOOD FLOW. *Physiological Reviews*. 1964;44:1–29.

13. Schelbert HR. Anatomy and physiology of coronary blood flow. *J Nucl Cardiol*. 2010;17:545–554.

14. Gould KL, Lipscomb K. Effects of coronary stenoses on coronary flow reserve and resistance. *The American Journal of Cardiology*. 1974;34:48–55.

15. Demer LL, Gould KL, Goldstein RA, Kirkeeide RL, Mullani NA, Smalling RW, Nishikawa A, Merhige ME. Assessment of coronary artery disease severity by positron emission tomography. Comparison with quantitative arteriography in 193 patients. *Circulation*. 1989;79:825–835.

16. Gould KL. Detecting and assessing severity of coronary artery disease in humans. *Cardiovasc Intervent Radiol*. 1990;13:5–13.

17. Li Y, Huang TT, Carlson EJ, Melov S, Ursell PC, Olson JL, Noble LJ, Yoshimura MP, Berger C, Chan PH, Wallace DC, Epstein CJ. Dilated cardiomyopathy and neonatal lethality in mutant mice lacking manganese superoxide dismutase. *Nat Genet*. 1995;11:376–381.

18. Di Carli M, Czernin J, Hoh CK, Gerbaudo VH, Brunken RC, Huang SC, Phelps ME, Schelbert HR. Relation among stenosis severity, myocardial blood flow, and flow reserve in patients with coronary artery disease. *Circulation*. 1995;91:1944–1951.

19. Picano E, Parodi O, Lattanzi F, Sambuceti G, Andrade MJ, Marzullo P, Giorgetti A, Salvadori P, Marzilli M, Distante A. Assessment of anatomic and physiological severity of single-vessel coronary artery lesions by dipyridamole echocardiography. Comparison with positron emission tomography and quantitative arteriography. *Circulation*. 1994;89:753–761.

20. Sambuceti G, Parodi O, Marcassa C, Neglia D, Salvadori P, Giorgetti A, Bellina RC, Di Sacco S, Nista N, Marzullo P. Alteration in regulation of myocardial blood flow in one-vessel coronary artery disease determined by positron emission tomography. *The American Journal of Cardiology*. 1993;72:538–543.

21. Uren NG, Melin JA, de Bruyne B, Wijns W, Baudhuin T, Camici PG. Relation between myocardial blood flow and the severity of coronary-artery stenosis. *New England Journal of Medicine*. 1994;330:1782–1788.

22. Rakusan K, Flanagan MF, Geva T, Southern J, Van Praagh R. Morphometry of human coronary capillaries during normal growth and the effect of age in left ventricular pressure-overload hypertrophy. *Circulation*. 1992;86:38–46.

23. Hermansen L, Wachtlova M. Capillary density of skeletal muscle in well-trained and untrained men. *J Appl Physiol*. 1971;30:860–863.

24. Andersen P. Capillary density in skeletal muscle of man. *Acta Physiol Scand*. 1975;95:203–205.

25. FACC DWM, MD CCJ, FACC HSCM, MD LAYJ, MD MC. Silent Ischemia During Coronary Occlusion Produced by Balloon Inflation: Relation to Regional Myocardial Dysfunction. *JAC*. 1987;10:491–498.

26. FACC AMHM, FACC VGM, MD RGR, FACC SGM, FACC GCTM, RDMS PD. Sequence of Mechanical, Electrocardiographic and Clinical Effects of Repeated Coronary Artery Occlusion in Human Beings:. *JAC*. 1985;5:193–197.

27. Nesto RW, Kowalchuk GJ. The ischemic cascade: temporal sequence of hemodynamic, electrocardiographic and symptomatic expressions of ischemia. *The American Journal of Cardiology*. 1987;59:23C–30C.

28. MD WW, MD PWS, MSc CJS, PhD JG, FACC HPKM, FACC PGHM, MD OMH. Effect of Coronary Occlusion During Percutaneous Transluminal Angioplasty in Humans on Left Ventricular Chamber Stiffness and Regional Diastolic Pressure-Radius Relations. *JAC*. 1986;7:455–463.

29. Dawson JR, Gibson DG. Regional left ventricular wall motion in pacing induced angina. *Br Heart J*. 1988;59:309–318.

30. Pozzoli MM, Salustri A, Sutherland GR, Tuccillo B, Tijssen JG, Roelandt JR, Fioretti PM. The comparative value of exercise echocardiography and 99m Tc MIBI single photon emission computed tomography in the diagnosis and localization of myocardial ischaemia. *European Heart Journal*. 1991;12:1293–1299.

31. Quiñones MA, Verani MS, Haichin RM, Mahmarian JJ, Suarez J, Zoghbi WA. Exercise echocardiography versus 201Tl single-photon emission computed tomography in evaluation of coronary artery disease. Analysis of 292 patients. *Circulation*. 1992;85:1026–1031.

32. Fioretti PM, Pozzoli MM, Ilmer B, Salustri A, Cornel JH, Reijs AE, Krenning EP, Reiber JH, de Feyter PJ, Roelandt JR. Exercise echocardiography versus thallium-201 SPECT for assessing patients before and after PTCA. *European Heart Journal*. 1992;13:213–219.

33. Gallik DM, Obermueller SD, Swarna US, Guidry GW, Mahmarian JJ, Verani MS. Simultaneous Assessment of Myocardial Perfusion and Left Ventricular Function During Transient Coronary Occlusion. *JAC*. 1995;25:1529–1538.

34. Forster T, McNeill AJ, Salustri A, Reijs AEM, El-Said E-SM, Roelandt JRTC, Fioretti PM. Simultaneous dobutamine stress echocardiography and technetium-99m isonitrile single-photon emission computed tomography in patients with suspected coronary artery disease. *JAC*. 1993;21:1591–1596.

35. Elhendy A, Geleijnse ML, Roelandt JRTC, van Domburg RT, TenCate FJ, Cornel JH, Reijs AEM, El-Said GM, Fioretti PM. Dobutamine-induced hypoperfusion without transient wall motion abnormalities: Less severe ischemia or less severe stress? *JAC*. 1996;27:323–329.

36. Leong-Poi H. Perfusion Versus Function: The Ischemic Cascade in Demand Ischemia: Implications of Single-Vessel Versus Multivessel Stenosis. *Circulation*. 2002;105:987–992.

37. Porter TR, Xie F, Silver M, Kricsfeld D, O'Leary E. Real-Time Perfusion Imaging With LowMechanical Index Pulse Inversion Doppler Imaging. *JAC*. 2001;37:748–753.

38. Global Use of Strategies to Open Occluded Coronary Arteries in Acute Coronary Syndromes (GUSTO IIb) Angioplasty Substudy Investigators. A clinical trial comparing primary coronary angioplasty with tissue plasminogen activator for acute myocardial infarction. *New England Journal of Medicine*. 1997;336:1621–1628.

39. Aversano T, Aversano LT, Passamani E, Knatterud GL, Terrin ML, Williams DO, Forman SA, Atlantic Cardiovascular Patient Outcomes Research Team (C-PORT). Thrombolytic therapy vs primary percutaneous coronary intervention for myocardial infarction in patients presenting to hospitals without on-site cardiac surgery: a randomized controlled trial. *JAMA*. 2002;287:1943–1951.

40. García E, Elízaga J, Pérez-Castellano N, Serrano JA, Soriano J, Abeytua M, Botas J, Rubio R, López de Sá E, López-Sendón JL, Delcán JL. Primary angioplasty versus systemic thrombolysis in anterior myocardial infarction. *JAC*. 1999;33:605–611.

41. Grines CL, Browne KF, Marco J, Rothbaum D, Stone GW, O'Keefe J, Overlie P, Donohue B, Chelliah N, Timmis GC. A comparison of immediate angioplasty with thrombolytic therapy for acute myocardial infarction. The Primary Angioplasty in Myocardial Infarction Study Group. *New England Journal of Medicine*. 1993;328:673–679.

42. Ribichini F, Steffenino G, Dellavalle A, Ferrero V, Vado A, Feola M, Uslenghi E. Comparison of Thrombolytic Therapy and Primary Coronary Angioplasty With Liberal Stenting for Inferior Myocardial Infarction With Precordial ST-Segment Depression. *JAC*. 1998;32:1687–1694.

43. Keeley EC, Boura JA, Grines CL. Primary angioplasty versus intravenous thrombolytic therapy for acute myocardial infarction: a quantitative review of 23 randomised trials. *Lancet*. 2003;361:13–20.

44. Boersma E, Mercado N, Poldermans D, Gardien M, Vos J, Simoons ML. Acute myocardial infarction. *Lancet*. 2003;361:847–858.

45. Ribichini F, Ferrero V, Wijns W. Reperfusion treatment of ST-elevation acute myocardial infarction. *Progress in Cardiovascular Diseases*. 2004;47:131–157.

46. Boden WE, Eagle K, Granger CB. Reperfusion strategies in acute ST-segment elevation myocardial infarction: a comprehensive review of contemporary management options. *J Am Coll Cardiol*. 2007;50:917–929.

47. Antman EM, Van de Werf F. Pharmacoinvasive therapy: the future of treatment for ST-elevation myocardial infarction. *Circulation*. 2004;109:2480–2486.

48. Bandh VS, Frojdh A, Swahn MRLE, Janzon M, Nielsen N-E, Diderholm ELUE, Jernberg T, Frostfeldt G, Lindahl B, Lindstrom G, Svensson E, Ahlberg GAFG, Saetre H, Karlsson EPJJ-E, Kristensson CASB-E, Ohlin BNLH, Hulting GDSJ, Magnusson GWEJO, Ekdahl S, Landgren YPKF, Holmgren B, Ryden S, Dellborg EBGM, Abrahamsson P, Svensson A-M, Naslund TWUU, Sinnerstad CSVB, Ahlstrom CJOANHDDMP, Falk S-BGNS-A, Perk B-MLOJ, Peterson BLLM, Risenfors KFMM, Y-Hassan JMES, Stjerna A, Thorsen MJVS, Nicol KERATACSHKP, Gustafsson G-BEG-SG, Abjorn ESSLWKC, Fanebust KPHHUBR, Lovheim THOO, August KTNARHTLV, Nilsson EVFH, Nyman HHATGMI, Fjelstad B, Johansson SOLP-A, Tornvall KSSP, Kahan KHDT, Hammarstrom ABBE, Carling L, Astrom L, Hedman BALA, Frisell J-E, Zingmark MSPA, Boman GLSDTHJHFPHHGBJSK, Ryttberg AAANTNOB, Brubakk KB-TFO, Brodersson THKNJFHETIKOPGKSHNG-SH, Svennberg L, Holst Silkeborg F Rømer Halden N T Granfeldt Skene B Bartholdson von M, Andersson A. Invasive compared with non-invasive treatment in unstable coronary-artery disease: FRISC II prospective randomised multicentre study. *The Lancet*. 2005;:1–8.

49. Cannon CP, Weintraub WS, Demopoulos LA, Vicari R, Frey MJ, Lakkis N, Neumann FJ, Robertson DH, DeLucca PT, DiBattiste PM, Gibson CM, Braunwald E, TACTICS (Treat Angina with Aggrastat and Determine Cost of Therapy with an Invasive or Conservative Strategy)--Thrombolysis in Myocardial Infarction 18 Investigators. Comparison of early invasive and conservative strategies in patients with unstable coronary syndromes treated with the glycoprotein IIb/IIIa inhibitor tirofiban. *New England Journal of Medicine*. 2001;344:1879–1887.

50. Fox KAA, Poole-Wilson PA, Henderson RA, Clayton TC, Chamberlain DA, Shaw TRD, Wheatley DJ, Pocock SJ, Randomized Intervention Trial of unstable Angina Investigators. Interventional versus conservative treatment for patients with unstable angina or non-ST-elevation myocardial infarction: the British Heart Foundation RITA 3 randomised trial. Randomized Intervention Trial of unstable Angina. *Lancet*. 2002;360:743–751.

51. Mehta SR, Cannon CP, Fox KAA, Wallentin L, Boden WE, Spacek R, Widimsky P, McCullough PA, Hunt D, Braunwald E, Yusuf S. Routine vs selective invasive strategies in patients with acute coronary syndromes: a collaborative meta-analysis of randomized trials. *JAMA*. 2005;293:2908–2917.

52. Arora S, Matsushita K, Qamar A, Stacey RB, Caughey MC. Early versus late percutaneous revascularization in patients hospitalized with non ST-segment elevation myocardial infarction: The atherosclerosis risk in communities surveillance study. *Cathet Cardiovasc Intervent*. 2017;290:1593.

53. Hoedemaker NPG, Damman P, Woudstra P, Hirsch A, Windhausen F, Tijssen JGP, de Winter RJ, ICTUS Investigators. Early Invasive Versus Selective Strategy for Non-ST-Segment Elevation Acute Coronary Syndrome: The ICTUS Trial. *J Am Coll Cardiol*. 2017;69:1883–1893.

54. Davies RF, Goldberg AD, Forman S, Pepine CJ, Knatterud GL, Geller N, Sopko G, Pratt C, Deanfield J, Conti CR. Asymptomatic Cardiac Ischemia Pilot (ACIP) study two-year follow-up: outcomes of patients randomized to initial strategies of medical therapy versus revascularization. *Circulation*. 1997;95:2037–2043.

55. Katritis DG, Ionnidis J. Percutaneous coronary intervention versus conservative therapy in nonacute coronary artery disease: a meta-analysis. *Circulation*. 2005;111:2906–2912.

56. Erne P, Schoenenberger MAW, Burckhardt MD, Zuber MM, Kiowski MW, Buser MPT, Dubach MP, Resink MTJ, Pfisterer PM. Effects of Percutaneous CoronaryInterventions in Silent IschemiaAfter Myocardial Infarction. *JAMA*. 2007;:1–7.

57. Boden WE, O'Rourke RA, Teo KK, Hartigan PM, Maron DJ, Kostuk WJ, Knudtson M, Dada M, Casperson P, Harris CL, Chaitman BR, Shaw L, Gosselin G, Nawaz S, Title LM, Gau G, Blaustein AS, Booth DC, Bates ER, Spertus JA, Berman DS, Mancini GBJ, Weintraub WS. Optimal Medical Therapy with or without PCI for Stable Coronary Disease. *New England Journal of Medicine*. 2007;356:1503–1516.

58. Lipinski MJ, McVey CM, Berger JS, Kramer CM, Salerno M. Prognostic Value of Stress Cardiac Magnetic Resonance Imaging in Patients With Known or Suspected Coronary Artery Disease. *J Am Coll Cardiol*. 2013;62:826–838.

59. Jahnke C, Nagel E, Gebker R, Kokocinski T, Kelle S, Manka R, Fleck E, Paetsch I. Prognostic Value of Cardiac Magnetic Resonance Stress Tests: Adenosine Stress Perfusion and Dobutamine Stress Wall Motion Imaging. *Circulation*. 2007;115:1769–1776.

60. Abbasi SA, Heydari B, Shah RV, Murthy VL, Zhang YY, Blankstein R, Steigner M, Jerosch-Herold M, Kwong RY. Risk stratification by regadenoson stress

magnetic resonance imaging in patients with known or suspected coronary artery disease. *The American Journal of Cardiology*. 2014;114:1198–1203.

61. Greenwood JP, Herzog BA, Brown JM, Everett CC, Nixon J, Bijsterveld P, Maredia N, Motwani M, Dickinson CJ, Ball SG, Plein S. Prognostic Value of Cardiovascular Magnetic Resonance and Single-Photon Emission Computed Tomography in Suspected Coronary Heart Disease: Long-Term Follow-up of a Prospective, Diagnostic Accuracy Cohort Study. *Ann Intern Med*. 2016;

62. Hachamovitch R. Comparison of the Short-Term Survival Benefit Associated With Revascularization Compared With Medical Therapy in Patients With No Prior Coronary Artery Disease Undergoing Stress Myocardial Perfusion Single Photon Emission Computed Tomography. *Circulation*. 2003;107:2900–2907.

63. Shaw LJ, Berman DS, Maron DJ, Mancini GBJ, Hayes SW, Hartigan PM, Weintraub WS, O'Rourke RA, DADA M, Spertus JA, Chaitman BR, Friedman J, Slomka P, Heller GV, Germano G, Gosselin G, Berger P, Kostuk WJ, Schwartz RG, KNUDTSON M, Veledar E, Bates ER, McCallister B, Teo KK, Boden WE, for the COURAGE Investigators. Optimal Medical Therapy With or Without Percutaneous Coronary Intervention to Reduce Ischemic Burden: Results From the Clinical Outcomes Utilizing Revascularization and Aggressive Drug Evaluation (COURAGE) Trial Nuclear Substudy. *Circulation*. 2008;117:1283–1291.

64. Berman DS, Kang X, Schisterman EF, Gerlach J, Kavanagh PB, Areeda JS, Sharir T, Hayes SW, Shaw LJ, Lewin HC, Friedman JD, Miranda R, Germano G. Serial changes on quantitative myocardial perfusion SPECT in patients undergoing revascularization or conservative therapy. *J Nucl Cardiol*. 2001;8:428–437.

65. Califf RM, Armstrong PW, Carver JR, D'Agostino RB, Strauss WE. 27th Bethesda Conference: matching the intensity of risk factor management with the hazard for coronary disease events. Task Force 5. Stratification of patients into high, medium and low risk subgroups for purposes of risk factor management. *JAC*. 1996;27:1007–1019.

66. MRCP RA-L, MRCPI DT, PhD H-MD, MRCP Sen S, FRCP KT, MRCP JD, MRCP TK, PhD MM, FRCP RK, FRCP ISM, MRCP SSN, MRCP RP, MRCP CC, MRCP YA, MRCP JH, FRCP CB, FRCP AS, FRCP RG, MRCP ST, MRCP RA, FRCP PJM, MRCP RW, PhD DC, MRCP MS-S, FRCP PSAT, MRCP DJED, FRCP PDPF, Al-Lamee R, Thompson D, Sen S, Tang K, Davies J, Keeble T, Kaprielian R, Malik IS, Nijjer SS, Petraco R, Cook C, Ahmad Y, Howard J, Shun-Shin M, Sethi A, Baker C, Sharp A, Ramrakha P, Gerber R, Talwar S, Assomull R, Foale R, Mayet J, Wensel R, Thom SA, Davies JE, Francis DP, Khamis R, Hadjiloizou N, Khan M, Kooner J, Bellamy M, Mikhail G, Clifford P, O'Kane P, Levy T, Swallow R, investigators O. Percutaneous coronary intervention in stable angina (ORBITA): a double-blind, randomised controlled trial. *The Lancet*. 2018;391:31–40.

67. ISCHEMIA Trial Research Group, MD DJM, MD JSH, PhD SMO, MD HRR, MD WEB, MD GWS, MHA SBM, MPH JASM, MD DBM, MD KPA, PhD LS, MD JSB, MD TBFJ, MD DOW, MD RAH, MPH YRM. International Study of Comparative Health Effectiveness with Medical and Invasive Approaches (ISCHEMIA) trial: Rationale and design. *American Heart Journal*. 2018;201:124–135.

68. Windecker S, Remondino A, Eberli FR, Jüni P, Räber L, Wenaweser P, Togni M, Billinger M, Tüller D, Seiler C, Roffi M, Corti R, Sütsch G, Maier W, Lüscher T, Hess OM, Egger M, Meier B. Sirolimus-eluting and paclitaxel-eluting stents for coronary revascularization. *New England Journal of Medicine*. 2005;353:653–662.

69. Kastrati A, Dibra A, Eberle S, Mehilli J, Suárez de Lezo J, Goy J-J, Ulm K, Schömig A. Sirolimus-eluting stents vs paclitaxel-eluting stents in patients with coronary artery disease: meta-analysis of randomized trials. *JAMA*. 2005;294:819–825.

70. Pijls NH, van Son JA, Kirkeeide RL, de Bruyne B, Gould KL. Experimental basis of determining maximum coronary, myocardial, and collateral blood flow by pressure measurements for assessing functional stenosis severity before and after percutaneous transluminal coronary angioplasty. *Circulation*. 1993;87:1354–1367.

71. Pijls NH, de Bruyne B, Peels K, Van Der Voort PH, Bonnier HJ, Bartunek J Koolen JJ, Koolen JJ. Measurement of fractional flow reserve to assess the functional severity of coronary-artery stenoses. *New England Journal of Medicine*. 1996;334:1703–1708.

72. Silber S, Albertsson P, Avilés FF, Camici PG, Colombo A, Hamm C, Jørgensen E, Marco J, Nordrehaug J-E, Ruzyllo W, Urban P, Stone GW, Wijns W, Task Force for Percutaneous Coronary Interventions of the European Society of Cardiology. Guidelines for percutaneous coronary interventions. The Task Force for Percutaneous Coronary Interventions of the European Society of Cardiology. European Heart Journal. 2005;26:804–847.

73. Pijls NHJ. Optimum guidance of complex PCI by coronary pressure measurement. *Heart*. 2004;90:1085–1093.

74. Bartunek J, Sys SU, Heyndrickx GR, Pijls NHJ, De Bruyne B. Quantitative coronary angiography in predicting functional significance of stenoses in an unselected patient cohort. *JAC* [Internet]. 1995;26:328–334. Available from: http://eutils.ncbi.nlm.nih.gov/entrez/eutils/elink.fcgi?dbfrom=pubmed&id=7608431&retmode=ref&cmd=prlinks

75. Pijls N, de Bruyne B, Peels K. Measurement of fractional flow reserve to assess the functional severity of coronary-artery stenoses. *… England Journal of …*. 1996;

76. Pijls NHJ, van Schaardenburgh P, Manoharan G, Boersma E, Bech J-W, van't Veer M, Bär F, Hoorntje J, Koolen J, Wijns W, De Bruyne B. Percutaneous Coronary Intervention of Functionally Nonsignificant Stenosis. *J Am Coll Cardiol*. 2007;49:2105–2111.

77. Fearon WF, Tonino PAL, De Bruyne B, Siebert U, Pijls NHJ, FAME Study Investigators. Rationale and design of the Fractional Flow Reserve versus Angiography for Multivessel Evaluation (FAME) study. *American Heart Journal*. 2007;154:632–636.

78. Tonino PAL, De Bruyne B, Pijls NHJ, Siebert U, Ikeno F, van 't Veer M, Klauss V, Manorharan G, Engstrom T, Oldroyd KG, Ver Lee PN, MacCarthy P, Fearon WF. Fractional flow reserve versus angiography for guiding percutaneous coronary intervention. *New England Journal of Medicine*. 2009;360:213–224.

79. van Nunen LX, Zimmermann FM, Tonino PAL, Barbato E, Baumbach A, Engstrom T, Klauss V, MacCarthy PA, Manoharan G, Oldroyd KG, Ver Lee PN, van't Veer M, Fearon WF, De Bruyne B, Pijls NHJ, FAME Study Investigators. Fractional flow reserve versus angiography for guidance of PCI in patients with multivessel coronary artery disease (FAME): 5-year follow-up of a randomised controlled trial. *Lancet*. 2015;386:1853–1860.

80. Zimmermann FM, Ferrara A, Johnson NP, van Nunen LX, Escaned J, Albertsson P, Erbel R, Legrand V, Gwon H-C, Remkes WS, Stella PR, van Schaardenburgh P, Bech GJW, De Bruyne B, Pijls NHJ. Deferral vs. performance of percutaneous coronary intervention of functionally non-significant coronary stenosis: 15-year follow-up of the DEFER trial. *European Heart Journal*. 2015;36:3182–3188.

81. Tonino PAL, De Bruyne B, Pijls NHJ, Siebert U, Ikeno F, van 't Veer M, Klauss V, Manoharan G, Engstrom T, Oldroyd KG, Ver Lee PN, MacCarthy PA, Fearon WF, FAME Study Investigators. Fractional flow reserve versus angiography for guiding percutaneous coronary intervention. *New England Journal of Medicine*. 2009;360:213–224.

82. Lockie T, Ishida M, Perera D, Chiribiri A, De Silva K, Kozerke S, Marber M, Nagel E, Rezavi R, Redwood S, Plein S. High-Resolution Magnetic Resonance Myocardial Perfusion Imaging at 3.0-Tesla to Detect Hemodynamically Significant Coronary Stenoses as Determined by Fractional Flow Reserve. *J Am Coll Cardiol*. 2011;57:70–75.

83. Panting JR, Gatehouse PD, Yang G-Z, Grothues F, Firmin DN, Collins P, Pennell DJ. Abnormal subendocardial perfusion in cardiac syndrome X detected by cardiovascular magnetic resonance imaging. *New England Journal of Medicine*. 2002;346:1948–1953.

84. Motwani M, Jogiya R, Kozerke S, Greenwood JP, Plein S. Advanced cardiovascular magnetic resonance myocardial perfusion imaging: high-spatial resolution versus 3-dimensional whole-heart coverage. *Circulation: Cardiovascular Imaging*. 2013;6:339–348.

85. Iskandrian AS. Adenosine myocardial perfusion imaging. *Journal of Nuclear Medicine*. 1994;35:734–736.

86. Hamon M, Fau G, Née G, Ehtisham J, Morello R, Hamon M. Meta-analysis of the diagnostic performance of stress perfusion cardiovascular magnetic resonance for detection of coronary artery disease. *J Cardiovasc Magn Reson*. 2010;12:29.

87. Baer FM, Smolarz K, Jungehülsing M, Theissen P, Sechtem U, Schicha H, Hilger HH. Feasibility of high-dose dipyridamole-magnetic resonance imaging for detection of coronary artery disease and comparison with coronary angiography. *The American Journal of Cardiology*. 1992;69:51–56.

88. Bhave NM, Freed BH, Yodwut C, Kolanczyk D, Dill K, Lang RM, Mor-Avi V, Patel AR. Considerations when measuring myocardial perfusion reserve by cardiovascular magnetic resonance using regadenoson. *J Cardiovasc Magn Reson*. 2012;14:89.

89. Dandekar VK, Bauml MA, Ertel AW, Dickens C, Gonzalez RC, Farzaneh-Far A. Assessment of global myocardial perfusion reserve using cardiovascular magnetic resonance of coronary sinus flow at 3 Tesla. *J Cardiovasc Magn Reson*. 2014;16:24.

90. Greenwood JP, Maredia N, Younger JF, Brown JM, Nixon J, Everett CC, Bijsterveld P, Ridgway JP, Radjenovic A, Dickinson CJ, Ball SG, Plein S. Cardiovascular magnetic resonance and single-photon emission computed tomography for diagnosis of coronary heart disease (CE-MARC): a prospective trial. *Lancet*. 2012;379:453–460.

91. Watkins S, Berry C, Oldroyd K. CMR versus SPECT for diagnosis of coronary heart disease. *Lancet*. 2012;379:2145–author reply 2147–8.

92. Schwitter J, Wacker CM, van Rossum AC, Lombardi M, Al-Saadi N, Ahlstrom H, Dill T, Larsson HBW, Flamm SD, Marquardt M, Johansson L. MR-IMPACT: comparison of perfusion-cardiac magnetic resonance with single-photon emission computed tomography for the detection of coronary artery disease in a multicentre, multivendor, randomized trial. *European Heart Journal*. 2008;29:480–489.

93. Schwitter J, Wacker CM, Wilke N, Al-Saadi N, Sauer E, Huettle K, Schönberg SO, Luchner A, Strohm O, Ahlstrom H, Dill T, Hoebel N, Simor T, MR-IMPACT Investigators. MR-IMPACT II: Magnetic Resonance Imaging for Myocardial Perfusion Assessment in Coronary artery disease Trial: perfusion-cardiac magnetic resonance vs. single-photon emission computed tomography for the detection of coronary artery disease: a comparative multicentre, multivendor trial. *European Heart Journal*. 2013;34:775–781.

94. Jaarsma C, Leiner T, Bekkers SC, Crijns HJ, Wildberger JE, Nagel E, Nelemans PJ, Schalla S. Diagnostic performance of noninvasive myocardial perfusion imaging using single-photon emission computed tomography, cardiac magnetic resonance, and positron emission tomography imaging for the detection of obstructive coronary artery disease: a meta-analysis. *J Am Coll Cardiol*. 2012;59:1719–1728.

95. Hussain ST, Paul M, Plein S, McCann GP, Shah AM, Marber MS, Chiribiri A, Morton G, Redwood S, MacCarthy P, Schuster A, Ishida M, Westwood MA, Perera D, Nagel E. Design and rationale of the MR-INFORM study: stress perfusion cardiovascular magnetic resonance imaging to guide the management of patients with stable coronary artery disease. *Journal of Cardiovascular Magnetic Resonance*. 2012;14:1–1.

96. Ishida N, Sakuma H, Motoyasu M, Okinaka T, Isaka N, Nakano T, Takeda K. Noninfarcted myocardium: correlation between dynamic first-pass contrast-enhanced myocardial MR imaging and quantitative coronary angiography. *Radiology*. 2003;229:209–216.

97. Pilz G, Bernhardt P, Klos M, Ali E, Wild M, Höfling B. Clinical implication of adenosine-stress cardiac magnetic resonance imaging as potential gatekeeper

prior to invasive examination in patients with AHA/ACC class II indication for coronary angiography. *Clin Res Cardiol*. 2006;95:531–538.

98. Paetsch I, Jahnke C, Wahl A, Gebker R, Neuss M, Fleck E, Nagel E. Comparison of dobutamine stress magnetic resonance, adenosine stress magnetic resonance, and adenosine stress magnetic resonance perfusion. *Circulation*. 2004;110:835–842.

99. Gebker R, Jahnke C, Manka R, Frick M, Hucko T, Kozerke S, Schnackenburg B, Fleck E, Paetsch I. High spatial resolution myocardial perfusion imaging during high dose dobutamine/atropine stress magnetic resonance using k-t SENSE. *International Journal of Cardiology*. 2012;158:411–416.

100. Gebker R, Frick M, Jahnke C, Berger A, Schneeweis C, Manka R, Kelle S, Klein C, Schnackenburg B, Fleck E, Paetsch I. Value of additional myocardial perfusion imaging during dobutamine stress magnetic resonance for the assessment of intermediate coronary artery disease. *Int J Cardiovasc Imaging*. 2012;28:89–97.

101. Gebker R, Jahnke C, Manka R, Hamdan A, Schnackenburg B, Fleck E, Paetsch I. Additional value of myocardial perfusion imaging during dobutamine stress magnetic resonance for the assessment of coronary artery disease. *Circulation: Cardiovascular Imaging*. 2008;1:122–130.

102. Rim S-J, Ha J-W, Lee M-H, Jang Y, Chung N. Left ventricular remodeling can be predicted with left ventricular volume response during dobutamine echocardiography after acute myocardial infarction. *Clin Cardiol*. 2008;31:259–264.

103. Bolognese L, Cerisano G, Buonamici P, Santini A, Santoro GM, Antoniucci D, Fazzini PF. Influence of infarct-zone viability on left ventricular remodeling after acute myocardial infarction. *Circulation*. 1997;96:3353–3359.

104. Scott AE, Semple SIK, Redpath TW, Hillis GS. Low-dose dobutamine adds incremental value to late gadolinium enhancement cardiac magnetic resonance in the prediction of adverse remodelling following acute myocardial infarction. *Eur Heart J Cardiovasc Imaging*. 2013;14:906–913.

105. Gargiulo P, Dellegrottaglie S, Bruzzese D, Savarese G, Scala O, Ruggiero D, D'Amore C, Paolillo S, Agostoni P, Bossone E, Soricelli A, Cuocolo A, Trimarco B, Perrone Filardi P. The prognostic value of normal stress cardiac magnetic resonance in patients with known or suspected coronary artery disease: a meta-analysis. *Circulation: Cardiovascular Imaging*. 2013;6:574–582.

106. Nandalur KR, Dwamena BA, Choudhri AF, Nandalur MR, Carlos RC. Diagnostic Performance of Stress Cardiac Magnetic Resonance Imaging in the Detection of Coronary Artery Disease. *J Am Coll Cardiol*. 2007;50:1343–1353.

107. Bruder O, Schneider S, Nothnagel D, Dill T, Hombach V, Schulz-Menger J, Nagel E, Lombardi M, van Rossum AC, Wagner A, Schwitter J, Senges J, Sabin GV, Sechtem U, Mahrholdt H. EuroCMR (European Cardiovascular Magnetic Resonance) Registry. *JAC*. 2009;54:1457–1466.

108. Bruder O, Wagner A, Lombardi M, Schwitter JR, van Rossum A, Pilz GN, Nothnagel D, Steen H, Petersen S, Nagel E, Prasad S, Schumm J, Greulich S, Cagnolo A, Monney P, Deluigi CC, Dill T, Frank H, Sabin G, Schneider S, Mahrholdt H. European cardiovascular magnetic resonance (EuroCMR) registry – multi national results from57 centers in 15 countries. *Journal of Cardiovascular Magnetic Resonance*. 2013;15:1–1.

109. Fritz-Hansen T, Hove JD, Kofoed KF, Kelbaek H, Larsson HBW. Quantification of MRI measured myocardial perfusion reserve in healthy humans: a comparison with positron emission tomography. *J Magn Reson Imaging*. 2008;27:818–824.

110. Schwitter J, Nanz D, Kneifel S, Bertschinger K, Buchi M, Knusel PR, Marincek B, Luscher TF, Schulthess von GK. Assessment of Myocardial Perfusion in Coronary Artery Disease by Magnetic Resonance : A Comparison With Positron Emission Tomography and Coronary Angiography. *Circulation*. 2001;103:2230–2235.

111. Morton G, Chiribiri A, Ishida M, Hussain ST, Schuster A, Indermuehle A, Perera D, Knuuti J, Baker S, Hedström E, Schleyer P, O'Doherty M, Barrington S, Nagel E. Quantification of Absolute Myocardial Perfusion in Patients With Coronary Artery Disease. *J Am Coll Cardiol*. 2012;60:1546–1555.

112. Miller CA, Naish JH, Ainslie MP, Tonge C, Tout D, Arumugam P, Banerji A, Egdell RM, Clark D, Weale P, Steadman CD, McCann GP, Ray SG, Parker GJM, Schmitt M. Voxel-wise quantification of myocardial blood flow with cardiovascular magnetic resonance: effect of variations in methodology and validation with positron emission tomography. *J Cardiovasc Magn Reson*. 2014;16:11.

113. Engblom H, Xue H, Akil S, Carlsson M, Hindorf C, Oddstig J, Hedeer F, Hansen MS, Aletras AH, Kellman P, Arheden H. Fully quantitative cardiovascular magnetic resonance myocardial perfusion ready for clinical use: a comparison between cardiovascular magnetic resonance imaging and positron emission tomography. *J Cardiovasc Magn Reson*. 2017;19:78.

114. Morton G, Jogiya R, Plein S, Schuster A, Chiribiri A, Nagel E. Quantitative cardiovascular magnetic resonance perfusion imaging: inter-study reproducibility. *Eur Heart J Cardiovasc Imaging*. 2012;13:954–960.

115. Larghat AM, Maredia N, Biglands J, Greenwood JP, Ball SG, Jerosch-Herold M, Radjenovic A, Plein S. Reproducibility of first-pass cardiovascular magnetic resonance myocardial perfusion. *J Magn Reson Imaging*. 2013;37:865–874.

116. Chih S, Macdonald PS, Feneley MP, Law M, Graham RM, McCrohon JA. Reproducibility of adenosine stress cardiovascular magnetic resonance in multi-vessel symptomatic coronary artery disease. *J Cardiovasc Magn Reson*. 2010;12:42.

117. Goykhman P, Mehta PK, Agarwal M, Shufelt C, Slomka PJ, Yang Y, Xu Y, Shaw LJ, Berman DS, Merz NB, Thomson LEJ. Reproducibility of myocardial perfusion reserve - variations in measurements from post processing using commercially available software. *Cardiovasc Diagn Ther*. 2012;2:268–277.

118. Ichihara T, Ishida M, Kitagawa K, Ichikawa Y, Natsume T, Yamaki N, Maeda H, Takeda K, Sakuma H. Quantitative analysis of first-pass contrast-enhanced myocardial perfusion MRI using a Patlak plot method and blood saturation correction. *Magn Reson Med*. 2009;62:373–383.

119. Wolff SD, Schwitter J, Coulden R, Friedrich MG, Bluemke DA, Biederman RW, Martin ET, Lansky AJ, Kashanian F, Foo TKF, Licato PE, Comeau CR. Myocardial first-pass perfusion magnetic resonance imaging: a multicenter dose-ranging study. *Circulation*. 2004;110:732–737.

120. Patel AR, Antkowiak PF, Nandalur KR, West AM, Salerno M, Arora V, Christopher J, Epstein FH, Kramer CM. Assessment of Advanced Coronary Artery Disease. *JAC*. 2010;56:561–569.

121. Giang TH, Nanz D, Coulden R, Friedrich M, Graves M, Al-Saadi N, Luscher TF, Schulthess von GK, Schwitter J. Detection of coronary artery disease by magnetic resonance myocardial perfusion imaging with various contrast medium doses: first European multi-centre experience. *European Heart Journal*. 2004;25:1657–1665.

122. Rieber J. Cardiac magnetic resonance perfusion imaging for the functional assessment of coronary artery disease: a comparison with coronary angiography and fractional flow reserve. *European Heart Journal*. 2005;27:1465–1471.

123. Nagel E, Klein C, Paetsch I, Hettwer S, Schnackenburg B, Wegscheider K, Fleck E. Magnetic resonance perfusion measurements for the noninvasive detection of coronary artery disease. *Circulation*. 2003;108:432–437.

124. Al-Saadi N, Nagel E, Gross M, Bornstedt A, Schnackenburg B, Klein C, Klimek W, Oswald H, Fleck E. Noninvasive detection of myocardial ischemia from perfusion reserve based on cardiovascular magnetic resonance. *Circulation*. 2000;101:1379–1383.

125. Ibrahim T, Nekolla SG, Schreiber K, Odaka K, Volz S, Mehilli J, Güthlin M, Delius W, Schwaiger M. Assessment of Coronary Flow Reserve:Comparison Between Contrast-Enhanced Magnetic Resonance Imaging and Positron Emission Tomography. *JAC*. 2002;39:864–870.

126. Plein S, Radjenovic A, Ridgway JP, Barmby D, Greenwood JP, Ball SG, Sivananthan MU. Coronary artery disease: myocardial perfusion MR imaging with sensitivity encoding versus conventional angiography. *Radiology*. 2005;235:423–430.

127. Lee DC. Magnetic Resonance Versus Radionuclide Pharmacological Stress Perfusion Imaging for Flow-Limiting Stenoses of Varying Severity. *Circulation*. 2004;110:58–65.

128. Hautvast GLTF, Chiribiri A, Lockie T, Breeuwer M, Nagel E, Plein S. Quantitative analysis of transmural gradients in myocardial perfusion magnetic resonance images. *Magn Reson Med*. 2011;66:1477–1487.

129. Chiribiri A, Hautvast GLTF, Lockie T, Schuster A, Bigalke B, Olivotti L, Redwood SR, Breeuwer M, Plein S, Nagel E. Assessment of Coronary Artery Stenosis Severity and Location. *JACC: Cardiovascular Imaging*. 2013;6:600–609.

130. Ishida M, Schuster A, Morton G, Chiribiri A, Hussain S, Paul M, Merkle N, Steen H, Lossnitzer D, Schnackenburg B, Alfakih K, Plein S, Nagel E. Development of a universal dual-bolus injection scheme for the quantitative assessment of myocardial perfusion cardiovascular magnetic resonance. *J Cardiovasc Magn Reson*. 2011;13:28.

131. Gatehouse PD, Elkington AG, Ablitt NA, Yang G-Z, Pennell DJ, Firmin DN. Accurate assessment of the arterial input function during high-dose myocardial perfusion cardiovascular magnetic resonance. *J Magn Reson Imaging*. 2004;20:39–45.

132. Gerber BL. Quantification of myocardial perfusion and myocardial perfusion reserve by positron emission tomography and cardiovascular magnetic resonance imaging. *J Am Coll Cardiol*. 2012;60:1556–1557.

133. Zierler KL. Theoretical basis of indicator-dilution methods for measuring flow and volume. *Circulation Research*. 1962;10:393–407.

134. Sourbron SP, Buckley DL. Tracer kinetic modelling in MRI: estimating perfusion and capillary permeability. *Phys Med Biol*. 2012;57:R1–33.

135. Rutland MD. Origin of the Patlak-Rutland plot. *Nuclear Medicine Communications*. 1996;17:441.

136. Tong CY, Prato FS, Wisenberg G, Lee TY, Carroll E, Sandler D, Wills J, Drost D. Measurement of the extraction efficiency and distribution volume for Gd-DTPA in normal and diseased canine myocardium. *Magn Reson Med*. 1993;30:337–346.

137. Tong CY, Prato FS, Wisenberg G, Lee TY, Carroll E, Sandler D, Wills J. Techniques for the measurement of the local myocardial extraction efficiency for inert diffusible contrast agents such as gadopentate dimeglumine. *Magn Reson Med*. 1993;30:332–336.

138. Diesbourg LD, Prato FS, Wisenberg G, Drost DJ, Marshall TP, Carroll SE, O'Neill B. Quantification of myocardial blood flow and extracellular volumes using a bolus injection of Gd-DTPA: kinetic modeling in canine ischemic disease. *Magn Reson Med*. 1992;23:239–253.

139. Pack NA, DiBella EVR. Comparison of myocardial perfusion estimates from dynamic contrast-enhanced magnetic resonance imaging with four quantitative analysis methods. *Magn Reson Med*. 2010;64:125–137.

140. Hsu LY, Groves DW, Aletras AH, Kellman P, Arai AE. A Quantitative Pixel-Wise Measurement of Myocardial Blood Flow by Contrast-Enhanced First-Pass CMR Perfusion Imaging. *JCMG*. 2012;5:154–166.

141. Zarinabad N, Chiribiri A, Hautvast GLTF, Ishida M, Schuster A, Cvetkovic Z, Batchelor PG, Nagel E. Voxel-wise quantification of myocardial perfusion by cardiac magnetic resonance. Feasibility and methods comparison. *Magn Reson Med*. 2012;68:1994–2004.

142. Wilke N, Jerosch-Herold M, Wang Y, Huang Y, Christensen BV, Stillman AE, Ugurbil K, McDonald K, Wilson RF. Myocardial perfusion reserve: assessment with multisection, quantitative, first-pass MR imaging. *Radiology*. 1997;204:373–384.

143. Jerosch-Herold M, Wilke N, Stillman AE. Magnetic resonance quantification of the myocardial perfusion reserve with a Fermi function model for constrained deconvolution. *Med Phys*. 1998;25:73–84.

144. Ourselin S, Rueckert D, Smith N. Functional Imaging and Modeling of the Heart. Springer; 2013.

145. Jerosch-Herold M, Swingen C, Seethamraju RT. Myocardial blood flow quantification with MRI by model-independent deconvolution. *Med Phys*. 2002;29:886–897.

146. Keeling SL, Kogler T, Stollberger R. Deconvolution for DCE-MRI using an exponential approximation basis. *Med Image Anal*. 2009;13:80–90.

147. Hautvast G, Chiribiri A, Zarinabad N, Schuster A, Breeuwer M, Nagel E. Myocardial Blood Flow Quantification From MRI by Deconvolution Using an Exponential Approximation Basis. *IEEE Trans Biomed Eng*. 59:2060–2067.

148. Neyran B, Janier MF, Casali C, Revel D, Canet Soulas EP. Mapping myocardial perfusion with an intravascular MR contrast agent: robustness of deconvolution methods at various blood flows. *Magn Reson Med*. 2002;48:166–179.

149. Chiribiri A, Schuster A, Ishida M, Hautvast G, Zarinabad N, Morton G, Otton J, Plein S, Breeuwer M, Batchelor P, Schaeffter T, Nagel E. Perfusion phantom: An efficient and reproducible method to simulate myocardial first-pass perfusion measurements with cardiovascular magnetic resonance. *Magn Reson Med*. 2012;69:698–707.

150. Schuster A, Zarinabad N, Ishida M, Sinclair M, van den Wijngaard JP, Morton G, Hautvast GL, Bigalke B, van Horssen P, Smith N, Spaan JA, Siebes M, Chiribiri A, Nagel E. Quantitative assessment of magnetic resonance derived myocardial perfusion measurements using advanced techniques: microsphere validation in an explanted pig heart system. 2014;:1–13.

151. Kroll K, Wilke N, Jerosch-Herold M, Wang Y, Zhang Y, Bache RJ, Bassingthwaighte JB. Modeling regional myocardial flows from residue functions of an intravascular indicator. *Am J Physiol*. 1996;271:H1643–55.

152. Bettencourt N, Chiribiri A, Schuster A, Ferreira N, Sampaio F, Pires-Morais G, Santos L, Melica B, Rodrigues A, Braga P, Azevedo L, Teixeira M, Leite-Moreira A, Silva-Cardoso J, Nagel E, Gama V. Direct comparison of cardiac magnetic resonance and multidetector computed tomography stress-rest perfusion imaging for detection of coronary artery disease. *J Am Coll Cardiol*. 2013;61:1099–1107.

153. Hsu L-Y, Kellman P, Arai AE. Nonlinear myocardial signal intensity correction improves quantification of contrast-enhanced first-pass MR perfusion in humans. *J Magn Reson Imaging*. 2008;27:793–801.

154. Hsu L-Y, Rhoads KL, Holly JE, Kellman P, Aletras AH, Arai AE. Quantitative myocardial perfusion analysis with a dual-bolus contrast-enhanced first-pass MRI technique in humans. *J Magn Reson Imaging*. 2006;23:315–322.

155. Christian TF, Rettmann DW, Aletras AH, Liao SL, Taylor JL, Balaban RS, Arai AE. Absolute myocardial perfusion in canines measured by using dual-bolus first-pass MR imaging. *Radiology*. 2004;232:677–684.

156. Christian TF, Aletras AH, Arai AE. Estimation of absolute myocardial blood flow during first-pass MR perfusion imaging using a dual-bolus injection technique: Comparison to single-bolus injection method. *J Magn Reson Imaging*. 2008;27:1271–1277.

157. Utz W, Greiser A, Niendorf T, Dietz R, Schulz-Menger J. Single- or dual-bolus approach for the assessment of myocardial perfusion reserve in quantitative MR perfusion imaging. *Magn Reson Med*. 2008;59:1373–1377.

158. Köstler H, Ritter C, Lipp M, Beer M, Hahn D, Sandstede J. Prebolus quantitative MR heart perfusion imaging. *Magn Reson Med*. 2004;52:296–299.

159. Kellman P, Hansen MS, Nielles-Vallespin S, Nickander J, Themudo R, Ugander M, Xue H. Myocardial perfusion cardiovascular magnetic resonance: optimized dual sequence and reconstruction for quantification. 2017;:1–14.

160. Gatehouse P, Lyne J, Smith G, Pennell D, Firmin D. T2* effects in the dual-sequence method for high-dose first-pass myocardial perfusion. *J Magn Reson Imaging*. 2006;24:1168–1171.

161. Algranati D, Kassab GS, Lanir Y. Why is the subendocardium more vulnerable to ischemia? A new paradigm. *AJP: Heart and Circulatory Physiology*. 2011;300:H1090–100.

162. Vermeltfoort IA, Raijmakers PG, Lubberink M, Germans T, van Rossum AC, Lammertsma AA, Knaapen P. Feasibility of subendocardial and subepicardial myocardial perfusion measurements in healthy normals with (15)O-labeled water and positron emission tomography. *J Nucl Cardiol*. 2011;18:650–656.

163. Chiribiri A, Bettencourt N, Nagel E. Cardiac magnetic resonance stress testing: results and prognosis. *Curr Cardiol Rep*. 2009;11:54–60.

164. Morton G, Ishida M, Schuster A, Hussain S, Schaeffter T, Chiribiri A, Nagel E. Perfusion cardiovascular magnetic resonance: Comparison of an advanced, high-resolution and a standard sequence. *Journal of Cardiovascular Magnetic Resonance*. 2012;14:1–1.

165. Motwani M, Maredia N, Fairbairn TA, Kozerke S, Radjenovic A, Greenwood JP, Plein S. High-Resolution Versus Standard-Resolution Cardiovascular MR Myocardial Perfusion Imaging for the Detection of Coronary Artery Disease. *Circulation: Cardiovascular Imaging*. 2012;5:306–313.

166. Zarinabad N, Hautvast G, Sammut E, Arujuna A, Breeuwer M, Nagel E,

Chiribiri A. Effects of tracer arrival time on the accuracy of high-resolution (voxel-wise) myocardial perfusion maps from contrast-enhanced first-pass perfusion magnetic resonance. *IEEE Trans Biomed Eng*. :1–1.

167. Costa MA, Shoemaker S, Futamatsu H, Klassen C, Angiolillo DJ, Nguyen M, Siuciak A, Gilmore P, Zenni MM, Guzman L, Bass TA, Wilke N. Quantitative Magnetic Resonance Perfusion Imaging Detects Anatomic and Physiologic Coronary Artery Disease as Measured by Coronary Angiography and Fractional Flow Reserve. *J Am Coll Cardiol*. 2007;50:514–522.

168. Bettencourt N, Chiribiri A, Schuster A, Ferreira N, Sampaio F, Duarte R, Santos L, Melica B, Rodrigues A, Braga P, Teixeira M, Simões L, Leite-Moreira A, Silva-Cardoso J, Nagel E, Portugal P, Gama V. Cardiac magnetic resonance myocardial perfusion imaging for detection of functionally significant obstructive coronary artery disease: a prospective study. *International Journal of Cardiology*. 2013;168:765–773.

169. Mordini FE, Haddad T, Hsu L-Y, Kellman P, Lowrey TB, Aletras AH, Bandettini WP, Arai AE. Diagnostic accuracy of stress perfusion CMR in comparison with quantitative coronary angiography: fully quantitative, semiquantitative, and qualitative assessment. *JACC: Cardiovascular Imaging*. 2014;7:14–22.

170. Motwani M, Kidambi A, Sourbron S, Fairbairn TA, Uddin A, Kozerke S, Greenwood JP, Plein S. Quantitative three-dimensional cardiovascular magnetic resonance myocardial perfusion imaging in systole and diastole. *J Cardiovasc Magn Reson*. 2014;16:19.

171. Manka R, Jahnke C, Kozerke S, Vitanis V, Crelier G, Gebker R, Schnackenburg B, Boesiger P, Fleck E, Paetsch I. Dynamic 3-dimensional stress cardiac magnetic resonance perfusion imaging: detection of coronary artery disease and volumetry of myocardial hypoenhancement before and after coronary stenting. *J Am Coll Cardiol*. 2011;57:437–444.

172. Jogiya R, Kozerke S, Morton G, De Silva K, Redwood S, Perera D, Nagel E, Plein S. Validation of Dynamic 3-Dimensional Whole Heart Magnetic Resonance Myocardial Perfusion Imaging Against Fractional Flow Reserve for the Detection of Significant Coronary Artery Disease. *JAC*. 2012;60:756–765.

173. Hansen MS, Sørensen TS. Gadgetron: An open source framework for medical image reconstruction. *Magn Reson Med*. 2012;69:1768–1776.

174. Cullen JHS, Horsfield MA, Reek CR, Cherryman GR, Barnett DB, Samani NJ. A myocardial perfusion reserve index in humans using first-pass contrast-enhanced magnetic resonance imaging. *JAC*. 1999;33:1386–1394.

175. Petersen SE, Aung N, Sanghvi MM, Zemrak F, Fung K, Paiva JM, Francis JM, Khanji MY, Lukaschuk E, Lee AM, Carapella V, Kim YJ, Leeson P, Piechnik SK, Neubauer S. Reference ranges for cardiac structure and function using cardiovascular magnetic resonance (CMR) in Caucasians from the UK Biobank population cohort. *J Cardiovasc Magn Reson*. 2017;19:18.

176. Petersen SE, Selvanayagam JB, Francis JM, Myerson SG, Wiesmann F, Robson MD, Ostman-Smith I, Casadei B, Watkins H, Neubauer S. Differentiation of athlete's heart from pathological forms of cardiac hypertrophy by means of geometric indices derived from cardiovascular magnetic resonance. *J Cardiovasc Magn Reson*. 2005;7:551–558.

177. Hudsmith LE, Petersen SE, Francis JM, Robson MD, Neubauer S. Normal human left and right ventricular and left atrial dimensions using steady state free precession magnetic resonance imaging. *J Cardiovasc Magn Reson*. 2005;7:775–782.

178. Alfakih K, Plein S, Thiele H, Jones T, Ridgway JP, Sivananthan MU. Normal human left and right ventricular dimensions for MRI as assessed by turbo gradient echo and steady-state free precession imaging sequences. *J Magn Reson Imaging*. 2003;17:323–329.

179. Authors/Task Force Members, McMurray JJV, Adamopoulos S, Anker SD, Auricchio A, Bohm M, Dickstein K, Falk V, Filippatos G, Fonseca C, Gomez-Sanchez MA, Jaarsma T, Kober L, Lip GYH, Maggioni AP, Parkhomenko A, Pieske BM, Popescu BA, Ronnevik PK, Rutten FH, Schwitter J, Seferovic P, Stepinska J, Trindade PT, Voors AA, Zannad F, Zeiher A, ESC Committee for Practice Guidelines (CPG), Bax JJ, Baumgartner H, Ceconi C, Dean V, Deaton C, Fagard R, Funck-Brentano C, Hasdai D, Hoes A, Kirchhof P, Knuuti J, Kolh P, McDonagh T, Moulin C, Popescu BA, Reiner Z, Sechtem U, Sirnes PA, Tendera M, Torbicki A, Vahanian A, Windecker S, Document Reviewers, McDonagh T, Sechtem U, Bonet LA, Avraamides P, Ben Lamin HA, Brignole M, Coca A, Cowburn P, Dargie H, Elliott P, Flachskampf FA, Guida GF, Hardman S, Iung B, Merkely B, Mueller C, Nanas JN, Nielsen OW, Orn S, Parissis JT, Ponikowski P. ESC Guidelines for the diagnosis and treatment of acute and chronic heart failure 2012: The Task Force for the Diagnosis and Treatment of Acute and Chronic Heart Failure 2012 of the European Society of Cardiology. Developed in collaboration with the Heart Failure Association (HFA) of the ESC. *European Journal of Heart Failure*. 2012;14:803–869.

180. Ponikowski P, Voors AA, Anker SD, Bueno H, Cleland JGF, Coats AJS, Falk V, González-Juanatey JR, Harjola V-P, Jankowska EA, Jessup M, Linde C, Nihoyannopoulos P, Parissis JT, Pieske B, Riley JP, Rosano GMC, Ruilope LM, Ruschitzka F, Rutten FH, van der Meer P, Authors/Task Force Members, Document Reviewers. 2016 ESC Guidelines for the diagnosis and treatment of acute and chronic heart failure. *European Journal of Heart Failure*. 2016;18:891–975.

181. Kim RJ, Wu E, Rafael A, Chen E-L, Parker MA, Simonetti O, Klocke FJ, Bonow RO, Judd RM. The Use of Contrast-Enhanced Magnetic Resonance Imaging to Identify Reversible Myocardial Dysfunction. *New England Journal of Medicine*. 2000;343:1445–1453.

182. Cheng ASH, Pegg TJ, Karamitsos TD, Searle N, Jerosch-Herold M, Choudhury RP, Banning AP, Neubauer S, Robson MD, Selvanayagam JB. Cardiovascular Magnetic Resonance Perfusion Imaging at 3-Tesla for the Detection of Coronary Artery Disease. *J Am Coll Cardiol*. 2007;49:2440–2449.

183. Plein S, Ryf S, Schwitter J, Radjenovic A, Boesiger P, Kozerke S. Dynamic contrast-enhanced myocardial perfusion MRI accelerated withk-t sense. *Magn Reson Med*. 2007;58:777–785.

184. Schuster A, Sinclair M, Zarinabad N, Ishida M, van den Wijngaard JPHM, Paul M, van Horssen P, Hussain ST, Perera D, Schaeffter T, Spaan JAE, Siebes M, Nagel E, Chiribiri A. A quantitative high resolution voxel-wise assessment of myocardial blood flow from contrast-enhanced first-pass magnetic resonance perfusion imaging: microsphere validation in a magnetic resonance compatible free beating explanted pig heart model. *Eur Heart J Cardiovasc Imaging*. 2015;16:1082–1092.

185. Villa ADM, Sammut E, Zarinabad N, Carr-White G, Lee J, Bettencourt N, Razavi R, Nagel E, Chiribiri A. Microvascular ischemia in hypertrophic cardiomyopathy: new insights from high-resolution combined quantification of perfusion and late gadolinium enhancement. *J Cardiovasc Magn Reson*. 2016;:1–11.

186. Kremser CB, O'Toole MF, Leff AR. Oscillatory hyperventilation in severe congestive heart failure secondary to idiopathic dilated cardiomyopathy or to ischemic cardiomyopathy. *The American Journal of Cardiology*. 1987;59:900–905.

187. Feld et al. JACC 1993. Cyclic respiratory pattern in HF. 2003;:1–4.

188. Yahima et al. Chest 1994. Irregular respiration in HF. 2007;:1–5.

189. McCrohon JA. Differentiation of Heart Failure Related to Dilated Cardiomyopathy and Coronary Artery Disease Using Gadolinium-Enhanced Cardiovascular Magnetic Resonance. *Circulation*. 2003;108:54–59.

190. Kramer CM, Barkhausen J, Flamm SD, Kim RJ, Nagel E, Society for Cardiovascular Magnetic Resonance Board of Trustees Task Force on Standardized Protocols. Standardized cardiovascular magnetic resonance (CMR) protocols 2013 update. J Cardiovasc Magn Reson. 2013;15:91.

191. Fang W, Zhang J, He Z-X. Myocardial ischemia in patients with dilated cardiomyopathy. *Nuclear Medicine Communications*. 2010;31:981–984.

192. Neglia D. Prognostic Role of Myocardial Blood Flow Impairment in Idiopathic Left Ventricular Dysfunction. *Circulation*. 2002;105:186–193.

193. Van den Heuvel AF, van Veldhuisen DJ, van der Wall EE, Blanksma PK, Siebelink H-MJ, Vaalburg WM, van Gilst WH, Crijns HJ. Regional myocardial blood flow reserve impairment and metabolic changes suggesting myocardial ischemia in patients with idiopathic dilated cardiomyopathy. *JAC* [Internet]. 2013;35:19–28. Available from: http://content.onlinejacc.org/article.aspx?articleid=1126188

194. Masci PG, Marinelli M, Piacenti M, Lorenzoni V, Positano V, Lombardi M, L'Abbate A, Neglia D. Myocardial Structural, Perfusion, and Metabolic Correlates of Left Bundle Branch Block Mechanical Derangement in Patients With Dilated Cardiomyopathy: A Tagged Cardiac Magnetic Resonance and Positron Emission Tomography Study. *Circulation: Cardiovascular Imaging*. 2010;3:482–490.

195. Neglia D, Parodi O, Gallopin M, Sambuceti G, Giorgetti A, Pratali L, Salvadori P, Michelassi C, Lunardi M, Pelosi G, Marzilli M, L'Abbate A. Myocardial Blood Flow Response to Pacing Tachycardia and to Dipyridamole Infusion in Patients With Dilated Cardiomyopathy Without Overt Heart Failure : A Quantitative Assessment by Positron Emission Tomography. *Circulation*. 1995;92:796–804.

196. Tio RA, Slart RHJA, de Boer RA, van der Vleuten PA, de Jong RM, van Wijk LM, Willems T, Lubbers DD, Voors AA, van Veldhuisen DJ. Reduced regional myocardial perfusion reserve is associated with impaired contractile performance in idiopathic dilated cardiomyopathy. *Neth Heart J*. 2009;17:470–474.

197. Parodi O, De Maria R, Oltrona L, Testa R, Sambuceti G, Roghi A, Merli M, Belingheri L, Accinni R, Spinelli F. Myocardial blood flow distribution in patients with ischemic heart disease or dilated cardiomyopathy undergoing heart transplantation. *Circulation*. 1993;88:509–522.

198. Hachamovitch R, Rozanski A, Hayes SW, Thomson LEJ, Germano G, Friedman JD, Cohen I, Berman DS. Predicting therapeutic benefit from myocardial revascularization procedures: are measurements of both resting left ventricular ejection fraction and stress-induced myocardial ischemia necessary? *J Nucl Cardiol*. 2006;13:768–778.

199. Hachamovitch R, Rozanski A, Shaw LJ, Stone GW, Thomson LEJ, Friedman JD, Hayes SW, Cohen I, Germano G, Berman DS. Impact of ischaemia and scar on the therapeutic benefit derived from myocardial revascularization vs. medical therapy among patients undergoing stress-rest myocardial perfusion scintigraphy. *European Heart Journal*. 2011;32:1012–1024.

200. Shaw LJ, Cerqueira MD, Brooks MM, Althouse AD, Sansing VV, Beller GA, Pop-Busui R, Taillefer R, Chaitman BR, GIBBONS RJ, Heo J, Iskandrian AE. Impact of left ventricular function and the extent of ischemia and scar by stress myocardial perfusion imaging on prognosis and therapeutic risk reduction in diabetic patients with coronary artery disease: results from the Bypass Angioplasty Revascularization Investigation 2 Diabetes (BARI 2D) trial. *J Nucl Cardiol*. 2012;19:658–669.

201. Hachamovitch R, Hayes SW, Friedman JD, Cohen I, Berman DS. A prognostic score for prediction of cardiac mortality risk after adenosine stress myocardial perfusion scintigraphy. *JAC*. 2005;45:722–729.

202. Berman DS, Abidov A, Kang X, Hayes SW, Friedman JD, Sciammarella MG, Cohen I, Gerlach J, Waechter PB, Germano G, Hachamovitch R. Prognostic validation of a 17-segment score derived from a 20-segment score for myocardial perfusion SPECT interpretation. *J Nucl Cardiol*. 2004;11:414–423.

203. Shaw LJ, Berman DS, Picard MH, Friedrich MG, Kwong RY, Stone GW, Senior R, Min JK, Hachamovitch R, Scherrer-Crosbie M, Mieres JH, Marwick TH, Phillips LM, Chaudhry FA, Pellikka PA, Slomka P, Arai AE, Iskandrian AE, Bateman TM, Heller GV, Miller TD, Nagel E, Goyal A, Borges-Neto S, Boden WE, Reynolds HR, Hochman JS, Maron DJ, Douglas PS. Comparative Definitions for Moderate-Severe Ischemia in Stress Nuclear, Echocardiography, and Magnetic Resonance Imaging. *JACC: Cardiovascular Imaging*. 2014;7:593–604.

204. Motwani M, Maredia N, Fairbairn TA, Kozerke S, Greenwood JP, Plein S. Assessment of ischaemic burden in angiographic three-vessel coronary artery disease with high-resolution myocardial perfusion cardiovascular magnetic resonance imaging. *Eur Heart J Cardiovasc Imaging*. 2014;15:701–708.

205. Morton G, Ishida M, De Silva K, Sicard P, Chiribiri A, Schuster A, Hussain S, Paul M, Perera D, Nagel E. Correlation between an angiographic and acardiac magnetic resonance score of myocardialjeopardy using standard and high-resolutionperfusion sequences. *J Cardiovasc Magn Reson*. 2011;13:P89.

206. Villa A, Sammut E, Shome JS, Razavi R, Plein S, Chiribiri A. Combined high-resolution assessment ofquantitative perfusion and late enhancement.Towards accurate estimation of the ischaemic burden in patients with coronary artery disease. *J Cardiovasc Magn Reson*. 2016;:1–2.

207. Manka R, Paetsch I, Kozerke S, Moccetti M, Hoffmann R, Schroeder J, Reith S, Schnackenburg B, Gaemperli O, Wissmann L, Wyss CA, Kaufmann PA, Corti R, Boesiger P, Marx N, Lüscher TF, Jahnke C. Whole-heart dynamic three-dimensional magnetic resonance perfusion imaging for the detection of coronary artery disease defined by fractional flow reserve: determination of volumetric myocardial ischaemic burden and coronary lesion location. *European Heart Journal*. 2012;33:2016–2024.

208. McDiarmid AK, Ripley DP, Mohee K, Kozerke S, Greenwood JP, Plein S, Motwani M. Three-dimensional whole-heart vs. two-dimensional high-resolution perfusion-CMR: a pilot study comparing myocardial ischaemic burden. *Eur Heart J Cardiovasc Imaging*. 2016;17:900–908.

209. Thygesen K, Alpert JS, White HD, Joint ESC/ACCF/AHA/WHF Task Force for the Redefinition of Myocardial Infarction. Universal definition of myocardial infarction. 2007. p. 2173–2195.

210. Kelle S, Chiribiri A, Vierecke J, Egnell C, Hamdan A, Jahnke C, Paetsch I, Wellnhofer E, Fleck E, Klein C, Gebker R. Long-term prognostic value of dobutamine stress CMR. *JACC: Cardiovascular Imaging*. 2011;4:161–172.

211. Karamitsos TD, Ntusi NA, Francis JM, Holloway CJ, Myerson SG, Neubauer S. Feasibility and safety of high-dose adenosine perfusion cardiovascular magnetic resonance. *J Cardiovasc Magn Reson*. 2010;12:66.

212. Plein S, Schwitter J, Suerder D, Greenwood JP, Boesiger P, Kozerke S. k-Space and time sensitivity encoding-accelerated myocardial perfusion MR imaging at 3.0 T: comparison with 1.5 T. *Radiology*. 2008;249:493–500.

213. Simon RM, Subramanian J, Li M-C, Menezes S. Using cross-validation to evaluate predictive accuracy of survival risk classifiers based on high-dimensional data. *Brief Bioinformatics*. 2011;12:203–214.

214. Varma S, Simon R. Bias in error estimation when using cross-validation for model selection. BioMed Central Ltd; 2006.

215. Blanche P, Dartigues J-F, Jacqmin-Gadda H. Estimating and comparing time-dependent areas under receiver operating characteristic curves for censored event times with competing risks. *Stat Med*. 2013;32:5381–5397.

216. Fihn SD, Gardin JM, Abrams J, Berra K, Blankenship JC, Dallas AP, Douglas PS, Foody JM, Gerber TC, Hinderliter AL, King SB, Kligfield PD, Krumholz HM, Kwong RYK, Lim MJ, Linderbaum JA, Mack MJ, Munger MA, Prager RL, Sabik JF, Shaw LJ, Sikkema JD, Smith CR, Smith SC, Spertus JA, Williams SV, Anderson JL, American College of Cardiology Foundation/American Heart Association Task Force. 2012 ACCF/AHA/ACP/AATS/PCNA/SCAI/STS guideline for the diagnosis and management of patients with stable ischemic heart disease: a report of the American College of Cardiology Foundation/American Heart Association task force on practice guidelines, and the American College of Physicians, American Association for Thoracic Surgery, Preventive Cardiovascular Nurses Association, Society for Cardiovascular Angiography and Interventions, and Society of Thoracic Surgeons. Circulation. 2012;126:e354–471.

217. Pencina MJ, D'Agostino RB, Vasan RS. Evaluating the added predictive ability of a new marker: from area under the ROC curve to reclassification and beyond. *Stat Med*. 2008;27:157–72– discussion 207–12.

218. Jacobs M, Benovoy M, Chang L-C, Arai AE, Hsu L-Y. Evaluation of an automated method for arterial input function detection for first- pass myocardial perfusion cardiovascular magnetic resonance. *J Cardiovasc Magn Reson*. 2016;:1–11.

219. Sammut E. Feasibility of high-resolution quantitative perfusion analysis in patients with heart failure. 2015;:1–11.

220. Wollny G, Ledesma-Carbayo MJ, Kellman P, Santos A. Exploiting quasiperiodicity in motion correction of free-breathing myocardial perfusion MRI. *IEEE Trans Med Imaging*. 2010;29:1516–1527.

221. Slart RHJA, Zeebregts CJ, Hillege HL, de Sutter J, Dierckx RAJO, van Veldhuisen DJ, Zijlstra F, Tio RA. Myocardial perfusion reserve after a PET-driven revascularization procedure: a strong prognostic factor. *J Nucl Med*. 2011;52:873–879.

222. Townsend DW. A combined PET/CT scanner: the choices. *Journal of Nuclear Medicine*. 2001;42:533–534.

223. Antoch G, Saoudi N, Kuehl H, Dahmen G, Mueller SP, Beyer T, Bockisch A, Debatin JF, Freudenberg LS. Accuracy of whole-body dual-modality fluorine-18-2-fluoro-2-deoxy-D-glucose positron emission tomography and computed tomography (FDG-PET/CT) for tumor staging in solid tumors: comparison with CT and PET. *J Clin Oncol*. 2004;22:4357–4368.

224. Bar-Shalom R, Yefremov N, Guralnik L, Gaitini D, Frenkel A, Kuten A, Altman H, Keidar Z, Israel O. Clinical performance of PET/CT in evaluation of cancer: additional value for diagnostic imaging and patient management. *Journal of Nuclear Medicine*. 2003;44:1200–1209.

225. Scarfone C, Lavely WC, Cmelak AJ, Delbeke D, Martin WH, Billheimer D, Hallahan DE. Prospective feasibility trial of radiotherapy target definition for head and neck cancer using 3-dimensional PET and CT imaging. *Journal of Nuclear Medicine*. 2004;45:543–552.

226. Pfannenberg AC, Aschoff P, Brechtel K, Müller M, Klein M, Bares R, Claussen CD, Eschmann SM. Value of contrast-enhanced multiphase CT in combined PET/CT protocols for oncological imaging. *Br J Radiol*. 2007;80:437–445.

227. Beyer T, Antoch G, Blodgett T, Freudenberg LF, Akhurst T, Mueller S. Dual-modality PET/CT imaging: the effect of respiratory motion on combined image quality in clinical oncology. *Eur J Nucl Med Mol Imaging*. 2003;30:588–596.

228. Brechtel K, Klein M, Vogel M, Mueller M, Aschoff P, Beyer T, Eschmann SM, Bares R, Claussen CD, Pfannenberg AC. Optimized contrast-enhanced CT protocols for diagnostic whole-body 18F-FDG PET/CT: technical aspects of single-phase versus multiphase CT imaging. *Journal of Nuclear Medicine*. 2006;47:470–476.

229. Goerres GW, Kamel E, Heidelberg T-NH, Schwitter MR, Burger C, Schulthess Von GK. PET-CT image co-registration in the thorax: influence of respiration. *Eur J Nucl Med Mol Imaging*. 2002;29:351–360.

230. Goerres GW, Burger C, Kamel E, Seifert B, Kaim AH, Buck A, Buehler TC, Schulthess Von GK. Respiration-induced attenuation artifact at PET/CT: technical considerations. *Radiology*. 2003;226:906–910.

231. Ratib O, Nkoulou R. Potential Applications of PET/MR Imaging in Cardiology. *J Nucl Med*. 2014;55:40S–46S.

232. Varoquaux A, Rager O, Poncet A, Delattre BMA, Ratib O, Becker CD, Dulguerov P, Dulguerov N, Zaidi H, Becker M. Detection and quantification of focal uptake in head and neck tumours: (18)F-FDG PET/MR versus PET/CT. *Eur J Nucl Med Mol Imaging*. 2014;41:462–475.

233. Paldino MJ, Yang E, Jones JY, Mahmood N, Sher A, Zhang W, Hayatghaibi S, Krishnamurthy R, Seghers V. Comparison of the diagnostic accuracy of PET/MRI to PET/CT-acquired FDG brain exams for seizure focus detection: a prospective study. *Pediatr Radiol*. 2017;47:1500–1507.

234. Judenhofer MS, Cherry SR. Applications for preclinical PET/MRI. *Semin Nucl Med*. 2013;43:19–29.

235. Rota Kops E, Ribeiro AS, Caldeira L, Hautzel H, Lukas M, Antoch G, Lerche C, Shah J. Attenuation correction for hybrid MR/PET scanners: a comparison study. *EJNMMI Phys*. 2015;2:A38.

236. Beyer T, Weigert M, Quick HH, Pietrzyk U, Vogt F, Palm C, Antoch G, Müller SP, Bockisch A. MR-based attenuation correction for torso-PET/MR imaging: pitfalls in mapping MR to CT data. *Eur J Nucl Med Mol Imaging*. 2008;35:1142–1146.

237. Hofmann M, Steinke F, Scheel V, Charpiat G, Farquhar J, Aschoff P, Brady M, Schölkopf B, Pichler BJ. MRI-based attenuation correction for PET/MRI: a novel approach combining pattern recognition and atlas registration. *Journal of Nuclear Medicine*. 2008;49:1875–1883.

238. Eiber M, Martinez-Möller A, Souvatzoglou M, Holzapfel K, Pickhard A, Löffelbein D, Santi I, Rummeny EJ, Ziegler S, Schwaiger M, Nekolla SG, Beer AJ. Value of a Dixon-based MR/PET attenuation correction sequence for the localization and evaluation of PET-positive lesions. *Eur J Nucl Med Mol Imaging*. 2011;38:1691–1701.

239. Martinez-Möller A, Souvatzoglou M, Delso G, Bundschuh RA, Chefd'hotel C, Ziegler SI, Navab N, Schwaiger M, Nekolla SG. Tissue classification as a potential approach for attenuation correction in whole-body PET/MRI: evaluation with PET/CT data. *Journal of Nuclear Medicine*. 2009;50:520–526.

240. Mehranian A, Zaidi H. Clinical Assessment of Emission- and Segmentation-Based MR-Guided Attenuation Correction in Whole-Body Time-of-Flight PET/MR Imaging. *J Nucl Med*. 2015;56:877–883.

241. Chun SY, Reese TG, Ouyang J, Guerin B, Catana C, Zhu X, Alpert NM, Fakhri El G. MRI-based nonrigid motion correction in simultaneous PET/MRI. *J Nucl Med*. 2012;53:1284–1291.

242. Petibon Y, Ouyang J, Zhu X, Huang C, Reese TG, Chun SY, Li Q, Fakhri El G. Cardiac motion compensation and resolution modeling in simultaneous PET-MR: a cardiac lesion detection study. *Phys Med Biol*. 2013;58:2085–2102.

243. Kolbitsch C, Ahlman MA, Davies-Venn C, Evers R, Hansen M, Peressutti D, Marsden P, Kellman P, Bluemke DA, Schaeffter T. Cardiac and Respiratory Motion Correction for Simultaneous Cardiac PET/MR. *J Nucl Med*. 2017;58:846–852.

244. Manber R, Thielemans K, Hutton BF, Wan S, McClelland J, Barnes A, Arridge S, Ourselin S, Atkinson D. Joint PET-MR respiratory motion models for clinical PET motion correction. *Phys Med Biol*. 2016;61:6515–6530.

245. Schlosser T, Nensa F, Mahabadi AA, Poeppel TD. Hybrid MRI/PET of the heart: a new complementary imaging technique for simultaneous acquisition of MRI and PET data. *Heart*. 2013;99:351–352.

246. Nensa F, Poeppel TD, Beiderwellen K, Schelhorn J, Mahabadi AA, Erbel R, Heusch P, Nassenstein K, Bockisch A, Forsting M, Schlosser T. Hybrid PET/MR imaging of the heart: feasibility and initial results. *Radiology*. 2013;268:366–373.

247. Bulluck H, White SK, Fröhlich GM, Casson SG, O'Meara C, Newton A, Nicholas J, Weale P, Wan SMY, Sirker A, Moon JC, Yellon DM, Groves A, Menezes L, Hausenloy DJ. Quantifying the Area at Risk in Reperfused ST-Segment-Elevation Myocardial Infarction Patients Using Hybrid Cardiac Positron Emission Tomography-Magnetic Resonance Imaging. *Circulation: Cardiovascular Imaging*. 2016;9:e003900.

248. Rischpler C, Langwieser N, Souvatzoglou M, Batrice A, van Marwick S, Snajberk J, Ibrahim T, Laugwitz K-L, Nekolla SG, Schwaiger M. PET/MRI early after myocardial infarction: evaluation of viability with late gadolinium enhancement transmurality vs. 18F-FDG uptake. *Eur Heart J Cardiovasc Imaging*. 2015;16:661–669.

249. Kero T, Nordström J, Harms HJ, Sörensen J, Ahlstrom H, Lubberink M. Quantitative myocardial blood flow imaging with integrated time-of-flight PET-MR. *EJNMMI Phys*. 2017;4:1.

250. Priamo J, Adamopoulos D, Rager O, Frei A, Noble S, Carballo D, Ratib O, Nkoulou R. Downstream indication to revascularization following hybrid cardiac PET/MRI: preliminary results. *Nuclear Medicine Communications*. 2017;38:515–522.

251. Nensa F, Schlosser T. Cardiovascular hybrid imaging using PET/MRI. *Rofo*. 2014;186:1094–1101.

252. Nensa F, Tezgah E, Poeppel TD, Jensen CJ, Schelhorn J, Köhler J, Heusch P, Bruder O, Schlosser T, Nassenstein K. Integrated 18F-FDG PET/MR imaging in the assessment of cardiac masses: a pilot study. *J Nucl Med*. 2015;56:255–260.

253. Ibrahim T, Nekolla SG, Langwieser N, Rischpler C, Groha P, Laugwitz K-L, Schwaiger M. Simultaneous positron emission tomography/magnetic resonance imaging identifies sustained regional abnormalities in cardiac metabolism and function in stress-induced transient midventricular ballooning syndrome: a variant of Takotsubo cardiomyopathy. *Circulation*. 2012;126:e324–6.

254. Dweck MR, Abgral R, Trivieri MG, Robson PM, Karakatsanis N, Mani V, Palmisano A, Miller MA, Lala A, Chang HL, Sanz J, Contreras J, Narula J, Fuster V, Padilla M, Fayad ZA, Kovacic JC. Hybrid Magnetic Resonance Imaging and Positron Emission Tomography With Fluorodeoxyglucose to Diagnose Active Cardiac Sarcoidosis. *JACC: Cardiovascular Imaging*. 2017;

255. Marchesseau S, Seneviratna A, Sjöholm AT, Qin DL, Ho JXM, Hausenloy DJ, Townsend DW, Richards AM, Totman JJ, Chan MYY. Hybrid PET/CT and PET/MRI imaging of vulnerable coronary plaque and myocardial scar tissue in acute myocardial infarction. *J Nucl Cardiol*. 2017;

256. Hyafil F, Schindler A, Sepp D, Obenhuber T, Bayer-Karpinska A, Boeckh-Behrens T, Höhn S, Hacker M, Nekolla SG, Rominger A, Dichgans M, Schwaiger M, Saam T, Poppert H. High-risk plaque features can be detected in non-stenotic carotid plaques of patients with ischaemic stroke classified as cryptogenic using combined (18)F-FDG PET/MR imaging. *Eur J Nucl Med Mol Imaging*. 2016;43:270–279.

257. Otton J, Morton G, Schuster A, Bigalke B, Marano R, Olivotti L, Nagel E, Chiribiri A. A direct comparison of the sensitivity of CT and MR cardiac perfusion using a myocardial perfusion phantom. *J Cardiovasc Comput Tomogr*. 2013;7:117–124.

258. Jerosch-Herold M. Quantification of myocardial perfusion by cardiovascular magnetic resonance. *Journal of Cardiovascular Magnetic Resonance*. 2010;12:57.

259. Hofmann M, Bezrukov I, Mantlik F, Aschoff P, Steinke F, Beyer T, Pichler BJ, Schölkopf B. MRI-based attenuation correction for whole-body PET/MRI: quantitative evaluation of segmentation- and atlas-based methods. *J Nucl Med*. 2011;52:1392–1399.

260. O' Doherty J, Schleyer P. An experimental phantom study of the effect of gadolinium-based MR contrast agents on PET attenuation coefficients and PET quantification in PET-MR imaging: application to cardiac studies. *EJNMMI Phys*. 2017;4:4.

261. Ouyang J, Li Q, Fakhri El G. Magnetic resonance-based motion correction for positron emission tomography imaging. *Semin Nucl Med*. 2013;43:60–67.

262. Huang C, Petibon Y, Ouyang J, Reese TG, Ahlman MA, Bluemke DA, Fakhri El G. Accelerated acquisition of tagged MRI for cardiac motion correction in simultaneous PET-MR: phantom and patient studies. *Med Phys*. 2015;42:1087–1097.

263. Vontobel J, Liga R, Possner M, Clerc OF, Mikulicic F, Veit-Haibach P, Voert Ter EEGW, Fuchs TA, Stehli J, Pazhenkottil AP, Benz DC, Gräni C, Gaemperli O, Herzog B, Buechel RR, Kaufmann PA. MR-based attenuation correction for cardiac FDG PET on a hybrid PET/MRI scanner: comparison with standard CT attenuation correction. *Eur J Nucl Med Mol Imaging*. 2015;42:1574–1580.

264. Røe ÅT, Frisk M, Louch WE. Targeting cardiomyocyte Ca2+ homeostasis in heart failure. *Curr Pharm Des*. 2015;21:431–448.

265. Maack C, O'Rourke B. Excitation-contraction coupling and mitochondrial energetics. *Basic Res Cardiol*. 2007;102:369–392.

266. Shannon TR, Wang F, Puglisi J, Weber C, Bers DM. A mathematical treatment of integrated Ca dynamics within the ventricular myocyte. *Biophys J*. 2004;87:3351–3371.

267. Bers DM. Cardiac excitation-contraction coupling. *Nature*. 2002;415:198–205.

268. Bers D. Excitation-Contraction Coupling and Cardiac Contractile Force. Springer Science & Business Media; 2012.

269. Harris DA, Das AM. Control of mitochondrial ATP synthesis in the heart. *Biochem J*. 1991;280 (Pt 3):561–573.

270. Balaban RS. Cardiac energy metabolism homeostasis: role of cytosolic calcium. *Journal of Molecular and Cellular Cardiology*. 2002;34:1259–1271.

271. Mootha VK, Arai AE, Balaban RS. Maximum oxidative phosphorylation capacity of the mammalian heart. *Am J Physiol*. 1997;272:H769–75.

272. Bers DM. Altered cardiac myocyte Ca regulation in heart failure. *Physiology (Bethesda)*. 2006;21:380–387.

273. Louch WE, Sejersted OM, Swift F. There goes the neighborhood: pathological alterations in T-tubule morphology and consequences for cardiomyocyte Ca2+ handling. *J Biomed Biotechnol*. 2010;2010:503906.

274. Gómez AM, Valdivia HH, Cheng H, Lederer MR, Santana LF, Cannell MB, McCune SA, Altschuld RA, Lederer WJ. Defective excitation-contraction coupling in experimental cardiac hypertrophy and heart failure. *Science*. 1997;276:800–806.

275. Heinzel FR, Bito V, Biesmans L, Wu M, Detre E, Wegner von F, Claus P, Dymarkowski S, Maes F, Bogaert J, Rademakers F, D'hooge J, Sipido K. Remodeling of T-tubules and reduced synchrony of Ca2+ release in myocytes from chronically ischemic myocardium. *Circulation Research*. 2008;102:338–346.

276. Gwathmey JK, Copelas L, MacKinnon R, Schoen FJ, Feldman MD, Grossman W, Morgan JP. Abnormal intracellular calcium handling in myocardium from patients with end-stage heart failure. *Circulation Research*. 1987;61:70–76.

277. Hasenfuss G, Mulieri LA, Leavitt BJ, Allen PD, Haeberle JR, Alpert NR. Alteration of contractile function and excitation-contraction coupling in dilated cardiomyopathy. *Circulation Research*. 1992;70:1225–1232.

278. O'Rourke B, Kass DA, Tomaselli GF, Kaab S, Tunin R, Marban E. Mechanisms of altered excitation-contraction coupling in canine tachycardia-induced heart failure, I: experimental studies. *Circulation Research*. 1999;84:562–570.

279. Guo A, Zhang C, Wei S, Chen B, Song L-S. Emerging mechanisms of T-tubule remodelling in heart failure. *Cardiovascular Research*. 2013;98:204–215.

280. Jeung M-Y, Germain P, Croisille P, ghannudi El S, Roy C, Gangi A. Myocardial tagging with MR imaging: overview of normal and pathologic findings. *Radiographics*. 2012;32:1381–1398.

281. Ingels NB, Daughters GT, Stinson EB, Alderman EL. Evaluation of methods for quantitating left ventricular segmental wall motion in man using myocardial markers as a standard. *Circulation*. 1980;61:966–972.

282. Brower RW, Katen ten HJ, Meester GT. Direct method for determining regional myocardial shortening after bypass surgery from radiopaque markers in man. *The American Journal of Cardiology*. 1978;41:1222–1229.

283. Meier GD, Bove AA, Santamore WP, Lynch PR. Contractile function in canine right ventricle. *Am J Physiol*. 1980;239:H794–804.

284. Arts T, Hunter WC, Douglas AS, Muijtjens AM, Corsel JW, Reneman RS. Macroscopic three-dimensional motion patterns of the left ventricle. *Adv Exp Med Biol*. 1993;346:383–392.

285. Myers JH, Stirling MC, Choy M, Buda AJ, Gallagher KP. Direct measurement of inner and outer wall thickening dynamics with epicardial echocardiography. *Circulation*. 1986;74:164–172.

286. Rankin JS, McHale PA, Arentzen CE, Ling D, Greenfield JC, Anderson RW. The three-dimensional dynamic geometry of the left ventricle in the conscious dog. *Circulation Research*. 1976;39:304–313.

287. Pelc LR, Sayre J, Yun K, Castro LJ, Herfkens RJ, Miller DC, Pelc NJ. Evaluation of myocardial motion tracking with cine-phase contrast magnetic resonance imaging. *Invest Radiol*. 1994;29:1038–1042.

288. Reese TG, Feinberg DA, Dou J, Wedeen VJ. Phase contrast MRI of myocardial 3D strain by encoding contiguous slices in a single shot. *Magn Reson Med*. 2002;47:665–676.

289. Jung B, Zaitsev M, Hennig J, Markl M. Navigator gated high temporal resolution tissue phase mapping of myocardial motion. *Magn Reson Med*. 2006;55:937–942.

290. Zerhouni EA, Parish DM, Rogers WJ, Yang A, Shapiro EP. Human heart: tagging with MR imaging--a method for noninvasive assessment of myocardial motion. *Radiology*. 1988;169:59–63.

291. Kuijer JPA, Marcus JT, Götte MJW, van Rossum AC, Heethaar RM. Three-dimensional myocardial strains at end-systole and during diastole in the left ventricle of normal humans. *J Cardiovasc Magn Reson*. 2002;4:341–351.

292. Moore CC, McVeigh ER, Zerhouni EA. Quantitative tagged magnetic resonance imaging of the normal human left ventricle. *Top Magn Reson Imaging*. 2000;11:359–371.

293. Amundsen BH, Helle-Valle T, Edvardsen T, Torp H, Crosby J, Lyseggen E, Støylen A, Ihlen H, Lima JAC, Smiseth OA, Slørdahl SA. Noninvasive myocardial strain measurement by speckle tracking echocardiography: validation against sonomicrometry and tagged magnetic resonance imaging. *J Am Coll Cardiol*. 2006;47:789–793.

294. Lima JA, Jeremy R, Guier W, Bouton S, Zerhouni EA, McVeigh E, Buchalter MB, Weisfeldt ML, Shapiro EP, Weiss JL. Accurate systolic wall thickening by nuclear magnetic resonance imaging with tissue tagging: correlation with sonomicrometers in normal and ischemic myocardium. *JAC*. 1993;21:1741–1751.

295. Kraigher-Krainer E, Shah AM, Gupta DK, Santos A, Claggett B, Pieske B, Zile MR, Voors AA, Lefkowitz MP, Packer M, McMurray JJV, Solomon SD, PARAMOUNT Investigators. Impaired systolic function by strain imaging in heart failure with preserved ejection fraction. *J Am Coll Cardiol*. 2014;63:447–456.

296. Ho E, Brown A, Barrett P, Morgan RB, King G, Kennedy MJ, Murphy RT. Subclinical anthracycline- and trastuzumab-induced cardiotoxicity in the long-term follow-up of asymptomatic breast cancer survivors: a speckle tracking echocardiographic study. *Heart*. 2010;96:701–707.

297. Buss SJ, Emami M, Mereles D, Korosoglou G, Kristen AV, Voss A, Schellberg D, Zugck C, Galuschky C, Giannitsis E, Hegenbart U, Ho AD, Katus HA, Schonland SO, Hardt SE. Longitudinal left ventricular function for prediction of survival in systemic light-chain amyloidosis: incremental value compared with clinical and biochemical markers. *J Am Coll Cardiol*. 2012;60:1067–1076.

298. Tower-Rader A, Betancor J, Popovic ZB, Sato K, Thamilarasan M, Smedira NG, Lever HM, Desai MY. Incremental Prognostic Utility of Left Ventricular Global Longitudinal Strain in Hypertrophic Obstructive Cardiomyopathy Patients and Preserved Left Ventricular Ejection Fraction. *J Am Heart Assoc*. 2017;6.

299. Schwarz K, Ahearn T, Srinivasan J, Neil CJ, Scally C, Rudd A, Jagpal B, Frenneaux MP, Pislaru C, Horowitz JD, Dawson DK. Alterations in Cardiac Deformation, Timing of Contraction and Relaxation, and Early Myocardial Fibrosis Accompany the Apparent Recovery of Acute Stress-Induced (Takotsubo) Cardiomyopathy: An End to the Concept of Transience. *J Am Soc Echocardiogr*. 2017;30:745–755.

300. Kalam K, Otahal P, Marwick TH. Prognostic implications of global LV dysfunction: a systematic review and meta-analysis of global longitudinal strain and ejection fraction. *Heart*. 2014;100:1673–1680.

301. Ojaghihaghighi Z, Alizadehasl A, Moladoust H, Ardeshiri M, Mostafavi A, Rezaeiyan N, Ojaghi SH, Safi F, Mikaeilpour A. Left Ventricular Torsional Parameters in Patients With Non-Ischemic Dilated Cardiomyopathy. *Arch Cardiovasc Imaging*. 2015;3.

302. Kanzaki H, Nakatani S, Yamada N, Urayama S-I, Miyatake K, Kitakaze M. Impaired systolic torsion in dilated cardiomyopathy: reversal of apical rotation at mid-systole characterized with magnetic resonance tagging method. *Basic Res Cardiol*. 2006;101:465–470.

303. Popescu BA, Beladan CC, Calin A, Muraru D, Deleanu D, Rosca M, Ginghina C. Left ventricular remodelling and torsional dynamics in dilated cardiomyopathy: reversed apical rotation as a marker of disease severity. *European Journal of Heart Failure*. 2009;11:945–951.

304. Tibayan FA, Lai DTM, Timek TA, Dagum P, Liang D, Daughters GT, Ingels NB, Miller DC. Alterations in left ventricular torsion in tachycardia-induced dilated cardiomyopathy. *The Journal of Thoracic and Cardiovascular Surgery*. 2002;124:43–49.

305. GRANT RP. NOTES ON THE MUSCULAR ARCHITECTURE OF THE LEFT VENTRICLE. *Circulation*. 1965;32:301–308.

306. Smerup M, Nielsen E, Agger P, Frandsen J, Vestergaard-Poulsen P, Andersen J, Nyengaard J, Pedersen M, Ringgaard S, Hjortdal V, Lunkenheimer PP, Anderson RH. The three-dimensional arrangement of the myocytes aggregated together within the mammalian ventricular myocardium. *Anat Rec (Hoboken)*. 2009;292:1–11.

307. Axel L, Wedeen VJ, Ennis DB. Probing dynamic myocardial microstructure with cardiac magnetic resonance diffusion tensor imaging. *J Cardiovasc Magn Reson*. 2014;16:89.

308. Harrington KB, Rodriguez F, Cheng A, Langer F, Ashikaga H, Daughters GT, Criscione JC, Ingels NB, Miller DC. Direct measurement of transmural laminar architecture in the anterolateral wall of the ovine left ventricle: new implications for wall thickening mechanics. *Am J Physiol Heart Circ Physiol*. 2005;288:H1324–30.

309. Kung GL, Nguyen TC, Itoh A, Skare S, Ingels NB, Miller DC, Ennis DB. The presence of two local myocardial sheet populations confirmed by diffusion tensor MRI and histological validation. *J Magn Reson Imaging*. 2011;34:1080–1091.

310. Sands GB, Gerneke DA, Hooks DA, Green CR, Smaill BH, Legrice IJ. Automated imaging of extended tissue volumes using confocal microscopy. *Microsc Res Tech*. 2005;67:227–239.

311. Gilbert SH, Benson AP, Li P, Holden AV. Regional localisation of left ventricular sheet structure: integration with current models of cardiac fibre, sheet and band structure. *European Journal of Cardio-Thoracic Surgery*. 2007;32:231–249.

312. Streeter DD, SPOTNITZ HM, PATEL DP, ROSS J, SONNENBLICK EH. Fiber orientation in the canine left ventricle during diastole and systole. *Circulation Research*. 1969;24:339–347.

313. PhD SN-V, MBBS ZK, PhD PFF, de Silva MBBS PhD R, PhD ADS, MD PK, MB L-AM, PhD AG, PhD PDG, PhD DE, BS EA, MSc MA-K, PhD PK, PhD DM, PhD RSB, PhD DNF, MD AEA, MD DJP. Assessment of Myocardial Microstructural Dynamics by In Vivo Diffusion Tensor Cardiac Magnetic Resonance. *JAC*. 2017;69:661–676.

314. Hales PW, Schneider JE, Burton RAB, Wright BJ, Bollensdorff C, Kohl P. Progress in Biophysics and Molecular Biology. *Progress in Biophysics and Molecular Biology*. 2012;110:319–330.

315. Chen J, Liu W, Zhang H, Lacy L, Yang X, Song S-K, Wickline SA, Yu X. Regional ventricular wall thickening reflects changes in cardiac fiber and sheet structure during contraction: quantification with diffusion tensor MRI. *Am J Physiol Heart Circ Physiol*. 2005;289:H1898–907.

316. SPOTNITZ HM, Spotnitz WD, Cottrell TS, Spiro D, SONNENBLICK EH. Cellular basis for volume related wall thickness changes in the rat left ventricle. *Journal of Molecular and Cellular Cardiology*. 1974;6:317–331.

317. Sammut E. LeGrice et al. Circ Res 1995. Mechanism of thickening of LV. 2013.

318. Dou J, Tseng W-YI, Reese TG, Wedeen VJ. Combined diffusion and strain MRI reveals structure and function of human myocardial laminar sheets in vivo. *Magn Reson Med*. 2003;50:107–113.

319. Costa KD, Takayama Y, McCulloch AD, Covell JW. Laminar fiber architecture and three-dimensional systolic mechanics in canine ventricular myocardium. *Am J Physiol*. 1999;276:H595–607.

320. Mori S, Frederiksen K, van Zijl PCM, Stieltjes B, Kraut MA, Solaiyappan M, Pomper MG. Brain white matter anatomy of tumor patients evaluated with diffusion tensor imaging. *Ann Neurol*. 2002;51:377–380.

321. Parmar H, Sitoh Y-Y, Yeo TT. Combined magnetic resonance tractography and functional magnetic resonance imaging in evaluation of brain tumors involving the motor system. *J Comput Assist Tomogr*. 2004;28:551–556.

322. Tseng W-YI, Wedeen VJ, Reese TG, Smith RN, Halpern EF. Diffusion tensor MRI of myocardial fibers and sheets: correspondence with visible cut-face texture. *J Magn Reson Imaging*. 2003;17:31–42.

323. Mekkaoui C, Huang S, Chen HH, Dai G, Reese TG, Kostis WJ, Thiagalingam A, Maurovich-Horvat P, Ruskin JN, Hoffmann U, Jackowski MP, Sosnovik DE. Fiber architecture in remodeled myocardium revealed with a quantitative diffusion CMR tractography framework and histological validation. *Journal of Cardiovascular Magnetic Resonance*. 2012;14:1–1.

324. Hsu EW, Muzikant AL, Matulevicius SA, Penland RC, Henriquez CS. Magnetic resonance myocardial fiber-orientation mapping with direct histological correlation. *Am J Physiol*. 1998;274:H1627–34.

325. SCHMID P, JAERMANN T, BOESIGER P, NIEDERER P, LUNKENHEIMER P, CRYER C, ANDERSON R. Ventricular myocardial architecture as visualised in postmortem swine hearts using magnetic resonance diffusion tensor imaging. *European Journal of Cardio-Thoracic Surgery* [Internet]. 2005;27:468–472. Available from: https://oup.silverchair-cdn.com/oup/backfile/Content_public/Journal/ejcts/27/3/10.1016/j.ejcts.2004.11.036/2/27-3-468.pdf?Expires=1497224609&Signature=Eh3Ko~X9qj~jJk7CnBKC50Pj9xFXTe3vF8LtNRWgsIzGdVYgG37cN~64bt5dYxlee~GMyoPZW5BIo1rOcevfwkoUz7-O4E7PR-gYRbQ0z1FpWOkvbmnikjeznzgO6WMGzDuiKGVLOyvUYLm9aq2nvCMI5r510-ktUmgU2YSmPzDQP8Hc8hXON1VNkS7l1W2zqtaDNiXLZrP4-XAQLgP5bu1tq0uqay4KXaJokBHkdIWQLH7FqTc1d0~JtGLHJ20gjjp0HqAjebnSKsqyNpAcIh4Q-bhMPxcyYO0KzlM1OT1e3emNmwO~OV2XDsAUo6YDimIMVvK~aLnNDsTGRmE0XQ__&Key-Pair-Id=APKAIUCZBIA4LVPAVW3Q

326. Healy LJ, Jiang Y, Hsu EW. Quantitative comparison of myocardial fiber structure between mice, rabbit, and sheep using diffusion tensor cardiovascular magnetic resonance. *J Cardiovasc Magn Reson*. 2011;13:74.

327. Dou J, Reese TG, Tseng W-YI, Wedeen VJ. Cardiac diffusion MRI without motion effects. *Magn Reson Med*. 2002;48:105–114.

328. Tseng WY, Reese TG, Weisskoff RM, Wedeen VJ. Cardiac diffusion tensor MRI in vivo without strain correction. *Magn Reson Med*. 1999;42:393–403.

329. Stoeck CT, Kalinowska A, Deuster von C, Harmer J, Chan RW, Niemann M, Manka R, Atkinson D, Sosnovik DE, Mekkaoui C, Kozerke S. Dual-phase cardiac diffusion tensor imaging with strain correction. *PLoS ONE*. 2014;9:e107159.

330. Ferreira PF, Kilner PJ, McGill L-A, Nielles-Vallespin S, Scott AD, Ho SY, McCarthy KP, Haba MM, Ismail TF, Gatehouse PD, de Silva R, Lyon AR, Prasad SK, Firmin DN, Pennell DJ. In vivo cardiovascular magnetic resonance diffusion tensor imaging shows evidence of abnormal myocardial laminar orientations and mobility in hypertrophic cardiomyopathy. *J Cardiovasc Magn Reson*. 2014;:1–16.

331. Reese TG, Weisskoff RM, Smith RN, Rosen BR, Dinsmore RE, Wedeen VJ. Imaging myocardial fiber architecture in vivo with magnetic resonance. *Magn Reson Med*. 1995;34:786–791.

332. Gamper U, Boesiger P, Kozerke S. Diffusion imaging of the in vivo heart using spin echoes--considerations on bulk motion sensitivity. *Magn Reson Med*. 2007;57:331–337.

333. Nielles-Vallespin S, Mekkaoui C, Gatehouse P, Reese TG, Keegan J, Ferreira PF, Collins S, Speier P, Feiweier T, de Silva R, Jackowski MP, Pennell DJ, Sosnovik DE, Firmin D. In vivo diffusion tensor MRI of the human heart: reproducibility of breath-hold and navigator-based approaches. *Magn Reson Med*. 2013;70:454–465.

334. Tseng WY, Reese TG, Weisskoff RM, Brady TJ, Wedeen VJ. Myocardial fiber shortening in humans: initial results of MR imaging. *Radiology*. 2000;216:128–139.

335. Wu MT, Tseng WYI, Su MYM, Liu CP, Chiou KR, Wedeen VJ, Reese TG, Yang CF. Diffusion Tensor Magnetic Resonance Imaging Mapping the Fiber Architecture Remodeling in Human Myocardium After Infarction: Correlation With Viability and Wall Motion. *Circulation*. 2006;114:1036–1045.

336. Tseng W-YI, Dou J, Reese TG, Wedeen VJ. Imaging myocardial fiber disarray and intramural strain hypokinesis in hypertrophic cardiomyopathy with MRI. *J Magn Reson Imaging*. 2006;23:1–8.

337. Deuster von C, Sammut E, Asner L, Nordsletten D, Lamata P, Stoeck CT, Kozerke S, Razavi R. Studying Dynamic Myofiber Aggregate Reorientation in Dilated Cardiomyopathy Using In Vivo Magnetic Resonance Diffusion Tensor Imaging. *Circulation: Cardiovascular Imaging*. 2016;9.

338. McGill L-A, Ismail TF, Nielles-Vallespin S, Ferreira P, Scott AD, Roughton M, Kilner PJ, Ho SY, McCarthy KP, Gatehouse PD, de Silva R, Speier P, Feiweier T, Mekkaoui C, Sosnovik DE, Prasad SK, Firmin DN, Pennell DJ. Reproducibility of in-vivo diffusion tensor cardiovascular magnetic resonance in hypertrophic cardiomyopathy. *J Cardiovasc Magn Reson*. 2012;14:86.

339. Drakos SG, Kfoury AG, Hammond EH, Reid BB, Revelo MP, Rasmusson BY, Whitehead KJ, Salama ME, Selzman CH, Stehlik J, Clayson SE, Bristow MR, Renlund DG, Li DY. Impact of mechanical unloading on microvasculature and associated central remodeling features of the failing human heart. *J Am Coll Cardiol*. 2010;56:382–391.

340. Edelman RR, Gaa J, Wedeen VJ, Loh E, Hare JM, Prasad P, Li W. In vivo measurement of water diffusion in the human heart. *Magn Reson Med*. 1994;32:423–428.

341. Rutz AK, Ryf S, Plein S, Boesiger P, Kozerke S. Accelerated whole-heart 3D CSPAMM for myocardial motion quantification. *Magn Reson Med*. 2008;59:755–763.

342. Klein S, Staring M, Murphy K, Viergever MA, Pluim JPW. elastix: a toolbox for intensity-based medical image registration. *IEEE Trans Med Imaging*. 2010;29:196–205.

343. Wang H, Stoeck CT, Kozerke S, Amini AA. Analysis of 3D cardiac deformations with 3D SinMod. *Conf Proc IEEE Eng Med Biol Soc*. 2013;2013:4386–4389.

344. Osman NF, Kerwin WS, McVeigh ER, Prince JL. Cardiac motion tracking using CINE harmonic phase (HARP) magnetic resonance imaging. *Magn Reson Med*. 1999;42:1048–1060.

345. Stuber M, Scheidegger MB, Fischer SE, Nagel E, Steinemann F, Hess OM, BOESIGER P. Alterations in the local myocardial motion pattern in patients suffering from pressure overload due to aortic stenosis. *Circulation*. 1999;100:361–368.

346. Asner L, Hadjicharalambous M, Chabiniok R, Peresutti D, Sammut E, Wong J, Carr-White G, Chowienczyk P, Lee J, King A, Smith N, Razavi R, Nordsletten D. Estimation of passive and active properties in the human heart using 3D tagged MRI. *Biomech Model Mechanobiol*. 2016;15:1121–1139.

347. Streeter DD, Bassett D. An Engineering Analysis of Myocardial Fiber Orientation in Pig‘S. *Anat Rec*. 1965;

348. Li W, Lu M, Banerjee S, Zhong J, Ye A, Molter J, Yu X. Ex vivo diffusion tensor MRI reflects microscopic structural remodeling associated with aging and disease progression in normal and cardiomyopathic Syrian hamsters. *NMR Biomed*. 2009;22:819–825.

349. Abdullah OM, Drakos SG, Diakos NA, Wever-Pinzon O, Kfoury AG, Stehlik J, Selzman CH, Reid BB, Brunisholz K, Verma DR, Myrick C, Sachse FB, Li DY, Hsu EW. Characterization of diffuse fibrosis in the failing human heart via diffusion tensor imaging and quantitative histological validation. *NMR Biomed*. 2014;27:1378–1386.